Universidad
Carlos III de Madrid

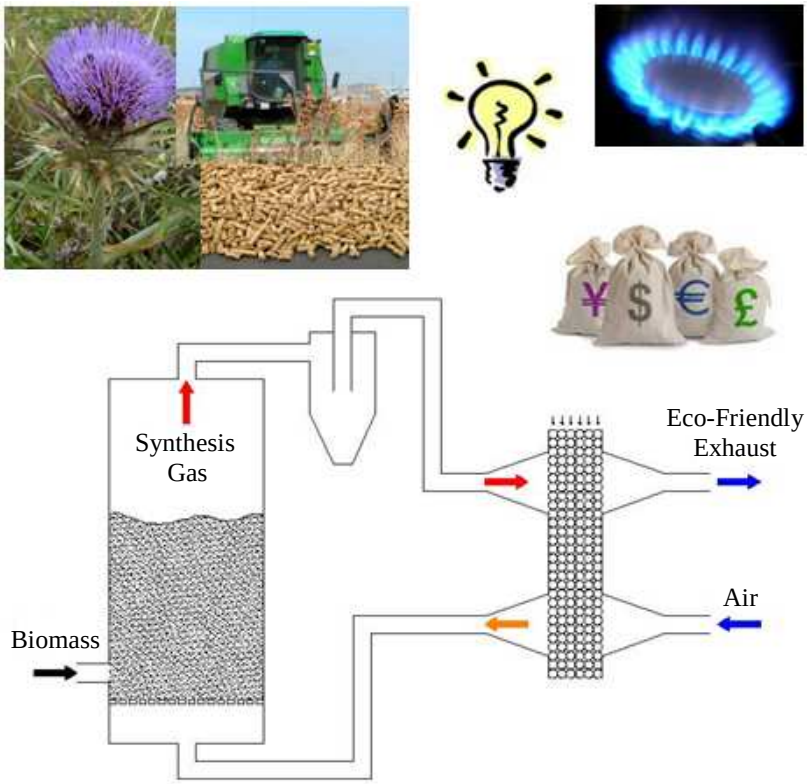

THE TECHNICAL AND ECONOMIC FEASIBILITY OF *CYNARA CARDUNCULUS* L. GASIFICATION

Alberto Gómez García, *PhD Thesis*

Carlos III University of Madrid. Polytechnic School
ISE Research Group
Thermal and Fluid Engineering Department
Leganés (Madrid, Spain), December, 2012

UNIVERSIDAD CARLOS III DE MADRID

TESIS DOCTORAL

“The Technical and Economic Feasibility of *Cynara Cardunculus* L. Gasification”

Autor:
Alberto Gómez García

Director:
Domingo Santana Santana

DEPARTAMENTO DE INGENIERÍA TÉRMICA Y DE FLUIDOS

Leganés, diciembre y 2012

TESIS DOCTORAL

“The technical and Economic Feasibility of *Cynara Cardunculus* L. Gasification”

Autor: Alberto Gómez García

Director/es: Domingo Santana Santana

Firma del Tribunal Calificador:

Firma

Presidente:

Vocal:

Secretario:

Calificación:

Leganés, de de

A mis padres, a Sandra y a Vanesa

Contents

List of Figures

List of Tables

List of Publications

Part of the work contained in this PhD Thesis has also been presented in the following conferences[(1)] and is intended to be submitted by the date of lecture of the thesis[(2)]:

- Gómez-García, A., Sánchez-Prieto, J., Villa-Briongos, J., Santana-Santana, D. Nueva aproximación en el modelado de reactores de gasificación en lecho fluidizado con aplicación a gasificación de biomasa, 7º Congreso Nacional de Ingeniería Termodinámica. Bilbao, España, 15-17 June. 2011.[(1)]

- Gómez-García, A., Sánchez-Prieto, J., Soria-Verdugo, A. Santana, D. MBHEF syngas conditioning: modelling approach and exergy optimisation, 4th International Symposium on Energy from Biomass and Waste. Venice, Italy, 12-15 November. 2012.[(1)]

- Assessment of the potential of the *Cynara cardunculus* L. gasification for bioenergy production. To be submitted.[(2)]

- MBHEF syngas conditioning: modelling approach and exergy optimisation. To be submitted. [(2)]

Besides, the author of the thesis has collaborated in the following works presented in conferences[(3)] and papers[(4)] while working on the thesis, but they are not included since their content is outside the scope of the present PhD Thesis.

- Hernández-Jiménez, F., Sánchez-Delgado, S., Gómez-García, A., Acosta-Iborra, A. Comparison between two-fluid model simulations and particle image analysis & velocimetry (PIV) results for a two-dimensional gas-solid fluidized bed. *Chemical Engineering Science 66, 3753-3772*, 2011.[(4)]

- Soria-Verdugo, A., García-Hernando, N., Gómez-García, A., García-Gutiérrez, L.M., Ruiz-Rivas, U. An evaluation of the DAEM model validity for wood pellets, 19th European Biomass Conference and Exhibition. From Research to Industry and Markets. Berlin, Germany, 6-10 June. 2011.[(3)]

- Sette, E., Gómez-García, A., Pallarés, D., Johnsson, F. Quantitative Evaluation of inert Solids Mixing in a Bubbling Fluidized Bed, 21th International Conference on Fluidized Bed Combustion. Naples, Italy, 3-6 June. 2012.[(3)]

- Sánchez-Prieto, J., Gómez-García, A., Villa-Briongos, J., Santana-Santana, D. Using DBM to Study the Effect of Biomass Feeding in the Dynamic Behavior of a Large-Scale Bubbling Fluidized Bed, 21th International Conference on Fluidized Bed Combustion. Naples, Italy, 3-6 June. 2012.[(3)]

- Hernández-Jiménez, F., Gómez-García, A., Santana, D., Acosta-Iborra, A. Characterization of the Gas interchange Between Bubble and Emulsion Using Two-Fluid Model Simulations, 21th International Conference on Fluidized Bed Combustion. Naples, Italy, 3-6 June. 2012.[3]

- Hernández-Jiménez, F., Gómez-García, A. Santana, D., Acosta-Iborra, A. Gas interchange between bubble and emulsion phases in a 2D fluidized bed as revealed by two-fluid model simulations. *Chemical Engineering Science* 2012. Accepted for publication.[4]

Agradecimientos

Llegado este momento, son muchas las personas a las que debo agradecer su apoyo. En primer lugar, a mi familia: mis abuelos, en especial a los que no han llegado a tiempo de verme alcanzar este sueño y siempre han estado ahí para lo que fuera, a mis padres por su cariño, paciencia, sacrificios y valores que me han inculcado para darme lo mejor y mi hermana por ser tan genuina, una gran persona y mejor hermana. Cualquier gesto se queda corto para agradecéroslo.

Gracias a Domingo, mi director de tesis, por su dedicación guiándome en el mundo de la investigación y apoyándome no solo en lo científico. Al resto de doctores del grupo ISE: Javi Villa, Antonio Acosta, Celia, Sergio, Antonio Soria, Ulpiano, Mercedes, Néstor, Carol, y los que están en vías de este camino tan largo y con los que he compartido buenos momentos: Fernando, Javi, Luis, Luismi, Edu, Jesús, Juan, Lucía, María, Mariano, Paula, Reyes, Javi, Borja, Alberto y Dani. También quiero dar las gracias al grupo de mecánica de fluidos por compartir su material de laboratorio con nosotros, a los técnicos de laboratorio Manolo, Carlos, David e Israel por su inestimable ayuda y a Cristina por sus ánimos constantes. A los que me olvido, sois tantos… muchas gracias también.

También quiero dar las gracias a todos mis amigos y colegas, de dentro y fuera del baile, colegio, instituto, universidad, barrio: Adela, Almudena, Andrés, Aurora, Borja, Carlos, el otro Carlos, Celia, David, Elena, Gabriel, Gema, Javi, Jeniffer, José, Josué, Juncal, Laura, Livia, Luis, Málik, María Lara, Marta, Mery, Noelia, Pablo Lamata, Salmerón, Sara, Svenka, Verónica… y a todos los demás que me dejo.

Finalmente, y no menos importante, mención especial a Vanesa, sin su cariño, afecto, ánimo y paciencia en esta época complicada para mi no habría sido posible realizar esta tesis.

Acknowledgement

In the last four years, the ISE research group has held several conferences related to its main research lines: fluidization and energy conversion technologies, and have been performed by some of the most important researches in these fields. I would like to thank them for having been a really good source of ideas for this thesis.

- Bo Leckner, *Chalmers University of Technology*.
- Filip Johnson, *Chalmers University of Technology*.
- Joachim Werther, *Hamburg University of Technology*.
- Piero Salatino, *Universit'a degli Studi di Napoli Federico II*.
- David Pallarés, *Chalmers University of Technology*.
- Allan Hayhurst, *University of Cambridge*.
- Naoko Ellis, *University of British Columbia*.
- Christoph Müller, *ETH of Zürich*.

Alberto Gómez Barea (University of Seville), your curiosity and devotion for the research has inspired me a lot. Besides, I would like to thank to John Grace and Andrés Mahecha from FRC at UBC (Vancouver) and, David Pallarés and Erik Sette from Energy Technology Division at Chalmers University (Göteborg) for hosting me in the summer stayships of 2010 and 2011 respectively. Thanks to all of you for your support, encourage and inspiration.

Resumen

La presente tesis doctoral analiza la viabilidad técnica y económica de la gasificación de *Cynara cardunculus* L. (cynara). El objetivo de este análisis es evaluar la producción de bioenergía por medio de la gasificación en reactores de lecho fluidizado y el posterior tratamiento del gas de síntesis (syngas) producido en dichos reactores para adecuar el syngas a las posibles aplicaciones como turbinas de gas y motores internos de combustión. Para lograr este objetivo, esta tesis propone la formulación de sendos modelos para evaluar los costes de generación de electricidad (**Capítulo 2**), el rendimiento del reactor (**Capítulo 3**) y la eficiencia de la depuración del syngas (**Capítulo 4**).

Con este propósito, se ha considerado la Comunidad Autónoma de Madrid (CAM) como caso base de estudio. El análisis realizado estima que la cynara tiene el potencial de proveer 1708 GWh al año, es decir, alrededor del 42% del suministro eléctrico nacional basado en biomasa excediendo en un 72% el suministro total de la electricidad procedente de la biomasa en la CAM. De este modo, la implementación de proyectos que utilicen la cynara como combustible podrían ayudar a reducir el consumo de energía de la CAM en un 0.05%, lo que supondría evitar hasta el 66% de las emisiones de CO_2 procedentes de la combustión de combustibles fósiles.

La evaluación económica llevada a cabo en el presente trabajo estudia el uso de dos tecnologías termoquímicas para la conversión de cynara en electricidad destinada a diferentes aplicaciones o a ser vendida a la red nacional. Dichas soluciones tecnológicas consideradas son: plantas de Turbinas de Gas en Ciclo Combinado (CCGT) y generadores de potencia en Motores de Combustión Interna (ICE). La solución CCGT ha sido estudiada para un rango de capacidades instaladas de 5-30 MW, mientras que la tecnología ICE ha sido analizada para un rango de 1-30 MW. Así pues, se realizó un análisis de sensibilidad para examinar los efectos de variables tales como la producción de biomasa, tasa de retorno del proyecto, costes de transporte y operación y mantenimiento de las plantas.

Para rendimientos de producción de cynara del orden de 17 t/ha considerando un planta de 8 MW como caso base de estudio, el análisis económico estima unos costes de producción de 21,60 c€/kWh y 24,32 c€/kW para las soluciones CCGT e ICE, respectivamente. Por tanto, las plantas CCGT son la mejor elección para tamaños de planta por encima de los 8 MW, mientras que las plantas ICE constituyen la tecnología más acorde por debajo de los 8 MW de tamaño de planta.

Con respecto a la tasa de retorno, los resultados muestran que para el mismo caso base de estudio considerado (8 MW), tasas de retorno del 10% suponen un coste de electricidad estimado en 16,69 c€/kWh para plantas CCGT y de 19,08 c€/kWh para

plantas ICE. Por el contrario, el empleo de tasas de retorno bajas (1%) dan un coste de electricidad de 12,70 y 15,13 c€/kWh para las opciones tecnológicas CCGT e ICE, respectivamente.

Sobre la inversión total de capital, ésta crece con el tamaño de planta representando hasta el 93 y 92% del total de las plantas CCGT e ICE, respectivamente. A tener en cuenta que estos porcentajes corresponden a 42,17M€ y 41,46 M€ respectivamente para el caso base de 8 MW. Sin embargo, las plantas ICE muestran una mayor economía de escala en términos de producción de energía. Además, los costes totales de operación para el mismo escenario de una planta CCGT se estimó en 2,94 M€ y alrededor de 3,65 M€ para una planta ICE.

En relación a las rutas termoquímicas de conversión de cynara, la gasificación de biomasa en un lecho fluidizado ha sido modelado para analizar dicho proceso para *Cynara cardunculus* L. considerando el comportamiento característico de la biomasa.

Se conoce muy bien que el estado térmico del lecho fluidizado y la generación de volátiles de la biomasa son cruciales en su operación y rendimiento. De hecho, el patrón de flujo de la fase burbuja controla el perfil de temperatura del lecho fluidizado que determina la devolatilización y las reacciones de craqueo de tars. Esto subyace en el hecho de que los compuestos alcalinos, caracterizados por un bajo punto de fusión, pueden transformarse en vapores y la llamada ceniza volante propensos a depositarse sobre las superficies de los combustores y/o reaccionar con las partículas del material inerte del lecho. De esta manera, la formación de aglomerados (precursores de la aglomeración del lecho) empezaría y así, la defluidización del lecho que llevaría a la parada del reactor. En consecuencia, una aproximación de modelado enfocada en la fase burbuja, que puede actuar como puntos calientes de “by-pass” influyendo los problemas derivados de las cenizas, puede ayudar a monitorizar la localización de regiones con riesgo de sinterización de ceniza y aglomeración de lecho y predecir funcionamientos indeseados de los reactores de lecho fluidizado.

En el presente trabajo se propone una nueva formulación para el modelado de reactores de gasificación de biomasa en lecho fluidizado considerando la devolatilización instantánea y picos de temperatura por la combustión de volátiles dentro del lecho. La fase burbuja y el balance de energía del lecho fluidizado se emplean para seguir la liberación gradual de volátiles de la biomasa a lo largo del lecho y comprobar el rendimiento del reactor de lecho fluidizado. La aproximación de modelado unidimensional y estacionario que se plantea usa un modelo de dos fases (burbuja y emulsión) con dos zonas (región densa del lecho y freeboard) para explicar la naturaleza compleja de la dinámica del reactor de lecho fluidizado. Por simplificación, no se consideran los efectos catalíticos de la fracción de ceniza de la biomasa.

Para la futura validación, ajuste y puesta a punto del modelo propuesto, se ha realizado un análisis de sensibilidad de la gasificación de cynara en lecho fluidizado, dentro del régimen burbujeante, y considerando las especificaciones de diseño de la planta piloto a escala del reactor de lecho fluidizado del Departamento de Ingeniería Térmica y de Fluidos en la Universidad Carlos III de Madrid. La campaña de simulación ha arrojado una composición de syngas (en base seca) de 4,79-14,84% para CO, 19,77-21,35% para CO_2, 6,11-15,00% para H_2 and 2,16-5,73% para CH_4. Además,

el poder calorífico inferior y contenido de tars del gas de síntesis caen en el rango de 2,25-6,25MJ/Nm^3 y 60-180g/Nm^3, respectivamente. Estos resultados corresponden a una relación de gastos másicos de biomasa y caudal de syngas generado de 1,309-2,392Nm^3/kg, incluyendo N_2.

El análisis de los resultados en comparación con la experimentación previa destaca: 1) la buena capacidad predictiva del modelo propuesto y 2) las discrepancias entre las simulaciones y los trabajos experimentales son atribuibles a la heterogeneidad de datos encontrados en la literatura, como por ejemplo, las diferentes composiciones de biomasa, condiciones de operación, material de lecho (catalítico) empleado, métodos de muestreo de gas y de tars, etc. Por lo tanto, investigación experimental adicional ayudaría a mejorar la capacidad predictiva del modelo propuesto.

Por último, se necesita el acondicionamiento del gas de síntesis producido en el reactor de lecho fluidizado para lograr las especificaciones de las plantas que operan con motores de combustión interna y turbinas de gas. De lo contrario, la carencia o ineficiencia de la limpieza del gas de síntesis podría conllevar a problemas operacionales in los equipos posteriores y entonces, paradas no planificadas con los costes extra de mantenimiento y reparación. Por ejemplo, las partículas finas arrastradas pueden ocasionar obstrucción y contaminación, mientras que los tars pueden condensar produciendo el taponamiento y atrición en filtros, conductos, intercambiadores de calor, etc. Además, el tratamiento del gas de síntesis para reducir las sustancias contaminantes que pudiera tener influiría en el rendimiento y los costes operacionales y de inversión de los equipos de limpieza de gas.

Actualmente, los sistemas de depuración de gases tienen el objetivo de reducir los niveles en partículas y tars por debajo de las concentraciones admisibles (mg/Nm^3) para los motores de combustión interna y turbinas de gas: 50-50 y 30-5, respectivamente. De este modo, como parte de la tesis, se propone el modelado y análisis de un filtro-intercambiador de calor en lecho móvil (MBHEF) como equipo de limpieza del gas de síntesis.

El filtro-intercambiador de calor en lecho móvil destaca por sus beneficios: operación a alta temperatura (700-800ºC, la temperatura de salida del reactor del gas de síntesis), sin obstrucción ni incremento de la presión durante su operación, que podría llevar a parar el proceso si se usaran otros métodos de depuración del syngas como filtros cerámicos, bolsas de filtro, etc. Además, dicho filtro en lecho móvil otorgaría una alta superficie de contacto entre el gas a tratar y el lecho sin arrastre ni elutriación de sólidos. Así, este tamaño compacto del equipo permitiría ahorrar costes. Finalmente, dicho equipo también evitaría costes adicionales derivados de las modificaciones del diseño del reactor de lecho fluidizado así como el empleo de aditivos y otros materiales catalíticos para eliminar y reducir el contenido de tars en el gas.

Por ello, se plantea una aproximación de modelado para simular la eliminación de partículas y tars en un filtro-intercambiador de calor en lecho móvil. El modelo bidimensional, adiabático y estacionario que se propone considera dos fases (gas y sólido) e ignora la conductividad térmica y difusión de materia. Respecto a los tars, su condensación se modela a través de la elección de compuestos representativos de las

clases de tars más importantes de acuerdo a la literatura: fenol (clase 2), naftaleno (clase 4) y pireno (clase 5).

El modelo también considera la influencia de la concentración de tars en el punto de rocío mientras que el modelo de filtración se ha tomado de la literatura. Además, se ha llevado a cabo un estudio de exergía con el fin de analizar la optimización del tamaño del equipo y ayudar a la elección de las condiciones de funcionamiento más económicas.

Se ha realizado un análisis de sensibilidad con el tamaño de partícula y la velocidad superficial de gas, los cuales han demostrado ser parámetros operativos clave. En dicho análisis de sensibilidad, se ha tomado como caso base de estudio una composición de gas de síntesis a partir de trabajos experimentales de la literatura. Por lo tanto, los mapas de temperatura y eficiencias de reducción de tars y partículas que se presentan muestran el rendimiento de dicho equipo para reducir el contenido de estos contaminantes.

Los resultados de las simulaciones indican la viabilidad de utilizar tal equipo como dispositivo de eliminación de tars, gracias a sus ventajas frente a otros métodos de depuración de gases con aceptables eficiencias de remoción de contaminantes, que van desde 88 hasta 94%. Como se observa, se pueden alcanzar eficiencias de, al menos, el mismo orden de magnitud que los alcanzables con el uso de lechos catalíticos o filtros de arena a temperaturas mucho menores y mayores que los logrados por medio de torres de lavado, precipitadores electrostáticos, filtros de tela y los absorbedores de lecho fijo. En caso de no alcanzar el nivel de reducción para cada aplicación final, el sistema MBHEF se puede utilizar como método eficaz de eliminación secundaria para la eliminación de tars del gas de síntesis previo a otro tratamiento, con las ventajas indicadas anteriormente en lugar de el resto de las tecnologías existentes.

Los resultados también señalan que bajas velocidades de gas (0,5-1m / s) y altos tamaños de partícula (400-700μm) son las condiciones más adecuadas para el ahorro de costes. Sin embargo, la optimización de la destrucción de exergía implica eliminar tars con bajo o muy bajo rendimiento de depuración, por lo que no se pueden optimizar simultáneamente la destrucción de exergía y la eficiencia de eliminación de tars y partículas.

La viabilidad técnica y económica de *Cynara cardunculus* L. mediante gasificación de lecho fluidizado se ha llevado a cabo en la presente tesis doctoral, demostrando la cynara como un prometedor cultivo energético para satisfacer las demandas de energía en lugares de clima mediterráneo como la CAM (caso de estudio en esta tesis). Además, la aproximación de modelado propuesto para predecir el rendimiento de los gasificadores en lecho fluidizado ha mostrado ser una herramienta útil para ayudar a otros métodos de diagnóstico en la prevención de la aglomeración del lecho y sinterización de las cenizas con el fin de evitar problemas de funcionamiento y de parada no programada de tales reactores. Finalmente, el uso del equipo MBHEF como método de limpieza del gas de síntesis ha sido analizado con la aproximación de modelado presentado en esta tesis. Este estudio indica que dicho equipo es muy efectivo para eliminar partículas y tars presentes en el gas de síntesis producido en el reactor de lecho fluidizado. De este modo, los problemas relacionados con la condensación tars como contaminación, obstrucción y atrición aguas abajo del reactor podrían evitarse.

Abstract

This PhD Thesis analyses the technical and economic feasibility of the gasification of one of the most promising energy crops in terms of biomass yield and plantation costs: *Cynara cardunculus* L. (cynara). The aim of this analysis is to assess the bioenergy production via fluidized bed gasification (FBG) and the ulterior treatment of the synthesis gas (syngas) produced in the FBG reactor to adequate it to end-use applications such as gas turbines and internal combustion engines. To achieve this objective, this thesis proposes a formulation model approach for evaluating the electricity generation costs (**Chapter 2**), the reactor performance (**Chapter 3**) and the syngas conditioning efficiency (**Chapter 4**).

For this purpose, the Autonomous Community of Madrid (CAM) has been taken as study case. The analysis estimates that the cynara has the potential to provide 1708 GWh yr^{-1}, that is, around 42% of national biomass-based electricity supply and exceeds 72% of total renewable-based electricity supply in CAM. Therefore, the implementation of cynara projects could help reducing the total energy consumption of CAM by 0.05%, what would suppose to avoid up to 66% of CO_2 emissions from fossil fuels.

The economic assessment performed in the present work evaluates the use of two thermochemical technologies for cynara conversion into electricity to be used for different applications or sold to the national grid. The technological solutions considered are: a Combined Cycle Gas Turbine (CCGT) plant and an Internal Combustion Engine (ICE) power generator. The CCGT solution was studied for an installed capacity range of 5-30 MW, while the ICE solution was analysed for a range of 1-30 MW. A sensitivity analysis was conducted to examine the effects of variables such as biomass yield, discount rate, transport cost, operation and maintenance.

For a cynara yield of 17 t/ha in an 8 MW plant as base case, the economic analysis estimates a production costs of 21.60 c€/kWh and 24.32 c€/kW for the CCGT and ICE solutions, respectively. Accordingly, CCGT plants are the best choice for a plant size above 8 MW, while ICE plants constitute the most suitable technology below 8 MW.

With regards to the discount rate, the results show that for the same base case (8 MW), for a discount rate of 10% the cost of electricity is estimated to be 16.69 c€/kWh for CCGT plants and 19.08 c€/kWh for ICE plants. On the contrary, the use of the lowest discount rate (1%) yields a cost of electricity of 12.70 and 15.13 c€/kWh for CCGT and ICE solutions, respectively.

Concerning to the total capital investment, it grows with the plant size, representing up to 93 and 92% of the total CCGT and ICE plant cost, respectively. Such percentages correspond to 42.17M€ and 41.46 M€ for a CCGT and ICE plant for a base case of 8 MW. Nevertheless, the ICE plants show a stronger economy of scale in energy

production than the CCGT solution. In addition to this, the total operating costs for an 8 MW CCGT scenario is estimated to be 2.94 M€ and around 3.65 M€ for an ICE plant.

In relation to the thermochemical conversion route of cynara, the gasification of biomass in a FB reactor has been modelled to analyse such process for *Cynara cardunculus* L. taking into consideration the particular biomass behavior.

It is well known that the FB reactor thermal state and the biomass volatiles generation are crucial in its operation and performance. Hence, the bubble flow pattern controls the FB temperature profile driving devolatilization and tars cracking kinetics. This underlies in the fact that alkali compounds of biomass fuels, which are featured by a low melting point, can transform into vapours and ash fly that are prone to deposit on heat surfaces in boilers and/or react with the particles of the inert bed material inside the FB. Thus, the formation of agglomerates (the so-called bed agglomeration) would start and then, the defluidization of FB leading to the shut-down of the FBG reactor. Therefore, a modelling approach focused on the bubble phase, which can act as "by-passing" hot spots inside the FB region influencing on ash-related problems, can help to monitor the location of ash sintering and bed agglomeration risk regions and predict undesired FBG reactor performance.

A new formulation for biomass FBG reactor modelling that considers the instantaneous devolatilization and temperature peaks due to volatiles combustion inside the FB region is proposed in the present work. A bubble phase and a FB energy balance are used to monitor the gradual release of biomass volatiles along the FB and to check the performance of the FBG reactor. The one-dimensional, steady-state proposed model uses a two-phase (bubble and emulsion) and two zone (bottom dense bed and upper freeboard) modelling approach to account for the complex nature of FBG reactor dynamics. Furthermore, no catalytic effects of ash composition from biomass are taken into consideration.

For further validation and tuning up of the model proposed, a sensitivity analysis of cynara gasification in FB, under bubbling regime, was performed considering the specification design of the pilot-plant scale FBG reactor in the Thermal and Fluid Engineering Department facilities at Carlos III University of Madrid. The simulation campaign yields a syngas composition (on dry basis) of 4.79-14.84% for CO, 19.77-21.35% for CO_2, 6.11-15.00% for H_2 and 2.16-5.73% for CH_4. Besides, the lower heating value and tar content of the syngas fall in the range of 2.25-6.25MJ/Nm^3 and 60-180g/Nm^3, respectively. These results correspond to a syngas-biomass flows ratio in the range of 1.309-2.392Nm^3/kg, accounting for N_2 in the raw syngas produced.

The analysis of the results in comparison with previous experiments stands out: 1) the good predictive capability of the model proposed and 2) the discrepancies between simulations and experimental works are attributable to the data heterogeneity found in the literature, that is, different biomass compositions, operating conditions, (catalytic) bed material used, sampling methods for syngas and tar compositions, etc. Hence, further experimental research would help improving the predictive capability of the proposed model.

Finally, the conditioning of the syngas produced from the FBG reactor is needed in order to achieve end-use requirements in ICE and gas turbines (GT) plants, since the

lack or inefficiency of syngas clean-up could lead to operational problems in downstream equipment and then, unscheduled shut-down and extra maintenance and repair costs. For example, particulate material can cause clogging and fouling, while tars can condensate producing blockage and attrition in filters, exit pipes, heat exchangers, etc. Furthermore, the syngas treatment to reduce its pollutants would influence the performance, investment and operational costs of the gas cleaning devices.

Nowadays, gas cleaning systems are aimed to reduce particulate and tars material levels below the allowable concentrations (mg/Nm^3) for ICE and GT devices: 50-50 and 30-5, respectively. Thus, as a part of the present thesis, the modelling and analysis of a moving bed heat exchange filter (MBHEF) is proposed as hot gas clean-up equipment.

The MBHEF stands out because its benefits: high temperature operation (700-800ºC the exhaust gas temperature from the FB reactor), no-clogging and non-pressure increase during operation, which can lead to unscheduled shut-down if using other typical hot gas cleaning devices such as ceramic filters, bag filters. Additionally, the MBHEF would provide a high contact area between gas and solids without entrainment nor elutriation of solids. This compact size equipment would allow saving costs. Eventually, the MBHEF solution for hot gas cleaning would also avoid extra costs derived from the reactor design modification and the use of additives/catalysts in order to remove tars.

It is presented a modelling approach for simulating tars and particulate removal in a MBHEF. The two-dimension, adiabatic, steady-state proposed model accounts for two-phase (gas and solid) and neglects conduction and mass diffusion. Tars condensation is modelled through representative tar class lumps: phenol (class 2), naphthalene (class 4), and pyrene (class 5) according to the literature. The model also considers tar concentration influence on tar dew point, while the filtration model is taken from literature. Furthermore, an exergy study was conducted in order to optimise the equipment size and help the choice of the less expensive operating conditions.

A sensitivity analysis was performed varying the particle size and superficial gas velocity as key operating parameters. To accomplish this, a syngas composition from experiments reported in the literature has been taken as study case. Thus, maps of temperature, tars abatement and particulate removal efficiencies are presented, which show the MBHEF performance for reducing impurities content.

The simulation results indicate the feasibility of use a MBHEF as tars removal equipment benefiting its advantages against other gas-cleaning methods with acceptable pollutant removal efficiencies, ranging 88-94%. As observed, the MBHEF yields efficiencies, at least, the same order of magnitude of the ones attainable with the use of catalytic crackers, venture scrubbers or sand filter at much lower temperatures and higher than the ones achieved by means of wash towers, wet electrostatic precipitators, fabric filters and fixed bed absorbers. In case of not reaching the reduction level for each end-use application, the MBHEF device can be used as effective secondary removal method for eliminating tars from the syngas, with the advantages stated above as opposed the rest of removal technologies.

Results also point out that low gas velocities (0.5-1m/s) and high particle size (400-700μm) for saving costs are the most suitable operating conditions. Nevertheless, the

exergy optimization involves low or very low tar removal efficiency so that the pollutant reduction and exergy cannot be optimised simultaneously.

The technical and economic feasibility of *Cynara cardunculus* L. via fluidized bed gasification carried out in the present PhD thesis has shown the cynara as a promising energy crop to meet energy demands in Mediterranean climate locations such the CAM (study case here). Besides, the modelling approach proposed for predicting the FBG reactors performance has been shown as a useful tool to help other diagnosis methods for the prevention of bed agglomeration and ash sintering in order to avoid operational problems and unscheduled shut-down of FBG reactors. Finally, the use MBHEF as hot gas clean-up method has been analysed by means of a modelling approach presented here. This study points out that the MBHEF is very effective equipment for removing particulate and tars from the syngas produced in FBG reactors. Thus, downstream tars-related problems such as fouling, blockage and attrition could be avoided.

Chapter 1

Introduction

Contents

1.1. Motivation of the thesis

This PhD Thesis presents a technical and cost assessment for producing and processing, via fluidized bed gasification, one of the most promising energy crops in Mediterranean climate countries (*Cynara cardunculus* L.) in the Autonomous Community of Madrid (Spain) in order to satisfy energy demand in an environmentally sustainable manner.

This PhD Thesis is intended to provide a simulation tool for evaluating costs for cultivating and processing *Cynara cardunculus* L. in terms of biomass yield, transport cost, operating costs, discount rate, price costs and potential useful energy when gasifying. This economic feasibility study includes the analysis of two technological solutions to determine the cost of electricity generation: Combined Cycle Gas Turbine (CCGT) plant and internal combustion engine (ICE) power generation. This economic evaluation uses a fluidized bed gasifier as thermochemical conversion route of *Cynara cardunculus* L. The analysis of the performance of the reactor and main downstream equipment is based on the reviews of the fluidized bed gasification reactors modelling and the synthesis gas (syngas) conditioning strategies for tar and particulate removal, which accounts for the particular biomass features such as high volatiles yield. This

study would allow achieving the end-use syngas requirements and offering economical and environmental solutions. This work proposes a new modelling approach for predicting the performance of such reactors in order to prevent from the in-bed hot spots generation, which can lead to operational problems as ash sintering and bed agglomeration and then, the unscheduled plant shutdown. Thereby, the simulations of the fluidized bed reactor performance can be a helpful guideline when conducting experiments in order to save time and costs in further reactor design and scale-up. In this PhD Thesis, the conditioning of gas produced from the gasifier is crucial, and then, a new moving bed design is proposed since it offers high tar and particulate abatement efficiencies in compact equipment. To evaluate the performance of the moving bed, this thesis presents the formulation for modelling and simulating a moving bed heat exchange filter for removing tars ant particulate (dust) from the syngas produced in order to avoid downstream problems as fouling or clogging due to tars condensation.

The final objective of this thesis is to provide a simulation tool addressed to evaluate costs of electricity production by means of gasification and two technological solutions (CCGT and ICE) as well as to predict the performance of fluidized bed gasifiers and moving beds with application to any biomass. The application to any biomass fuel of cost, gasification and tars removal models presented in this PhD Thesis would be attained by adopting the corresponding input data for models proposed: biomass cultivation costs, biomass yield, power plant size (energy demand), biomass and inert bed material properties, operating conditions of both reactor and moving bed, end-use syngas requirements.

1.2. Objectives of the thesis

The overall objective of the thesis is to assess the potential of *Cynara cardunculus* L. via fluidized bed gasification for bioenergy production in the Autonomous Community of Madrid context (Spain). To achieve this, the key objectives of the PhD thesis are:

- To analyse the influence of annual biomass yield, transport cost, operating costs, technology solution, operating reactor conditions and plant size on the price cost of *Cynara cardunculus* L.
- To provide a modelling approach tool for simulating fluidized bed reactors with application to biomass gasification.
- To study the effect of operating conditions of such reactor on the syngas quality.
- To propose a new moving bed modelling approach as simulation tool for tar and particulate removal saving experimental investigation costs.
- To analyse the theoretical tar and particulate removal efficiency by moving bed technology.

1.3. Thesis layout

This PhD Thesis is presented in a manuscript form, with a few modifications in order to avoid overlap or repetition of some parts that could hinder its readability and understanding. Chapters 2 and 3 are intended to be published together with chapter 4 as well. As follows, a summary of main topics covered by this PhD Thesis is presented:

Chapter 1 introduces the problem derived of fossil fuel dependence, the alternatives energy sources to maintain the current lifestyle in a sustainably manner and the choice adopted: biomass as energy source. Thus, one of the most promising biomass conversion technology, gasification fluidized bed, is described: basic fundamentals for understanding and advantages. Eventually, main drawbacks of biomass gasification in fluidized beds to be overcome are also showed, which are featured by the model approach in **Chapter 3**.

Chapter 2 evaluates the potential for bioenergy production of *Cynara cardunculus* L. in the Autonomous Community of Madrid (Spain). This economic assessment uses the syngas yield predictions of *Cynara cardunculus* L. gasification obtained by the model approach proposed in **Chapter 3**. The cost evaluation for bioenergy production considers two technological solutions: CCGT plant and ICE power generator. This feasibility study analyses the effect of operating costs, biomass transport costs, technology (ICE and CCGT) and operating reactor conditions on the cost price for different annual biomass productions.

Chapter 3 presents a modelling approach for predicting the performance of biomass gasification in fluidized beds reactors, considering unique features of biomass and fluidized beds in a simple manner. Furthermore, *Cynara Cardunculus* L. gasification in fluidized bed is evaluated in terms of magnitude and trends of syngas quality: gas composition, Low Heating Value (LHV) and tar content for operating conditions (bed temperature, fluidizing gas inlet, equivalence ratio, fluidization state). Simulations results are then compared with experimental works from literature.

Chapter 4 shows a model to predict and evaluate removal of main tars compounds and particulate (dust) material in a moving bed heat exchange filter in order to satisfy gas requirement of end-use syngas applications: engines and turbines. Tars condensation and particulate material are evaluated. The influence of operating conditions: superficial gas velocity and particle size are analysed for the economical equipment design in terms of pressure drop. An exergy analysis is also performed to find optimised operating conditions that meet syngas quality for applications in turbines and engines.

Chapter 5 summarizes the main conclusions of the previous chapters and suggests future perspectives of this research.

Finally, the **Appendix** section provides the guidelines adopted in the current PhD Thesis about estimating physical and thermodynamical properties of permanent gases and tars as well as the justification of some important simplifications made for modelling approaches of chapters 3 and 4.

1.4. State of the art

1.4.1. The need of reducing fossil fuel dependence

So far, combustible fossil fuels have been the main industry feedstock in manufacturing a wide variety of products (producer gas, raw products as intermediate fuels in others industries or processes - the so-called syngas or bio-oils -, town gas, electricity, heating, etc) after the industrial revolution by the 1800, displacing biomass as energy source. Thus, fossil fuels as energy source mean a qualitative leap for power generation and industry, so that, yielding products and services for the society what made possible a better lifestyle all over the world.

Since then, the energy consumption of fossil fuels such as gas, oil and coal, have rapidly increased in the last century as a consequence of the energy demand growth to satisfy energy requirements of industries and the lifestyle by the population in developed countries, as well as the new incipient consumers from the so-called emergent countries. The industrialization of developing countries and the increase of world population are also contributing to this scenario. Figure 1.1 shows the primary energy growth from 1850 to 2008.

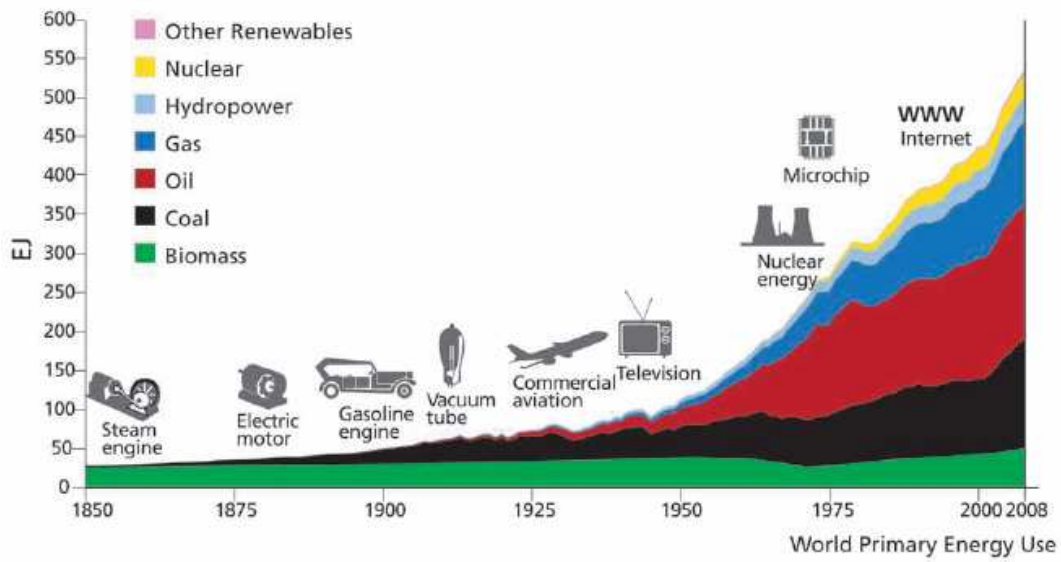

Figure 1.1: Evolution of primary energy shown as absolute contributions by different energy source (EJ). Biomass refers to traditional biomass until the most recent decades when it became more prevalent and now accounts for one-quarter of biomass energy. New renewables have emerged in the last few decades. Updated from Nakicenovic et al. (1998).

As said, previous to the steam engine development, the energy consumption was basically based on biomass. With the discovery of electric motor and the gasoline engine, the biomass energy was displaced by the fossil fuels in scarce 25 years. This was consequence of the low energy density, or calorific value (CV), of biomass (~8GJ/t for 50% of humidity) in contrast to the CV of fossil fuels (28J/t, 42GJ/t and 56GJ/t for coal, mineral oil and liquefied natural gas respectively), what converted the biomass in an energy source economically unfeasible to be transported over large distances. In addition, the electric bulbs around 1900 also replaced town gas as light source, leading to a “marginal” role of the biomass in large scale energy generation. Then, the societies

have become more and more dependent on combustible fossil fuels. This dependence increase has been more remarkable in the last 60 years while the biomass contribution to primary energy has practically remained unchanged. The fact that biomass conversion technologies have been less competitive than traditional electric energy conversion systems has contributed to this situation along the past.

Nowadays, the fossil fuels are so important that they account for up to 78% of primary energy share as denoted in figure 1.2, by 2009. On the contrary, the biomass energy only represents around 7.4%, around 10 times lower than the contribution share of gas, oil and coal together. Obviously, this share of primary energy over the last 40 years has affected the environment in many ways. For example, many scientific studies reveal that CO_2 levels have increased 31% and CH_4 levels have been doubled the last 200 years as well as 20Gtons of carbon have been added due to deforestation. All this has strongly contributed to the raise of the global average surface temperature, around 0.4-0.8ºC, in the last century above the baseline of 14ºC. Besides, precipitation has increased by 5-10% in the northern hemisphere last century and decreased in drier regions. Artic sea ice thinned by 40% and decreased by 10-15% in area since the 1950s too. Thus, global mean sea levels have grown at an average annual rate of 1-2mm the last century (Sims, 2004).

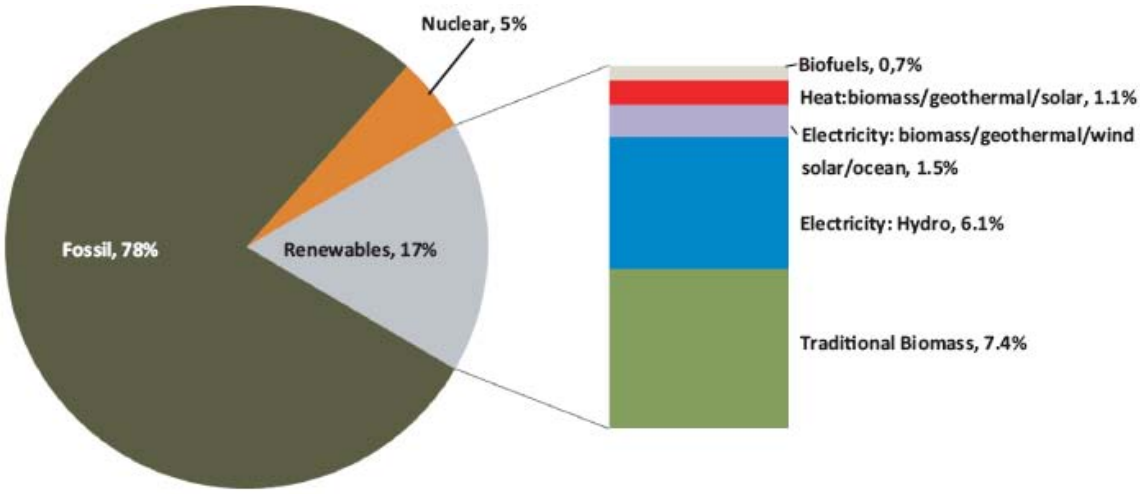

Figure 1.2: Share of primary energy use, 2009, from GEA 2012: Global Energy Assessment report.

In addition to environmental implications, the climate change may affect health through a range of pathways: increase of frequency and intensity of heat waves, reduction in cold related deaths, floods and droughts increase, changes in the distribution of vector-borne diseases and effects on the risk of disasters and malnutrition. All these effects are likely to be predominately negative and impact most heavily on low-income countries where adaptation capacity is weakest but also on the most vulnerable groups in developed countries (Haines et al., 2006).

Energy is vital for social and economic development though there are enough evidences alerting us of that our current lifestyle and power generation model based on fossil fuels are not sustainable from an environmental point of view. In addition, derived health risks are recently being accepted. Thereby, actions have to be taken and

addressed to mitigate greenhouse gases (GHG) emissions, and therefore, reduce global warming.

1.4.2. An aimed change towards a sustainable development

The success in the attainment of mitigating GHG emissions lays on switching to a fully renewable energy system with no or low associated GHG emissions as much as possible. From some time ago, we have become aware enough of the relevance and magnitude of the problem. In fact, generating electricity, heat and biofuels has become a high priority in the energy policy strategies at national and global level (Resch et al., 2008). Hence, several strategies can be carried out: application of energy savings programs focused on energy demand reduction and energy efficiency in industrial (Lee and Chen, 2009) and domestic (Martiskainen and Coburn et al., 2011) fields spheres, research and development of less polluting fuel-to-energy processes such biomass conversion technologies (McKendry, 2002), sustainable renewable energy systems (Panwar et al., 2011; Shi and Chew, 2012), methods and tools to evaluate the availability of renewable energy sources (RES) (Angelis-Dimakis et al., 2011) and investigation of CO_2 capture and storage techniques (Herzog et al., 1997; Herzog and Golomb, 2004).

Among all abovementioned strategies to alleviate climate change problems, the use of RES has been given much attention due to its definition: energy that can be used again and again with low environmental impact, it means, zero or almost zero emissions of air pollutant and GHG.

RES includes biomass, hydropower, solar, geothermal, wind and marine energy finding many usages as observed in table 1.1, what points out its great potential to be profited as energy source (Fischer and Schrattenholzer, 2001; Cornelissen et al., 2012). As can be observed in table 1.1, RES have many applications, either industrial (power generation by means of hydropower, wind or modern biomass) or domestic (urban heating, solar home system, solar dryers and cookers or water heaters).

Energy source	**Energy conversion and application options**
Hydropower	Power generation
Modern biomass	Heat and power generation, pyrolysis, gasification, digestion
Geothermal	Urban heating, power generation, hydrothermal, hot dry rock
Solar	Solar home system, solar dryers, solar cookers
Direct Solar	Photovoltaic, thermal power generation, water heaters
Wind	Power generation, wind generators, windmills, water pumps
Wave	Numerous designs
Tidal	Barrage, tidal stream

Table 1.1: Main energy conversion and usage options of main RES (Demirbas, 2006).

Among several studies, Fischer and Schrattenholzer (2001) analysed the bioenergy potential in 11 world regions (figure 1.3) considering separately five crop groups: wheat, rice, other grains, protein feed and other food crops. This study, based on the calculation of above-ground biomass and primary food produce ratio and the fraction of

parts with available potential for energy use, calculates the yield rates for each of the eleven regions in the world. The results, influenced by the corresponding climate, soil quality, water availability and the crop, indicates how the bioenergy potential tends to increase over the time due to the agricultural progress by 2050. From estimation results obtained by this work stands out the big share from Sub-Saharan Africa, Latin America and Caribbean regions with around the half part of the 275 EJ estimated. Currently, the energy primary demand is roughly 500 EJ (figure 1.1) and by 2050 is expected to be around 550 EJ (Shell, 2008). As observed in figure 1.3, the tendency is to increase the use of bioenergy meeting energy demands in order to improve health and environment quality as well as accessibility to energy worldwide.

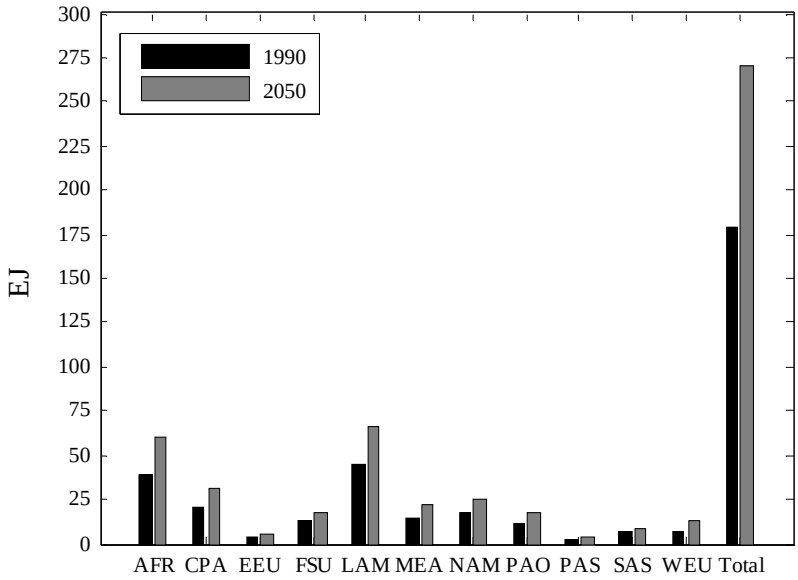

Figure 1.3: Bioenergy potential of crops residues and grasslands [EJ] comparing 1950 and 2050 for 11 regions: Sub-Saharan Africa (AFR), Centrally Planned Asia & China (CPA), Central & Eastern Europe (EEU), Former Soviet Union (FSU), Latin America & the Caribean (LAM), Midle East & North Africa (MEA), North America (NAM), Pacific OECD (PAO), Other Pacific Asia (PAS), South Asia (SAS), Western Europe (WEU) and total of previous regions. The estimated values for 2050 only consider the low estimates. Adapted from Fischer and Schrattenholzer (2001).

However, as Haberl et al. (2010) reveals, not all the studies and reviews aimed at estimating bioenergy potentials span the same range of values: 28-128EJ/year (Erb et al., 2009), 34-120EJ/year (WBGU, 2009), 65-300EJ/year (van Duren et al., 2009), 300-650EJ/year (Hoogwijk et al., 2005), 215-1272EJ/year (Smeets et al., 2007), 120-330EJ/year (Dornburg et al., 2008; 2010) and 60/810EJ/year (Bauen et al., 2009). This wide range of results may lead to misundertandings so that some caution should be taken in consideration when estimating bioenergy potential ranges because of the assumptions made and available data. In fact, Haberl et al. (2010) points out that the high-end of bioenergy potential ranges estimated by some studies are implausible due to: 1) an overestimation of the available area for bio-energy crops due to insufficient consideration of constraints; 2) a too high yield expectations resulting from extrapolation of plot-based studies to large, less productive areas; and 3) no

consideration of possible effects of future climate change on the bioenergy potential. Hence, as conservative criteria, bioenergy potential study and assumptions made by Fischer and Schrattenholzer (2001) has been chosen as basis, whose high-end bioenergy potential (275EJ) matches the value 270EJ estimated by Haberl et al. (2010).

On the other hand, additionally to the wide scope of potential applications and bioenergy potential, RES system development can also solve the presently most crucial tasks according to Zakhidov (2008):

- Improving energy supply reliability and organic fuel economic;
- Solving problems of local energy and water supply;
- Increasing the standard of living and level of employment of the local population;
- Ensuring sustainable development of the remote regions in the desert and mountains zones;
- Implementation of the obligations of the countries with regard to fulfilling the international agreements relating to environmental protection.

1.4.3. Why biomass as fuel for energy purposes?

Solar, wind, hydropower and tidal energy sources are promising because of their potential since they offers great chances for reducing the environmental impact of human activities with a high share in the current energy demand if exploited (figure 1.4). However, many efforts are recently being addressed to biomass as fossil fuel substitute for power and heat generation.

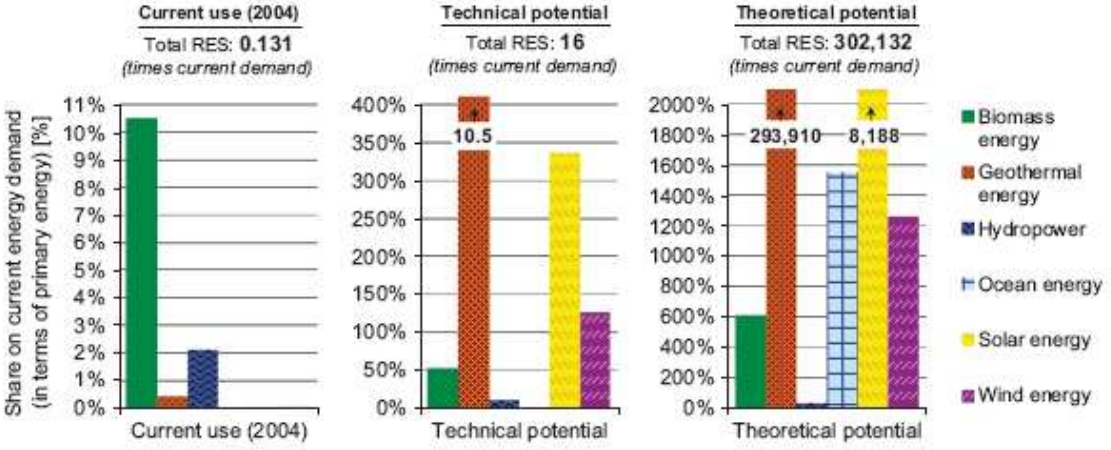

Figure 1.4: Current use (2004), technical and theoretical potentials for several RES compared to current energy demand (476EJ in 2004), at global scale. Adapted from Johansson et al. (2004) and Rogner et al. (2004).

The growing interest in biomass as energy source lays on renewability, environmental and socio-political benefits as Basu (2010) stands out.

Firstly, renewability benefits are derived from biomass definition. Biomass is the plant material constantly formed by the interaction of CO_2, air, water, soil and sunlight via photosynthesis. As a result, carbohydrates forming building blocks of biomass are

produced. Thus, the solar energy driving photosynthesis is stored in the chemical bonds of the structural components of biomass. When biomass is processed efficiently, either chemically or biologically, the energy content stored in the chemical bonds, in combination with oxygen oxidizes CO producing CO_2 and water. Then, the process is cyclical since CO_2 is available to produce new biomass (McKendry, 2002). In other words, biomass grows and is renewable in contrast to fossil fuels like coal, oil and gas. A crop cut this year will grow next year while a tree cut today may grow up within a decade. Therefore, biomass is not likely to be depleted with consumption. This is the reason why the biomass use is rising so fast, especially for energy production.

Secondly, the environmental benefits from biomass are numerous. The net addition of CO_2 to the atmosphere via biomass combustion is considered to be zero. Even when gasified, CO_2 emissions are slightly less than those from combustion (table 1.2). In regard to sulphur content, most virgin biomass contains little to no sulphur saving costs for SO_2 and H_2S removal. Concerning to nitrous oxide emissions, biomass combustion systems yield very low levels in comparison to fired-fossil-fuels systems (Van Loo and Koppejan, 2008). However, gasification systems produce nitrogen compounds in the form of N_2 or NH_3, relatively easily removable. Additionally, highly toxic pollutants such as dioxin and furan, they are not likely to form as opposed to combustion systems.

Thirdly, socio-political benefits are substantial. On the one hand, biomass is a locally grown resource so that it is free from uncertainties such as global political landscape which happens in supply and price of imported fossil fuels, even within short times. On the other hand, this locally character involves the development of associated industries for biomass growing, collecting and transporting. This could create up to 20 times more employment than that created by a coal/oil-based plant according to some authors (Van Loo and Koppejan, 2008), what would have a positive impact on the local economy.

Emission	Pulverized-coal Combustion	Gasification	Combined Natural-Gas Combustion
CO_2 (kg/1000 MWh)	0.77	0.68	0.36
Water use (l/1000 MWh)	4.62	2.84	2.16
SO_2 (kg/MWh)	0.68	0.045	0
NO_x (kg/MWh)	0.61	0.082	0.09
Total solids (kg/100 MWh)	0.98	0.34	~0

Table 1.2: Comparison of emissions from electricity-generation technologies. Adopted from graphs by Stiegel, 2005.

When processing biomass, the achievable useful energy density from further syngas processing depends on the physical and chemical biomass properties (composition, density, particle size, LHV), the conversion technology (fluidization state, gasifying agent, etc) and the operating conditions. Table 1.3 summarizes most important properties of some biomasses as well as the corresponding value ranges according to study developed by Neves et al. (2011).

Fuel	C	H	O	N	S	Ash	Moisture	HHV	Reference
Rice husks	48.36	5.13	32.79	0.72	0.31	12.50	6.80	16.79	Tsai et al. (2007)
Cardoon	42.78	4.40	43.69	0.64	0.09	8.40	n.a.	18.20	Encinar et al. (2000)
Switchgrass	49.40	5.80	42.00	0.58	0.11	4.60	5.00	19.53	Agblevor et al. (1995)
Apricot pulp	48.98	5.43	38.31	2.38	n.a.	4.70	10.30	18.40	Özbay et al. (2008)
Pine sawdust	50.30	6.00	43.50	0.10	n.a.	0.20	3.41	20.60	Oasmaa and Kuoppala (2003)
Beech wood	49.47	5.57	44.39	0.16	0.02	0.47	7.80	19.30	Schröder (2004)
min	36.89	4.40	23.46	0.00	0.00	0.20	3.41	15.29	
average	47.93	5.86	41.55	0.92	0.09	3.93	7.67	18.90	
max	59.05	8.87	51.28	8.72	0.31	23.50	16.28	26.70	

Table 1.3: Proximate and ultimate analysis (mass % of dry fuel) and HHV (MJ/kg dry fuel) of some biomasses used in the work of Neves et al. (2011). n.a.: not available.

In general terms, three types of product syngas with different calorific value can be distinguished according to the operation method of gasification. The syngas obtained by gasification of biomass can yield low CV (4-7MJ/Nm^3) when using air and air/steam what provides a gas suitable for boiler, turbine or engine operation, medium CV (10-18MJ/Nm^3) using O_2/steam and high CV (around 40MJ/Nm^3) using H_2 (McKendry, 2002; Gómez-Barea and Leckner, 2010). Thus, the biomass conversion by gasification can provide a suitable syngas for pipeline distribution and feedstock for synthesis of liquid into biofuels, but if combustion also allows producing energy, even more than gasification, why gasification is a promising fuel conversion technology?

1.4.4. Gasification: a promising conversion technology

Gasification is a thermochemical conversion method of solid fuels into useful product gas with a wide variety of applications: it can be burnt in boilers, kilns, turbines, gas engines and fuel cells or used as raw gas for synthesis of fuels or chemicals of interest in the industry. Then, there are many reasons that make gasification a technology with remarkable commercial attraction for industries and businesses:

- Gasification provides significant environmental benefits (table 1.2). For example, lower GHG emissions can be achieved instead of using combustion. This result in less expensive downstream flue-gas cleaning treatment: electrostatic precipitators, selective catalytic reducers, CO_2 capture and sequestration. In this sense, established technologies to capture CO_2 from a gasification plant are available but not for a combustion plant.
- As total water consumption is much less than that of a conventional power plant (table 1.2), a gasification plant can be designed to recycle and reuse its process water.
- Gasification plants also produce significantly lowers emissions of others major air pollutants like SO_2 and particulates.
- Gasification also yields high overall efficiency (38-41%) for power generation against to combustion. Thereby, gasification offers lower production costs.
- A process plant that uses natural gas as feedstock can utilise locally available biomass or organic waste instead. Thus, dependence on imported natural gas can

- be notably reduced. Finally, supply volatility and price rising of fossil fuels determining medium and long term economic feasibility of such plants can be eliminated.
- Polygeneration is a unique feature of a gasifier plant. For instance, it can deliver steam for process, electricity for grid and gas for synthesis, what provides a good product mix. In addition, in case of high-sulphur fuels, a gasifier plant can produce sulphur as a by-product. In cases of high-ash fuel, slag or fly ash can be obtained, which have application in cement manufacture.

Why gasification instead of combustion? Benefits from gasification

At first sight, one may think that combustion is undoubtedly preferable for heat and power production because some energy content is lost in the gasification process. On the contrary, gasification offers more advantages.

On the one hand, as stated above, lower overall costs in downstream flue-gas cleaning equipment can be achieved. Two reasons support this statement: the volume of gas produced by gasification for a given fuel throughout is much less than that from direct combustion plants and, the GHG and others air pollutants emissions (SO_2 and particulates for example) are also lowers. Therefore, smaller devices and less numbers of treatment units are required with gasification compared to combustion in order to meet limits stated in national and global policies.

On the other hand, gas as feedstock or final product can be more easily transported and distributed than a solid fuel among all industrial and domestic (individual houses or even medium-size to large community) customers. Furthermore, gas transportation is cheaper than solid fuel for combustion.

Additionally, a gasified fuel can be used in a wider range of application than can its precursor solid fuel. For instance, glass blowing and drying cannot use dirty flue gas from combustion of coal or biomass, but they can use heat from the cleaner and more controllable combustion of gas generated through gasification.

Finally, gasification-based energy system allows producing value-added chemicals as a side stream, the so-called polygeneration that is not available in direct combustion. Meanwhile, gasification plants are smaller, less bulky and expensive (gasifier and compression ignition engine) in contrast to combustion plants (boiler, steam engine and condenser) for electricity or mechanical work in a remote location.

1.4.5. Conversion technology choice of study: fluidized bed gasification

To all aforementioned biomass properties that suppose benefits from an environmental and energy point of view with its consequent social and economic impacts, it has to be remarked the great advantages that the combination of gasification and fluidized bed technology in contrast with fixed or entrained beds offers. For instance, FBG systems are featured by high mass and energy transfer coefficients providing high mixing fuel and reaction rates inside the dense region, allowing giving controllability process,

feedstock versatility in terms of nature, distribution of size and shape and ease to scale-up (Kunii and Levenspiel, 1991).

Because of all these reasons, there has been a great interest in developing predictive models of the performance of fluidized bed gasification reactors (FBGR's) in order to save costs in design and optimization. For instance, Mahecha-Botero et al. (2007) and Gómez-Barea and Leckner (2010) group in their reviews all models and mathematical studies proposed since the 50s, remarking strong and weak spots as well as some guidelines in modelling of FBGR's. Also, Gómez-Barea and Leckner (2010) pay attention to special features of the biomass behaviour in FBGR's such as devolatilization, char and tars conversion models.

To the author's best knowledge, most efforts about FBGR modelling have been focused on carbon gasification as Kaushal et al. (2010) point out while studies devoted to biomass FBGR modelling are scarce (Fiaschi and Michelini, 2001; Corella and Sanz, 2005; Radmanesh et al., 2006). Although differences between biomass and coal in terms of properties, reactivity or devolatilization kinetics are often neglected at modelling, coal gasification information is exploited to model biomass gasification. Furthermore, biomass properties are critical in the reactor performance. Then, dealing with biomass FBGR modelling, various fundamental aspects affecting reactor performance should be considered.

1.4.6. Review of concepts about biomass fluidized bed gasification

The aim of this introduction is to give a short and the main insights of the fluidization phenomena and basics fundamentals of thermal conversion methods of solid fuels as well as their properties, advantages and drawbacks that characterize such processes. The final goal is to make a better understanding of the concepts and theories appearing in the following chapters of the thesis for the readers, even if they are not so familiar for them.

Introduction to Biomass Fluidized Bed Gasification Technology

Regarding biomass gasification in a fluidized bed process a lot of concepts and phenomena are involved, interconnected between them so that the issue cannot be so easy to understand, since many physical and chemical mechanisms occurs inside such reactors. Therefore, the modelling of such processes and the designing of such equipment convert this kind of study in a challenging task.

As follows, a short presentation of fluidized bed technologies, thermal conversion processes and biomass gasification are given. More insights about all these issues can be found from the corresponding papers, review works, books and handbooks to which the reader is gently addressed. For instance, the review of Gómez-Barea and Leckner (2010) and references there-in give a greatly detailed basis and settle guidelines in biomass gasification fluidized bed reactor modelling.

Fluidized Bed Technologies

Fluidization is the operation by which solid particles are transformed into a fluid-like state by suspension in a gas or liquid (Kunii and Levenspiel, 1991). Thus, this contact method has unusual but profitable properties and characteristics, useful in engineering.

The fluidization technology can be grouped according to the fluidization state of the bed, it means, the superficial velocity/minimum fluidization velocity ratio (U_0/U_{mf} ratio). It is known that the solid bed material can be fluidized when gas flow exceeds the corresponding U_{mf} value for the solid given, that is, depending on the physical properties of the gas and the solid, the gas flow or pressure drop required to fluidized a bed of solids is set (Geldart, 1973). Then, solids can be sort out in different groups according to their behavior when they are fluidized, as figure 1.5 shows.

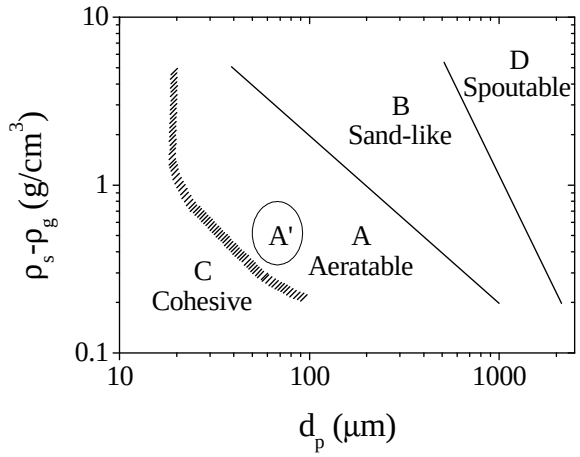

Figure 1.5: Geldart classification of solids (Geldart, 1973).

On the other hand, when a fluid is flowed with a superficial velocity, U_0, through a bed of solid particles, different values of the fluidization velocity for the same kind of solid bed can yield a very different behavior during fluidization as figure 1.6 shows with the U_0/U_{mf} ratio. Hence, the value of U_0 sets the fluidization state inside a FBR.

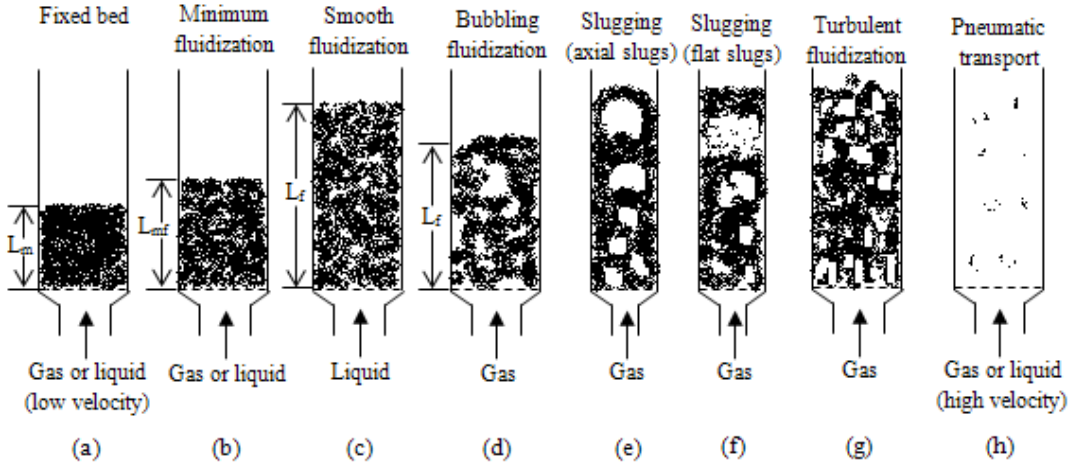

Figure 1.6: Different fluidization regimes with U_0, adapted from Kunii and Levenspiel (1991).

Fluidization properties

From long time ago, research about the behavior of solids when they are fluidized by a gas flow revealed interesting and promising findings on fluidization properties with applicability for industry (Kunii and Levenspiel, 1969; Davidson and Harrison, 1963; Geldart, 1973). These properties, which allow a new type of design of processes manipulating solids with or no chemical conversion, are depicted in the figure 1.7 and listed as follows:

i. Objects can float over the fluidized bed (figure 1.7(a)).
ii. The fluidized bed keeps a horizontal level, even the recipient is inclined (figure 1.7(b)).
iii. When an orifice is done, the particles inside flow out the recipient in form of a jet as a liquid (figure 1.7(c)).
iv. In multiples fluidized bed systems, the height in all fluidized beds equals if they are connected among them (figure 1.7(d)).

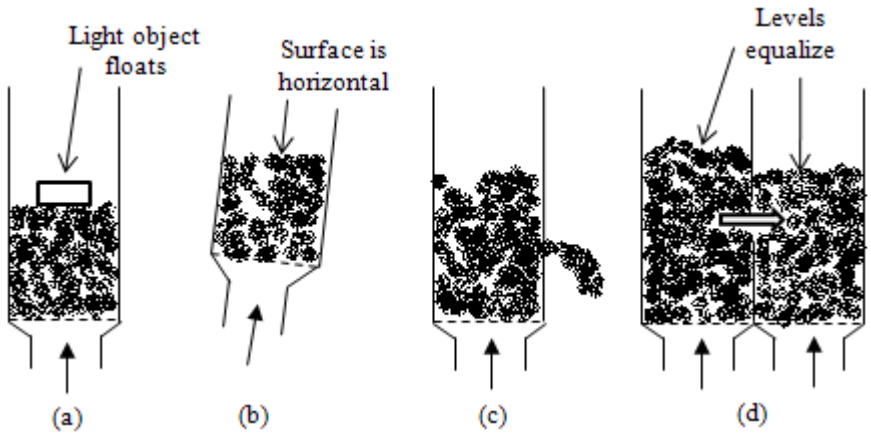

Figure 1.7: Most relevant properties of fluidized beds, adapted from Kunii and Levenspiel (1991).

The aforementioned fluidization properties give a unique performance if applied to reactors, heat exchangers, adsorbers and others much equipment so that benefits from fluidization can be profited in industry.

Table 1.4 stands out specific properties, advantages and drawbacks of main fluidization regimes such as: fixed bed, moving bed, bubbling and turbulent bed, fast fluidized bed and pneumatic transport; applied to chemical conversion.

All these features of the different fluidization regimes are related to particle processing, gas-solid contacting, gas and solid conversion, pressure drop, heat exchange/transport and temperature distribution. The way they affect to the performance of each fluidized bed (FB) systems is described.

Type of contacting / Property	Conversion	Temperature distribution in the Bed	Gas-solid reaction	Gas-phase reactions (Catalyst)	Heat Exchange & Heat transport	Particles	Pressure Drop
Fixed Bed	Close to 100% of theoretical conversion with PF of gas and temperature control (hard) is possible	Large temperature gradient can occur when much heat is involved	Unsuited for continuous operations but batch operations yield non-uniform product	Only for very slow or non-deactivating catalyst. Serious problems in temperature control, limiting the unit size	Limiting factor in scale-up due to inefficient exchange. Larger size is nedeed	Must be large and uniform. A poor temperature control solids may sinter and clog the reactor	As size particle is large, pressure drop is not a problem
Moving Bed	Flexible and close to ideal countercurrent and cocurrent contacting allows close to 100% of theorical conversion	Temperature gradient can be controlled with gas flow or minimized with large solid circulation	For fairly uniform size feed with little or no fines. Large-scale operations can be possible	For large granular rapidly deactivated catalyst. Fairly large-scale operations possible	Heat transport by solids recirculation can be large but inefficient heat exchange due to high heat capacity of solids	Large and uniform. Top size fixed by kinetics of solids recirculation, and bottom size by fluidizing velocity in reactor	Intermediate between fixed and FBs
Bubbling and Turbulent Bed	For continuous operation, solids mixing and gas bypassing yield poorer performance than other reactor types. For high conversion, staging or other special design is required	Temperature practically constant. Control by heat exchange or continuous feed and removal of solids	Wide range of solids and large-scale operations at uniform temperature are possible. Excellent for coninuous operations, yielding uniform product	For small granular or powdery non-friable catalyst. Can handle rapid deactivation of solids. Excellent control of the temperature allowing large-scale operations	Efficient heat exchange and large heat transport by circulating solids. Thus, heat problems are rarely limiting in scale-up	Wide size distribution and much fines are possible. Attrition of particles and erosion of vessels can be serious	For deep FBs pressure drop is high resulting in high consumption
Fast FB & Pneumatic transport	Gas and solid flows both close to cocurrent PF. Then, hogh conversion is possible	Temperature gradients in the direction of solids flow. It may be severe and dificult to control	Suitable for rapid reactions. Recirculation of fines is crucial	Suitable for rapid reactions. Serious attrition of the catalyst	Intermediate between fluidized and moving bed	Fine solids, top size governed by U_{mf}. Erosion equipment and particles attrition are severes	Low for fine particles but can be considerable for larger particles

Table 1.4: Comparison of some types of contacting for reacting gas-solid FB systems Kunii and Levenspiel (1991).

On the other hand, when FB technology is applied to reactor design, others characteristics has to be emphasized:

i. Very high mixing rates of solids, leading to practically isothermal conditions throughout the reactor. Thus, the operation of FBs can be simply and reliably controlled.
ii. The whole system of well-mixed solids represents a large thermal flywheel, responding slowly to changes in the operating conditions and resisting rapid temperature changes. This gives a large safety margin in avoiding temperature runaway for the case of high exothermic reactions when FBs are operated, for example.

iii. High energy and mass transfer between gas and particles compared to others contacting methods.
iv. High rate of heat transfer between the FB and an immersed object, leading to small surface areas in related equipment.
v. Suitable for large-scale processes.
vi. The solids circulation between two FBs allows removing or adding great amount of heat in large reactors.

Finally, FB technology has a lot of applications in the industry since the characteristics and the benefits from fluidization phenomena can be used in processes such of:

- Drying/washing of solid particles.
- Heat exchange.
- Mechanical sieving based on the size, density or shape distribution.
- Gasification, combustion and incineration.
- Calcinations and carbonatation.
- Catalytical reactions, as coal and petrol cracking.
- Reaction of synthesis of new raw products.
- Adsorption and ionic exchange.
- Crystallization.
- Bioengineering process: bioreactors.

Thermal Conversion Processes

The main thermal conversion processes of biomass can be sort out in three groups: pyrolysis, gasification and combustion, as illustrated in the figure 1.8 depending on the operating conditions and the specifications design of the equipment involved. As follows, these thermal technologies are briefly presented.

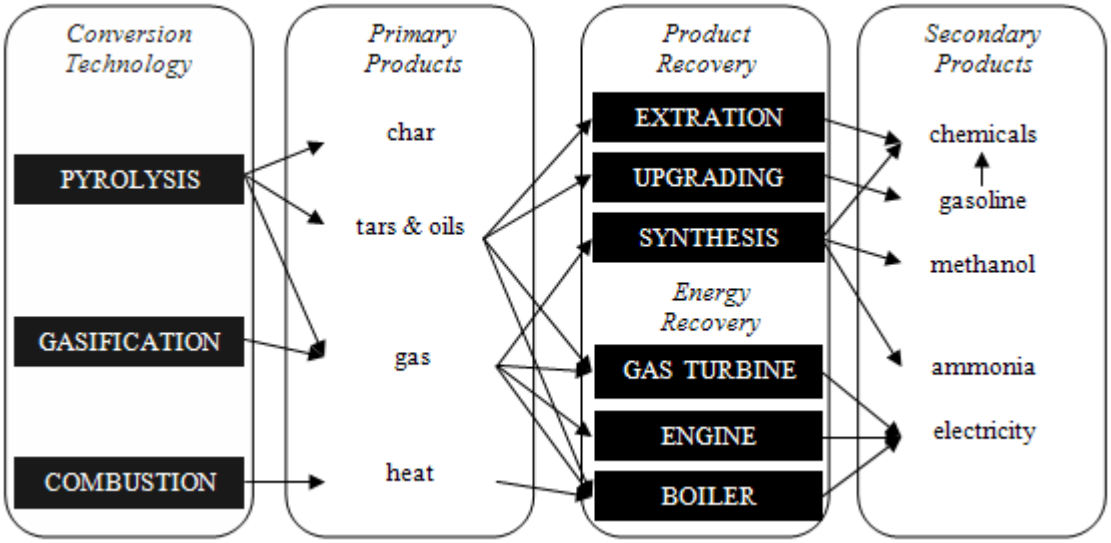

Figure 1.8: Main thermal conversion processes of biomass. Adapted from Bridgwater (1994a).

Pyrolysis

Pyrolysis is the breaking down of a material into liquid (bio-oil or bio-crude) as well as solid and gaseous fractions by means of heat in absence of air at around 300-500ºC. It is also the first step of the gasification or combustion of biomass. When biomass is undergoing pyrolysis, it yields char-coal, permanent gases (CO, CO_2, H_2, H_2O and CH_4) and tars or condensable gases of pretty higher molecular weight than permanent gases.

Although efficiencies up to 80% can be reached (Aston University and DK Teknik, 1993; EU, 1999; Aston University, 1996), pyrolysis has some problems that need to be overcome: the poor thermal stability and the corrosivity of the oil. Thus, overcoming these drawbacks by lowering the oxygen content and removing the alkali fraction, pyrolysis can make pyrolysis a more attractive process.

Gasification

Gasification is the partial oxidation of the biomass at high temperatures (700-900ºC) converting it into a combustible gas mixture suitable for: direct burning; as a fuel for gas turbines/engines; as a feedstock in the production of chemicals as methanol for use in transportation, for example. Here, gasification is very briefly defined as in the next section more details will be given about the types of gasification technologies.

Combustion

The combustion technology, typically used in converting energy stored in fuels to heat, mechanical power or electricity, produces hot gases around 800-1000ºC when is applied for burning biomass with a moisture content less than 50% unless biomass is pre-dried, otherwise, biomass with a high moisture content is better suited to biological conversion processes. The scale of the combustion power plants range widely, from a very small scale (i.e. domestic use) to large-scale industrial plants in the range of 100-3000MW. Furthermore, co-combustion of biomass in coal-fired power plants seems to be an attractive option due to their high conversion efficiency (Mitsui Babcock, 1997; Aston University and DK Teknik, 1993; EU, 1999).

These plants usually yield conversion efficiencies of 20-40%. Higher values are obtained in +100MWe plants or if biomass co-combusted in coal-fired power plants.

Gasification: Chemistry, Thermodynamics and Technologies

Gasification involves the breakdown of large and heavy molecules of solid hydrocarbons into simpler and lighter ones collected as the so-called product gas.

Chemistry and Thermodynamics

When studying gasification, with whatever kind of solid fuel, the steps comprised by the whole process of gasification can be summarized (figure 1.9): pyrolysis (devolatilization), gasification and combustion. This figure deals with the use of

biomass as fuel but for others fuels, the only differences are just in the relative fractions of permanent gases, tars and char-coal vary and its physical and chemical properties.

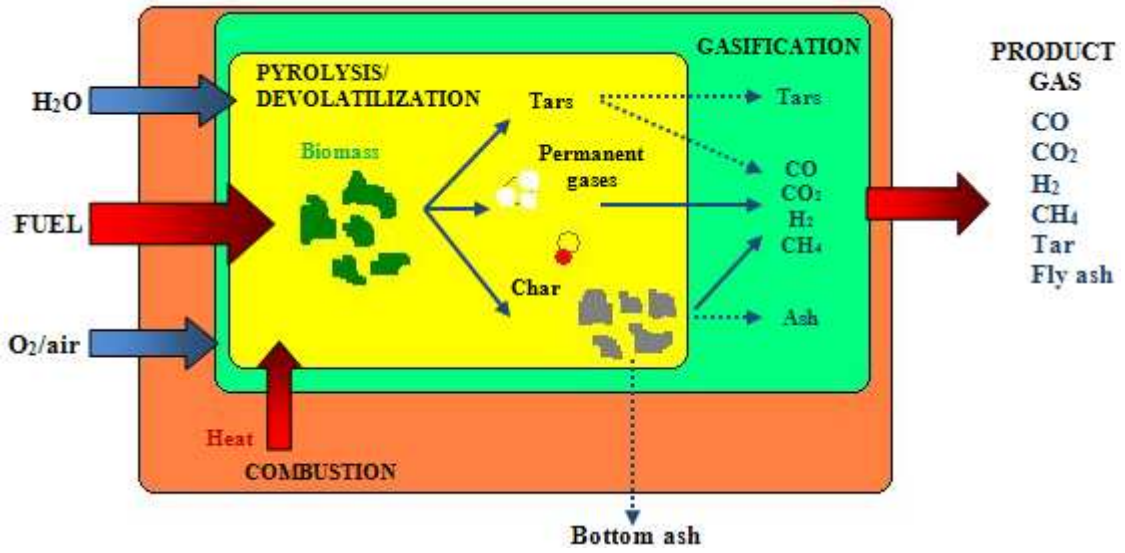

Figure 1.9: Processes in a gasifier: pyrolysis/devolatilization of solid fuel and reforming/gasification of the resulting gaseous products and char. Adapted from Gómez-Barea and Leckner (2010).

The chemical behavior of any fuel is described by means of reactions rates and the stoichiometry of the reactions involved. Here, the main chemical reactions of the reaction network that can happen in such a process are listed in table 1.5. It should be noted that in such a complex reaction network, some reactions are exothermic (combustion ones) and others ones are endothermic (char gasification and tar cracking ones) so that the fuel feeding with the corresponding fuel chemistry and the operating conditions set allows a FBGR to operate under autothermal conditions.

Stoichiometry	**Heat of reaction (kJ/mol)**	**Name of the reaction**
Char combustion		
$C + 1/2O_2 \rightarrow CO$	-111	Partial combustion
$C + O_2 \rightarrow CO_2$	-394	Complete combustión
Char gasification		
$C + CO_2 \rightarrow 2CO$	+173	Boudouard reaction
$C + H_2O \rightarrow CO + H_2$	+131	Steam gasification
$C + 2H_2 \rightarrow CO_2 + 2H_2O$	-75	Hydrogen gasification
Homogeneous reactions		
$H_2 + 1/2O_2 \rightarrow H_2O$	-283	Carbon monoxide oxidation
$CO + 1/2O_2 \rightarrow CO_2$	-242	Hydrogen oxidation
$CH_4 + 2O_2 \rightarrow CO_2 + 2H_2O$	-283	Methane oxidation
$CO + H_2O \rightarrow CO_2 + H_2$	-41	Water gas-shift reaction
Tar cracking reaction. (Tar assumed as C_nH_m)		
$C_nH_m + (n/2)O_2 \rightarrow nCO + (m/2)H_2$	Highly endothermic (200-300)	Partial oxidation
$C_nH_m + nCO_2 \rightarrow (m/2)H_2 + 2nCO$		Dry reforming
$C_nH_m + nH_2O \rightarrow (m/2+n)H_2 + nCO$		Steam reforming
$C_nH_m + (2n-m/2)H_2 \rightarrow nCH_4$		Hydrogenation
$C_nH_m \rightarrow (n-m/4)C + (m/4)CH_4$		Thermal cracking

Table 1.5: Chemistry and thermodynamics of biomass gasification.

When simulating a FBGR, the combination of mass and heat transfer mechanisms, reaction network, stoichiometry and reaction rates, can allow predicting the performance of the reactor. In fact, as it will be explain in next chapters, reactions from the table 1.3, with gas-solid contact inside the FB as well, play a key role in products distribution, that is, the gas composition that the FBGR yields.

Technologies

Gasification technologies can be grouped according to several criteria such as the way the heat is provided to the reactor, the so-called gasification concept: autothermal and allothermal gasification (figure 1.10) and the fluidization state of the bed material: fixed bed, moving bed, fluidized bed and entrained flow.

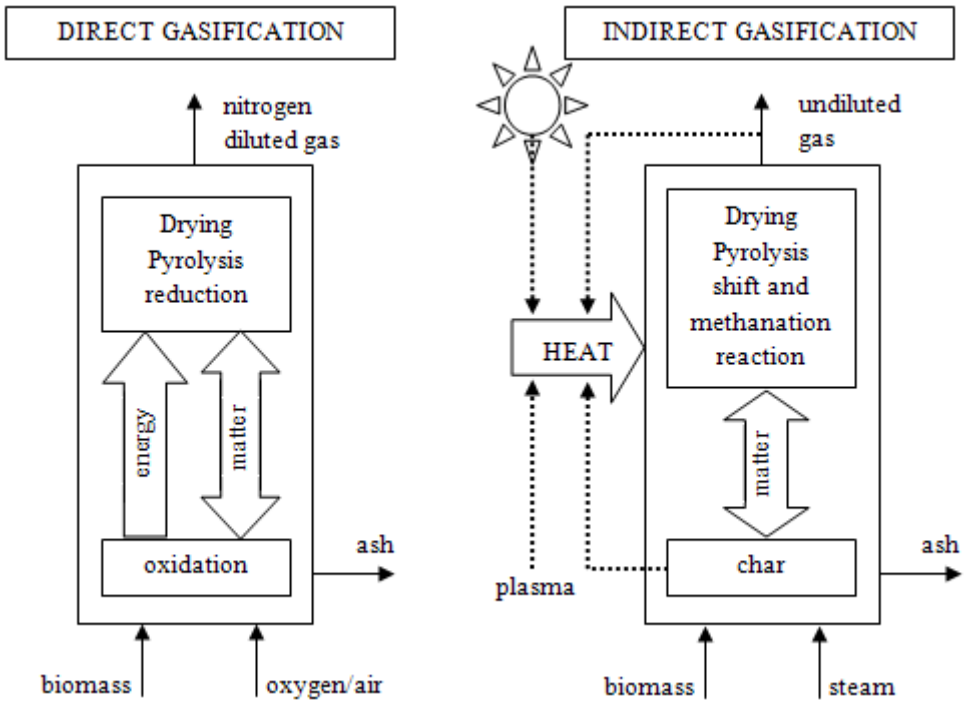

Figure 1.10: Direct and indirect gasification processes. Adapted from Belgiorno et al. (2003).

Direct and Indirect Gasifiers

As gasification is an endothermic process, energy is required to ignite the reactor. In direct or autothermal gasification, the energy to heat up, dry and pyrolyze the biomass generally comes from the sensible heat of the gases and the combustion of the dry biomass. This energy can account around 6-10% of the heat of combustion of dry biomass (Reed and Levie, 1984). Thus, using oxygen or air the partial oxidation takes place releasing energy from the fuel. When air is used as fluidizing and gasifying agent, a LHV gas is produced (4-7MJ/Nm^3) while oxygen gasification produces a medium heating value gas (10-18MJ/Nm^3). The main advantages of direct gasification are summarized in being a very simple and largely self-regulating process.

In indirect or allothermal gasification, steam is used as gasifying agent and the necessary heat is obtained from an external energy source, which allows generating a gas of medium value of LHV (14-18MJ/Nm^3). Furthermore, indirect gasification can be sort out depending on whether heat is supplied from external (plasma or solar gasification) or internal sources (by recirculation streams of char or gas).

Fixed Bed Gasifiers

In fixed bed gasifiers the bed material is not fluidized, it means, the fluidization velocity is set below the minimum fluidization value for the corresponding bed material and gas. There are different configurations of fixed bed gasifiers depending on the fuel feeding location in the reactor, shown in figure 1.11. They are: updraft, downdraft and crossdraft gasifiers.

In downdraft gasifiers, the biomass and the gasifying agent flow in the same direction. The biomass is fed at the reactor top part and the gasifying agent is blown in the heart of the reactor. The syngas produced leaves the reactor after passing the combustion zone what leads to low tar content and high temperature (around 800ºC).

On the other hand, in updraft gasifiers, the fuel moves downwards after being fed in the top of the reactor while the gasifying agent, fed at the bottom through a grate, flows upwards. Then, biomass runs through drying, devolatilization combustion and reduction yielding volatiles that partly condense on the biomass and partly exits with the gas. Thus, the gas leaves the reactor near the pyrolysis zone with high tar content and low temperature (200-300ºC). This configuration is able for wet biomasses and a wide range of size particle fuel.

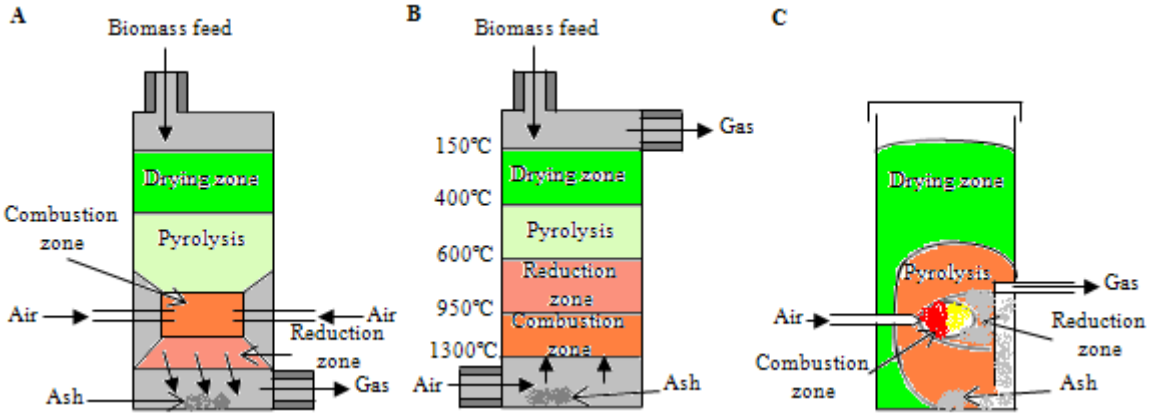

Figure 1.11: Sketches of the reaction zones in an downdraft (A), updraft (B) and crossdraft (C) fixed bed gasifier. Figures A and B are adapted from Foley and Barnard (1985). Figure C is adapted from Olofsson et al. (2005).

Finally, crossdraft gasifiers main feature is the cross flow of biomass and gasifying agent since this enters from one side while the biomass moves downwards. The syngas produced leaves the reactor at the same level of inlet gasifying agent. Therefore, the combustion and gasification region is located in the inlet gasifying agent. Hence, the gas leaves the gasifier at high temperature (around 900ºC) with very low of tar content.

Fluidized Bed Gasifiers

The main feature of fluidized bed gasifiers is the promotion of fluidization of material bed. The gasifying agent is blown through a bed of solid material at a sufficient velocity to keep the bed in suspension. The fuel particles can be fed at the top either the bottom part of the reactor and they are mixed in the fluidized bed so that they rapidly reach the bed temperature. Thus, the fuel is pyrolysed fast yielding large amount of volatiles. Simultaneously, gasification and tar conversion reactions take place in the gas phase. The gasification can be conducted in two types of fluidized beds: bubbling and circulating fluidized bed (figure 1.12).

The bubbling fluidized bed (BFB) is a well-established technology. This type of reactors is divided into two parts: a lower region for the fluidized bed and an upper part called freeboard. The BFB operates with adjusting the gas velocity to avoid the transport of the FB. For this reason, the ash particles are blown out of the bed. The syngas produced can typically reach temperatures of 800-900ºC with moderate or relatively high tar and particulate content. Furthermore, the BFB gasifiers are sensible to the biomass geometry since this property affect to the fluid-dynamic performance of the bed.

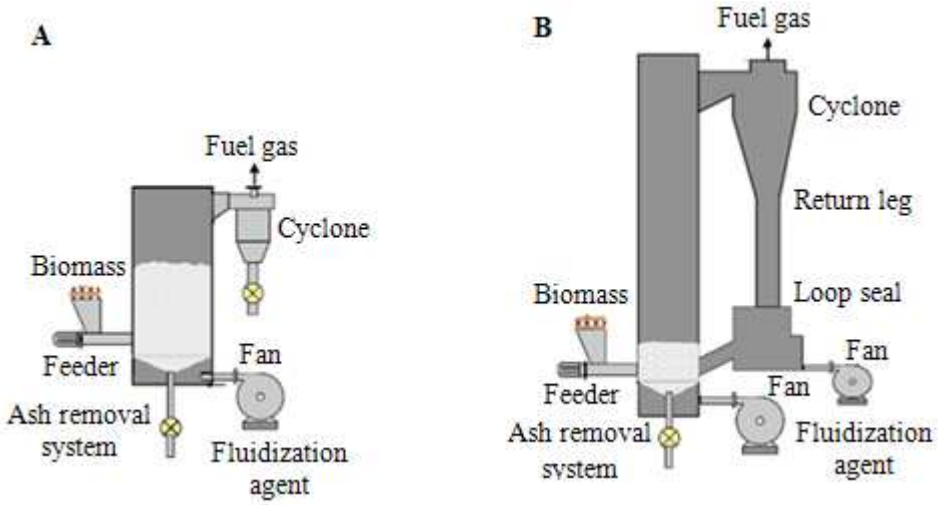

Figure 1.12: Bubbling Fluidized Bed gasifier (A) and Circulating Fluidized Bed gasifier (B). Adapted from Gómez-Barea and Leckner (2010).

The circulating fluidized bed (CFB) gasifiers operate at higher gas velocity than BFB gasifiers. This promotes no clear difference between fluidized bed and freeboard regions. Additionally, the higher gas velocity enhances mixing of solid bed and biomass particles, leading to fully isothermal conditions in the fluidized bed. However, higher amount of particulate and bed material are blown out of the reactor. Thus, a cyclone recirculates this solid material collected to the gasifier. The CFB gasifiers allow achieving higher LHV and char conversion as well as lower tar content in the syngas compared to performance of BFB gasifiers.

Entrained Flow Gasifiers

The entrained flow (EF) gasifiers, commonly used for coal since they can be slurry-fed, usually operates at high temperatures (1000-1200ºC) and high pressures (25-60bar) at large capacities (>100MWth). These gasifiers are characterized by short residence times and very low tar level in the syngas. As gasifying agent, air and pure oxygen are used and conversion close to 100% can be achieved. However, small fuel particles are mandatory for proper performance of such gasifiers.

Table 1.6 shows the main strength and weak points of the different FBG technologies described above. This table lists the feasibility and convenience of each FBG technology for each purpose. This summarize is aimed to help in choosing the proper technology for gasifying biomass in FB taking into account the syngas quality, char conversion or scale-up potential. Furthermore, this table would also help to consider further conditioning to be required in order to improve LHV, lower pollutant emissions, for instance.

Charateristics [a]	**Fixed bed**		**Fluidized bed**		**Indirect gasifier**	
	Updraft	**Downdraft**	**Bubbling**	**Circulating**	**Char**	**Gas**
Carbon conversion	****	****	**	****	*****	**
Thermal efficiency	*****	****	***	****	***	***
CGE	*****	***	***	****	***	***
Turndown ratio	***	**	****	****	****	****
Start-up facility	*	*	***	***	*****	*****
Magement facility	****	***	**	**	*	*
Control facility	**	**	****	****	*****	*****
Scale-up potential	***	*	***	*****	***	***
Sized feed elasticity	****	*	**	**	**	**
Moisture feed elasticity	****	**	***	***	*	*
Ash feed elasticity	*	*	****	****	***	****
Fluffy feed elasticity	****	**	*	***	***	*
Sintering safety	*	*	***	*****	*****	***
Mixing	*	*	****	*****	*****	****
Cost safety	*****	****	**	**	*	*
Tar content	*	*****	**	***	**	**
Particulate content	*****	***	***	**	**	****
LHV	*	*	*	**	*****	*****

Table 1.6: Comparison of different FBGR technologies: main characteristics, advantages and drawbacks: [a] *poor, **fair, ***good, ****very good, *****excellent (Bridgwater, 1994a; Juniper, 2000; Belgiorno et al., 2003).

As follows, table 1.7 gives quantitative performance of the qualitative description about FB technologies stated previously. This table presents the typical values range of syngas composition, LHV and tar and particulate content in the syngas. As denoted by this table, the increase of gas velocity yields higher H_2 and CO content and LHV except for the EF gasifier that gives a lower LHV than the CFB technology. In addition to this, there is more tar conversion though particles concentration is bigger because of the use of higher gas velocities.

Process	Gas composition (%, dry)					LHV (MJ/Nm^3)	Tar (g/Nm^3)	Particles (g/Nm^3)
	H_2	CO	CO_2	CH_4	N_2			
FBU	15-21	10-22	11-13	1-5	37-63	4-5.6	0.01-6	0.1-8
FBD	10-14	15-20	8-10	2-3	53-65	3.7-5.1	10-150	0.1-3
BFB	15-22	13-15	13-15	2-4	44-57	3.6-5.9	2-30	8-100
CFB	17-36	36-51	7-15	0.1-1	0-39	11.4-18	1-20	8-100
EF	29-40	39-45	18-20	0.1-1	0.1-9	8.8-9.3	-	-

Table 1.7: Properties of syngas produced by different types of gasification technologies (Hasler and Nussbaumer, 1999; Beenackers, 1999).

Particular case: Biomass Gasification in Fluidized Bed Reactor

There are quite a lot literature regarding to the process description of the biomass gasification in fluidized bed reactors (Basu, 2010; Gómez and Leckner, 2010) settling basic insights, guidelines or more detailed description for helping and addressing FBR's modelling with biomass gasification application.

Figure 1.13 depicts briefly but clearly the main physical and chemical phenomena governing the performance of such reactors. Biomass gasification is a very complex thermal conversion process since there are several phenomena taking place at the same time: biomass drying, volatiles release, gas and solids mixing, mass and heat transfer between bubbles and the so-called emulsion phase, mass diffusion through reactant particles (as char for instance) and chemical homogeneous and heterogeneous reactions in bubbles as well as in the surface reactant solids.

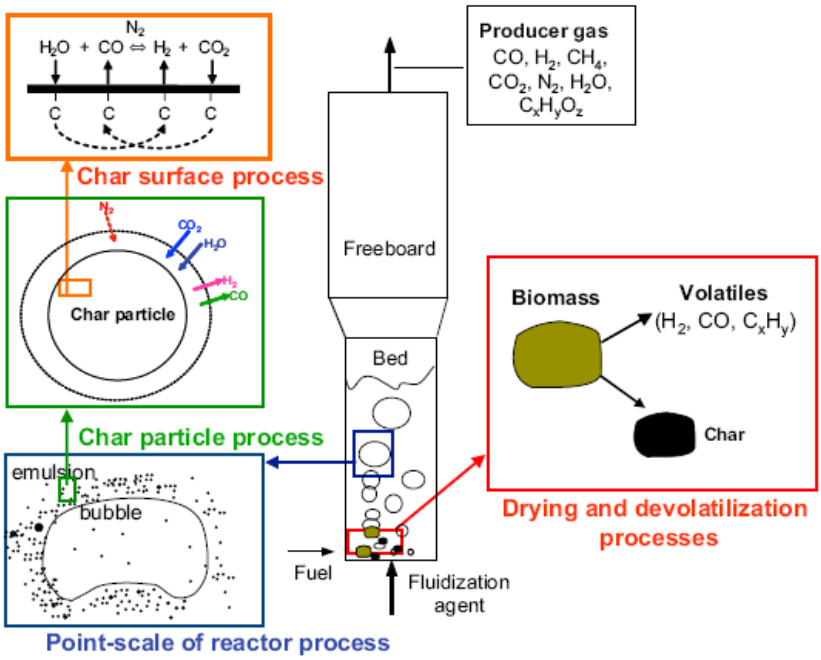

Figure 1.13: Description of processes in FBGRs. Adapted from Gómez-Barea and Leckner (2010).

A gasification process can be understood tracking a biomass particle fed to the reactor. Thus, when a biomass particle is fed to the reactor, it undergoes a series of conversion processes: at first, drying and devolatilization, subsequently oxidation of volatiles and char, and eventually, char gasification by steam and carbon dioxide.

Furthermore, once the fuel particle has been injected into the fluidized bed, it immediately experiences shrinkage and primary fragmentation due to the thermal stresses and internal pressures caused by the release of volatiles. Then, secondary fragmentation, attrition of char and char conversion because of char reactions take place. Thus, the gas flow pattern distributes the char and the devolatilizing fuel particles through the bed, establishing a gas environment where these reactant solid particles are converted.

1.4.7. Operational constraints of biomass fluidized bed gasification

The operation of fluidized beds is not exempt of risks that can lead to an unscheduled shutdown. Two main operational problems govern operation of fluidized bed reactors: bed agglomeration and tar formation.

The first mentioned problem, bed agglomeration, deals with the ash composition of biomass fuels processed in such reactors. This phenomenon is crucial since it can provoke to stop the operation. Furthermore, ash sintering enhances bed agglomeration as well as it can reduce the efficiency of heat surface boilers. Ash sintering also causes plugging and fouling because of forming deposits on surfaces. Both phenomena are usually traced by the temperature and pressure drop fluctuations as they depend on the melting point of alkali metals.

The second one, tar formation, mainly affects on syngas composition, that says, the quality of syngas produced. This would involve higher costs to conditioning the syngas in order to adequate its end-use and avoid downstream problems: plugging and fouling of particle filters, coolers and suction engines, for example.

Ash sintering and bed agglomeration

There are many ash-related operating problems in combustors and gasifiers: slagging, fouling and corrosion. However, the major ash-related problem encountered in fluidized bed combustors and gasifiers is bed agglomeration which can result in total defluidization of the bed and an unscheduled plant shutdown in the worst cases (Öhman et al., 2000). Ash sintering can also lead to bed agglomeration as well and finally, total defluidization of the bed.

All these ash-related operating problems comes from the low melting point of alkali components of biomass fuels (700-1000ºC, Davidsson et al., 2007), and then, its ash composition as stated in table 1.8 (Natarajan et al., 1998). This work points out the influence of chemical composition of ash, alkalis and metallic oxides, on the initial agglomeration temperature in combustion and gasification conditions using two different bed materials (quartz and lime). Results from table 1.8 reveal the importance of ash composition on the value at which bed agglomeration can take place.

The ash-forming elements occur as internal or external mineral grains, salts such as chlorides (KCl) and sulfates (K_2SO_4), or associated with the organic matrix of the fuel. Depending on the operating conditions, the salts may vaporize while the mineral grains will undergo phase transformations and approach each other to form fly ash particles.

Then, vapors and fly ash particles may be deposited on heat surfaces in boilers and /or react with the particles of the bed inert material in FB initiating the formation of deposits and agglomerates. These reactions can take place either in the solid phase (bed) or in the gas phase (Arvelakis et al., 2003).

Property	Ash composition (%)										Quartz	Lime	Quartz	Lime
Fuel	SiO_2	Al_2O_3	Fe_2O_3	MgO	CaO	K_2O	MnO_2	TiO_2	Na_2O	P_2O_5	T^a (ºC)	T^a (ºC)	T^b (ºC)	T^b (ºC)
Rice Husk	96.26	0.56	0.48	0.05	0.81	1.03	0.08	0.07	0.22	0.44	1009	>1020	>1020	>1020
Bagasse	73.19	8.29	5.37	2.53	4.14	4.11	0.14	0.65	0.67	0.91	>1020	>1020	>1020	>1020
Cane trash	69.13	7.83	5.07	2.39	3.91	3.88	0.13	6.17	0.64	0.85	890	905	834	n.a.
Olive flesh	36.20	3.60	4.25	12.40	18.20	18.20	0.01	0.02	1.70	4.00	933	>1020	880	n.a.

Table 1.8: Initial agglomeration temperatures for combustion (a) and gasification conditions (b) for several biomass fuels (Natarajan et al., 1998). n.a.: not available.

It is very important to take into account this aspect because the biomass-fuel of interest in this PhD Thesis, *Cynara cardunculus* L., exhibits the highest ash and mineral contents among most popular energy crops with 117 g/kg of ash, 1.8g/kg of Al, 27.8 g/kg of Ca, 13.1 g/kg of Cl, 19.3 g/kg of K, 12.8 g/kg of Fe (Monti et al., 2008). In this way, *Cynara cardunculus* L. would be one of the energy crops with higher operational problems risk. Consequently, efforts are being addressed to diagnose, to monitor and to prevent from fouling, slagging and corrosion tendencies for the cynara-based power plants in recent years. For example, Aho et al. (2008) have proposed the use of co-firing or blend-fuels as another type of measure to avoid such operational problems.

On the other hand, figure 1.14 shows a typical agglomeration test. As observed, the pressure drop bed starts to decrease while the bed temperature rapidly rises. At the end, the pressure drop along the bed dramatically falls since the fluidization of the bed. Consequently, a shutdown should be required to solve the problem and restart the operation.

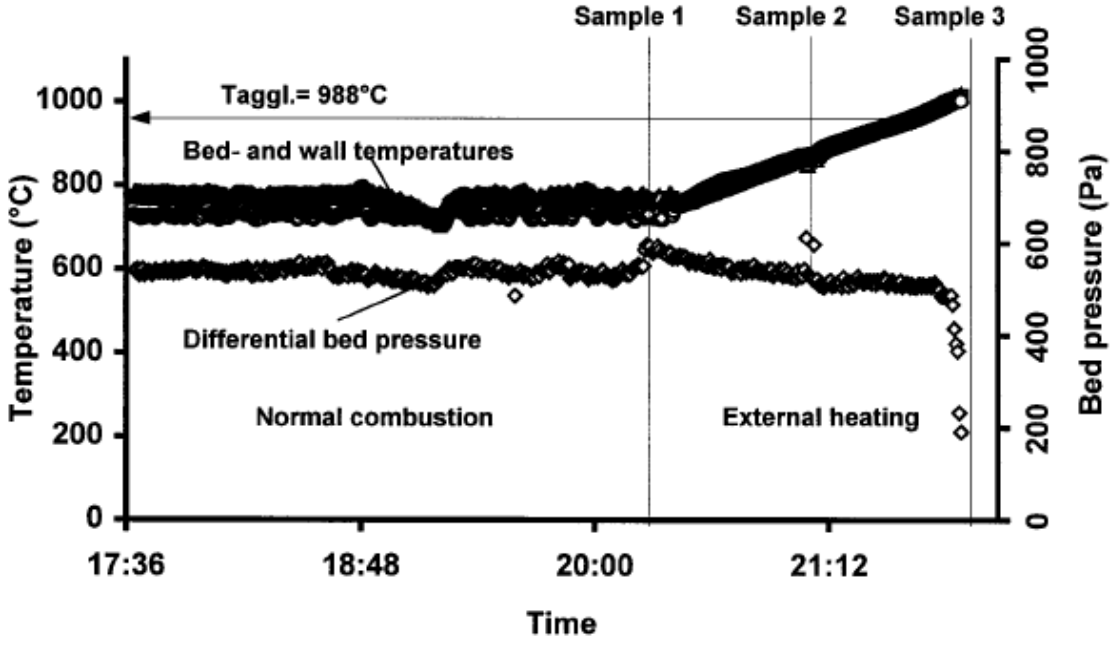

Figure 1.14: Typical agglomeration test (Öhman et al., 2000).

Nowadays, interest in detecting and preventing bed agglomeration has grown. Methods for counteracting defluidization phenomena have been recently reviewed in Bartels et al. (2008). The counteraction methods can be divided into methods for implementation in existing processes such as operational actions, changing the fuel supply rate to the process and the use of alternative bed materials; and improved reactor design by means of the installation of mechanical devices to break the aggregates such as stirring blades or rotating distributors. For example, Gómez-Hernández et al. (2012) use a rotating distributor as an attempt to re-fluidize water induced defluidized systems, both shallow beds (h/D=0.75) and deep beds (h/D=1.5). Results from this work stands out the potential of rotating distributor as technological solution to be applied in fighting the unwanted defluidization phenomena.

Tars formation

Tars or tar fraction in biomass, representing up to half of primary pyrolysis products from devolatilization, is a very complex mixture of chemical species with a heavier molecular weight than permanent gases and the so-called C_2 and C_3 fraction. Tars comprise a broad range of chemical species tending to be refractory and difficult of being removed by means of thermal, catalytic and physical processes. This fraction of condensable hydrocarbons includes from single ring compounds as benzene to 5-ring aromatic compounds with others oxygenated compounds and polycyclic aromatic hydrocarbons (PAH).

The importance of reducing tar content in syngas lies on tar fraction can greatly affect on the gas composition (syngas quality) and cause serious operational problems by blocking when condensing in downstream equipment such as particles filters, coolers and suction engine (figure 1.15). For this reason, tar fraction plays a key role both in reactor performance and designing gas cleaning downstream systems before using the syngas produced (Li and Suzuki, 2009).

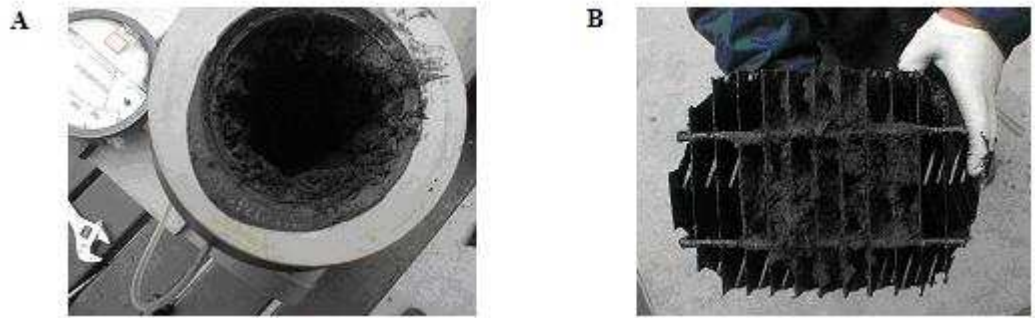

Figure 1.15: Plugging of piping (A) and fouling of equipment (B) from **http://www.thersites.nl/**.

Kiel et al. (2004) recently evidenced the importance of tar class concentration and even tar lumping when estimating the temperature at which tars condensation can take place. Thus, this property is a useful and valuable parameter to the right design tar removal equipment and choice of the operating conditions of reactors for producing syngas.

On the other hand, Devi et al. (2003) has reviewed the primary measures for tar elimination from previous studies highlighting results, strong and weak points of each method. Kiel et al. (2004) have developed proper methods for the measurement and classification of tar, based on a clear definition and with focus on the impact of tar in downstream processes. This work deals with tar formation in air-blown, atmospheric-pressure fluidised-bed gasification in order to assess the practical and economic feasibility of most primary measures. Finally, Zwart et al. (2009) judge the technical and economical suitability of two up-scalable tar removal methods (OLGA and Partial Oxidation) connected to low-temperature gasification.

As observed, many efforts have been addressed to minimize tar formation in new reactor and downstream process designs and to reduce tars content in existing processes.

1.5. Notation

D Fluidized bed/reactor diameter, [m].

d_p Particle diameter, [m].

h Fluidized bed/reactor height, [m].

L Fluidized bed height, [m].

U_{mf} Minimum fluidization velocity, [m/s].

U_0 Superficial gas velocity, [m/s].

U_0/U_{mf} Fluidization state of a bed, [-].

Abbreviations

BFB Bubbling Fluidized Bed.

BGFB Biomass Gasification in Fluidized Bed.

CCGT Combined Cycle Gas Turbine.

CFB Circulating Fluidized Bed.

CV	Calorific value.
ICE	Internal Combustion Engine.
EF	Entrained Flow.
FB	Fluidized Bed.
FBD	Fixed Bed Downdraft.
FBG	Fluidized Bed Gasification.
FBU	Fixed bed Updraft.
GHG	Greenhouse gases.
HHV	High heating value.
LHV	Low heating value.
PAH	Polycyclic aromatic hydrocarbons.
RES	Renewable energy source.
syngas	Synthesis gas.

Greek letters

ρ	Density, [kg/m^3].

Subscripts

f	Fluidized bed.
g	Gas.

mf Minimum fluidization.

m Stoichiometric coefficient in chemical reactions, number of atoms of an element.

n n stoichiometric coefficient in chemical reactions, number of atoms of an element.

p Particle.

s Solid.

Bibliography

Agblevor, F.A., Besler, S., Wiselogel, A.E. 1995. Fast pyrolysis of stored biomass feedstocks. *Energy & Fuels* 9(4), 635-640.

Angelis-Dimakis, A., Biberacher, M., Domínguez, J., Fiorese, G., Gadocha, S., Gnansounou, E., Guariso, G., Kartalidis, A., Panichelli, L., Pinedo, I., Robba, M. 2011. Methods and tools to evaluate the availability of renewable energy sources. *Renewable and Sustainable Energy Reviews* 15(2), 1182-1200.

Aho, M., Gil, A., Taipale, R., Vainikka, P., Vesala, H. 2008. A pilot-scale fireside deposit study of co-firing Cynara with two coals in a fluidized bed. *Fuel* 87(1), 58-69.

Arvelakis, S., Gehrmann, H., Beckmann, M., Koukios, E.G. 2003. Agglomeration problems during fluidized bed gasification of olive-oil residue: evaluation of fractionation and leaching as pre-treatments. *Fuel* 82(10), 1261-1270.

Bartels, M., Lin, W., Nijenhuis, J., Kapteijn, F., van Ommen, J.R. 2008. Agglomeration in fluidized beds at high temperatures: mechanisms, detection and prevention. *Progress In Energy and Combustion Science* 34(5), 633-666.

Bauen, A., Berndes, G., Juginger, M., Londo, M., Vuille, F., Ball, R., Bole, T., Chudziak, C., Faaij, A., Mozaffarian, H. 2009. Bioenergy – A sustainable and Reliable Energy Source. A review of Status and Prospects. Main Report. International Energy Agency Bioenergy.

Basu, P. 2010. Biomass gasification and pyrolysis. Practical design. Eds. Elsevier, Oxford, UK.

Beenackers, A.A.C.M. 1999. Biomass gasification in moving beds, a review of European technologies. *Renewable Energy* 16(1-4), 1180-1186.

Belgiorno, V., De Feo, G., Della Rocca, C., Napoli, R.M.A. 2003. Energy from gasification of solid wastes. *Waste Management* 23(1), 1-15.

Bridgwater, A.V. 1994a. Catalysis in thermal biomass conversion. *Applied Catalysis A-General* 116(1-2), 5-47.

Cornelissen, S., Koper, M., Deng, Y.Y. 2012. The role of bioenergy in a fully sustainable global energy system. *Biomass and Bioenergy* 41, 21-33.

Davidson, J.F., Harrison, D. 1963. Fluidised particles. 1st ed.. Cambridge University Press, Cambridge, UK.

Davidsson, K.O., A mand, L.E., Leckner, B, Kovacevik, B., Svane, M., Hagstrom, M., Pettersson, J.B.C., Pettersson, J., Asteman, H., Svensson, J.E.; Johansson, L.G. 2007. Energy & Fuels 21 (1), 71–81.

Demirbas, A. 2006. Global renewable energy sources. Energy Sources, Part A: Recovery, Utilization and Environmental Effects 28(8), 779-792.

Devi, L., Ptasinski, K. J., Janssen, F. J. J. G. 2003. A review of the primary mesures for tar elimination in biomass gasification processes. *Biomass & Bioenergy* 24, 125-140.

Dornburg, V., Faaij, A.P.C., Verweij, P., Langeveld, H., van de Ven, G., van Keulen, H., van Diepen, K., Meeusen, M., Banse, M. Ros, J. 2008. Biomass Assessment. Assessment of Global Biomass Potentials and Their Links to Food, Water, Biodiversity, Energy Demand and Economy. Netherlands Environmental Assessment Agency.

Dornburg, V., van Vuuren, D., van de Ven, G., Langeveld, H., Meeusen, M., Banse, M., van Oorschot, M., Ros, J., Jan van den Born, G., Aiking, H. 2010. Bioenergy revisited: key factors in global potentials of bioenergy. *Energy Environmental Science* 3(3), 258-267.

Encinar, J.M., Gónzalez, J.F., González, J. 2000. Fixed-bed pyrolysis of Cynara cardunculus L. Product yields and compositions. *Fuel Processing Technology* 68(3), 209-222.

Erb, K.H., Haberl, H., Krausman, F., Lauk, C., Plutzar, C., Steinberger, J.K., Müller, C., Bondeau, C., Waha, K., Pollack, G. 2009. Eating the planet: Feeding and Fuelling the World Sustainably, Fairly and Humanely – A scoping Study. Institute of Social Ecology, Potsdam, Institute of Climate Impact Research. Social Ecology Working Paper 116. Vienna. ISSN 1726-3816.

Fischer, G., Schrattenholzer, L. 2001. Global bioenergy potentials through 2050. *Biomass and Bioenergy*, 20(3), 151-159.

Foley, G., Barnard, G. 1985. Biomass Gasification in Developing Countries. Earthscan, London, UK.

GEA 2012: Global Energy Assessment 2012 – Towards a Sustainable Future. Cambridge University Press, Cambridge, UK and New York, USA and the International Institute for Applied Systems Analysis (IIASA), Laxenburg, Austria.

Geldart, D. 1973. Types of Gas Fluidization. *Powder Technology* 7(5), 285-292.

Gómez-Barea, A. Leckner, B. 2010. Modelling of biomass gasification in fluidized bed. *Progress In Energy and Combustion Science* 36(4), 444-509.

Gómez-Hernández, J., Soria-Verdugo, A., Villa-Briongos, J., Santana, D. 2012. Fluidized bed with a rotating distributor operated under defluidization conditions. *Chemical Engineering Journal* 195, 198-207.

Haines, A., Kovats, R.S., Campbell-Lendrum, D., Corvalan, C. 2006. Climate change and human health: Impacts, vulnerability and public health. *Journal of the Royal Institute of Public Health* 120(7), 585-596.

Hasler, P., Nussbaumer, T. 1999. Gas cleaning for IC engine applications from fixed bed biomass gasification. *Biomass and Bioenergy* 16(6), 385-395.

Herzog, H., Drake, E., Adams, E. 1997. CO2 Capture, reuse and storage technologies for mitigating global climate change: a white paper, final report. DOE No DE-AF22-96PC01257. Energy Laboratory, Massachusetts Institute of Technology, Massachusetts, USA.

Herzog, H., Golomb, D. 2004. Carbon Capture and Storage from Fossil Fuel Use. In Encyclopedia of Energy (C.J. Cleveland, ed.) et al. pp. 277-287. Elsevier Science Inc., New York, USA.

Hoogwijk, M., Faaij, AA., Eickhout, B. de Vries, B., Turkenburg, W. 2005. Potential of biomass energy out to 2100, for four IPCC SRES land-use scenarios. *Biomass & Bioenergy* 29(4), 225-257.

Johansson, T.B., McCormickm K., Neij, L., Turkenburg, W. 2004. The potentials of renewable energy thematic background paper, January 2004.

Juniper Consultancy Services Ltd. 2000. Pyrolysis & gasification of waste: a worldwide technology & business review. Volume 2: Technologies & Processes.

Kiel, J. H. A., van Paasen, S. V. B., Neeft, J. P. A., Devi, L., Ptasinski, K. J., Janssen, F. J. J. G. 2004. Primary measures to reduce tar formation in fluidized-bed biomass gasifiers. *Final Report SDE project P1999-12. Energy Research Centre of the Netherlands, ECN. Report ECN-C-04-014, The Netherlands*.

Kunii, D., Levenspiel, O. 1991. Fluidization Engineering, 2nd ed. Butterworth-Heinemann. Stoneham, Massachutssets, USA.

Lee, T.-Y., Chen, C.L. 2009. Wind-photovoltaic capacity coordination for a time-of-use rate industrial user. *IE transactions on Renewable Power Generation* 3(2), 152-167.

Martiskainen, M., Coburn, J. 2011. The role of information and communication technologies (ICTs) in household energy consumption/prospects for the UK. *Energy Efficiency* 4(2), 209-221.

McKendry, P. 2002. Energy production from biomass (part 3): gasification technologies. *Bioresource Technology* 83(1), 55-63.

Monti, A., Di Virgilio, N., Venturi, G. 2008. Mineral composition and ash content of six major energy crops. *Biomass & Bioenergy* 32(3), 216-223.

Nakicenovic, N. Grubler, A., McDonald, A. 1998. Global Energy Perspectives. International Institute for Applied Systems Analysis (IIASA) and World Energy Council (WEC) (eds). Cambridge University Press, Cambridge, UK.

Natarajan, E., Öhman, M., Gabra, M., Nordin, A., Liliedahl, T. 1998. Experimental determination of bed agglomeration tendencies of some common agricultural residues in fluidized bed combustión and gasification. *Biomass & Bioenergy* 15(2), 163-169.

Neves, D., Thunman, H., Matos, A., Tarelho, L., Gómez-Barea, A.2011. Characterization and prediction of biomass pyrolysis products. *Progress In Energy and Combustion Science* 37(5), 611-630.

Oasmaa, A., Kuoppala, E., 2003. Fast pyrolysis of forestry residue. 3. Storage stability of liquid fuel. *Energy & Fuels* 17(4), 1075-1084.

Öhman, M., Nordin, A., Bengt-Johan, S., Backman, R., Hupa, M. 2000. Bed agglomeration characteristics during fluidized bed combustión of biomass fuels. *Energy & Fuels* 14(1), 169-178.

Olofsson, I., Nordin, A., Sönderlimd, U. 2005. Initial review and evaluation of process technologies and systems suitable for cost-efficient medium-scale gasification for biomass to liquid fuels. ISSN 1653-0551. ETPC Report 05-02, Energy Technology & Thermal Process Chemistry, University of Umeå, Sweden.

Özbay, N., Apaydin-Varol, E., Uzun, B.B., Pütün, A.E. 2008. Characterization of bio-oil obtained from fruit pulp pyrolysis. *Energy* 3(8), 1233-1240.

Panwar, N.L., Kaushik, S.C., Kothari, S. 2011. Role of renewable energy sources in environmental protection: A review. *Renewable and Sustainable Energy Reviews* 15(3), 1513-1524.

Reed, T.B., Levie, B. 1984. A simplified model of the stratified downdraft gasifier. In: The International Bio-Energy Directory and Handbook. Washington, D.C., USA, pp. 379-389.

Resch, G., Held, A., Faber, T., Panzer, C., Toro, F., Haas, R. 2008. Potentials and prospects for renewable energies at global scale. *Energy Policy* 36(11), 4048-4056.

Rogner, H.H. et al. 2004. Energy resources. In World Energy Assessment – 2004 update. United Nations Development United Nations Department of Economic Affairs, World Energy Council, 2004 (Chapter 5).

Schröder, E. 2004. Experiments on the pyrolysis of large beechwood particles in fixed beds. *Journal of Analytical Applied Pyrolysis* 71(2), 669-694.

Shell. 2008. Shell energy scenarios to 2050. Shell International BV.

Shi, L., Chew, M.Y.L. 2012. A review on sustainable design of renewable energy systems. *Renewable and Sustainable Energy Reviews* 16(1), 192-207.

Siegel, G.J. 2005. Overview of gasification technologies. Global Energy and Energy Project (GCEP) Advanced Coal Workshop, Provo, UT.

Sims, R.E.H. 2004. Renewable energy: a response to climate change. *Solar Energy*, 76(1-3), 9-17.

Smeets, E.M.W., Faaij, A.P.C., Lewandowski, I.M., Turkenburg, W.C. 2007. A bottom-up assessment and review of global bio-energy potentials to 2050. *Progress In Energy and Combustion Science* 33(1), 56-106.

Tsai, W.T., Lee, M.K., Chang, Y.M. 2007. Fast pyrolysis of rice husks: product yields and compositions. *Bioresource Technology* 98(1), 22-28.

Van Loon, S., Koppejan, J. 2008. The Handbook of Biomass Combustion and Co-firing. Task 32. Earthscan, London.

Van Vuuren, Detlef, .P., Van Vliet, J., Stehfest, E. 2009. Future bio-energy potential under various natural constraints. *Energy Policy* 37(11), 4420-4230.

WBGU: Future Bioenergy and Sustainable Land Use. 2009. Earthscan.

Zakhidov, R.A., 2008. Central Asian countries energy system and role of renewable energy sources. Applied Solar Energy 44(3), 218-223.

Zwart, R.W.R. 2009. Gas cleaning downstream biomass gasification. *Status Report. Energy Research Centre of the Netherlands, ECN. Report ECN-E-08-078 Petten, The Netherlands*.

Chapter 2

Assessment of the potential of *Cynara cardunculus* L. gasification for bioenergy production

Contents

2.1. Introduction

Fossil fuels provide about 46% of the total electricity supply in Spain, where nearly half of the energy comes from Combined Cycle Gas Turbine (CCGT) plants (Secretaría de Estado de Energía, 2010). This dependence on fossil fuels leaves the region in a vulnerable position in front of the rise of fuel prices and supply shocks. To control the European energy consumption, the European directive [2009/28/EC] has set a 20% target for the overall share of energy from Renewable Energy Sources (RES) by 2020. So far, renewable resources in Spain represent around 11% of the total primary energy consumption (Secretaría de Estado de Energía, 2010). Hydro and biomass resources

account for half of the Spanish renewable energy production. Among renewable resources, biomass is the only fuel available for renewable combustion based electricity generation (Evans et al., 2010). This characteristic has resulted in a growing demand for biomass resources such as biomass residues and dedicated energy crops. In 2010, over 4 thousand GWh were generated using biomass, accounting for 1.4% of the total Spanish electricity supply (Secretaría de Estado de Energía, 2010).

The Commission of the European Communities (CEC) indicates that RES targets might be impossible to achieve without using more biomass (CEC, 2005). In Spain, the energy production from this type of resource has been successfully promoted. This is the case of the Autonomous Community of Madrid (CAM), where, according to the "Energy Plan for CAM", the energy production from biomass has to increase by 69.8% for the period 2003-2012 (Mosquera et al., 2011).

Recently, the use of energy crops as a feedstock for energy production is gaining a lot of popularity. For example, in the U.K. approximately $66 million has been provided to help encourage the use of energy crops for energy production (ECOFYS, 2011). Of this, the New Opportunities Fund provided approximately $33 million for energy crops power generation and around $3 million for small-scale biomass/combined heat and power projects (ECOFYS, 2011). The main advantages of energy crops are that can be grown on marginal and degraded land, and require low inputs (McKendry, 2002).

In the Mediterranean region, one of the most promising energy crops is *Cynara cardunculus* L. (cynara) due to its potential for biomass production. This agrees with the findings made by Mosquera et al. (2011) who state that small, medium and large projects are possible due to there is enough land in CAM to cultivate energy crops as cynara. The biomass obtained from this type of crops can be transformed into energy through several conversion routes. This study will only be focused on the thermochemical conversion of biomass into electricity. Three primary technologies stand out for this purpose: pyrolysis, gasification and direct combustion.

Pyrolysis is the first step in combustion and gasification processes, where it is followed by total or partial oxidation of the primary products. The main advantage of pyrolysis technology is that can provide a liquid fuel able to substitute for fuel oil in any static heating or electricity generation application (Bridgwater, 1999). However, pyrolysis is one of the most capital intensive electricity generation technologies comparable with nuclear (Evans et al., 2010). Biomass gasification technology has attracted the highest interest as it offers high efficiencies compared to combustion and pyrolysis. Conversion efficiencies up to 50-60% may be reached if biomass integrated gasification/combined gas steam cycles are used (McKendry, 2002; Caputo et al., 2005). Biomass gasification is also an "eco-friendly" technology which produces lower emissions than the aforementioned ones, allowing it to meet environmental directives and policies for mitigating GHG emissions (Evans et al., 2010). The classification of gasification is based on several parameters: types of gasifiers, gasification temperature, heating, and gasification agent (Bhaskar et al., 2011). Over the years, different types of gasifier configurations have been developed: downdraft gasifiers, FB's, updraft, etc. This study will only be focused on FB gasifiers (FBG). These systems are featured by high mass and energy transfer coefficients providing high mixing fuel and reaction rates

inside the dense region. This allows increasing controllability process, feedstock versatility in terms of nature, distribution of size and shape, and ease to scale-up (Kunii and Levenspiel, 1991). The gaseous product of gasification (syngas) is an energy rich mixture of CO, CO_2, H_2, CH_4 and other impurities such as nitrogen, sulphur and tars. This syngas can be used as fuel to power gas turbines or in internal combustion engines (ICE) for electricity generation. The use of fluid bed configurations are being considered in applications ranging from 5 to 300 MW (Caputo et al., 2005). Combustion has been the traditional process to generate heat and electricity from biomass since ancient times. However, despite being the oldest, combustion is the most inefficient technology between the aforementioned conversion routes (Bridgwater, 2003). Thus, the choice of the best suited conversion technology is crucial to make an efficient use of the land available, biomass and reduce fossil-fuel consumption.

This study aims to determine the technical and economic performance of cynara gasification for bioenergy production in the CAM. The gasification process has been evaluated using a predictive model, focused on the particular behavior of biomass. The model includes a realistic approach of the biomass gasification process, accounting for the bubble phase temperature influence on tar cracking and ash sintering. The technical and economic assessment of product gas from gasification has been conducted for two technological solutions to determine the cost of electricity generation: CCGT and ICE plants. The electricity obtained from these processes can be used for different applications or sold to the national grid. Moreover, the production of energy crops such as cynara can help to rural development and local producers by providing a new market for farm production, while producing clean energy.

2.1.1. *Cynara cardunculus L.*

Cynara cardunculus L. is an herbaceous perennial plant with C3-type metabolism, which normally grows on fallow land and road verges. In Spanish climate conditions, its cycle goes from October to September with the main growth rate from March to June (Fernández et al., 2009). *Cynara cardunculus* L. is commonly known as “Cardoon", when it is grown for horticultural purposes. However, if the crop is grown for energy purposes, “Cynara" is preferable (Fernández and Curt, 2005). Tables 2.1 and 2.2 present a comparison between cynara and other C3-type crops that in recent years have been under study due to their good attributes as energy crops.

Parameters	Unit	Reed canary grass	Cynara	Giant Reed
Harvesting cycle	months		10	7-12 (Oder et al., 2008)
No. of cycle in a year		1-2 (Adler et al., 2007)	1	1
Fertilizer requierement	kg/ha N	50-140	50-100	50-100
Plant density	plants/ha	9,984-19,768 (Odero et al., 2008)	10,000 (Fernández et al., 2006)	9,000 (Christou et al., 2005)
Moisture at harvest		10-23 (Lewandowski et al, 2003)	12 (Fernández and Curt, 2005)	50-60 (Odero et al., 2008)
Biomass yield	ta/ha/cycle	7-13 (Sankari et Mela, 1998)	10-20 (Fernández et al., 2006)	3-37
Heating value	MJ/kg	16.6[*1]-19.12[*2] ([*1] Burvall, 1997; [*2] Greenhalf et al., 2012)	15-16 (Fernández et al., 2009)	14.8-18.8
Characteristic		Lignocellulosic biomass	Lignocellulosic biomass/oil seed	Lignocellulosic biomass

Table 2.1: Comparison between cynara, reed canary grass and giant reed.

Reed canary grass	Cynara	Giant Reed
Heat and power	Heat and power	Biofuel
Biofuel	Seed oil and biodiesel	Industrial fiber
Paper pulp	Paper pulp	Phytoremediation
	Green forage	
	Pharmacological active compounds: cynarin and silymarin	
	Phytoremediation	

Table 2.2: Applications of cynara, reed canary grass and giant reed.

Cynara is an annual crop, well adapted to Mediterranean conditions, which has a high biomass yield potential on poor quality soils. It is capable to produce 10-20 tonnes of biomass per hectare per year and the lifetime of the plantation is 15 years. In Mediterranean rainfed conditions (~450 mm rainfall $year^{-1}$) cynara yields about 17 t fresh matter ha^{-1} $year^{-1}$ with 12% moisture (15 t dry matter ha^{-1} $year^{-1}$) on average (Fernández and Curt, 2004). One of the main advantages of cynara is that can be grown in non-irrigated land and is well suited for seed propagation. On average, it has the same fertilizer requirements as Giant reed and lower than Reed canary grass. Cynara has a lower heating value (LHV) in the range of 15-16 MJ/kg and mean moisture content (12%) lower than reed canary grass and giant reed. All these characteristics allow producers to avoid land rental, drying costs and problems related to storage of the biomass. Therefore, cynara benefits represent a low cost option compared to other energy crops and give producers a suitable choice for biomass production, while attaining profitable sales growth.

Besides being used for horticultural and energy purposes, *Cynara cardunculus* L. can also be used as a renewable source to decontaminate polluted sites. For example, Papazoglou and Rozakis (2011) explored the possibility of using cynara to decontaminate a cadmium polluted site and found that cynara seems to be a promising candidate to achieve low price decontamination of soil, while producing clean energy.

2.2. Materials and methods

2.2.1. *Cynara cardunculus* L. properties

Thermogravimetric analysis was performed in a TA instruments Q500 type thermogravimetric analyser for determination of proximate analysis of cynara (moisture, ash content, volatile matter and fixed carbon). Ultimate analysis was obtained using a CHNS analyser (Leco TruSpec CHN-S), i.e., weight percent of carbon, hydrogen, nitrogen, and sulphur in the cynara samples. The percentage of oxygen was determined by difference. Ultimate and proximate analysis was conducted using ASTM standards. The cynara LHV was estimated using a bomb calorimeter (6300, Parr Inc.). These experiments were performed at the Thermal and Fluid Engineering Department facility of Carlos III University of Madrid. Table 2.3 presents the *Cynara cardunculus* L. chemical properties, which are going to be used for further calculations.

Parameter	Unit	Value
Ultimate analysis (% d.b.)		
C	%	46.57
H	%	5.86
N	%	0.83
O[a]	%	46.62
S	%	0.0012
LHV	MJ/kg	16.55
Proximate analysis (% w.b.)		
Moisture	%	8.7
Ash	%	8.95
Volatiles	%	68.16
Fixed Carbon	%	14.19

Table 2.3: Characterization of *Cynara cardunculus* L. [a] by difference.

2.2.2. *Cynara cardunculus* L. potential in the Autonomous Community of Madrid (CAM)

In order to calculate the cynara-based energy potential, it is necessary to estimate the area available to cultivate cynara. This area has already been estimated by Mosquera et al. (2011), evaluating the biomass production from cynara in CAM using a Geographic Information System (GIS) tool. The potential area to cultivate *Cynara cardunculus* L. is presented in table 2.4.

Possible restrictions	Potential area (ha)	Potential lignocellulosic biomass (tonnes of DM/year)
With no SPA [a] restrictions	63,061	977,500
With possible SPA [a] restrictions	24,564	382,500
Total	87,625	1,360,000

Table 2.4: Potential area to cultivate *Cynara cardunculus* L. in the Autonomous Community of Madrid.
[a] Special Protected Area.

As can be seen from table 2.4 the total potential area to cultivate cynara in CAM is 87,625 ha. However, this study will not take into consideration land with possible special protected area restrictions. Therefore, the energy potential will be only based in the 63,061 ha available. The LHV used to assess the energy potential was extracted from table 2.3.

2.2.3. *Cynara cardunculus* L. gasification

2.2.3.1. Facility

The reactor considered for this analysis has been defined according to specification design of the pilot-plant scale Biomass Bubbling Fluidized Bed Gasifier (BBFBG) in the Thermal and Fluid Engineering Department facility of Carlos III University of Madrid. The gasification plant incorporates storage and handling sections, and a BBFBG for the production of syngas. The gas stream (syngas) obtained from gasification can be used to produce electricity, process heat and power. The gasification plant has the characteristics shown schematically in figure 2.1.

On the other hand, table A1 (Appendix A) shows the operating conditions such as pressure, bed temperature, equivalence ratio, fluidization state (U_0/U_{mf}), bed material, particle and density of bed material and reactor design (diameter and height of the bed and the freeboard regions) of experimental facilities employed in the corresponding investigations in order to set the frame of biomass gasification simulations in the bubbling regime.

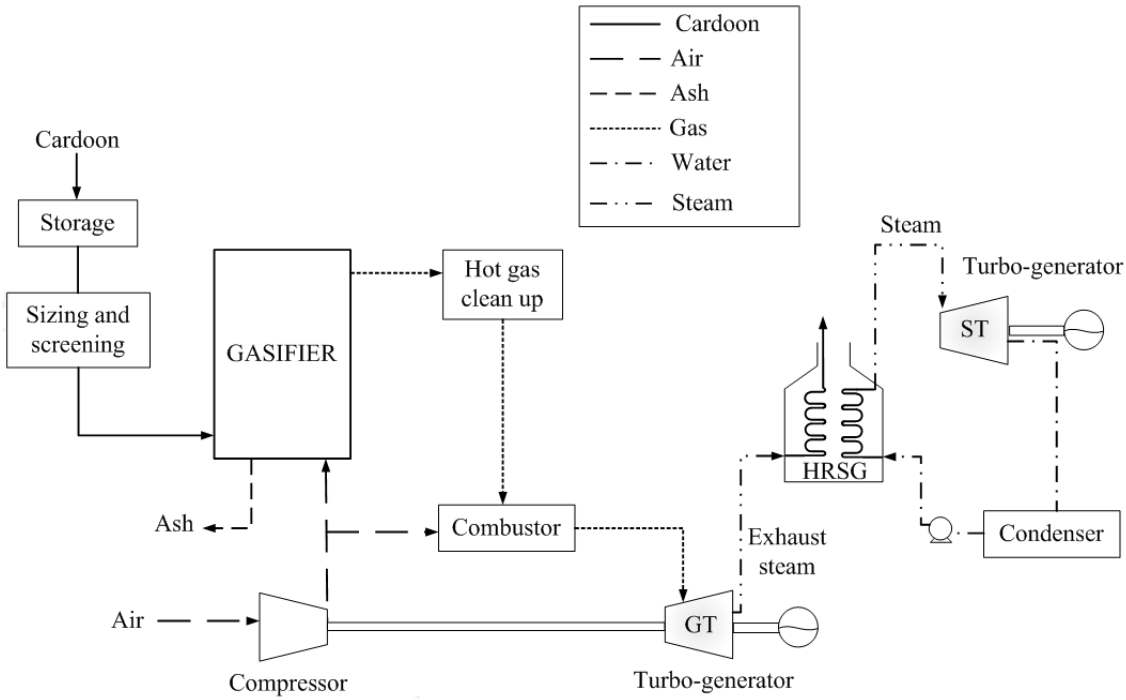

Figure 2.1: Fluidized bed gasification, followed by a combined gas-steam cycle power generation - CCGT plant.

In order to determine the potential production of electricity from cynara-based syngas and evaluate its economic competitiveness, two technological solutions have been considered: CCGT plant and ICE power generator. A process flow diagram for each technology is shown schematically in figures 2.1 and 2.2, respectively. With respect to the CCGT plant, the syngas produced from the BBFBG is fed into the hot gas clean-up system to collect and remove the contained “impurities" (dust and tars). Then, the clean gas is used as fuel into the combined gas-steam cycle to generate electricity for the production process. The surplus of electricity is sold to the national grid. As can be seen from figure 2.2, the ICE plant incorporates storage and handling section, and a fluidized bed gasifier analogous to the CCGT solution. The syngas produced is fed into the cold gas clean-up system to remove “impurities". Gas cleaning is a very important process as impurities such as tars may cause damage to the downstream equipment and inhibit the operation of the engine (attrition, fouling and clogging related problems). Hence, the overall gasification efficiency decreases. Gas cleaning is achieved by using a cyclone separator and moving bed system (MBHEF). The MBHEF system removes condensable material from the gas flow into the solid mass flow, collected on the bottom part of the system. That is, the gas inlet with condensable material (here tars) enters to the device and goes out free of tars or with a low tar content. The gas resultant

from the cleaning process is then used as fuel into an ICE power generator to generate electricity for the production process. The surplus of electricity is sold to the national grid.

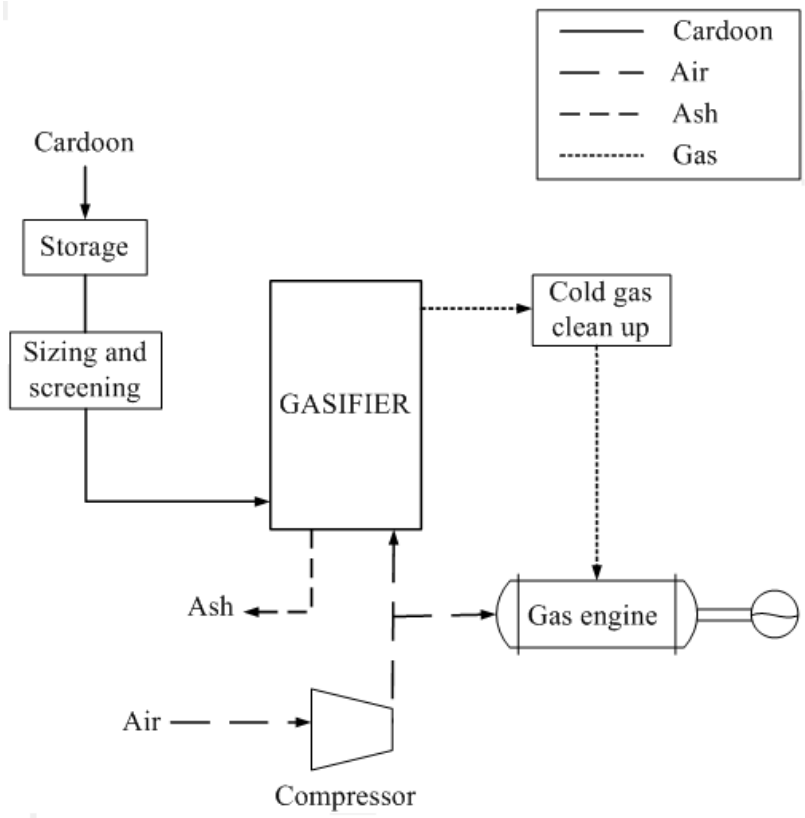

Figure 2.2: Fluidized bed gasification, followed by an internal combustion engine power generator - ICE plant.

The simulation of the biomass gasification in a fluidized bed reactor was performed with the model approach presented in detail in the following chapter, **Chapter 3**.

2.2.4. Costs assessment

A detailed economic analysis has been made for cynara conversion to electricity on the basis of its cost including a minimum desired profit margin on the investment. This study evaluates the cost of electricity for new CCGT and ICE plants.

In order to estimate the cost of electricity for these technologies, a model for each of the items involved in the cynara processing has been considered. The four main studied blocks are highlighted in figure 2.3, i.e., crop properties, agricultural activities, transport and conversion technology. Figure 2.3 explains the calculation process to assess the cost of electricity of cynara.

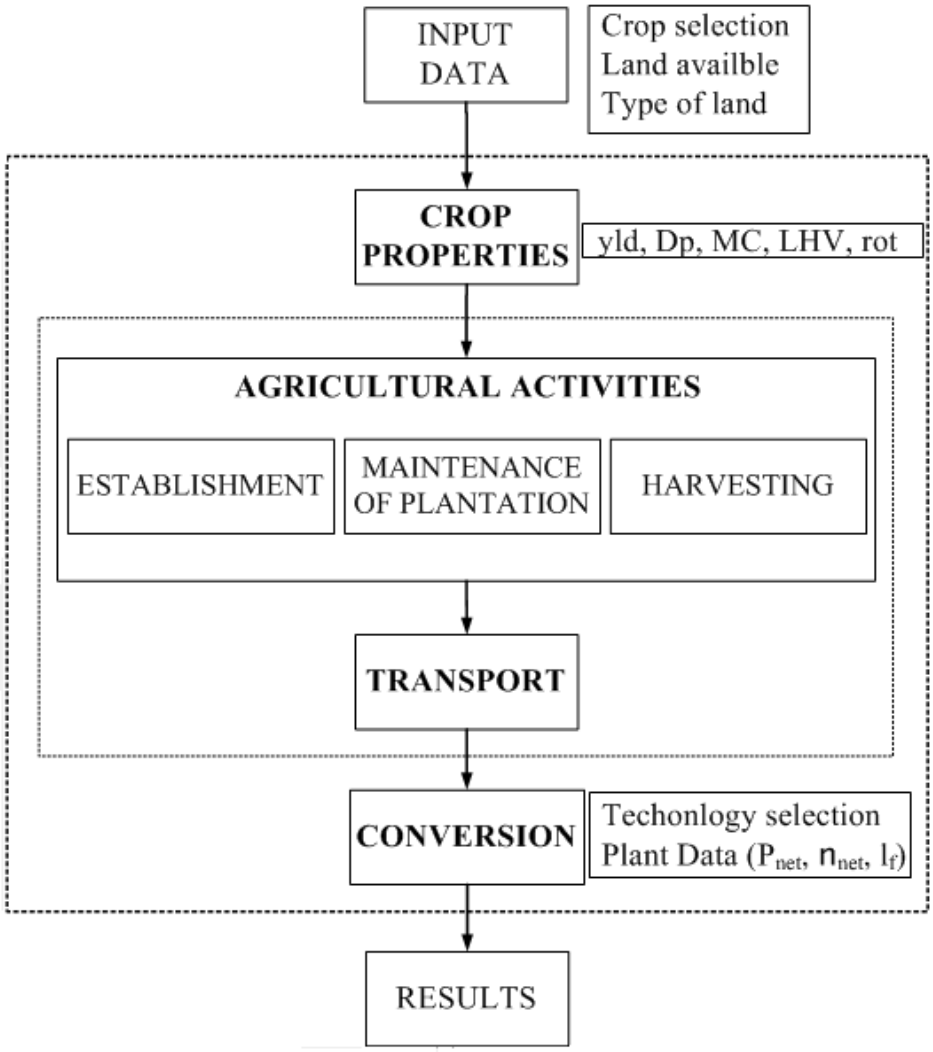

Figure 2.3: Schematic cost model.

The methodology used to assess the cost of electricity production is based on the work of van den Broek et al. (2000). This method is based on spreading the costs equally over the years, i.e., converting the costs into annuities. The costs per kWh of electricity (COE) produced are determined by Eq. (2.1), and are based on the NPV (Net Present Value) of the costs and of the revenues (van den Broek et al., 2000).

$$COE = \frac{3.6\sum_{i=1}^{i}\left(ecc_i \sum_{y=1}^{n} \frac{f_i(y)}{(1+dr)^y}\right)}{\eta_{net} \cdot LHV \cdot 1000 \cdot yld \cdot rot \cdot \sum_{y=1}^{n} \frac{f_{yld}(y)}{(1+dr)^y}} + \frac{\sum_{j=1}^{j}\left(ppc_j \sum_{y=1}^{n} \frac{f_j(y)}{(1+dr)^y}\right)}{P_{net} \cdot 8760 \cdot 1000 \cdot l_f \sum_{y=1}^{n} \frac{f_e(y)}{(1+dr)^y}} \quad (2.1)$$

where:
COE = cost of electricity [€/kWh];
i = number of energy crop cost items with different time pattern;
ecc_i = cost of energy crop item i [€ha^{-1}] ;
n = total number of years in the project lifetime;
$f_i(y)$ = number of times per hectare that cost item i occurs in year y in the plantation;

d_r = discount rate;
η_{net} = net power plant efficiency;
LHV = lower heating value on dry basis [GJ t^{-1}];
yld = average annual yield of energy crop [t ha^{-1} yr^{-1}];
rot = harvest rotation cycle [yr];
$f_{yld}(y)$ = binary figure (0 or 1) to indicate whether the energy crop is harvested in year y;
ppc_j = cost of power plant cost item [€] ;
$f_j(y)$ = number of times that cost item j occurs in year y in the power plant;
P_{net} = net installed electric capacity of the power plant [MWe];
l_f = load factor [h];
$f_e(y)$ = binary figure (0 or 1) to indicate whether power is produce in year y [h];
j = number of power plant cost items with different time pattern;

The first part of Eq. (2.1) represents the energy crop costs takes into consideration the costs involved in the agricultural activities of cynara. To be able to assess these types of costs, data on the timing and frequency of the cost items is required, i.e., how many times a certain cost item occurs in each year of plantation's lifetime. The cost of agricultural activities and yield data of cynara plantations are also necessary. These data are presented in tables 2.7 and 2.8 and are represented by the parameters $f_i(y)$, $f_j(y)$, $f_{yld}(y)$, $f_e(y)$ and ecc_i of Eq. (2.1). It is assumed that cynara is planted near the processing plant and receives initial irrigation to ensure good establishment, i.e., irrigation only during the first year of the plantation (Panoutsou, 2007). In the first year, management is more intensive than during the rest of the plantation's lifetime. It is also considered that cynara can be only harvested once in a calendar year.

The second part of Eq. (2.1) refers to the power plant cost, which takes into consideration the technology conversion costs. To estimate these, adopted equipment, investment, O&M costs and efficiency data of the power plant are necessary. Therefore, a process simulation was carried out for each stage of the production process of both CCGT and ICE solutions. With respect to the CCGT solution, a standard plant was considered for the simulation, with unit operations and equipment shown in figure 2.1. The CCGT plant incorporates a FBG for the production of syngas with a LHV around 6.36 MJ/Nm^3. It is assumed that the fumes generated by combustion processes are treated with NO_x and SO_x removal equipment and fumes filters. In the fumes treatment, it is also considered ashes storage, ashes extraction, fans, fumes ductworks and discharge stack. The combustor is designed to burn the syngas coming from the gasifier with air, in order to deliver the resulting gases to the turbine. It is assumed a complete combustion of syngas with oxygen inside the reactor, yielding only the completely oxidized combustion products. With respect to the ICE solution, the standard plant configuration considered for the simulation is shown in figure 2.2. The main advantage of the ICE plant is that the engines can be fueled by low-quality gases, reducing the technical risk of the power plant compared to the CCGT solution. It has been assumed a maximum capacity for a single engine of 1 MW (Baratieri et al., 2009). The ICE is designed to run with a mixture of syngas and oxygen for fuel. It is considered the combustion of syngas with 10% excess air. Due to the low moisture content in cynara (~

12%), there is no need to include a heat-recovery dryer in the plant configuration of both technologies. The operating and process parameters used for the simulation are listed in table 2.5. The combustion reactions used in the combustor (R1) and ICE (R2) design are presented in table 2.6. The power plant cost (ppc_j) for each technology analysed is presented in table 2.8.

Equipment	Process parameters	Value	Unit
CCGT plant			
Compressor	Pressure (in)	0.1	MPa
	Pressure (out)	0.9	MPa
	Temperature (in)	15	ºC
	Isoentropic efficiency	85	%
Gasifier	Temperature syngas (out)	327.81	ºC
	Temperature, flue gas (out)	1057.18	ºC
	Thermal efficiency	86	%
Gas turbine	Pressure (in)	900	kPa
	Pressure (out)	100	kPa
	Temperature (in)	1057.18	ºC
	Temperature (out)	907.87	ºC
	Isoentropic efficiency	88	%
HRSG	Pressure (in)	9	MPa
	Temperature, flue gas (in)	907.87	ºC
	Temperature, flue gas (out)	130	ºC
	Temperature, steam (out)	480	ºC
Steam turbine	Pressure (in)	9	MPa
	Pressure (out)	0.9	MPa
	Temperature (in)	480	ºC
	Temperature (out)		
	Isoentropic efficiency	90	%
Condenser	Pressure (out)	900	kPa
ICE plant			
Compressor	Pressure (in)	0.1	MPa
	Pressure (out)	0.9	MPa
	Termmperature (in)	15	ºC
	Isoentropic efficiency	85	%
Gasifier	Temperature syngas (out)		ºC
Cyclone	Temperature		ºC
	Pressure loss		kPa
	Removal efficiency	80	%
Bag filter	Temperature		ºC
	Pressure loss		kPa
	Removal efficiency		%
ICE	Temperature syngas (in)	33.93	ºC
	Temperature syngas out (in)	721.94	ºC
	Electrical efficiency	35	%

Table 2.5: Parameters adopted for the CCGT and ICE plant.

Reaction number	Combustion reactions
R1	$0.1484CO + 0.2098CO_2 + 0.15H_2$ $+0.573CH_4+0.4025N_2+0.221C_2H_6$ $+ 0.3411O_2 + 1.28536N_2 \Rightarrow 0.4597CO_2 + 0.3309H_2O + 1.6850N_2$
R2	$0.1484CO + 0.2098CO_2 + 0.15H_2$ $+0.573CH_4+0.4025N_2+0.221C_2H_6 + 0.37527O_2$ $+ 1.41173N_2 \Rightarrow 0.4597CO_2 + 0.3309H_2O + 1.814247N_2 + 0.034115O_2$

Table 2.6: Reactions used in CCGT and ICE plants design.

The simulation results from the gasification model and literature collected data were processed by different analytical tools such as mass and energy balances, material and substance flow analysis in order to design the aforementioned plants. Cost estimating techniques and cost correlations were also utilised. These correlations are based on Caputo et al. (2005) methodology to assess the purchased equipment, capital and operating costs. The total plant cost (TC) has been evaluated as the sum of the total capital investment costs (TCI) and total operating costs (TOC) over the plant lifetime.
With respect to the TCI, these were defined as the sum of all direct and indirect plant costs. The direct plant costs (TDC) include cost items such as: purchased equipment, piping, electrical, civil works, installation, auxiliary services, instrumentation and controls and site preparation costs (table 2.8). On the other hand, the indirect plant costs (TIC) include all costs associated with engineering and start-up. The total operating costs (TOC) have been determined as the sum of operating labour, ash transport, ash disposal, purchased biomass, biomass transport, maintenance and insurance costs (table 2.8).

The biomass transport costs (BTC) have been defined by equation Eq. (2.2):

$$BTC = \frac{3}{4}\sqrt{\frac{0.036 \cdot P_{net} \cdot OH}{\pi \cdot \eta_{net} \cdot LHV \cdot yld}}\,\frac{F_B}{V_c} \qquad (2.2)$$

where:
F_B= Biomass feeding the gasifier [t yr^{-1}];
V_c = Vehicles capacity [t];
C_{st}= Specific transport cost [€km^{-1}];
OH= operation hours.

		Cost items of *Cynara cardunculus* L. plantation (ecc_i)							Power plant cost items ($p\ pc_j$)	
		Establishment	Fertilization	Chemical weeding[a]	Mechan. weeding[a]	Pest control	Harvesting[a]	Land cost[c]	Invest	O&M
	Year	$f_1(y)$	$f_2(y)$	$f_3(y)$	$f_4(y)$	$f_5(y)$	$f_6(y)=f_{yld,cl}(y)$	$f_7(y)$	$f_1(y)$	$f_2(y)=f_e(y)$
*	1	1	0	1	1	0	1	1	1	1
	2	0	1	0	0	1	1	1	0	1
	3	0	1	0	0	1	1	1	0	1
	4	0	1	0	0	1	1	1	0	1
	5	0	1	1	1	1	1	1	0	1
	6	0	1	0	0	1	1	1	0	1
	7	0	1	0	0	1	1	1	0	1
	8	0	1	0	0	1	1	1	0	1
	9	0	1	0	0	1	1	1	0	1
	10	0	1	1	1	1	1	1	0	1
	11	0	1	0	0	1	1	1	0	1
	12	0	1	0	0	1	1	1	0	1
	13	0	1	0	0	1	1	1	0	1
	14	0	1	0	0	1	1	1	0	1
	15	0	1	0	0	1	1	1	0	1

Table 2.7: Timing of various cost items in the *Cynara cardunculus* L. plantations and power plant. Symbols used are according to Eq. (2.1). * First rotation.

Parameter	Value CCGT plant	Value ICE plant	Unit	Parameter	Value CCGT plant	Value ICE plant	Unit
General financial data				**Harvesting**			
Requiered IRR	20	20	%	Harvesting & baling	161.90	161.90	€ha^{-1}
Total cynara area	63,061	-	ha	Loading cost	8.70	8.70	€ha^{-1}
Land rent cost	120	120	€ha^{-1}yr^{-1}				
Interes rate for rents	0	0	%	**Plant Data**			
Labour cost	25000	25000	€yr^{-1}	Net electrical capacity	8	8	MW
Working days per year	333	333	d yr^{-1}	Net electrical efficiency	58	28	%
				Load factor	80	80	%
General physical data				Investment	42173255	41466688	€yr^{-1}
Cynara yield	17	17	t ha^{-1}yr^{-1}	Total direct plant costs	36789798	39352814	€yr^{-1}
Density plantation	10000	10000	plants ha^{-1}	PE costs	17944858	8532730	€yr^{-1}
Moisture content at harvest	12	12	%w	Piping costs	1001574	747198	€yr^{-1}
Density of cynara	0.114	0.114	t m^{3}	Electrical work costs	2670479	21240854	€yr^{-1}
LHV of cynara	16.55	16.55	MJ kg^{-1}	Civil work costs	3508729	3508729	€yr^{-1}
				Direct Installation	5383458	2857116	€yr^{-1}
Establishment				Auxiliary services	2691729	1056937	€yr^{-1}
Land preparation	73.13	73.13	€ha^{-1}	Instrumentation and controls	1794486	704625	€yr^{-1}
Ploughing	48.08	48.08	€ha^{-1}	Site preparation	1794486	704625	€yr^{-1}
Harrowing	25.05	25.05	€ha^{-1}	Total indirect plant costs	5383458	2113874	€yr^{-1}
Fertilizer	133.80	133.80	€ha^{-1}	O&M cost	2944884	3795915	€yr^{-1}
Fertilization labour	7.50	7.50	€ha^{-1}	Purchased biomass costs	614253	1258363	€yr^{-1}
Seed cost	60.00	60.00	€ha^{-1}	Biomass cost	26	26	€yr^{-1}
Sowing labour	24.04	24.04	€ha^{-1}	Ash transport cost	127434	261062	€yr^{-1}
Initial irrigation	38.00	38.00	€ha^{-1}	Ash disposal cost	49329	101056	€yr^{-1}
Pest control	18.00	18.00	€ha^{-1}	Biomass transportation costs	3776	11073	€yr^{-1}
Pest control labour	12.30	12.30	€ha^{-1}	Specific vehicle transport costs	1.14	1.14	€km^{-1}
Fuel and lubricants	6.00	6.00	€ha^{-1}	Effective load truck	20	20	t
				Operating labour	425810	425810	€yr^{-1}
Maintenance of plantation				Personnel transport costs	37351	76518	€yr^{-1}
Chemical weeding	44.02	44.02	€ha^{-1}	Maintenance	1265198	1244001	€yr^{-1}
Mechanical weeding	25.50	25.50	€ha^{-1}	Insurance and general	421733	414667	€yr^{-1}

Table 2.8: Financial, physical and cost data on the cultivation of *Cynara cardunculus* L. cultivation.

2.3. Results and discussion

2.3.1. *Cynara cardunculus L.* potential

The potential electricity production from cynara in the Autonomous Community of Madrid is presented in Table 2.9.

Possible restrictions	Potential Area (ha)	Potential electricity production (ktoe/year)	Potential electricity production (GW he/year)
With no SPA a restrictions	63,061	385	1,708
With possible SPA a restriction	24,564	150	668
Total	87,625	535	2,337

Table 2.9: Potential electricity production from *Cynara cardunculus* L. in the Autonomous Community of Madrid. [a] Special Protected Area.

The results show that by growing *Cynara cardunculus* L. on the 63,061 ha available in CAM, cynara could supply about 1708 GWh yr^{-1}. This electricity production represents around 42% of national biomass-based electricity share and exceeds 72% of total renewable-based electricity supply in CAM for the year 2009. The implementation of cynara projects could help to reduce the total energy consumption of CAM by 0.05%.

2.3.2. Thermoeconomic analysis

The economic performance of cynara-based syngas is presented in figures 2.4-9. The CCGT solution was studied for a capacity range of 5-30 MW, while the ICE solution was analysed for a range of 1-30 MW. Although the two technological solutions proposed in this study are based on identical gasification sections, these differ in their operating conditions and overall energy conversion efficiency. Therefore, to illustrate the results of the CCGT and ICE scenarios, the cost of electricity was varied in terms of the installed electric capacity, biomass yield and discount rate. The influence of plant size in the TC, TCI and TOC has also been analysed.

The cost of electricity for each technology as a function of the installed electric capacity is depicted in figure 2.4. As can be seen in the range 6-30 MW, the CCGT solution provides lower values of COE compared with the ICE solution. Such behavior is influenced by the electrical costs corresponding to the engines. That is, as plant size increases, this technology is penalized by the number of engines required to meet the power demand.

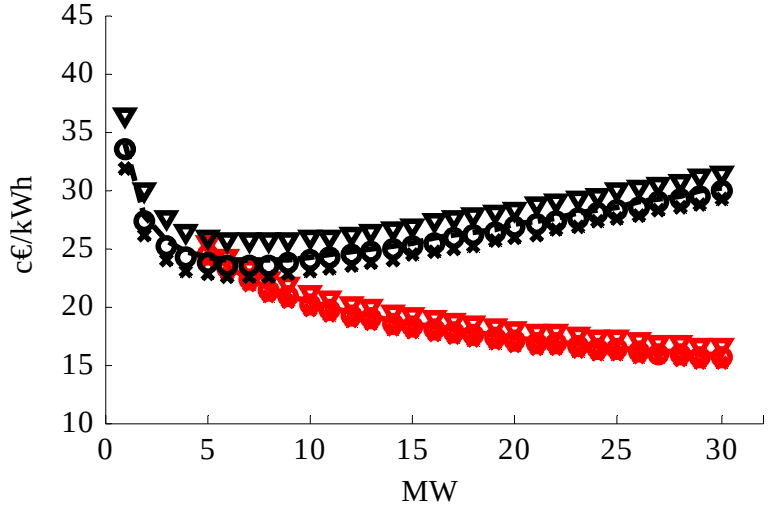

Figure 2.4: Effect of plant size and technologies on the cost of electricity from *Cynara cardunculus* L. Red values refers to CCGT plants and black to ICE for 10 t/ha(∇), 17 t/ha (-),20 t/ha (o) and 40 t/ha (x).

Figure 2.5 shows the effect of biomass yield on the cost of electricity for each scenario considered. Note that cynara-based electricity production can be more economically feasible as the energy crop yield increases. As observed, in the range 6-30 MW, cynara-based electricity generated in a CCGT plant is cheaper to produce than in the ICE plant. For instance, for a cynara yield of 17 t/ha, an 8 MW CCGT plant could produce electricity for 21.60 c€/kWh. On the contrary, an ICE plant with the same installed capacity as the case analysed before could produce electricity for 24.32 c€/kWh.

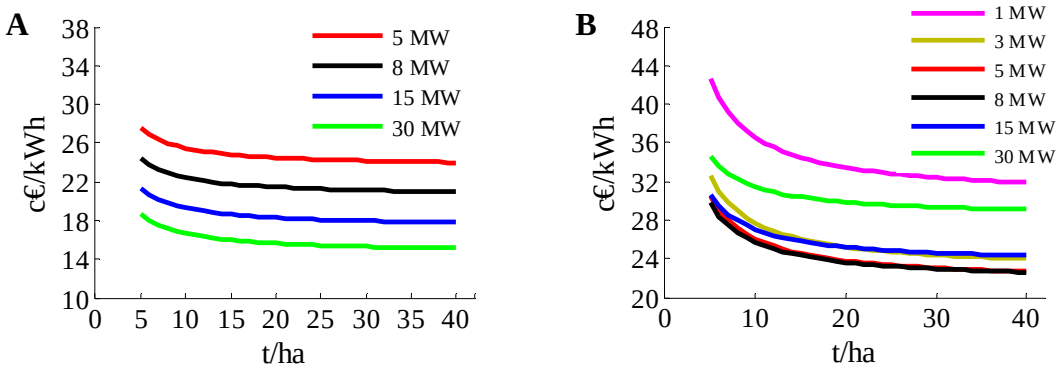

Figure 2.5: Cost of electricity generation from *Cynara cardunculus* L. for different biomass yields for CCGT (A) and ICE (B) solutions.

The influence of discount rate on the cost of electricity production for each technology is presented in figure 2.6. For example, for an 8 MW CCGT plant, the value of COE is estimated to be 16.69 c€/kWh using a discount rate of 10%. As for ICE solution, a plant with similar conditions as the case analysed before could produce electricity for 19.08 c€/kWh. For an installed capacity of 8 MW the values of COE for CCGT and ICE solutions, using the lowest discount rate (1%) are around 12.70 and 15.13 c€/kWh, respectively. As can be seen, the cost of electricity obtained for these technologies is higher than fossil-fuel and other renewable technologies. Such elevated cost is attributable to the power plant investment comprised in this analysis.

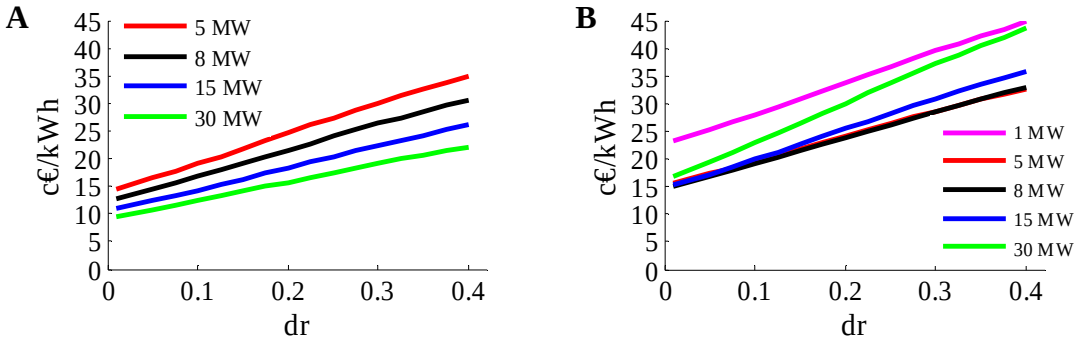

Figure 2.6: Effect of discount rate on cost of electricity generation from *Cynara cardunculus* L. for CCGT (A) and ICE (B) solutions.

Figure 2.7 shows the trend in total plant cost for each technology according to the installed electric capacity. The results indicate that the ICE solution is the most suitable technology for cynara-based electricity production when the installed capacity is below 8 MW. On the other hand, CCGT technology is the most suitable when the power output is above 8 MW.

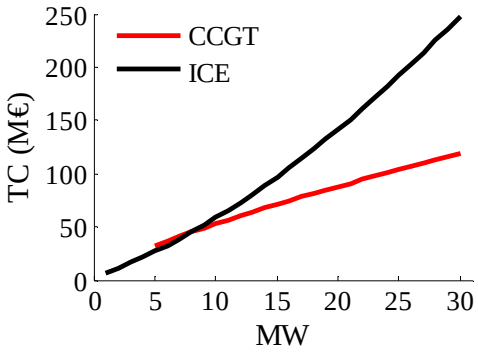

Figure 2.7: Total cost (TC) for different plant sizes and technologies using *Cynara cardunculus* L.

The effect of plant size on total capital investment (TCI) is described in figure 2.8. This figure shows that the values of TCI grow as the installed capacity increases. Nevertheless, the ICE plant exhibits a stronger economy of scale in energy production than CCGT solution. These types of costs represent about 93 and 92% of the total CCGT and ICE plant cost, respectively. It can be observed that in the range 9-30 MW, the ICE plant is characterized by higher values of TCI compared with CCGT plant. For example, for an 8 MW CCGT plant the value of TCI is estimated to be 42.17 M€, while the investment necessary for an ICE plant is around 41.46 Me. Although there is not a big difference between these technologies, note that the ICE plants approximately double the amounts of electrical material and equipment than the CCGT solution. Therefore, the development of cynara projects should be supported by adequate financial incentives to attract potential investors. Such incentives could include tax reductions to supply the local market, exonerations when using local feedstocks, tax exemption and production subsidy for cultivating cynara, and value-added tax exemptions for imported machinery and equipment. Loans for the purchase of equipment, materials, and services used for the design, construction, and installation of cynara projects should also be considered. For instance, in the Autonomous Community of Madrid, plants which produce electricity or energy from biomass receive an incentive payment of 75 €/kW and a maximum subsidy of 30% over the eligible costs.

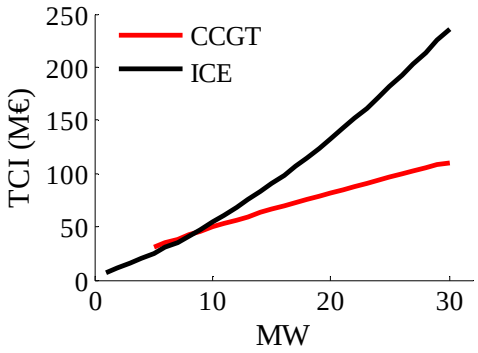

Figure 2.8: Total capital investment (TCI) for different plant sizes and technologies using *Cynara cardunculus* L.

Figure 2.9 illustrates the total operating costs for each technology as a function of the plant size. The figure shows that for any plant scale it is more expensive to run an ICE than a CCGT plant. This trend is due to the ICE plant requires the maintenance of more rotating equipment than CCGT solution. For example, for an 8 MW CCGT plant the value of TOC is estimated to be 2.94 M€, while the costs for an ICE plant is around 3.65 M€. Important sources of cost reduction can be the optimization of operating and maintenance activities.

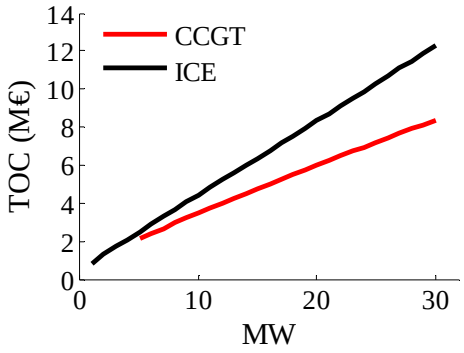

Figure 2.9: Total operating costs for different plant sizes and technologies using *Cynara cardunculus* L.

2.4. Conclusions

A techno-economic analysis has been performed in order to assess the potential of *Cynara cardunculus* L. gasification for bioenergy production. For this purpose, the Autonomous Community of Madrid (CAM) has been taken as a study case. However, the methodology presented here can be used as a tool to assess the potential of other biomass resources. The results show that cynara has the potential to provide around 42% of national biomass-based electricity supply and exceeds 72% of total renewable-based electricity supply in CAM. The thermochemical technology selected for the conversion of cynara into bioenergy is gasification due to its high efficiencies and lower emissions.

The economic comparison has been carried out on the basis of the estimating the energy crop and power plant cost of cynara in the Spanish context. The cost of cynara-generated electricity varies widely and depends on the biomass yield, conversion technologies, operation and maintenance.

The results indicate that ICE power generators are the most suitable technologies when the power output required is below 8 MW. Such behavior is influenced by the electrical costs corresponding to the engines. This technology is penalized by the number of engines required to meet the electricity demand. On the contrary, for an installed electric capacity above 8 MW, CCGT plants are the best choice.

It has been determined that an 8 MW CCGT plant could produce electricity from *Cynara cardunculus* L. for 21.60 c€/kWh, as compared to 24.32 c€/kWh for electricity from an ICE plant. Furthermore, the results point out that ICE plants are more expensive to run than CCGT plants at any scale. This trend is due to the ICE plant

requires the maintenance of more rotating equipment than CCGT solution. For example, for an 8 MW plant the value of TOC for the CCGT scenario is estimated to be 2.94 M€, while the costs for an ICE plant is around 3.65 M€.

Although the cost of electricity obtained for both technologies is higher than fossil-fuel and other renewable sources, this elevated cost is attributable to the power plant investment. Therefore, this study recommends the development of cynara projects supported by adequate financial incentives to attract potential investors.

As is shown in this paper, the production of energy crops such as *Cynara cardunculus* L. can help to rural development and local producers by providing a new market for farm production, while producing clean energy.

2.5. Notation

U_0/U_{mf} Fluidization state of a bed, [-].

Abbreviations

BBFBG Biomass Bubbling Fluidization Gasifier.

BTC Biomass transport costs.

CAM Autonomous Community of Madrid.

CCGT Combined Cycle Gas Turbine.

CEC Commission of the European Communities.

CHNS Carbon, hydrogen, nitrogen, sulphur content.

COE Cost of electricity.

DM Dry matter.

FBG Fluidized Bed Gasification.

GHG Green House Gas.

GIS Geographic Information System.

GT Gas Turbine.

HRSG Heat Recovery and Steam Generator.

ICE Internal Combustion Engine.

LHV Low Heating Value.

MBHEF Moving Bed Heat Exchange Filter.

O&M Operation & Management.

RES Renewable energy source.

ST Steam Turbine.

TC Total plant cost.

TCI Total capital investment.

TDC Total direct costs.

TOC Total operating costs.

Subscripts

mf Minimum fluidization.

Bibliography

Adler, P.R., Del Grosso, S.J., Parton, William J. 2007. Life-cycle assessment of net greenhouse-gas flux for bioenergy cropping systems. *Ecological Applications* 17(3), 675-691.

Baratieri, M., Baggio, P., Bosio, B., Grigiante, M., Longo, G.A. 2009. The use of biomas syngas in IC engines and CCGT plants: A comparative analysis. *Applied thermal Engineering* 29(16), 3309-3318.

Bhaskar, T., Bhavya, B., Singh, R., Naik, D.V., Kumar, A., Goyal, H.B.. 2011. Chapter 3 - Thermochemical conversion of biomass to biofuels. In Ashok Pandey, Christian Larroche, Steven C. Ricke, Claude-Gilles Dussap, and Edgard Gnansounou, editors, Biofuels, pages 51-77. Academic Press, Amsterdam. ISBN 978-0-12-385099-7.

Bridgwater, A.V., Meier, D., Radlein, D. 1999. An overview of fast pyrolysis of biomass. *Organic Geochemistry* 30(12), 1479-1493.

Bridgwater, A.V. 2003. Renewable fuels and chemicals by thermal processing of biomass. *Chemical Engineering Journal* 91(23), 87-102.

Burvall, J. 1997. Influence of harvest time and soil type on fuel quality in reed canary grass (phalaris arundinacea l.). *Biomass & Bioenergy* 12(3), 149-154.

Caputo, A.C., Palumbo, M., Pelagagge, P.M., Scacchia, F. 2005. Economics of biomass energy utilization in combustion and gasification plants: effects of logistic variables. *Biomass & Bioenergy* 28(1), 35-51.

Christou, M., Fernandez, J., Gosse, G., Venturi, G., Bridgwater, A., Scheurlen, K., Obernberger, I., Van be Beld, B., Soldatos, P., Reinhardt, G. 2005. Bio-energy chains from perennial crops in south europe. BIO-ENERGY CHAINS.

Commission of the European Communities (CEC). 2005. Biomass action plan. Technical Report, COM(2005) 628 final.

ECOFYS. 2011. Financing renewable energy in the European energy market. Technical Report, ECOFYS Netherlands BV.

Evans, A., Strezov, V., Evans, T.J. 2010. Sustainability considerations for electricity generation from biomass. *Renewable and Sustainable Energy Reviews* 14(5), 1419-1427.

Fernández, J., Curt, M.D. 2004. Low-cost biodiesel from cynara oil. Proceedings of the 2nd World Conference and Exhibition on Biomass for Energy, Industry and Climate Protection, pag. 109-113, 10-14 May, Rome, Italy.

Fernández, J., Curt, M.D. 2005. State of the art of *Cynara cardunculus L*. as an energy crop. Proceedings of the 14th European Biomass Conference, pag. 22-25, 17-21 October, Paris, France.

Fernández, J., Curt, M.D., Aguado, P.L. 2006. Industrial applications of *Cynara cardunculus* L. for energy and other uses. *Industrial Crops and Products*, 24(3), 222-229. ISSN 0926-6690. 2005 Annual Meeting of the Association for the Advancement of Industrial Crops: The International Conference on Industrial Crops and Rural Development.

Fernández, J., Sánchez, J., Esteban, B., Checa, M., Aguado, P.L., Curt, M.D., Mosquera, F., Romero, L. 2009. Potential lignocellulosic biomass production from

dedicated energy crops in marginalized agricultural land of Spain. Proceedings of the 17th European Biomass Conference, pag. 131-137, June-July, Hamburg, Germany.

Greenhalf, C.E., Nowakowski, D.J., Bridgwater, A.V., Titiloye, J., Yates, N., Riche, A., Shield, I. 2012. Thermochemical characterisation of straws and high yielding perennial grasses. *Industrial Crops and Products* 36(1), 449-459.

Kunii, D., Levenspiel, O. 1991. Fluidization Engineering, 2nd ed. Butterworth-Heinemann. Stoneham, Massachutssets, USA.

Lewandowski, I., Scurlock, J.M.O., Lindvall, E., Christou, M. 2003. The development and current status of perennial rhizomatous grasses as energy crops in the us and europe. *Biomass & Bioenergy* 25(4), 335-361.

Mosquera, F., Sánchez, J., Esteban, B., Checa, M., Aguado, P.L., Curt, M.D., and Fernández, J. 2011. Assessment of the potential biomass production from cardoon (*Cynara cardunculus* L.) in the autonomous community of Madrid. Proceedings of the 19th European Biomass Conference, pages 404-408.

Odero, D., Gilbert, R., Ferrell, J., Helsel, Z. 2008. Production of giant reed for biofuel. SS-AGR-318, pages 1-4.

Panoutsou, C. 2007. Socio-economic impacts of energy crops for heat generation in northern greece. *Energy Policy* 35(12), 6046-6059.

Papazoglou, E.G., Rozakis, S. 2011. Cardoon cultivation for combined bioenergy production and cadmium phytoextraction: an economic evaluation. Proceedings of the 3rd International CEMEPE & SECOTOX Conference, pag. 637-642, June, Skiathos island, Greece.

Sankari, H.S., Mela, T.J.N 1998. Characteristics of reed canary grass (phalaris arundinacea l.) breeding lines compared at three experimental sites in Finland. Biomass for Energy and Industry: 10th European Conference and Technology Exhibition: Proceedings of the International Conference, pages 894–896.

Secretaria de Estado de Energía. 2010. La energía en España. Technical Report, Ministerio de Industria, Turismo y Comercio.

van den Broek, R., van den Burg, T., van Wijk, A., Turkenburg, W.. 2000. Electricity generation from eucalyptus and bagasse by sugar mills in Nicaragua: A comparison with fuel oil electricity generation on the basis of costs, macro-economic impacts and environmental emissions. *Biomass & Bioenergy* 19(5), 311-335.

Chapter 3

Modelling approach of biomass gasification in fluidized bed reactor

Contents

In modelling FBRs, several phenomena need to be coupled to accurately characterize the main performance variables. Conservation balances of matter and energy need to be established to track the evolution of system state variables, such as species concentrations and temperature along the reactor. These equations need to be coupled with information on the geometry, physics, stoichiometry, thermodynamics, heat and mass transfer, reaction rates and flow patterns of the different phases in the reactor.

Reviewing the literature, it can be seen there are many points of view to describe a FBR, depending on what aspects the modeler wants to focus on most. Based on the review of previous research and experimental evidences, the guidelines, assumptions and modelling strategy of a new formulation approach to describe such systems are exposed in this chapter as follows.

3.1. Introduction

As a consequence of the impact of FB technology in the development of gasification process, modelling task has been a very valuable and useful tool in comprehension of such processes, particularly dealing with biomass gasification.

As some authors have remarked, biomass is indeed but young coal, with a higher volatile matter, humidity and alkali content and lower char fraction in comparison to coal. Thus, although differences between processes handling biomass and coal are not so much modelling biomass gasification in FBs has been hardly addressed since most of works have been based on previous experiences regarding coal instead of biomass.

Since research makes progress, more and more models have been developed as well as more reviews about gasification in FBs have been carried out to settle the guidelines in modelling FB gasification processes.

To date, an extensive number of FBR models have been proposed along the past half century (Mahecha-Botero et al., 2007; Gómez-Barea and Leckner, 2010). Thereby, the objective of this section is just to present and summarize chronologically the more relevant works and reviews concerning to modelling FB gasification, from the classical and pioneering reactor models to the current state-of-the-art. Thus, each model incorporates a different set of assumptions leading to different expressions for simulating the reactor performance.

On the other hand, it has to be remarked that FB gasification processes are a very complex phenomena and they can be studied with CFD and non-CFD models. The following review focus mostly on non-CFD models, using gas as fluidizing fluid and considering both catalytic and non-catalytic bed material, since non-CFD models are much less computational intensive than CFD models and they are capable of giving accurate results in a wide range of applicability.

3.2. Review of fluidized bed reactor modelling

When talking about FBR modelling, we have to take into account the complexity of FB and gasification phenomena, even more if biomass is the fuel involved. This means that FBRs and the modelling strategies can be sort out in many ways, making FBR

modelling reviews a difficult task. Furthermore, one could speak about FBR models developed and FBR modelling reviews. In this way, firstly, criteria to classify FBR modelling are described. Secondly, in a chronological way, FBR modelling reviews with their main insights given are presented.

According to the FBR modelling reviews of Radmanesh et al. (2006) and Gómez-Barea and Leckner (2010) of the last decades, FBR models can be basically grouped in two approaches: equilibrium models (the so-called black box models) and fluidization models. The first approach just estimates the final composition of the product gas without considering the underlying chemical and transport phenomena. In contrast, the second kind of model, CFD and non-CFD models, takes into account both the kinetics and the fluid-dynamics of the FB. Here, in these kind of models, drying and pyrolysis can be considered as equilibrium stages (Robert et al., 1988; Yan et al., 1998; Mansaray et al., 2000, Altafini et al., 2003) or not (Radmanesh et al. 2006; Ji et al., 2009).

Regarding the modelling reviews existing in the literature, as follows the most relevant works are presented in FBR modelling history, only dealing with non-CFD models.

The most historical developments in fluidization and FBR modelling date from the 1950's: the concept of two-phase fluidization (Toomey and Johnstone, 1952) and the first FBR model (Shen and Johnstone, 1955). Afterwards, the previous reviews of FBR modelling were performed in the 1970's and 1980's, dealing only with the bubbling flow regime. Obviously, there have been advances in FBR modelling which have been covered in next reviews recently. Therefore, the most recent FBR modelling reviews are the most documented and detailed works.

Along the 1970's, several works pay attention to FBR modelling, focusing on several aspects. For instance, Grace (1971) classified FBR models in two groups based on their complexity: simple models and bubbling bed models. The first ones composed of two parallel one-dimensional single-phase reactors containing at least three parameters while the second ones are based on bubble properties. Moreover, this work showed that models of that time differed in many features, so, not necessarily the higher complexity lead to better predictions.

On the other hand, Calderbank and Toor (1971), Pyle (1972), Yates (1975) and Horio and Wen (1977) studied several models of that time. Calderbank and Toor (1971), based on the work of Orcutt (1962) and Calderbank (1967), discussed the importance of the nature of the reacting system, that is, how it can define the complexity of the model: slow reactions may be modelled as simple CSTRs whereas very fast reactions are likely to be controlled by gas exchange. As well, they denote that gas bypassing and gas exchange are key variables in the reactor performance. Pyle (1972) remarked the need to set important or critical features for reactor design and questioned if those features could be implemented in reactor models. Others models as the ones of Davidson and Harrison (1963), Patridge and Rowe (1966) and Kunii and Levenspiel (1989) were analysed qualitatively. Yates (1975) discussed the classification proposed by Grace (1971). Horio and Wen (1977) proposed three levels of complexity in FBR models: a first one containing more than three adjustable parameters, a second one

comprising models that use average parameters estimated from operating conditions in the middle height of the reactor and a third level using parameters varying along the FB height. Moreover, this review also suggested that for FBRs operating with a value of the superficial gas velocity several times higher than U_{mf}, the dense phase concentrations predicted are not so critical since the dense phase only accounts for a small fraction in the bottom bed.

In the 1980's, there are some remarkable works in FBR modelling: Grace (1981), Fane and Wen (1982), Van Swaaij (1985) and Grace (1986a, 1986b).

Grace (1981) reviewed FBR modelling field since the 1940's, sorting out models based on several aspects: phases considered, equimolar mass transfer, bubble size, mixing in the emulsion phase, isothermatily, time variation and application. Afterwards, the same author stood out main advantages (e.g. temperature uniformity, high heat and mass transfer, low pressure drop and large/small scale of operation) and drawbacks (e.g. bypassing, backmixing, and entrainment) of FBs and provided some useful analytical expressions for simple reacting FB systems (Grace, 1986a). Meanwhile, in another review of models of that time is presented, dealing with fluidization regimes, phase division, bubble size estimation, dense phase mixing and equimolar mass transfer (Grace, 1986b). This review also focused on the models of May (1959), Orcutt (1962) and Grace (1984).

On the other hand, Fane and Wen (1982) grouped models by means of the method proposed by Horio (1977) as well as gave some insights for gas-phase and gas-solid reactions according to reaction kinetics. Van Swaaij (1985) also used the classification of Horio (1977) distinguishing three levels of complexity and giving importance to calculate reactor parameters as a function of the vertical coordinate instead of using average values. This work reviewed mass transfer coefficient, interfacial area and bubble rising velocity as well.

In the last decade there have been some recent and more comprehensive reviews in FBR Modelling concerning to more particularly biomass gasification, for example: Ho (2003), Mahecha-Botero et al. (2007), Basu (2009), Gómez-Barea and Leckner (2010) and Puig-Arnavat et al. (2010).

Ho (2003) was one of the first researchers in distinguishing between pseudo-homogeneous, two-phase and multiple-region models. The author also emphasized the art aspect of multiphase modelling and stood out that no single model is likely to be applicable in all cases too.

Mahecha-Botero (2007) and Gómez-Barea and Leckner (2010) extensively reviewed most of works about FBR modelling, highlighting both advantages and drawbacks of models proposed as well as remarking some important insights in modelling strategies of such systems. Mahecha-Botero (2007) also proposed a new mechanistic formulation for simulating a broad range of FBRs as it can be seen in the work of Mahecha-Botero (2009). This new formulation considers pseudo-phase approach, any geometry (one, two or three dimensions), convective transport, equimolar interphase mass transfer, catalytic reactions, fluidization regime variation calculated by probabilistic averaging of adjacent flow regimes (Abba et al., 2003b) as others remarkable features (e.g. selective

removal of species by membranes, heat and mass dispersion, fuel feeding distribution along the height) detailed in the study.

Basu (2009) reviewed works focused on pyrolysis and gasification chemistry, depicting main types of models in order to design such systems. This review paid mostly attention to gasification kinetics, char reactivity, pyrolysis models and modelling strategies. The author also concluded that models developed for coal gasification were not necessarily applicable to biomass gasification in FBs unless certain suitable modifications were made. Basu concluded that the major obstacle is to correctly fit kinetic parameters based on experimental research which is able to predict reactor performance under a wider range of operating conditions and more accurately.

Gómez-Barea and Leckner (2010) devoted special attention to all phenomena involved in biomass gasification: drying and devolatilization models, char and tar conversion models, homogeneous kinetics, comminution of solid particles, tar cracking models as well as a detail description of main FBRs with a comparison among all them. This review also summarized most important trends observed in FBR modelling in order to settle some guidelines for further improvements in FBR modelling for leading to better predictions of reactor performance. This work stood out which information (adjustable parameters, operating conditions) is missing or not clear in each structure model and also concluded that devolatilization and kinetic expressions greatly affect simulation results (e.g. gas composition, tar content, char conversion), char and tar conversion are the processes whose modelling is least satisfactory and validation should be desired at lab-scale or larger scale in testing the models proposals.

Puig-Arnavat et al. (2010) have analysed several gasification models (see references therein) based on thermodynamic equilibrium, kinetics and artificial neural networks. This study points out the usefulness of thermodynamic models as preliminary comparison tool for investigating the influence of the most important fuel and process parameters and maximum achievable yield of a desired product with no dependence of gasifier design, what cannot give high accurate in results for all cases. The kinetic models are computationally more intensive but give accurate and detailed results. Nevertheless, they contain parameters that limit their applicability to different plants.

Finally, CFD models apply governing conservation equations (heat, mass and momentum) in order to describe fluid flow, heat and mass transfer and chemical reactions (devolatilization, gasification) occurring in 2D (Oevermann et al., 2009; Gerber et al., 2010) and 3D (Sofialidis and Faltsi, 2001) FB geometries. The CFD models allow understanding the dynamic process inside the reactors. CFD models have recently gained interest due to the combination of increased computer efficiency and advanced numerical techniques (Wang and Yan, 2008). However, most of CFD works focus on the pyrolysis in FB systems (Papadikis et al., 2008; 2009a; 2009b; 2009c) nowadays.

3.3. Model description

The objective of the proposed model is to provide a map of basic properties of FBG process: composition, Low Heating Value (LHV) and tar content of gas produced for operating conditions (bed temperature, fluidizing gas inlet temperature, ER, U_0/U_{mf}, etc) corresponding to the performance of an autothermal biomass gasifier by means of an overall energy balance in the FB limits.

To accomplish this goal, a model development is needed. Hence, the fundamental equations have to be established. The equations, fundamentals and assumptions on which the model is based can be grouped into four modelling categories:

i. Conservation equations: mass balance for all chemical species considered in the system and an energy balance for any phase into which the reactor is divided.
ii. Fluidization hydrodynamic and transport correlations, from fluidized bed experiments for non-reactive systems.
iii. Kinetic rate equations to describe key chemical reactions such as devolatilization, gasification and combustion.
iv. Closure equations or conditions: equations not included above such as initial conditions, boundary conditions or additional correlations.

The fundamental assumptions of the proposed FBGR model approach are presented from generalized concepts to more detailed aspects. The conservation equations for mass and overall energy balance (MB and OEB respectively), kinetic model (KM) and estimation of physical properties needed in the main or secondary calculations are presented. A schematic of the reactor appears in figure 3.1.

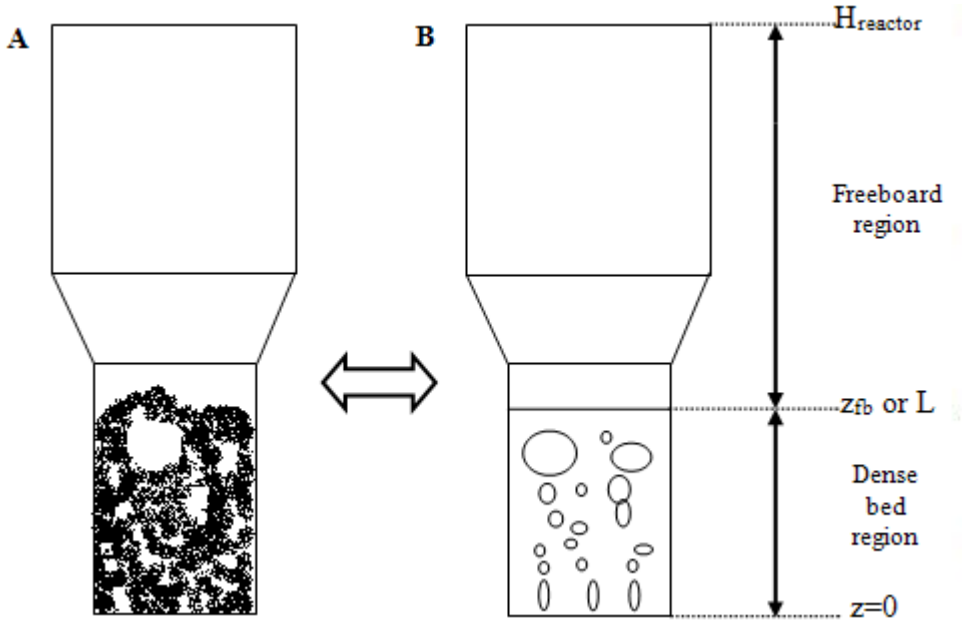

Figure 3.1: Definition of regions in FBR (not to scale). 3.1A shows an axial 2D view of a fluidized bed with bubbles rising up within the bed. 3.1B depicts the fluidized bed outlined in 3.1A as an axial 2D view representing solid bed material as a continuous media and bubbles.

3.3.1. General assumptions and fluid-dynamic formulation

The biomass gasification in a FBR is a very complex process. Many phenomena are involved inside the reactor: biomass devolatilization, comminution of solids particles, chemical reactions, fluidization, mass and heat transfer between phases, etc. A new formulation presented is focused on the particular behaviour of biomass.

As follows, the model is explained to attain the modelling objective: a realistic approach of the biomass gasification process accounting for the bubble phase temperature which can influence on tar cracking and ash sintering. The development of the model is sort out in: general assumptions, conservation equations, kinetic model assumptions and method of calculation.

Prior to describe the model development, main hypothesis are presented. This establishes the frame on which conservation equations are constructed and kinetics applied. Thus, general assumptions of the proposed model are:

1. The FBR is modelled as a steady-state one-dimensional (axial profile) adiabatic reactor. Hence, there is no time dependence of states-variables as well as no horizontal variation of any variable.
2. The main features of the new formulation proposed in this work are:
    i. Isothermal conditions in the emulsion phase due to high energy transfer and solids mixing inside the dense region. The temperature in the emulsion phase is assumed as constant. The reactant solids temperature is assumed to be the emulsion phase value.
    ii. Energy balance for the bubble phase according to Ross et al. (2004) (table 3.2). It includes energy term due to chemical reactions and energy transfer term between bubble and emulsion phase. This last term deals with heat transfer by radiation, convection and gas bulk flow, being the last two ones expressed by the coefficient H_{BE} (table 3.1).
    iii. Instantaneous devolatilization (Radmanesh et al., 2006). The devolatilization process yields gases which form the so-called endogenous bubbles (Bruni et al., 2002; Solimene et al., 2003). These volatiles, f_{vol}, are assigned to the bubble phase appearing gradually along the FB height (Kaushal et al., 2010).
3. The model is based on the two-phase fluidization theory of Toomey and Johnstone (1952). The volumetric flow is divided into bubble and emulsion phases. The gas excess is assumed to rise as a solids-free bubble phase at velocity U_B while the gas in the emulsion phase is set as U_{mf}. Eq. (3.1) gives the assumed flow distribution.

$$Q_T = Q_B + Q_E \tag{3.1}$$

$$Q_0 = U_0 \cdot A_T = U_B \cdot A_B + U_E \cdot A_E \quad \text{at } z=0 \tag{3.2}$$

In Eq. (3.2) subscript "0" refers to the reactor inlet (z=0), where no reaction has taken place. Therefore, Eq. (3.2) is only valid at the reactor inlet. The cross-sectional areas for each phase:

$$A_B = \varepsilon_B \cdot A_T \quad (3.3), \qquad A_E = (1-\varepsilon_B)\cdot A_T \quad (3.4)$$

Eq. (3.2) shows the phase division and how the volumetric flow is distributed between the bubble and emulsion phases at the reactor inlet. If it is assumed that the emulsion phase superficial velocity is U_{mf} at z=0, then:

$$U_0 = U_{B)z=0} + U_{mf} \quad (3.5)$$

4. Gas flows in both the bubble and emulsion phases are modelled as plug flow reactor (PFR), as Yan et al. (1998) propose. The solid phase, forming by inert solid particles and reactant solids (char, soot, etc), is modelled as continuous stirred tank reactor (CSTR).

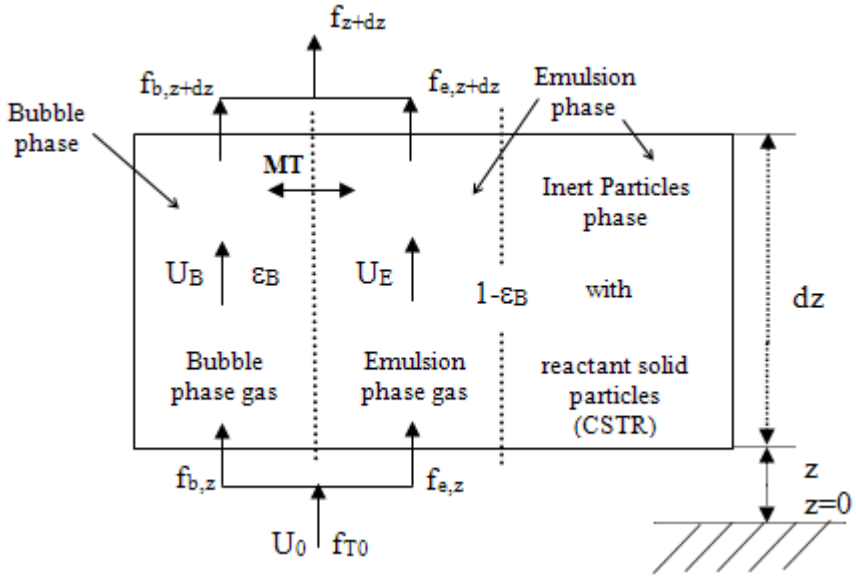

Figure 3.2: Schematic of control volume element of FBG. Gas in bubble and emulsion phase rises up with chemical reactions taking place and mass and convective transfer occurring between phases. At the same time, heterogeneous reactions yield gases that are transferred to the emulsion phase.

5. The relative amount of reactant solid is small compared to the inert bed particles fraction in the bed (Radmanesh et al., 2006). Hence, the solid volume fraction is assumed to be constant along the reactor height. In both the bed and freeboard regions, the physical properties are assumed to be uniform for any reactant solid particle.
6. The grid region in the fluidized bed is neglected since the jet penetration height in the fluidized bed is usually small compared to the bed expanded height and it hardly influences the process in large-scale systems (Gómez-Barea and Leckner, 2010).
7. Bubble throughflow velocity, $U_{th,}$ is considered by some authors (Grace and

Clift, 1974; Leckner et al., 1991; Pallarés and Johnsson, 2006) and based on experimental results with no agreement on the extent of throughflow. Furthermore, Grace and Clift (1974) summarized the results from experimental works dealing with the gas flow division in fluidized beds in Eq. (3.6):

$$U_{vis} = U_0 - m \cdot U_{mf} \qquad 0 \le z \le z_{fb}, \text{ (3.6)}$$

where "m", based on experimental data, varies in a wide range (1-18). For simulations in this PhD Thesis, m has been set as 1, corresponding to the standard two-phase theory of Toomey and Johnstone.

8. Visible bubble flow, U_{vis} and throughflow are related by means of Eq. (3.7) while the emulsion phase is assumed to remain as U_E at any height. The visible bubble flow affects the bubble rising velocity, u_{br}:

$$U_B = U_{vis} + u_{br} \qquad 0 \le z \le z_{fb}, \text{ (3.7)}$$

where u_{br} corresponds to the bubble rise velocity in isolation in a freely infinite bed (Davidson and Harrison, 1963).

9. The other fluid-dynamic parameters, tables 3.1 and 3.2, are calculated according to experimental correlations. To note that all these fluidization correlations are based on experimental results for non-reactive systems.

Parameter	Correlation (units explained in "Notation")		Reference
Re_{mf}	$Re_{p,mf} = \sqrt{33.7^2 + 0.0408 \cdot Ar} - 33.7$	(3.8)	Wen and Yu (1966)
	$Re_{pmf} = \frac{d_p \cdot \rho_g \cdot U_{mf}}{\mu}$ (3.9), $Ar = \frac{d_p^3 \cdot \rho_g \cdot (\rho_s - \rho_g) \cdot g}{\mu^2}$	(3.10)	
u_t	$Re_p = \frac{d_p \cdot U_0 \cdot \rho_g}{\mu}$ (3.11), $u_t = \left(\frac{4 \cdot d_p \cdot (\rho_s - \rho_g) \cdot g}{3 \cdot \rho_g \cdot c_D} \right)^{0.5}$	(3.12)	Kunii and Levesnpiel (1991)
	with $c_D = \frac{24}{Re_p} \cdot \left[1 + \left(8.1716 \cdot e^{-4.0655 \cdot \phi}\right) \cdot \left(Re_p\right)^{0.0964 + 0.5565 \cdot \phi}\right] + \ldots$	(3.13)	
	$\ldots \frac{73.69 \cdot \left(e^{-5.0748 \cdot \phi}\right) \cdot Re_p}{Re_p + 5.378 \cdot e^{6.2122 \cdot \phi}}$		
d_B	$d_B = d_{BM} - \left(d_{BM} - d_{B0}\right) \cdot e^{\left(-0.3 \cdot z / D_t\right)}$	(3.14)	Mori and Wen (1975)
	$d_{B0} = 87.16 \cdot \left(A_T \cdot \left(U_0 - U_{mf}\right) / n_d\right)^{2/5}$	(3.15)	
	$d_{BM} = 163.78 \cdot \left(A_T \cdot \left(U_0 - U_{mf}\right)\right)^{2/5}$	(3.16)	
u_{br}	$u_{br} = 0.711 \cdot \sqrt{g \cdot d_B}$	(3.17)	Davidson and Harrison (1963)
ε_B	$\varepsilon_B = \frac{1}{1 + u_{br} / U_{vis}}$	(3.18)	Leckner et al. (1991)

Table 3.1: Correlations for estimating fluid-dynamic properties of both the bottom dense region and the freeboard region.

Parameter	Correlation (units explained in "Notation")			Reference
a_B	$a_B = 6 \cdot \frac{\varepsilon_B}{d_B}$		(3.19)	Kunii and Levesnpiel (1991)
k_{BE}	$k_{BE} = \frac{U_{mf}}{3} + \left(\frac{4 \cdot D_{im} \cdot \varepsilon_{mf} \cdot u_B}{\pi \cdot d_B} \right)^{0.5}$		(3.20)	Sit and Grace (1981)
H_{BE}	$H_{BE} = 4.5 \cdot \left(\frac{U_{mf} \cdot \rho_g \cdot C_{p,g}}{d_b} \right) + 5.85 \cdot \left(\frac{\left(k_g \cdot \rho_g \cdot C_{p,g}\right)^{1/2} \cdot g^{1/4}}{d_b^{5/4}} \right)$		(3.21)	Kunii and Levesnpiel (1991)
F_{bex}	$F_{bex} = 1 + \frac{1.032 \cdot \left(U_0 - U_{mf}\right)^{0.57} \cdot \rho_g^{0.083}}{\rho_p^{0.166} \cdot U_{mf}^{0.063} \cdot D_t^{0.445}}$	if $D_t < 0.0635$	(3.22)	Babu et al. (1978)
	$F_{bex} = 1 + \frac{14.31 \cdot \left(U_0 - U_{mf}\right)^{0.738} \cdot d_p^{1.006} \cdot \rho_p^{0.376}}{\rho_g^{0.126} \cdot U_{mf}^{0.937}}$	if $D_t \geq 0.0635$	(3.23)	
F_s	$F_s = F_\infty + \left(F_{s,fb} - F_\infty\right) \cdot \exp\left(-a \cdot \left(z - z_R\right)\right)$		(3.24)	Wen and Chen (1982)
	$F_{s,fb} = 3.07 \cdot 10^{-9} \cdot A_T \cdot d_{BM} \cdot \left(\rho_g^{3.5} \cdot g^{0.5} \cdot \mu^{-2.5}\right) \cdot \left(U_t - U_{mf}\right)^{2.5}$		(3.25)	
	$F_{\infty,n} = E_{\infty,n} \cdot x_{fines}$		(3.26)	
	$a = 4 \cdot \frac{U_t}{U_0}$		(3.27)	
E_∞	$E_{\infty,} = 0.011 \cdot \rho_s \cdot \left(1 - \frac{U_t}{U_0}\right)^2$	if $U_t < U_0$	(3.28)	Wen and Chen (1982)
	$E_\infty = 0$	if $U_t > U_0$	(3.29)	

Table 3.2: Continuation of table 3.1.

To note that the bubble-emulsion mass transfer coefficient, k_{BE}, is calculated for all species taking into account the respective diffusivities. Regarding the FB height, this variable can be estimated in several ways, but here, the height at which the freeboard height is reached is estimated by a bed expansion coefficient, F_{bex}, proposed by Babu et al. (1978).

10. Ideal gas behavior is assumed in order to calculate changes in volumetric flow due to reactions as Jiang and Morey (1992), Abba et al. (2002) and Mahecha-Botero et al. (2007, 2009) propose. There is a relationship between molar flow and molar concentration at any reactor height, given for the volumetric flow at the corresponding height, Eq. (3.30). The total molar flow is expressed as:

$$f_T = f_B + f_E \qquad 0 \leq z \leq z_{fb}, \ (3.30)$$

$$f_T = C_T \cdot Q_T = C_B \cdot Q_B + C_E \cdot Q_E = f_B + f_E \qquad (3.31)$$

In these equations, the ideal gas law is considered implicitly. From Eq. (3.31), a general expression for molar concentration according to this assumption can be obtained at any reactor height, for each phase φ (bubble and emulsion):

$$C_{\varphi} = \frac{P_{\varphi}}{Z \cdot R \cdot T_{\varphi}} = \frac{f_{\varphi}}{Q_{\varphi}} = \frac{f_{\varphi}}{U_{\varphi} \cdot A_{\varphi}} \qquad \text{at any reactor height, } z, \text{ (3.32)}$$

Then, from Eq. (3.32), molar concentrations for any species "i" are obtained:

$$C_{Bi} = \frac{p_{Bi}}{Z \cdot R \cdot T_B} = \frac{f_{Bi}}{U_B \cdot A_B} \qquad \text{(3.33)}, \qquad C_{Ei} = \frac{p_{Ei}}{Z \cdot R \cdot T_E} = \frac{f_{Ei}}{U_E \cdot A_E} \qquad \text{(3.34)}$$

11. The boundary conditions for temperature, pressure and composition, in the lowest part of the freeboard region are the same as the exit conditions at the top of the dense bed region (De Souza-Santos, 1989, 2007).
12. Inventory of solids entrained. In fluidization, inert and reactant solids from the bed can be entrained and elutriated according to the operating conditions and physical properties of gas flowing through the FB.
    Although there is an extensive literature on entrainment and elutriation models of inert solids from fluidized beds as outlined by Wen and Chen (1982) and Gómez-Barea and Leckner (2010), this phenomenon is modelled by the correlation suggested by Wen and Chen (1982) in this PhD Thesis for simplicity. Nevertheless, there are practically no studies related to entrainment of solid reactants as char and soot coming from gasification reactions. Therefore, entrainment of reactant solids is not considered for the sake of simplicity.
    Finally, the importance and influence of char generation and entrainment in the freeboard in the final conversion of char during a FBG process has been proved (Miccio et al., 1999). However, in this PhD Thesis, attrition of reactant particles is not considered due to the lack of information based on experiments of entrainment and attrition of biomass fuels.

3.3.2. Conservation equations

In addition to general assumptions for FBG reactors, fluidization correlations and kinetic models at any reactor height, conservation equations are needed to close the system in order to describe the reactor performance at desired operating conditions.

The required conservation equations are mole and energy balances (table 3.3). Firstly, the mass balance (MB) for the dense bed and the freeboard regions are explained. Secondly, the energy balance (EB) for the dense bed region, the freeboard region and the overall energy balance (OEB) in the FB limits are described to close the equation set for simulating FBRs with application to biomass gasification. Thus, the model is constructed applying general assumptions defined above. It solves mole and energy balance for bubble and emulsion phase in the FB region and mole and energy balance in the freeboard region.

Mole Balances	
Bubble phase (Dense bed region)	
$$\frac{df_{Bi}}{dz} = A_T \cdot \left(a_B \cdot k_{BE} \cdot \left(C_{Ei} - C_{Bi}\right) + f_{vol} + \varepsilon_B \cdot \sum_{j=1}^{N_B} \nu_{ij} \cdot r_{Bj} \right)$$	(3.35)
Emulsion phase (Dense bed region)	
$$\frac{df_{Ei}}{dz} = A_T \cdot \left(a_B \cdot k_{BE} \cdot \left(C_{Bi} - C_{Ei}\right) + \left(1-\varepsilon_B\right) \cdot \left(\varepsilon_{mf} \cdot \sum_{j=1}^{N_E} \nu_{ij} \cdot r_{Ej} + \left(1-\varepsilon_{mf}\right) \cdot \sum_{j=1}^{N_E} \nu_{ij} \cdot r_{sj} \right)\right)$$	(3.36)
Freeboard region	
$$\frac{df_{fbi}}{dz} = A_{fb} \cdot \varepsilon_{fb} \cdot \sum_{j=1}^{N_g} \nu_{ij} \cdot r_{g\,j}$$	(3.37)
Energy Balances	
Bubble phase (Dense bed region)	
$$\frac{dT_B}{dz} = \frac{A_T \cdot \varepsilon_B \cdot \left[H_{BE} \cdot \left(T_E - T_B\right) - \sum_{j=1}^{N_g} \Delta H_j \cdot r_{Bj} + \frac{6}{d_B} \cdot k_{SB} \cdot \varepsilon_p \left(T_E^4 - T_B^4\right) \right]}{\sum_{i=1}^{N_i} f_{Bi} \cdot c_{p\,i}}$$	(3.38)
Emulsion phase (Dense bed region)	
Isothermal phase (T_E=T_p)	(3.39)
Freeboard region	
$$\frac{dT_F}{dz} = \left(\begin{array}{c} A_{fb} \cdot \left[\varepsilon_{fb} \cdot \sum_{j=1}^{N_g} \Delta H_j \cdot r_{g\,j} + \left(1-\varepsilon_{fb}\right) \cdot \varepsilon_{fb}^{*} \cdot \sum_{j=1}^{N_{g-s}} \Delta H_j \cdot r_{g-s\,j} \right] - \\ \sum_{i=1}^{N_i} \Delta H_i \cdot \frac{df_{fb\,i}}{dz} - A_{fb} \cdot U_w \cdot \left(T_{fb} - T_{ext}\right) \end{array} \right) \Big/ \sum_{i=1}^{N_i} f_{fb\,i} \cdot c_{p\,i}$$	(3.40)

Table 3.3: Model conservation equations for mole and energy balances.

3.3.2.1. Mole balance in the dense bed region

A mole balance for all species in the bubble and emulsion phases is applied to every control cell (figure 3.2). The structure of these conservation equations considers the most important phenomena in variation of molar flows. Separate mole balances are described for the gas and solids phases, explained as follows.

Gas phase mole balance

The mole balance formulation for any chemical species "i" in the bubbles and emulsion gas is described in table 3.3. It is important to notice that mass balances are written in molar flow rate terms for convenience (Mahecha-Botero et al., 2007). This form of equation simplifies the simulations, especially, when the overall number of

moles or volumetric gas flow can vary appreciably along the reactor height. This is a typical situation in biomass gasification reactors, since biomass has high volatile matter content (McKendry, 2002).

On the other hand, the mass balances for the bubble and emulsion phases account for mass transfer between phases, volatiles release and chemical reactions. These features are defined as follows:

- Equimolar interphase mass transfer (MT in figure 3.2), k_{BE}: mass transfer between phases, for any specie, due to molar concentration gradient is calculated with the corresponding bulk temperature at any FB height. Here, the bulk temperature is defined as the FB temperature which accounts for the contribution of the bubble and emulsion phase temperatures.
- Volatiles. The volatile content is assigned to the bubble phase as Bruni et al. (2002) and Solimene et al. (2003) propose. The release of volatiles (endogenous bubbles) is modelled by the term f_{vol}. It gradually takes the matter volatile fraction from biomass feeding to the reactor, that means, biomass volatiles composition is added up to the bubble phase along the FB height.
- Chemical reactions of existing species in the respective phases. The reaction set is introduced in the next section. The bubble phase considers homogeneous and tar cracking reactions. The emulsion phase includes homogeneous and heterogeneous gas-solid reactions.

Solid phase mole balance

A mole balance for any reactant solid "n" of interest: typically char and soot, is defined in the emulsion phase, involving heterogeneous reactions. The corresponding control volume for the solid phase fraction, at any reactor height, is $(1-\varepsilon_B)\cdot(1-\varepsilon_{mf})$.

As noted in assumption 4, perfect mixing for solids is assumed. Hence, char conversion is supposed to be the same at any FB height.

According to the char conversion iteration loop (figure 3.3), the char conversion (X_{char}) is discretized in each control volume for the reaction rates calculation of heterogeneous reactions (table 3.6). Besides, there is no mass transfer of solids between the bubbles and the emulsion phase: all inert and reactant solids remain in the emulsion phase.

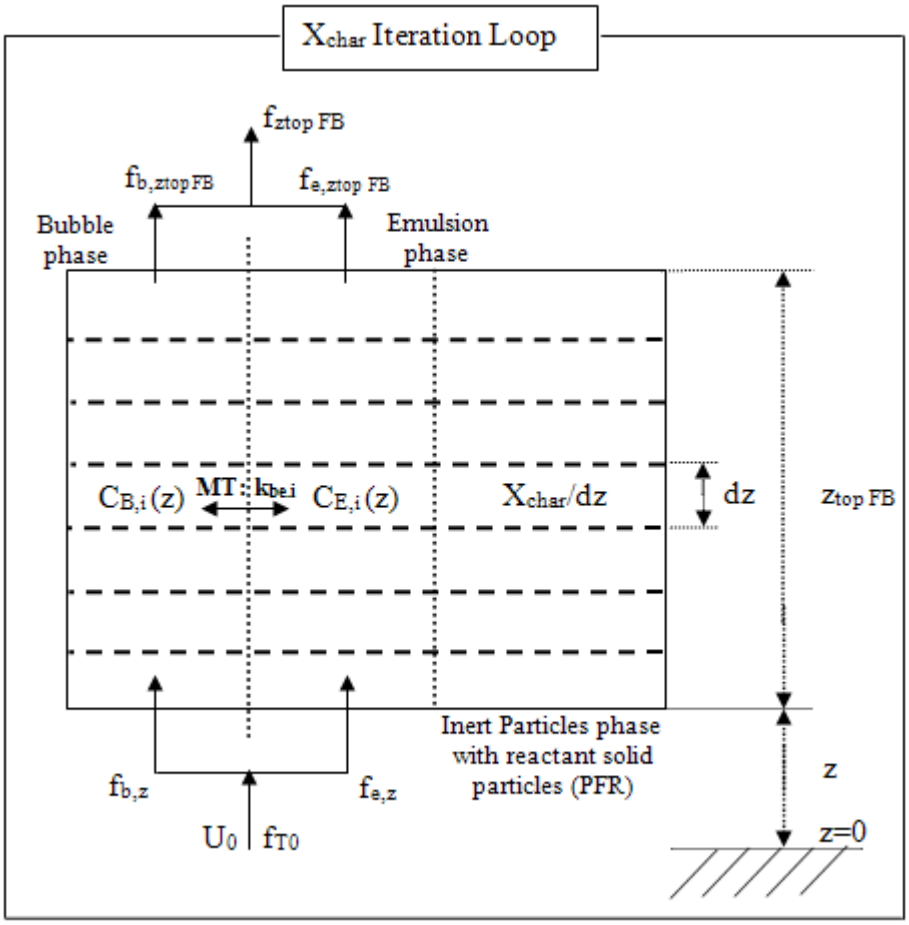

Figure 3.3: Detail of the mole balance in the fluidized bed region: mass transfer between phases ($k_{be,i}$) and gas-solid reactions.

3.3.2.2. Mole balance in the freeboard region

In the freeboard region, the mole balance considers both homogeneous and heterogeneous reactions. In addition, a mole balance for all species in the gas phase, modelled as PFR, is applied to every control cell. Besides, tar cracking reactions are considered to take place in the gas phase.

3.3.2.3. Energy balance in the dense bed region

Concerning to the thermal state of the bubble phase, the temperature profile evolution is affected by chemical reactions and heat transfer between phases by radiation, convection and flow of the bulk gas. Thereby, bubbles can act as “by-pass” yielding peaks of temperature (hot spots) which can enhance ash sintering and bed agglomeration and, then, the unscheduled and undesirable shut-down of the reactor.

The appearance of these so-called hot spots in the bubble phase is consequence of the high concentration of combustible gases coming from devolatilization. Furthermore, volatiles are more reactive than char with the oxygen molecules. After oxygen depletion, the gas composition is balanced by gasification reactions, typically

endothermic and which would lower the bubble phase temperature. Meanwhile, the emulsion phase is assumed to keep its temperature constant at any height.

3.3.2.4. Energy balance in the freeboard region

Some authors, as De Souza-Santos (2005, 2007) and Hemati et al. (2008), model the freeboard as a PFR distinguishing two phases: a gas and a solid phase, with energy exchange between them and the surroundings. As this PhD Thesis is focused on the dense bed region, the gas and the solids in the freeboard are considered to be one isothermal phase characterized by T_F, the freeboard temperature, as a function of z coordinate (height of the reactor).

The energy balance predicts the temperature profile evolution taking into account standard reaction enthalpies and energy losses in cases of non-adiabatic condition. The influence of the variation of molar flow of any species is also considered. As the reactor is considered to operate adiabatically, there is no heat exchange with the surroundings, U_w, in table 3.3.

On the other hand, the homogeneous gas-gas reactions and the heterogeneous reactions involving tar cracking reactions are assumed to occur in the gas fraction, ε_{fb}.

3.3.2.5. Overall energy balance

The purpose of the OEB is to allow getting a map of operating conditions that correspond to the performance of an autothermal gasifier of biomass. Thus, a respective map of performance reactor referred to quality syngas, it means, gas composition, LHV and tar content can be obtained.

The OEB in the limits of the FB is considered based on the energy flow entering at the reactor and the energy flow leaving the FB where bubbles reach the freeboard surface and coalescence completely (Ross et al., 2005; Ji et al., 2009; Gómez-Barea and Leckner, 2010). The OEB, that compares the energy input and output in the FB limits and acts a closure equation, is defined in the following equation:

$$HHV_{biomass} + Q_{preheater} + Q_{drying} = HHV_{char\_unreacted} + HHV_{syngas} + Q_{ncg} + Q_{syngas} \qquad (3.41)$$

The left side term represents the reactor energy input, which consists of: energy content transported by the biomass, $HHV_{biomass}$, preheated fluidizing gas, $Q_{preheater}$, and energy associated to biomass humidity, Q_{drying}. The energy output term (right side term) accounts for: higher heating value unreacted char, $HHV_{char\_unreacted}$, energy content from synthesis gas, HHV_{syngas}, sensible heat of syngas, Q_{syngas}, and of non-combustible gas, Q_{ncg}.

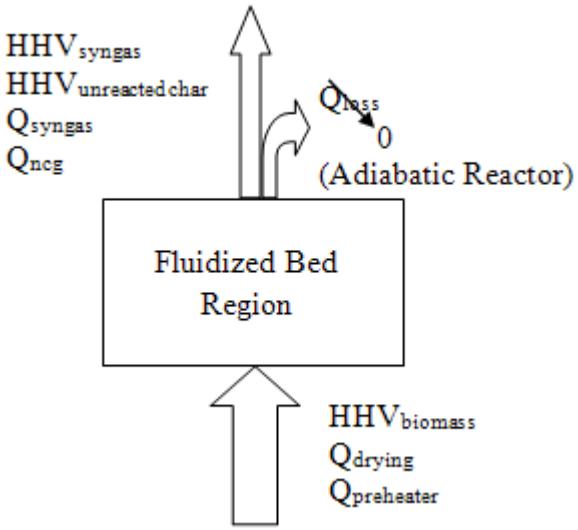

Figure 3.4: Energy balance in the limits of the FBR.

The OEB is addressed to check the performance of the reactor by means of varying the operating conditions for a set of biomass, fluidizing gas and FB design. This procedure would yield synthesis gas in an autothermal gasification process with FB technology.

3.4. Kinetic model

Another key step in FBG reactor modelling is to identify the species involved in reaction network as well as the reaction rate equations and the kinetic models to describe the biomass kinetic behaviour. Therefore, depending on how many species, kind of devolatilization, char and tar conversion models and reaction rate set for taking into account gasification and combustion processes inside reactor, simulation results can vary widely, even for the same set of operating conditions. However, all these topics are interrelated (Ji et al., 2009), and they are affected by devolatilization kinetics, species and lumping considered (Hajaligol et al., 1982; Nunn et al., 1985; Radmanesh et al., 2006).

The biomass kinetic behavior description is key in FBGR modelling due to the complex biomass nature. It requires the identification of the species involved in the reaction network, the lumping criteria and the reaction rate equations. Hence, model predictions can vary widely. This underlies in the complex nature of biomass. In fact, tar fraction can represent up to half of primary pyrolysis products from devolatilization.

3.4.1. Chemical species and lumping

The number of compounds is set according to what species are needed to describe their chemical behaviour and the biomass one. In biomass gasification processes running in FBRs, the typical required species are:

- O_2 and N_2 (inert) come from air inlet to the reactor. Due to high reaction rate of combustion reactions, O_2 is practically depleted at the reactor inlet.

- Non-condensable gases (H_2,, CO, CO_2, and CH_4), H_2O, C_2H_6 and tar (gas) come from biomass devolatilization (parameters from the work of Nunn et al. (1985)). The reaction rates composing the kinetic model for homogeneous reactions are shown later on in table 3.9.
- Although tar lumping is key in the final gas composition and an important source of uncertainty in model predictions, tar fraction is modelled according to Boroson et al. (1989) and tar (gas) is assumed as benzene according to Simell and Kurkela (1993) in this PhD Thesis. This will be discussed in next section.
- C_2H_6 represents non-condensable species of higher molecular weight than CH_4: from ethane to propane.
- Char fraction, which is the mass fraction remaining after devolatilization, is modelled as carbon (C). Char gasification and combustion reactions (tables 3.6 and 3.7) yield non-condensable gases. For the sake of simplification, a uniform conversion model with constant properties of char is considered. It is considered that char combustion reaction accounts for diffusion and chemical reaction as a series step process, while gasification char reactions by CO_2 and H_2O are described by a Langmuir-Hinshelwood mechanism.
- No soot generation is considered.
- Biomass is free of nitrogen and sulphur compounds.
- No catalysis activity of ash is considered.

3.4.2. Kinetic reaction network

From a chemical point of view, biomass is a source of volatile organic compounds. Gasification reactors yield these reaction products. As seen from the literature, gasification is a complex process involving several phenomena occurring simultaneously such as devolatilization, tar cracking, gasification and combustion processes (Gómez-Barea, 2010).

In this sense, to simplify model understanding, the kinetic reaction network is divided into four parts or submodels: devolatilization, char conversion, homogeneous reactions and tar conversion model. All submodels are based on global mechanisms.

3.4.2.1. Devolatilization model

The pyrolysis or devolatilization is a process consisting of biomass thermal degradation in absence of oxygen/air which leads to formation of solid (char), liquid (tar) and gaseous products (volatiles).

There is significant literature concerning devolatilization biomass modelling what have led to several points of view for modelling pyrolysis (Várhegyi et al., 1997; Semino and Tognotti, 1998; Moghdateri, 2006; Di Blasi, 2008).

On the one hand, pyrolysis models can describe the thermal decomposition of biomass by means of concentration evolution of individual components such as permanents gases (CO, CO_2, CH_4, H_2 and H_2O for example) or with pseudo-components or lumps: char, tars, volatiles and gases. For instance, Hajaligol et al.

(1982) and Nunn et al. (1985) have studied biomass devolatilization using the first type of approach whereas Koufopanos et al. (1989) based their investigations on lumps approach models.

Additionally, the lump models for primary pyrolysis can be sort out in two sub-categories as well: one-stage and multi-stage mechanism. They are based on the type of interaction between the pseudo-components, that is, direct reactions governing the kinetics for one-stage mechanisms or direct and parallel reaction networks for multi-stage mechanisms (Di Blasi, 2008). Figure 3.5A denotes the case of pseudo-components with no interaction among them while figure 3.5B depicts a possible chemical route in which the lumps react through direct and parallel reactions. For example, Koufopanos et al. (1989) established two reactions to yield $(volatile+gases)_1$ and $(char)_1$. Next, by means of a third reaction, other volatiles and char can appear in the form of so-called $(volatile+gases)_2$ and $(char)_2$. In this way, $(volatile+gases)_1$ and $(char)_1$ act as intermediates in the reaction scheme.

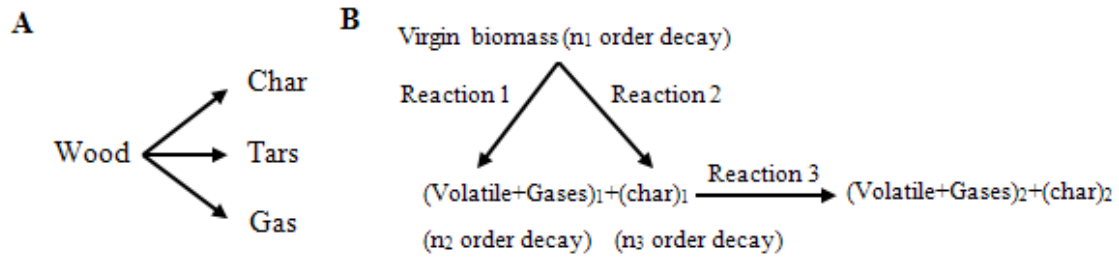

Figure 3.5: One-component mechanism for primary pyrolysis proposed by Shafizadeh and Chin (1977) (A) and multi-component mechanism for primary pyrolysis proposed by Koufopanos et al. (1989) (B).

On the other hand, Gómez-Barea and Leckner (2010) distinguish two kinds of devolatilization models. The first one is an instantaneous devolatilization which is assumed to occur at the reactor inlet so that a non-zero molar concentration profile for any specie is defined (Robert et al., 1988; Zhang et al., 1998; 1999; Ross et al., 2005). Furthermore, this pyrolysis model has been usually used for coal along the time. The second category of devolatilization models is based on kinetics from experiments at different temperatures and heating rates for a wide variety of biomasses (Hajaligol et al., 1982; Nunn et al., 1985; Boroson et al. 1989; Radmanesh et al., 2006). This second category can also be subdivided into global kinetics mechanism models (Di Blasi, 2008), distributed activation energy models (De Diego et al., 2002) and structural models (Chen et al., 1998; Niksa, 2000). Note that pyrolysis models of biomass proposed by Shafizadeh and Chin (1977) and Koufopanos et al. (1989) can also be stated as kinetic models too.

The simplification degree of the devolatilization model depends on how important two main phenomena occur in the FB reactor: convective transport time (mixing solid time) and devolatilization time (Ross et al., 2000; Gómez-Barea and Leckner, 2010). The relative importance of both phenomena can be evaluated by the Damkohler number, Da_{vol}, (Radmanesh et al., 2006; Gómez-Barea and Leckner, 2010), expressed as follows:

$$Da_{vol} = \frac{convective\ transport\ time}{devolatilization\ time} = \frac{L/U_0}{t_{dev}} \tag{3.42}$$

The convective transport time is assumed as residence time for a PFR, the same way that both bubble and emulsion phases are supposed to flow up in the fluidized bed. Meanwhile, the devolatilization time is calculated from kinetic data of the work conducted by Nunn et al. (1985), exposed in table 3.4.

Typically, the Damkohler number has a value around 7-14 (Radmanesh et al., 2006). In physical terms, this means that devolatilization occurs in the bottom zone, near the reactor inlet. Therefore, instantaneous devolatilization can be assumed. Furthermore, gases released from devolatilization are added gradually along the FB height because of gas mixing according to Kaushal et al. (2010).

Product	E_i (J/mol)	log k_{0i} (s^{-1})	y^* (wt %)
CO	61028	3.36	17.05
CO_2	59774	3.77	5.97
CH_4	69388	3.79	1.91
H_2O	48070	3.35	5.14
HCHO	53922	3.51	1.99
CH_3CHO	89034	5.80	1.4
C_2H_4	80256	4.41	1.17
C_2H_6	99066	5.87	0.17
C_3H_6	178904	11.20	0.41
Total gases	49324	2.88	41.01
Weight loss	68970	4.53	92.97

Table 3.4: Devolatilization parameters of each species.

3.4.2.2. Char conversion model

Solid particles have several features controlling physical and chemical phenomena (diffusion and reaction) in gas-solid reactions such as: shape, size and porosity. Consequently, solid conversion strongly depends on these particle properties as well as temperature, pressure inside the particle and the gas velocity surrounding the particle. Thus, solid conversion modelling becomes a challenge.

To note that any gas-solid reaction needs an intimate contact between gas and the reactant part of particles to yield reaction products. However, to make this possible, before occurring the chemical reaction, the reactant gas has to reach the particle surface, or even travel within the particle structure if solid is porous. Therefore, there are several series steps involved in a gas-solid reaction to be taken into account:

- Diffusion of reactant gas in the gas layer surrounding the particle.
- Diffusion of reactant gas within the channels existing in the particle.
- Adsorption of reactants on the surface of the particle.
- Chemical reaction on the surface of the particle. Reactant converts into products.
- Desorption of products off the surface of the particle.
- Diffusion of product gas within the channels existing in the particle.

- Diffusion of product gas in the gas layer surrounding the particle.

As stated, particle properties and operating conditions influence the relative importance of each step. Nevertheless, among all steps, one is the limiting and controlling step in the whole process and the solid conversion yield.

Gómez-Barea and Leckner (2010) have reviewed char conversion models existing in the literature which have been applied in FBR modelling to date. It should be noted that the choice and use of a char conversion model should be based on experimental evidences about the type of biomass of interest. Table 3.5 shows the basics features of each model.

Char conversion model	Features
Uniform Conversion Model (UCM)	uniform conversion and density with time
	constant size particle, $d_p=d_{p0}$
	reaction on the particle surface
	particle and local conversion are the same
	particle effectiveness factor of 100%
Shrinking Unreacted Particle Model (SUPM)	reaction on the particle surface
	ash peels off, if exists
	$d_p=d_{p0}(1-x_c)^{1/3}$
	appropriate for relatively non-porous char
Shrinking Unreacted Core Model (SUCM)	reaction at the core surface
	ash layer remains attached
	$d_p=d_{p0}$
	$d_c=d_{p0}(1-x_c)^{1/3}$
	valid for initially non-porous char
Progressive Model with Shrinking (reacting) Particle (PMSP)	reaction throughout the particle
	ash peels off, if exists
	$d_p=d_p(x_c)$
	extension of SUPM for porous char
Progressive Model with Shrinking (reacting) Core (PMSC)	reaction throughout the particle
	ash layer remains attached
	$d_p=d_{p0}$ but $d_c=d_c(x_c)$
	extension of SUCM for porous char

Table 3.5: Basic features of the most important char conversion models existing in the literature.

On the contrary, figure 3.6 depicts the temporal evolution of solid particle according to each model (with no time-scale).

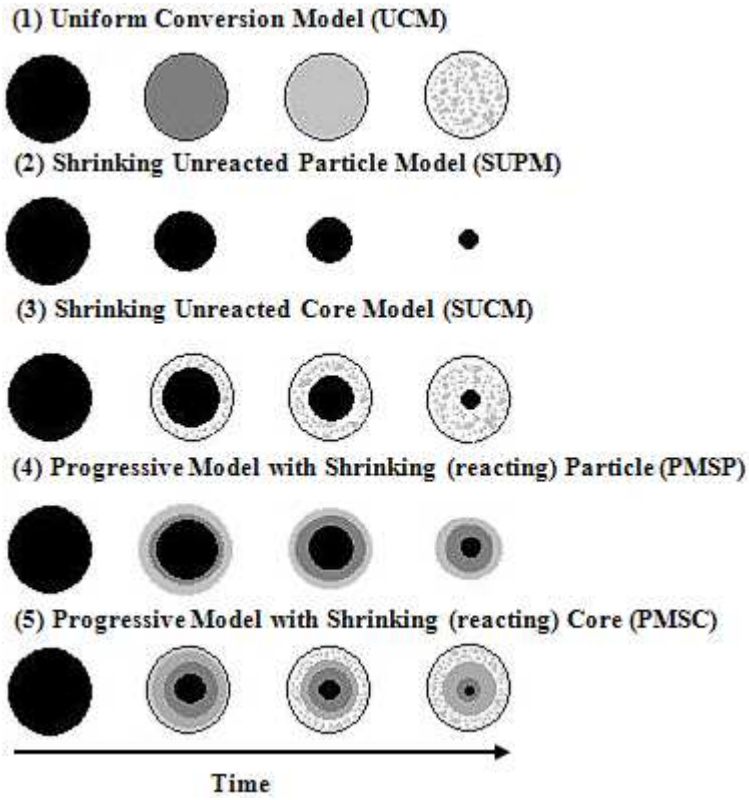

Figure 3.6: Single particle char conversion models. Black colour means unreacted carbon. White colour means ash. Grey scale means intermediates states of the particle conversion. Models (1) to (3) are the classical ones while models (4) and (5) are extension of (2) and (3) for porous char, allowing particle to take place within the shrinking core/particle. Figure adapted from Gómez Barea and Leckner (2010).

On the other hand, in the FBR modelling, two point-scales of view can be distinguished: the reactor scale and the particle scale. Obviously, the strategy adopted leads to a group of assumptions to make and the modelling of FBRs. Here, in spite of the complex nature of solid conversion models, the purpose of the work is to focus on the reactor scale, not the particle one. Therefore, the features of the char conversion model are listed as follows, based on the UCM:

- Uniform conversion, density and particle size with time.
- Particle properties: shape, density and particle size, do not change.
- Particle and local conversion are the same.
- Chemical reaction takes place on the surface of the particle.
- Kinetic constant of reaction R1 computes taking account diffusion and chemical reaction as a series step process:

$$k_{(1)} = \frac{1}{1/k_g + 1/k_r} \tag{3.43}$$

Where k_g expresses the diffusion of gas through the solid and k_r represents the kinetic constant of the combustion reaction (R1).

The chemistry of char, both gasification and combustion heterogeneous reactions, is presented in tables 3.6, 3.7 and 3.8.

There is a competitive consumption involving O_2, CO_2 and H_2O, so, this makes it difficult to know how much H_2O and O_2 are consumed in each reaction. For this reason, two splitting factors are defined: α and β. Parameter α defines the CO/CO_2 distribution of carbon from char to CO and CO_2 in char combustion reaction, while β defines the same distribution of species in char gasification reaction.

The splitting factor α includes the product distribution in CO and CO_2 because char combustion can be due to partial oxidation and complete oxidation simultaneously. The basic reactions, merged in reaction R3 according to Agarwal and Linjewile (1995), involve:

$$C + O_2 \rightarrow CO_2$$

$$C + \frac{1}{2}O_2 \rightarrow CO$$

On the other hand, the heterogeneous water gas shift reaction can consume steam by the reactions presented below. Then, both char gasification reactions are merged in R3 with another splitting factor, β, fixed as 1.2 by Matsui et al. (1985):

$$C + H_2O \rightarrow CO + H_2$$

$$C + 2H_2O \rightarrow CO_2 + 2H_2$$

Finally, the CO_2 gasification reaction is considered in the reaction set as R5.

No.	Reaction	Kinetic equation (mol/m^{3}s)	Reference
R3	$\alpha C + O_2 \rightarrow 2(\alpha-1)CO + (2-\alpha)CO_2$	$r = k_r \cdot C_{O_2}$	Field et al. (1967)
R4	$C + H_2O \rightarrow (2-\beta)CO + (\beta-1)CO_2 + \beta H_2$	$r = \frac{k_{(2)} \cdot C_{H_2O}}{1 + K_{k\_H_2O} \cdot C_{H_2O} + K_{k\_H_2} \cdot C_{H_2} + K_{k\_CO} \cdot C_{CO}}$	Matsui et al. (1985)
R5	$C + CO_2 \rightarrow 2CO$	$r = \frac{k_{(3)} \cdot C_{CO_2}}{1 + K_{k\_CO_2} \cdot C_{CO_2} + K_{k\_CO} \cdot C_{CO}}$	Matsui et al. (1987a; 1987b)

Table 3.6: Kinetic rate expressions of heterogeneous reactions in biomass gasification simulations.

No.	Reaction	Units	Reference
R3	$k_r = 5.957 \cdot 10^2 \cdot T_p \exp\left(-\frac{149{,}440}{R \cdot T_p}\right) \cdot \frac{6}{d_p}$	1/s	Field et al. (1967)
	$\alpha = \frac{1 + 2 \cdot fr}{1 + fr}$, $fr = 4.72 \cdot 10^{-3} \cdot \exp\left(\frac{37{,}737}{R \cdot T_p}\right)$		Agarwal and Linjewile (1995)

Table 3.7: Kinetic parameters of char combustion reaction.

No.	Reaction	Units	Reference
R4	$k_{(2)} = 2.39 \cdot 10^{2} \cdot \exp\left(-\frac{129{,}000}{R \cdot T}\right) \cdot \frac{\rho_{char}}{M_{char}} \cdot (1 - X)$	1/s	Matsui et al. (1985)
	$K^{(2)}_{k\_H_2O} = 3.16 \cdot 10^{-2} \cdot \exp\left(-\frac{30{,}100}{R \cdot T}\right)$	m^3/mol	
	$K^{(2)}_{k\_H_2} = 5.36 \cdot 10^{-2} \cdot \exp\left(-\frac{59{,}800}{R \cdot T}\right)$	m^3/mol	
	$K^{(2)}_{k\_CO} = 8.25 \cdot 10^{-5} \cdot \exp\left(-\frac{96{,}100}{R \cdot T}\right)$	m^3/mol	
R5	$k_{(3)} = 4.89 \cdot 10^{7} \cdot \exp\left(-\frac{268{,}000}{R \cdot T}\right) \cdot \frac{\rho_{char}}{M_{char}} \cdot (1 - X)$	1/s	Matsui et al. (1987a; 1987b)
	$K^{(3)}_{k\_CO_2} = 6.60 \cdot 10^{-2}$	m^3/mol	
	$K^{(3)}_{k\_CO} = 1.2 \cdot 10^{-1} \cdot \exp\left(-\frac{25{,}500}{R \cdot T}\right)$	m^3/mol	

Table 3.8: Kinetic parameters of char gasification reactions.

3.4.2.3. Homogeneous kinetic reactions

Besides devolatilization and char conversion processes, gas species undergo homogeneous reactions. These reactions, gasification and combustion of permanent gases, can happen in both bubble and emulsion phases in the dense bed region as well as in the freeboard region in the FBG reactor.

Regarding exothermic combustion reactions of H_2, CO, CH_4 and C_2H_6, R6-R8 and R11 (table 3.9), may occur in the bubble and emulsion phases with the corresponding temperatures and gas composition at any reactor height. Once depletion of O_2 has happened, water-gas shift reaction and steam reforming, R9 and R10 may take place until the equilibrium state is reached.

No.	Reaction	Kinetic equation (mol/m^3s)	Reference
R6	$H_2 + \frac{1}{2}O_2 \rightarrow H_2O$	$r = 1.08 \cdot 10^{10} \cdot \exp\left(-\frac{125{,}525}{R \cdot T}\right) \cdot C_{O_2} \cdot C_{H_2}$	Kerinin and Shifrin (1993)
R7	$CO + \frac{1}{2}O_2 \rightarrow CO_2$	$r = 1.78 \cdot 10^{10} \cdot \exp\left(-\frac{180{,}032}{R \cdot T}\right) \cdot C_{CO} \cdot C_{H_2O}^{0.5} \cdot C_{O_2}^{0.25}$	Dryer and Glassman (1973)
R8	$CH_4 + \frac{1}{2}O_2 \rightarrow CO + 2H_2$	$r = 1.58 \cdot 10^{10} \cdot \exp\left(-\frac{202{,}641}{R \cdot T}\right) \cdot C_{CH_4}^{0.7} \cdot C_{O_2}^{0.8}$	Dryer and Glassman (1973)
R9	$CO + H_2O \rightarrow CO_2 + H_2$	$r = 2.778 \cdot \left(-\frac{12{,}560}{R \cdot T}\right) \cdot \left(C_{CO} \cdot C_{H_2O} - \frac{C_{CO_2} \cdot C_{H_2}}{K_{eq}}\right)$	Biba et al. (1978)
		$K_{eq} = 0.022 \cdot \exp\left(-\frac{3.473 \cdot 10^{4}}{R \cdot T}\right)$	
R10	$CH_4 + H_2O \rightarrow CO + 3H_2$	$r = 3.3 \cdot 10^{10} \cdot \exp\left(-\frac{2.4 \cdot 10^{5}}{R \cdot T}\right) \cdot C_{CH_4}^{1.7} \cdot C_{H_2}^{-0.8}$	Jess (1995)
R11	$C_2H_6 + 2.5O_2 \rightarrow 2CO + 3H_2O$	$r = 2.67 \cdot 10^{8} \cdot T^{0.5} \cdot \exp\left(-\frac{20131}{T}\right) \cdot C_{O_2} \cdot C_{C_2H_6}$	Zimont and Trushin (1969)

Table 3.9: Kinetic rate expressions of homogeneous reactions in biomass gasification simulations.

3.4.2.4. Tar conversion model

Due to the high volatile matter content in biomass, up to roughly half of primary pyrolysis products, tars can greatly influence on the gas composition and cause serious operational problems by blocking when condensing in downstream equipment. Thereby, tar fraction plays a key role both in reactor performance and designing gas cleaning downstream equipment before using the syngas produced. Then, it is important to choose carefully the lump species (lumping criteria) for the tar fraction at modelling FBR systems in order to study and to improve the efficiency of gas cleaning systems (Gerun et al., 2008).

As presented in the introduction section, tar fraction is a very complex mixture of components with a heavier molecular weight than permanent gases and the so-called C_2 and C_3 fraction. This fraction of tars comprises a wide range of chemical species which tend to be refractory and then, difficult of being removed by means of thermal, catalytic and physical processes (Li and Suzuki, 2009).

Despite of the complex nature of tars, some research works have dealt with it in order to elucidate the reaction network involved and to improve the predictions of tars kinetic models in FBRs. For instance, one single mechanism to understand the tar formation and evolution in reacting atmosphere in FBRs with the temperature is the one proposed by Elliot (1988), figure 3.7.

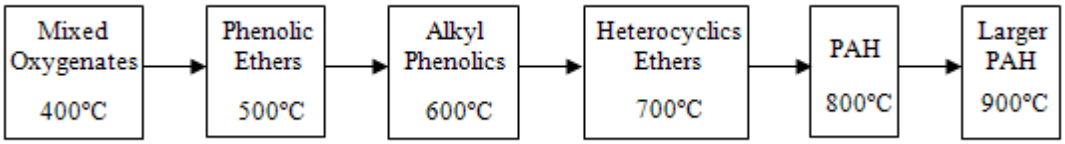

Figure 3.7: Scheme of tars evolution with temperature proposed by Elliot (1988).

Investigations addressed to study the tars properties with temperature have also been conducted. Kiel et al. (2004) concluded that tars can be sort out in 5 groups or classes, table 3.10. This study also stands out the dependence and importance of the dew tar point with the tar composition and concentration (figure 3.8). Another detailed and complex tar classification has been proposed by Milne and Evans (1998).

Tar class	Properties	Representative compounds
1	Very heavy tars, cannot be detected by GC	Determined by substracting the GC-detectable tar fraction from the total gravimetric tar
2	Tars contaning hetero atoms, highly water soluble compounds	Pyridine, phenol, cresols, quinoline, isoquinoline, dibenzophenol
3	Normally light hydrocarbons with single ring, do not pose a problem concerning to solubility and condensability	Toluene, ethylbenzene, xylenes, styrene
4	2 and 3 rings compounds, condense at low temperature even at very low concentration	Indene, naphthalene, methylnaphthalene, biphenyl, acenaphthalene, fluorene, phenanthrene, anthracene
5	larger than 3-ring, condense at high-temperatures at low concentrations	Fluoranthene, pyrene, chrysene, perylene, coronene

Table 3.10: List of classes of tars by Kiel et al. (2004).

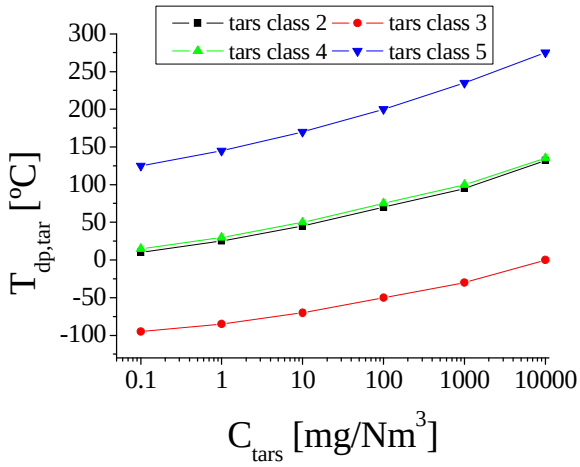

Figure 3.8: Tar dew point with tar concentration for different classes of tar (Kiel et al., 2004).

As Gómez-Barea and Leckner (2010) point out, tar modelling has been focused on simplifying the tar formation, conversion scheme as well as all the kinetic data for estimating the reaction rates. Notably, most conversion schemes are global mechanisms, with no representation of elementary steps which explain the interaction among tar lumps. This FBR modelling review also stands out that, to date, all research gives kinetics of the tar formation and secondary decomposition.

Gómez-Barea and Leckner (2010) have reviewed tar conversion models in last decades concluding that three different types of approach for tar modelling can be distinguished. The first procedure for tar lump modelling, the simplest method, consists of taking one compound that represents gravimetric tar for describing the tar concentration in FBR systems. In the second way, specie is chosen as lump compound: acetol ($C_3H_6O_2$) (Morf, 2002), anisole (C_7H_8O) (Fiorenza et al., 2007), phenol (C_6H_6O) (Ji et al., 2009), toluene (C_7H_8) (Taralas et al., 2003), naphthalene ($C_{10}H_8$) (Morf et al., 2002) or benzene (C_6H_6) (Petersen and Werther, 2005), for being qualitatively representative of a tar class. Eventually, the third approach considers a continuous representation of the tar mixture that evolves with time. This late procedure assumes the reactivity of a given compound depending on its molecular weight.

Then, it can be seen that there is no agreement in tar lumping but several tar modelling strategies lacking more insights in how tar reaction network occurs in order to obtain more descriptive and accurate tar conversion models. Further research might lead to better predictions of tar conversion in FBR systems (Gómez-Barea and Leckner, 2010).

For this reason, the tar conversion model assumed in this PhD Thesis for FBGR modelling is based on a global mechanism. The tar cracking model adopted considers benzene as tar lump since benzene can account up to 60-80% of tar fraction (Simell and Kurkela, 1993). Then, benzene would play a key role in tar decomposition (Jess, 1996a). Furthermore, the kinetic rate at which benzene would break into simpler species (permanent gases) and gravimetric tar (inert tar) is supposed to take place by means of a single-step mechanism (Boroson et al., 1989), presented in table 3.11. The yield of tar

cracking into permanent gases and inert tar is described by the stoichiometry of Boroson et al. (1989) as well (table 3.12). Finally, this tar conversion model is assumed to occur in both the bottom dense region and the freeboard region.

No.	Reaction	Kinetic equation (kg/m^{3}s)	Reference
R12	$tar(gas) \rightarrow \upsilon_{H_2} H_2(g) + \upsilon_{CH_4} CH_4(g) + \upsilon_{CO} CO(g) + \upsilon_{CO_2} CO_2(g) + \upsilon_{tar} tar_{inert}$	$r = \upsilon_i \cdot 10^{4.98} \cdot \exp\left(-\frac{93}{R \cdot T}\right) \cdot C_{tar}$	Boroson et al. (1989)

Table 3.11: Kinetic rate expressions of the tar conversion model used in biomass gasification simulations.

Component	ν_i
H_2	0.0173316
CH_4	0.0884052
CO	0.5633160
CO_2	0.1109316
Secondary tar	0.22

Table 3.12: Stoichiometric coefficients for tar cracking model proposed by Boroson et al. (1989).

The reason why the tar conversion model of Boroson et al. (1989) is chosen is due to that it has widely applied so far: Rath et al. (2002), Wurzenberger et al. (2002) and Radmanesh et al. (2006) are some examples.

3.5. Physical and transport properties

Since many transport properties depend on physical properties is necessary to estimate their respective values for both the bubble and emulsion phases, at any reactor height. Physical and transport properties are always considered as a function of temperature and gas composition. Tables 3.13 and 3.14 show the respective correlations for estimating the physical and transport properties for pure components as well as the multicomponent mixtures. Most of these properties are based on physical-chemical parameters as Lennard-Jones (Ω_μ) and Stockmayer Potential (Ω_k), dipolar moment (μ_p) or collision diameter (σ), summarized in tables C1 and F3, from Appendixes C and F respectively.

Correlation for pure components		Correlation for mixture		Ref[a]
Viscosity				
$\mu = 2.6693 \cdot 10^{-6} \cdot \frac{\sqrt{M \cdot T}}{\sigma^2 \cdot \Omega_\mu}$	(3.44)	$\mu_{mix} = \sum_{a=1}^{N} \frac{x_a \cdot \mu_a}{\sum_{b=1, b \neq a}^{N} x_b \cdot \phi_{ab}}$	(3.45)	Bird et al. (2002)
$\Omega_\mu = \frac{1.16145}{(T^*)^{0.14874}} + \frac{0.52487}{e^{(0.7732 \cdot T^*)}} + \frac{2.16178}{e^{(2.43787 \cdot T^*)}}$	(3.46)			
$\phi_{ab} = \frac{1}{\sqrt{8}} \cdot \left(1 + \frac{M_a}{M_b}\right)^{-1/2} \cdot \left[1 + \left(\frac{\mu_a}{\mu_b}\right)^{1/2} \cdot \left(\frac{M_b}{M_a}\right)^{1/4}\right]^2$	(3.47)			
$T^* = \frac{T}{\varepsilon_{kB}}$	(3.48)			

Table 3.13: Correlations for estimating physical and transport properties.

Correlation for pure components		Correlation for mixture		Ref[a]
Thermal conductivity				
$k = 8.31 \cdot 10^{-2} \cdot \frac{\sqrt{T/M}}{\sigma^2 \cdot \Omega_k}$	(3.49)	$k_{mix} = \sum_{a=1}^{N} \frac{x_a \cdot k_a}{\sum_{b=1,b\neq a}^{N} x_b \cdot \phi_{ab}}$	(3.50)	Bird et al. (2002)
with $\Omega_k = \Omega_\mu + 0.2 \cdot \frac{\delta^2}{T^*}$	(3.51)			
and $\delta = \frac{\left(3.162 \cdot 10^{-25} \mu_p\right)^2}{2 \cdot \left(\left(10^{-10} \cdot \sigma\right)^3\right) \cdot \varepsilon_{kB} \cdot k_B}$	(3.52)			
Diffusivity				
$D_{ab} = \frac{1.8583 \cdot 10^{-3} \cdot T^{3/2} \cdot \sqrt{\frac{1}{M_a} + \frac{1}{M_b}}}{P \cdot \sigma_{ab}^2 \cdot \Omega}$ *1	(3.53)	$D_{a,m} = \left(1 - x_a\right) \Big/ \left(\sum_{\substack{b=1 \\ b\neq a}}^{N} \frac{x_a}{D_{ab}} \right)$ *2	(3.54)	*1 Bird et al. (2002)
with $\sigma_{ab} = 0.5 \cdot \left(\sigma_a + \sigma_b\right)$ *1	(3.55)			*2 Wilke (1950)
Heat capacity				
Eq. (D.1) explained in Appendix D				JANAF Database
Heat transfer coefficient between sand and gas				
$\frac{h_p \cdot d_p}{k_{mix}} = 2 + 0.6 \cdot \mathrm{Re}_p^{1/2} \cdot \mathrm{Pr}^{1/3}$	(3.56)			Ranz (1952)
with $\mathrm{Re}_p = \frac{d_p \cdot U_g \cdot \rho_{g_{mix}}}{\mu_{mix}}$	(3.57)			
and $\mathrm{Pr} = \frac{c_p \cdot U_g}{k_{mix}}$	(3.58)			

Table 3.14: Continuation of table 3.13.

Finally, the gas mixture diffusivity coefficient is estimated by the method proposed by Wilke (1950), equation (3.54). This correlation is based on the diffusivity coefficients of binary mixtures, D_{ab}, estimated previously by Bird et al. (2002). The parameter x_a refers to molar fraction of a compound.

3.6. Calculation strategy

The simulation code for the gasifier solves simultaneously mole and energy balances in each control volume element for both FB and freeboard region. Additionally, fluid-dynamic parameters, physical and transport properties of species are calculated with correlations and estimations methods presented in tables 3.1, 3.2, 3.13 and 3.14.

Figure 3.9 explains the calculation process. A predictive variable step method is used to solve the mole and energy conservation equations. This method uses the optimised parameters of convergence (table 3.15) to monitors the absolute and relative errors of calculations. This operation is performed, by the block labelled as “control of errors”,

after each control volume in order to check the accuracy of the size step predicted. For the dense region, the model also iterates the char conversion value in the bed.

Regarding to the OEB, the bed temperature is iterated based on the Eq. (3.41) as some authors propose (Robert et al., 1988; Ross et al., 2005). Here, operating conditions (bed temperature, gas fluidizing temperature, ER and U_0/U_{mf}) are checked by means of the OEB to test the reactor performance until satisfying the tolerance (1E-6 in this work). Also, the tolerance value can be set close to 0 corresponding to the behaviour of an adiabatic gasifier or higher than 0, acting as a reactor with energy losses.

The simulation software is developed in Matlab R2010a. This calculation methodology allows, firstly, to draw a possible map of the syngas properties at the corresponding operating conditions, secondly, to gain more control of simulation results at any bed temperature and thirdly, to speed up the simulation calculations.

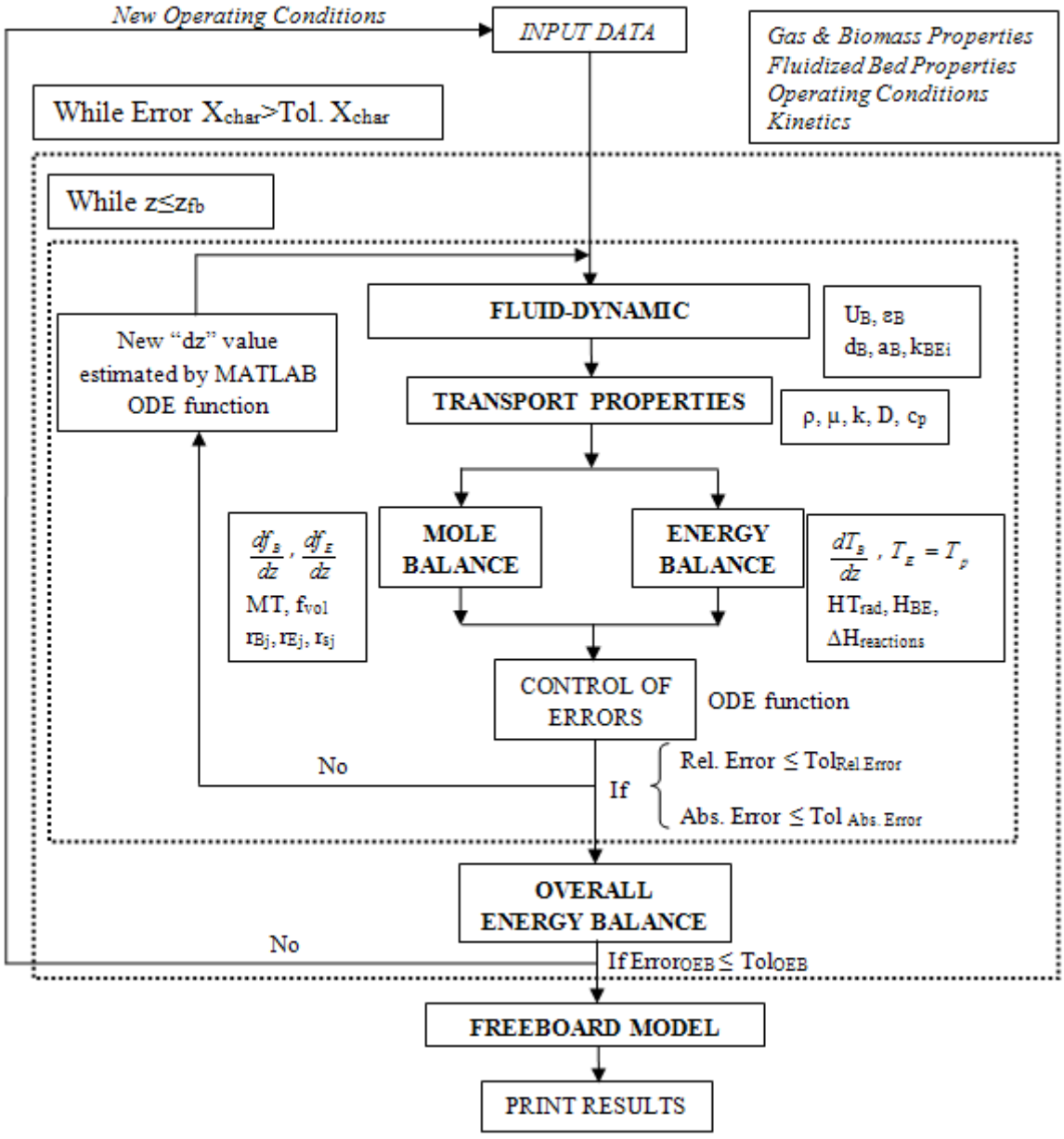

Figure 3.9: Diagram of the calculation strategy for the model proposed.

Parameter	Value
Relative tolerance	1.00E-03
Absolute tolerance	1.00E-06
Initial size step (dz)	1.00E-12
Maximum size step (dz)	1.00E-03

Table 3.15: Convergence parameters used in simulation campaign.

3.7. Results and discussion

Prior to discuss the predictive capability of the model approach proposed, the fluid-dynamic regime studied (bubbling regime) is presented. The figure 3.10 is addressed to compare the experimental works used for testing the proposed model and the predictions model from a fluid-dynamic point of view. To perform this analysis it should be noted that all cases are related to hot conditions (gasification operating conditions). On the contrary, the fluidization regime map is adapted from the work of Grace (1986c), for cold conditions (ambient temperature and pressure).

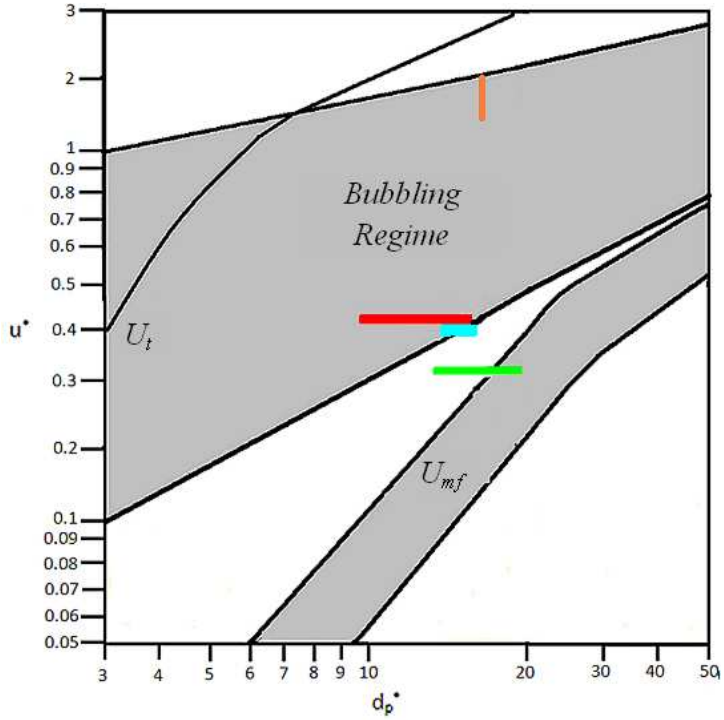

Figure 3.10: Location of experimental works of Narváez et al. (1996) (green), Gómez-Barea et al. (2005) (blue) and Alimuddin and Lim (2008) for testing of the proposed model and simulations run (orange) in the general fluidization regime map, adapted from the work of Grace (1986c).

With the available information, coloured lines for the corresponding works can be observed. Almost all lines drop in the bubbling regime but the one related to the experimental study of Gil et al. (1999) and to the operating conditions range performed in simulations. For these two cases bubbling fluidization could not be assured. However, it is expected that all operating conditions ranges drop above incipiently fluidization regime in hot conditions, assuring bubbling fluidization. Therefore, it can be said that the operating conditions considered for testing the proposed model are fair as figure 3.10 denotes. This is because of the similar dynamic behaviour in the experimental reactors and the one simulated.

It should be taken into account that simulation results are constraints to the overall energy balance in the FB limits as stated in previous section. The overall energy balance is addressed to determine the operating conditions that assure biomass gasification in a FB. The further aim would be to simplify the gasification phenomena referred to biomass devolatilization (energy and mass transfer from the biomass particle and the FB). Thus, simulation results are firstly discussed without paying attention to errors in overall energy balance. Later on, the analysis of the overall energy balance will be performed and linked to the following analysis of the model approach performance.

To evaluate the proposed model, a sensitivity analysis has been performed. Since the further objective in future investigations is to validate the model experimentally, reactor parameters used for simulations have been defined according to specification design of the pilot-plant scale BFBG reactor in the Thermal and Fluid Engineering Department facilities of University Carlos III of Madrid (table 3.16). The simulations obtained were compared with some experimental works from literature (Narvaez et al., 1996; Gil et al. 1999; Gómez-Barea et al., 2005; Campoy et al., 2009; Alimuddin and Lim, 2008) in terms of order of magnitude and trends of key properties in FBGRs: composition, LHV and tar content of the gas produced.

Distributor	**Value**	**Unit**	**Bed material properties**	**Value**	**Unit**
Number of orificies	177		ρ_s	2500	kg/m^3
Diameter of orifice	1,00E-03	m	d_p	400	μm
			ε	0.5	
			ϕ	0.8	
Reactor			**Operating conditions**	**Value**	**Unit**
Fluidized bed region			P	101325	Pa
L/D ratio	1.5	m	T_{preh}	150-300	ºC
Diameter	0.1413	m	T_{bed}	700-850	ºC
Freeboard region			ER	0.15-0.4	
Diameter	2.000	m	U_0/U_{mf}	6.5-11	
Total height	2.5	m			

Table 3.16: Bed (inert material) properties, design specifications of the FBR and operating conditions in simulation campaign.

It should be noted that temperature range performed in simulations comprises 700-830ºC while temperature range in investigations of Gil et al. (1999) and Alimuddin and Lim (2008) are 718-733 and 780-830ºC respectively. Thus, some differences in results are expected.

3.7.1. Simulation of gasification of *Cynara Cardunculus* L.

Table 3.17 shows simulation results of molar gas composition as dry basis (d.b.) for operating conditions range of interest in bubbling regime. On dry basis, the simulation of gasification of *Cynara Cardunculus* L. in a BFBG reactor yields a syngas with 4.79-14.84% of CO, 19.77-21.35% of CO_2, 6.11-15.00% of H_2 and 2.16-5.73% of CH_4. The lower heating value (LHV) and tar content of the syngas fall in the range of 2.25-6.25MJ/Nm^3 and 60-180g/Nm^3, respectively, as figure 3.11(A-B) shows. Eventually,

the FBG process simulation also yields a syngas-biomass ratio range of 1.309-2.392Nm^3/kg, accounting for N_2 in the raw syngas produced.

Run	T_{bed} (ºC)	T_{preh} (ºC)	*ER*	*FS*	Gas/Fuel (Nm^3/kg)	Gas composition (% d.b.)							T_B	
						CO	CO_2	H_2	CH_4	N_2	C_2H_6	Tar (gas)	Mean	Max
1	820	150	0.15	6.5	1.405	14.84	20.98	15.00	5.73	40.25	2.21	0.99	824.0	1009.0
2	780	200	0.2	8	1.568	11.32	21.15	12.01	4.53	47.91	1.75	1.34	820.1	1029.3
3	750	250	0.2	9	1.537	10.27	21.31	11.84	4.32	48.61	1.76	1.89	808.0	1034.1
4	760	250	0.15	9	1.309	12.28	21.35	13.81	5.04	42.38	2.26	2.87	804.0	1036.1
5	730	200	0.4	7	2.392	5.59	20.10	7.10	2.59	63.38	0.77	0.47	822.7	988.7
6	740	200	0.25	7	1.766	8.54	20.88	10.79	3.85	53.21	1.42	1.30	802.8	1030.3
7	830	200	0.2	7	1.627	13.15	20.44	12.65	4.92	46.61	1.80	0.42	842.0	1008.0
8	770	300	0.3	10	1.974	8.19	20.27	8.83	3.28	57.44	1.22	0.76	849.3	1055.8
9	700	200	0.4	10	2.311	4.79	19.96	6.11	2.16	65.36	0.81	0.83	850.1	1102.7
10	800	300	0.35	8	2.235	8.04	19.77	8.25	3.17	59.52	1.06	0.20	850.2	983.1
11	810	200	0.3	6.5	2.050	9.63	19.94	9.64	3.74	55.62	1.26	0.17	838.1	964.9
12	740	300	0.2	11	1.494	9.90	20.92	11.13	4.05	49.72	1.83	2.44	825.0	1130.9
13	790	300	0.3	7	2.006	8.79	20.09	9.25	3.48	56.66	1.24	0.49	847.9	1035.5
14	760	150	0.4	11	2.368	6.10	20.08	6.19	2.37	64.07	0.80	0.39	870.8	1054.2

Table 3.17: Gas composition (% d.b.) expressed as molar fraction, for corresponding feasible gasification operating conditions.

Figure 3.11 describes a map of LHV and tar content, respectively, as a function of operating conditions listed in table 3.14. As it can be seen in figure 3.11A, half of points fall in typical range for LHV, 4-6MJ/Nm^3 (McKendry, 2002) but points 5, 9 and 14 (2.31-2.61MJ/Nm^3) fall out the area enclosed by these experimental works (rectangle of dash line). Although the point 1 falls out, it can be considered inside this area as well as the points 8, 11 and 13 (3.59-3.99MJ/Nm^3), since they are close to the lowest LHV limit value, 4MJ/Nm^3. This difference is attributed to the tar cracking kinetics incertitude, which will be discussed later on. However, about 78% of the simulation points fall in the expectable range under this assumption.

Tar cracking kinetics incertitude also influences tar content model predictions (figure 3.11B) which differ from experiments (Narváez et al., 1996; Gil et al., 1999): 2-20g/Nm^3. As can be seen, the order of magnitude only matches nearly half of the points: 5, 7, 8, 9, 10, 11, 13 and 14 (62.27-89.61g/Nm^3), while the rest exceed the typical maximum value (20g/Nm^3). Therefore, one may presumably guess that the tar lumping and tar cracking model assumed are not so accurate.

As can be seen, Figure 3.11B shows the differences between simulations results and experiments conducted by Narváez et al. (1996), Gil et al. (1999) and Gerber et al. (2010) in LHV and tar content. The main reason why predictions do not agree so well can be explained by several important factors. The different nature of the lump compound used for simulations and the tar gravimetric fraction measured in experiments can yield tar content results that differ from experimental values. Bed material (sand, char, use of additives, etc), alkali and heavy metals from ash composition can also play an important role in the syngas quality (LHV, tar content) due they can act as tar cracking catalysts. For example, Gómez-Barea et al. (2005) and Campoy et al. (2009) use olivine and calcite as bed material in the FBG process. Gerber

et al. (2010) simulate a FBG process using char as bed material yielding up to 55g/Nm^3 of inert tar under adiabatic conditions.

On the other hand, if tar content is generally overpredicted, the tar kinetic model yields less permanent gases (mainly CO and H_2) and less gas flow production than expected. Taken into account the chemical network adopted for this study (tables 3.6-9 and 3.11-12), tar cracking is considered to take place through tar thermal cracking (Boroson et al., 1989). It is well known that decomposition of tars occurs by a wide number of reactions: combustion, gasification, thermal and catalytic ones. Here, combustion and gasification reactions with steam, hydrogen, methane and dioxide carbon have not been considered. Catalytic reactions of tars have not been taken into account since there is not so much information and the performance of the reactor would be adjusted by a coefficient method (Kaushal et al., 2010).

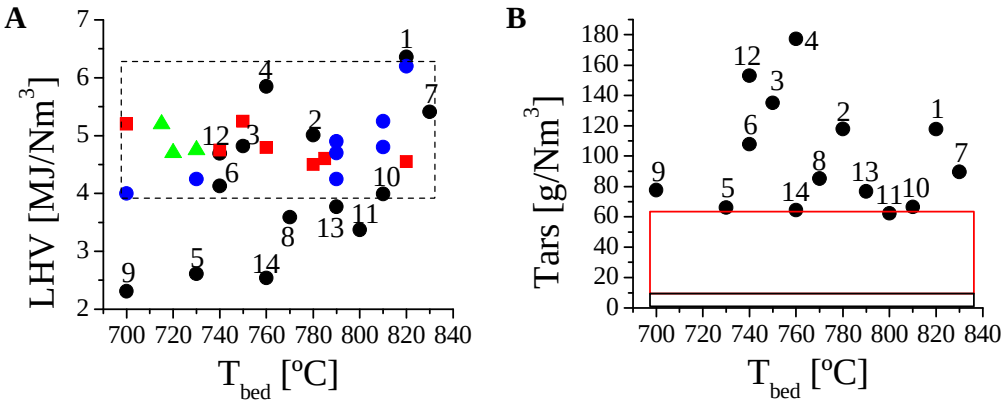

Figure 3.11: Map of LHV (A) and tar content values (B) for feasible gasification operating conditions. 3.11A compares simulation results (black) with experimental works of Narváez et al. (1996) (blue), Gómez-Barea et al. (2005) (red) and Alimmudin and Lim (2008) (green). Figure 3.11B shows discrepancies between simulation results (black) and experiments of Corella et al. (1999) (black square) and Gerber et al. (2010) (red square).

In order to elucidate the main causes of tar content discrepancies a temperature and molar gas composition profiles have been developed. For all the simulations, the temperature profile has shown a good agreement with works of Robert et al. (1988) and Ross et al. (2005). As an example, figure 3.12 shows the temperature axial profile along the reactor height for runs 1, 3, 8 and 13, where the bubble and emulsion phase temperatures are detailed in a zoomed region.

As can be seen, there is a bubble phase temperature increase with height, due to the O_2 depletion by volatiles combustion reactions as expected. Homogeneous gas-gas reactions are much faster than char consumption reactions. Additionally, the gas composition profile in figures 3.12(A-B) and 3.13(A-B) stand out the onset of hot spots in bubbles. This is noticeable at the reactor inlet, where the temperature raises quickly up to 980-1130ºC. This temperature peak may influence on the ash sintering and bed agglomeration what can cause problems in FBR's operation. Thereby, the prediction of hot spots location with high risk of defluidization would help to avoid reactor operational problems. For example, Natarajan et al. (1998) and Öhman et al. (2000)

have respectively reported bed agglomeration onset in FBR's at 900 ºC and 1000 ºC. Afterward, the bubble temperature drops since the heat transfer between phases prevails over the energy release from exothermic reactions. The lower the oxygen concentration, the less exothermic reactions contribution is (figures 3.14 and 3.15). In the zoomed region a second soft raise can be observed, followed by a gradual decrease after O_2 depletion. This is due to the combustion of remaining volatiles, which adds up heat. As can be seen, endothermic gasification reactions and bubble-emulsion heat transfer play a key role in the FB thermal state until reaching freeboard surface.

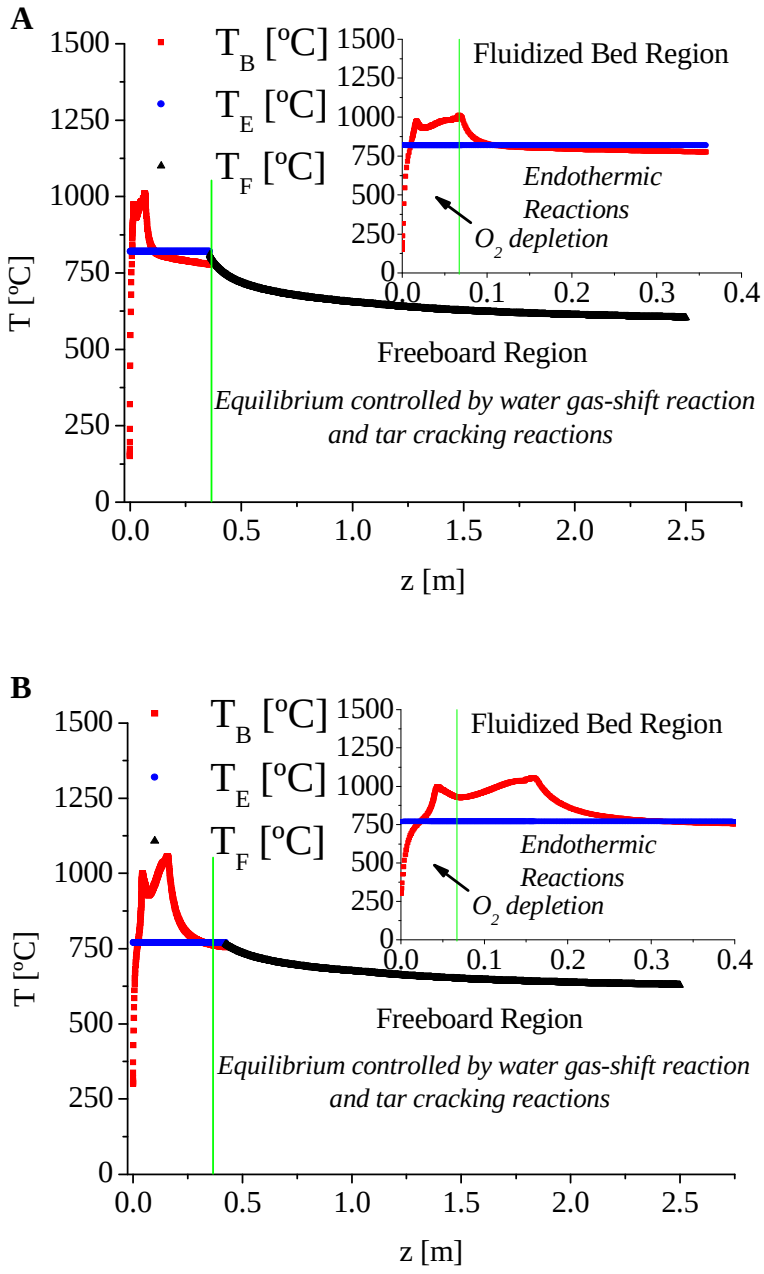

Figure 3.12: Temperature profiles including bubble and emulsion phases in the fluidized bed region and the freeboard region of the gasification reactor. Cases 1(A) and 3(B) from table 3.17 are represented as examples.

The freeboard temperature profile shows a soft temperature drop because of endothermic reactions of water gas-shift and tar cracking as in experiments (Narváez et al., 1996; Gil et al., 1999; Gómez-Barea, 2005).

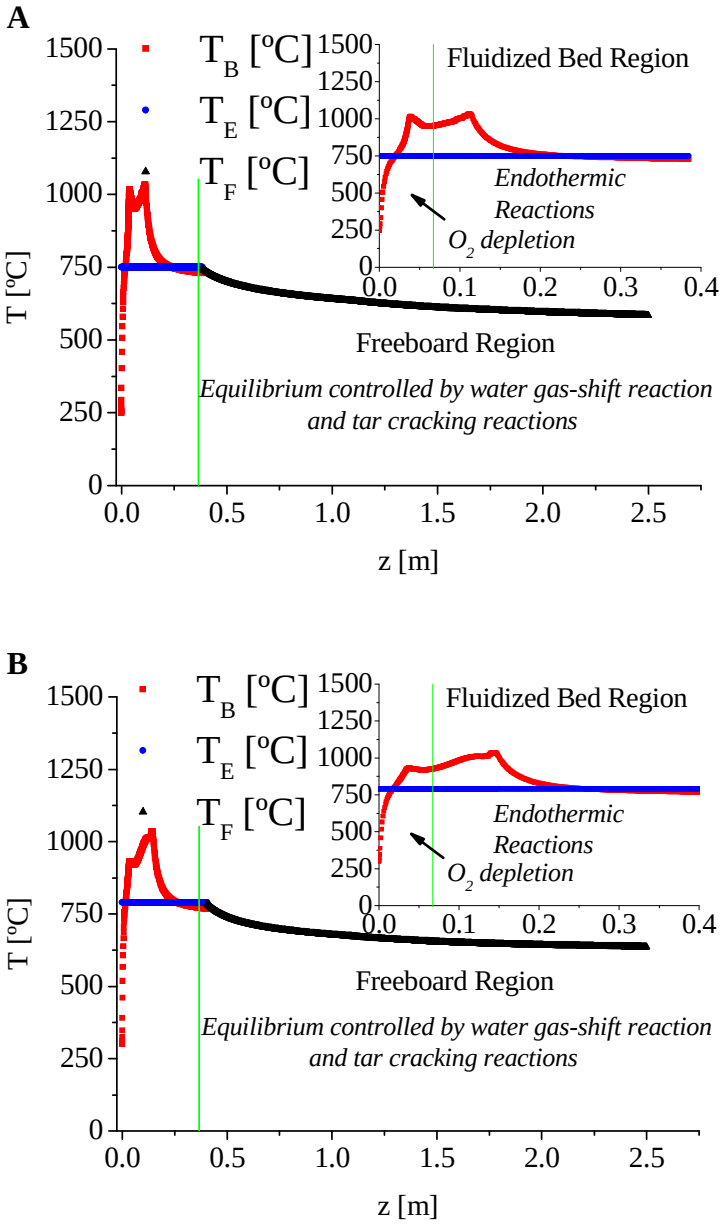

Figure 3.13: Temperature profiles including bubble and emulsion phases in the fluidized bed region and the freeboard region of the gasification reactor. Cases 8 (A) and 13 (B) from table 3.17 are represented as examples.

Molar gas composition profiles in both dense bed and freeboard region are depicted in figure 3.14(A-D) and 3.15(A-B) for runs 1, 3, 8 and 13 as well. A great composition variation occurs in the bed region due to fast combustion reactions (dense zoomed region). This also matches up with the main temperature change in the axial profile. In contrast to this, water-gas shift and tar cracking reactions play a major role in the gas composition adjustment in the freeboard region. The reactions yield H_2O and light compounds as CO, CO_2 and H_2.

As can be seen in the dense zoomed region reactive tars (benzene) becomes significantly important at some reactor height. Afterwards, in the freeboard region tars decrease until they reach an asymptotic value (0.17-2.87%), while the other species involved are balanced by equilibrium reactions (R9, R10).

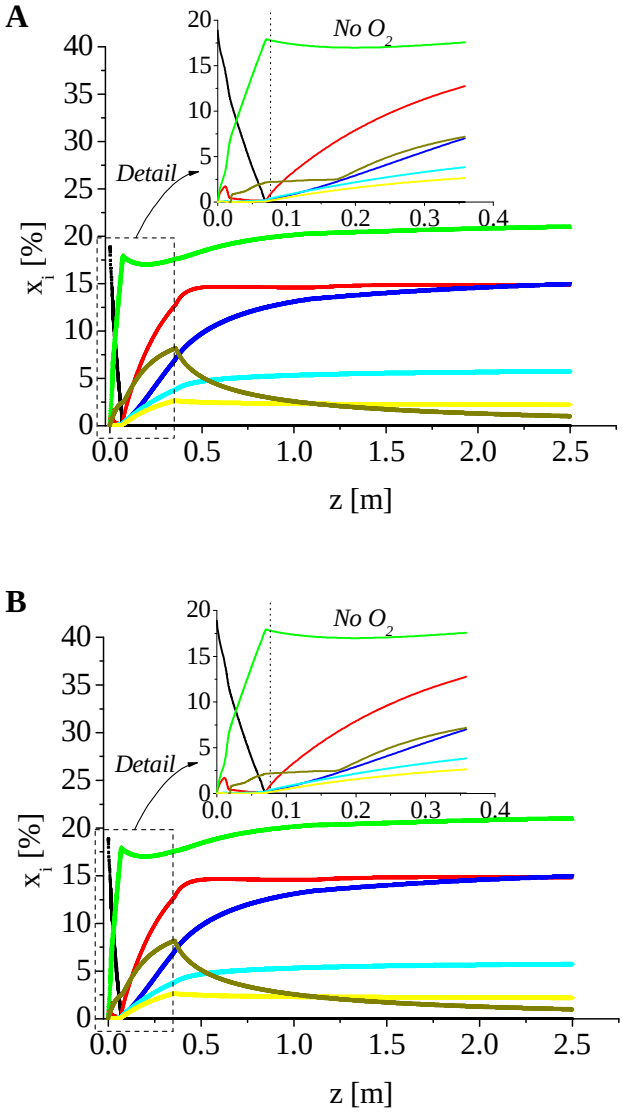

Figure 3.14: Molar gas composition profile (d.b.) of O_2 (black), CO (red), CO_2 (green), H_2 (dark blue), CH_4 (light blue), C_2 fraction (yellow) and tar (gas) (dark yellow) including bubble and emulsion phases in the fluidized bed region and the freeboard region of the gasification reactor. Cases 1(A) and 3(B) from table 3.17 are represented as examples.

As expected, O_2 is totally consumed around 2.5-5 cm above the distributor. The profiles for the rest of species vary softer than for the O_2 but the CO_2. According to that, it can be concluded that the CO_2 evolution is strongly linked to O_2 depletion. Furthermore, the CO, H_2 and CH_4 fractions grow rapidly because of the volatiles release and tar cracking reaction.

Although CO_2 and H_2 concentration predictions are higher than experimental results (Gómez-Barea, 2005) as well as CH_4 concentration predicted is lower than the CH_4

measured by Gómez-Barea et al (2005) and Alimuddin and Lim (2008). The composition predicted also suits reasonably well with values observed in literature. C_2 fraction predictions (0.77-2.26%) agree well with the range 0.2-3.3% and 2% measured by Gil et al. (1999) and Narváez et al. (1996), respectively. Note that the lumping criterion is crucial for the C_2 fraction determination.

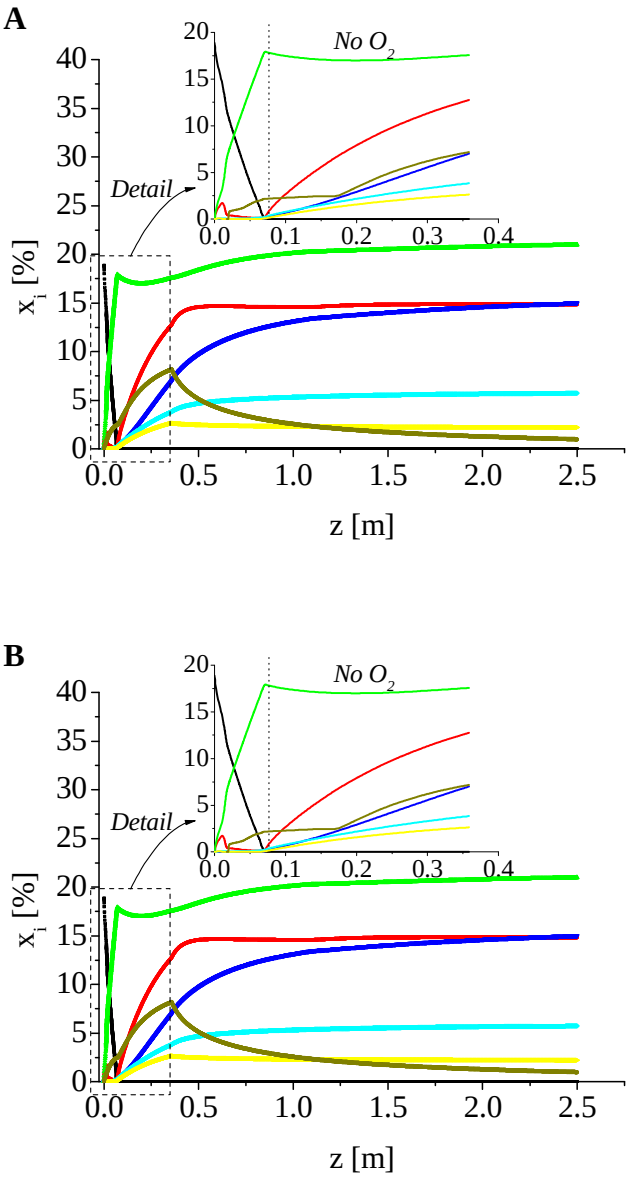

Figure 3.15: Molar gas composition profile (d.b.) of O_2 (black), CO (red), CO_2 (green), H_2 (dark blue), CH_4 (light blue), C_2 fraction (yellow) and tar (gas) (dark yellow) including bubble and emulsion phases in the fluidized bed region and the freeboard region of the gasification reactor. Cases 8 (A) and 13 (B) from table 3.17 are represented as examples.

Table 3.18 shows others important gasification properties that indicate the quality of the operation: HHV (2.57-7.02MJ/Nm^3), syngas flow produced (3.483-7.324Nm^3/h), cold and hot efficiencies (32.74-54.70% and 37.20-59.69%, respectively) and char conversion(24.48-87.77%).

Run	HHV (MJ/Nm^3)	Q_{gas} (Nm^3/h)	Cold eff (%)	Hot eff (%)	X_{char} (%)
1	7.02	4.690	54.70	59.69	36.59
2	5.54	5.190	48.11	52.77	42.20
3	5.34	5.377	45.38	49.70	36.24
4	6.47	6.742	46.85	51.02	24.48
5	2.90	3.802	38.25	43.09	80.66
6	4.58	4.406	44.63	49.10	47.13
7	5.96	4.311	53.85	59.28	51.68
8	3.97	5.544	43.40	48.38	59.19
9	2.57	5.565	32.74	37.20	54.48
10	3.72	4.077	46.16	51.79	87.77
11	4.41	3.483	50.14	55.80	82.05
12	5.19	7.324	42.94	47.15	28.46
13	4.16	4.890	46.30	51.58	67.51
14	2.80	5.589	36.84	41.99	77.31

Table 3.18: Others properties of the gasification quality: higher heating value (HHV), syngas flow produced, gasification efficiency and char conversion (X_{char}).

In regards to the simulations accuracy, the table 3.19 shows the error in the mass balance for both the dense bed region and the freeboard region. The error committed in the OEB is also shown.

Run	$Error_{BMbed}$ (%)	$Error_{BMfb}$ (%)	$Error_{BE}$ (%)
1	0.0980	0.0978	18.07
2	0.0388	0.0386	19.47
3	0.0647	0.0645	20.72
4	0.0971	0.0969	22.29
5	0.1370	0.1368	11.37
6	0.1479	0.1477	18.16
7	0.0839	0.0837	15.84
8	0.1103	0.1101	14.93
9	0.1526	0.1525	8.49
10	0.1420	0.1418	12.87
11	0.1307	0.1305	13.45
12	0.1015	0.1013	19.85
13	0.1253	0.1252	14.66
14	0.0530	0.0528	8.32

Table 3.19: Errors in mass and energy balance of simulations performed.

As it can be seen, the mass balance errors in the bed region and the freeboard region from 0.0388 to 0.1526% and from 0.0386 to 0.1525% respectively. Therefore, the choice of convergence parameters optimised (table 3.15) was right.

With respect to the OEB error, this varies in the range of 8.49-22.29%, what evidences the influence and importance of some key factors, such as uncertainty in tars lumping criteria, inaccuracy of tar cracking kinetic network modelling and the no consideration of catalytic effects of bed material (sand, char, etc) due to the lack of information related to that, in the FBR performance predictions as stated previously. This is in accordance with what Gómez-Barea and Leckner (2010) stand out: devolatilization and kinetic expressions greatly affect simulation results and modelling of char and tar conversion processes is least satisfactory; while Basu and Kaushal

(2009) point out: the major obstacle is to correctly fit kinetic parameters based on experimental investigation which is able to predict reactor performance, more accurately and for a wider range of operating conditions.

3.7.2. Model verification

The model developed for predicting the performance of BFBG reactors and presented in this PhD Thesis was compared against the experiments conducted by Campoy et al. (2009), which study air-steam gasification of biomass in a fluidised bed. Thus, air, air/steam and air/steam with oxygen enriched gasification processes are simulated in order to evaluate the predictive capability of the model.

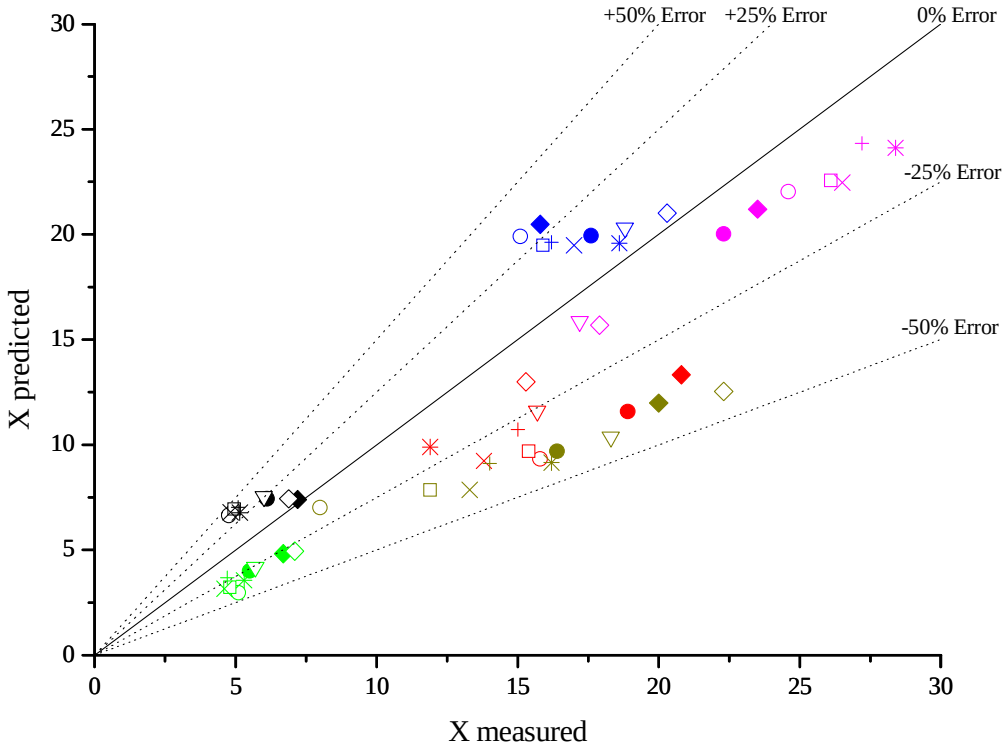

Figure 3.16: Comparison of molar gas composition of CO (red), CO_2 (blue), H_2 (dark yellow), CH_4 (green), Q_{gas} (pink) and LHV (black) from simulations with the experiments 1 (o), 2 ( ), 3 (x), 4 (+), 5 (*), 6 (·), 7 (∇), 8 (♦) and 9 (◊) carried out but Campoy et al. (2009).

As it can be seen, figure 3.16 exhibits the differences between the model predictions and experiments 1-9 carried out by Campoy et al. (2009). Around two-thirds of the predictions are inside the ± 25% error region. For example, for experiment 9 the composition obtained for CO_2 is 21% against 20% reported by Campoy et al. (2009). On the contrary, the simulation of experiment 2 yields a H_2 composition of 7.5% against 12%. The discrepancies found in this analysis are based on the aforementioned factors: tar criteria lumping, tar cracking kinetics and catalytic effects by bed material and ash composition from biomass. Although some simulations differ from experimental work,

the comparative study has proved that this model is a useful tool to yield a first reliable estimation about the FBGR performance and the biomass gasification quality. Therefore, the information provided by this model can be used to select the suitable technology for further processing.

3.8. Conclusions

A new approach in the formulation of biomass FBGR, which is based on the two-phase fluidization theory, has been proposed. This new scheme focuses on biomass behavior and characterizes the phenomena that take place in the bubble phase: temperature peaks due to volatiles combustion and instantaneous devolatilization. These phenomena are considered by an energy balance and a gradual addition of volatiles, both in the bubble phase. Global kinetic reactions have also been assumed.

A sensitivity analysis of the operating conditions has been conducted to test the proposed model. The simulation results show that this model can be used as a tool for designing biomass FBGR's:

- Gas composition of main components (CO, CO_2, H_2 and CH_4) and LHV,
- Temperature profiles and hot spots predictions,
- Tar content.

According to the simulation campaign and the model verification, it has been proven the model as a predictive tool in order to help others diagnosis methods in detecting important operational problems in FBR’s such as high tar concentration, ash sintering and bed agglomeration. The presence of impurities (ash melt fly and tars) may damage and inhibit downstream equipment operation by attrition, fouling and clogging. With respect to ash sintering, which is mainly caused by the bubbles ”by-pass”', those ash sintering-related risk regions can be detected by the temperature peaks reflected in the temperature profiles. This factor as well as the bed agglomeration can lead to FBG's defluidization and unscheduled reactor shut-down.

On the other hand, the discrepancies between model predictions and experimental works from literature are higher than expected. Gómez-Barea and Leckner (2010) state that devolatilization and kinetic expressions greatly influence simulation results (e.g. gas composition, tar content, char conversion). Such variations are related to the uncertainty in tars lumping criteria, inaccuracy of tar cracking kinetics and different use of tars measurement methods, as the tar content prediction suggests. Accordingly, Basu and Kaushal (2009) concluded that the major obstacle is to correctly fit kinetic parameters based on experimental research. This adjustment would be able to predict more accurately the reactor performance under a wider interval of operating conditions.

Furthermore, among the hypotheses considered, Gómez-Barea and Leckner (2010) stands out that char and tar conversion are the processes whose modelling is least satisfactory. Therefore, validation should be desired at lab-scale or larger scale in testing the models proposals. Thus, further experimental work would be addressed to tune up the proposed model approach here, in order to improve its predictive capacity. This

experimental research would be carried out in the pilot-plant scale BBFBG in the Thermal and Fluid Engineering Department facility of Carlos III University of Madrid (figure 3.15).

Figure 3.15: Pilot-plant scale Biomass Bubbling Fluidized Bed Gasifier (BBFBG).

3.9. Notation

Ar Arquimeder number, [-].

A_{fb} Cross-sectional area of reactor in freeboard region, [m^2].

A_T Cross-sectional area of the reactor at any height, [m^2].

a_B Interfacial area between bubbles and emulsion phases per unit bed volume unit, [m^2/m^3].

a Constant of the entrainment model, [m^{-1}].

C Molar concentration of species “i”, [mol/m^3].

C_{Bi} Molar concentration of species “i” in bubble phase, [mol/m^3].

C_{Ei} Molar concentration of species “i” in emulsion phase, [mol/m^3].

c_D Drag coefficient, [-].

c_p Heat capacity, [J/kg K].

D Diffusivity of species a in a multicomponent mixture of species, [m^2/s].

D_t Fluidized bed diameter, [m].

Da Damkohler number, [-].

d_B Bubble diameter, [m].

d_{B0} Initial bubble diameter at the distributor, [m].

d_{BM} Maximum bubble diameter due to total coalescences of bubbles, [m].

d_p Particle diameter, [m].

d_p^* Dimensionless particle diameter, [-].

F_∞ Flux of particles above the transport disengaging height, [kg/m^2s].

F_{bex} Bed expansion factor [-].

F_s Flux of particles in the freeboard, [kg/m^2s].

f_{Bi} Molar flow of species “i” in bubble phase, [mol/s].

f_{Ei} Molar flow of species “i” in emulsion phase, [mol/s].

f_{fb} Molar flow of gaseous species “i” in the freeboard region, [mol/s].

f_{T0} Total molar flow at the reactor inlet, [mol/s].

fr Product CO/CO_2 ratio, [-].

f_{vol} Molar flow of volatiles release at any height in the FB region, [mol/s].

g Gravity, [m^2/s].

K Adsorption kinetic constant [units depending on the reaction].

k Thermal conductivity, [W/m K]. Chemical reaction kinetic constant (units depending on the reaction).

k_{BE} Bubble-emulsion mass transfer coefficient, [m^3/m^2s].

k_{SB} Stefan-Boltzmann constant, [W/m^2K^4].

H_{BE} Bubble-emulsion heat transfer coefficient, [W/m^2 K].

h_p Gas-particle heat transfer coefficient, [W/m^2 K].

L/D Fixed bed height/bed reactor diameter ratio, [-].

M Molecular weight, [kg/kmol].

m Visible bubble flow parameter, [-].

N Number of reactions.

N_g Number of homogeneous reactions and heterogeneous tar cracking reactions in freeboard region.

$N_{g\text{-}s}$ Number of heterogeneous gas-solid reactions in freeboard region.

N_i Chemical species in bubble and emulsion phase. total chemical species in the freeboard region that participate in homogeneous and heterogeneous tar cracking reactions.

n_d Number of orifice openings in the distributor.

P Pressure, [Pa].

Pr Prandlt number, [-].

Q Volume flow, [m^3/s]. Heat flux, [J/s].

R Ideal gas constant, [J/mol K].

Re Reynolds number, [-].

r_{Bj} Reaction rate of homogenous reaction “j” in bubble phase, [mol/m^3s].

r_{Ej} Reaction rate of homogenous reaction “j” in emulsion phase, [mol/m^3s].

r_{sj} Reaction rate of heterogeneous reaction “j” in emulsion phase, [mol/m^3s].

$r_{g\,j}$ Reaction rate of homogeneous reaction “j” and heterogeneous tar cracking reactions in the gas fraction in the freeboard region, [mol/m^3s].

$r_{g\text{-}s\,j}$ Reaction rate of heterogeneous gas-solid reaction “j” in reactant solid fraction in the freeboard region, [mol/m^3s].

T Temperature, [K].

$T_{dp,tar}$ Tars dew point, [K].

T_F Freeboard temperature, [K].

T_R Standard temperature, [K].

t Time, [s].

U_0 Superficial velocity, [m/s].

U_B Bubble phase velocity, [m/s].

U_E Emulsion phase velocity, [m/s].

U_{mf} Minimum fluidization velocity, [m/s].

U_t Terminal velocity, [m/s].

U_w Overall bed to surroundings heat transfer coefficient, [W/m^{2}K].

u_{br} Velocity of a single bubble in an infinite freely-bubbling bed, [m/s].

u^* dimensionless gas velocity, [-].

X_{char} Conversion of char.

x_{fines} Elutriable/entrainable solid material fraction [-].

Z Acentric factor.

z Height, [m]. Axial position, [m].

z_{fb} Position of freeboard surface, [m].

$z_{reactor}$ Position of exit of reactor, [m].

Abbreviations

BFBG Bubbling Fluidized Bed Gasifier.

CFD Computational fluid-dynamics.

CSTR Continuous Stirred Tank Reactor.

EB Energy balance.

ER Equivalence Ratio. Air-Biomass ratio.

FBR Fluidized Bed Reactor.

FBG Fluidized Bed Gasifier. Fluidized Bed Gasification.

FBGR Fluidized Bed Gasification Reactor.

FS Fluidization State, [-].

KM Kinetic model.

LHV Low Heating Value, [J/kg].

HHV High Heating Value, [J/kg].

MB Mole balance.

MT Mass Transport.

OEB Overall energy balance in the limits of the fluidized bed region.

PFR Plug Flow Reactor.

UCM Uniform Conversion Model.

Greek letters

α Stoichiometric coefficient for char combustion reaction.

β Stoichiometric coefficient for char gasification reaction.

ΔH Reaction enthalpy, [J/mol].

δ Dimensionless parameter for transport properties, [-].

ε_B Volume fraction of bubbles. void fraction of bubble phase at any reactor height.

ε_{fb} Volume fraction of gas in the freeboard region at any reactor height.

ε_{fb}^* Volume fraction of solids in the freeboard region at any reactor height.

ε_{kb} Boltzmann constant [m^2 kg s^{-2} K^{-1}].

ε_{mf} Porosity of bed inert material.

ε_p Emissivity of bed inert material.

μ Viscosity, [kg/m s].

μ_p Dipole moment, [D].

ν_{ij} Stoichiometric coefficient for gaseous species “i” in reaction “j”.

ν_{nj} Stoichiometric coefficient for solid species “n” in reaction “j”.

ρ Density of gas, [kg/m^3].

ρ_s Density of inert bed material, [kg/m^3].

σ Collision diameter, [Å].

ϕ Contribution factor for pairs of species in a mixture in the properties calculation.

φ Phase in the fluidized bed.

Ω_k Stockmayer potential.

Ω_μ Lennard-Jones potential.

Subscripts

0 Value of variable at the reactor inlet. z=0.

a First chemical specie in a binary system of components.

ab Binary system of chemical species.

b Second chemical specie in a binary system of components.

bed Bed region. Inert particles bed.

B Bubble phase in bed region.

char Char material.

dev Devolatilization.

drying Heat of evaporation.

E Emulsion phase in bed region.

ext External.

fb Freeboard region.

g Gas.

i Chemical species “i” involved or not in a reaction in bubble and emulsion phase. Chemical species “i” involved or in a reaction in the freeboard region.

im Property of chemical specie “i” in a mixture of components.

j Chemical reaction.

loss Energy loss to surroundings.

mf Minimum fluidization.

mix Gas mixture.

ncg Non-combustible gases.

p Particle.

preh Preheater.

r Reaction.

syngas Synthesis gas.

T Total.

t Terminal.

vis Visible.

vol Volatiles.

∞ Surroundings.

Bibliography

Abba, I.A., Grace, J.R., Bi, H.T., Thompson, M.L. 2003b. Spanning the flow regimes: a generic fluidized bed reactor model. *AIChE Journal* 49(7), 1838–1848.

Agarwal, P.K., Linjewile, T.M. 1995. The influence of product CO/CO_2 ratio on the ignition and temperature history of petroleum coke particles in incipiently gas-fluidized beds. *Fuel* 71, 12-16.

Alimuddin, Z., Lim, M.T. 2008. Bubbling fluidized bed biomass gasification. Performance. process findings and energy analysis. *Renewable Energy* 33(10), 2339-2343.

Altafini, C.R., Wamder, P.R., Barreto, R.M. 2003. Prediction of working parameters of a wood waste gasifier through an equilibrium model. *Energy Conversion and Management* 44(17), 2763-2777.

Babu, S.P., Shah, B., Talwalker, A. 1978. Fluidization correlations for coal gasification materials-minimum fluidization velocity and fluidized bed expansion ratio. *AIChE Journal Symp. Ser.* 74, 176-186.

Basu, P, Kaushal, P. 2009. Modelling of pyrolysis and gasification of biomass in fluidized beds: a review. *Chemical Product and Process Modelling* 4(1), 21 (47 pp.). ISSN (Online) 1934-2659, DOI: 10.2202/2659.1338.

Biba, V., Macak, J., Klose, E.J., Malecha, J. 1978. Mathematical Model for the Gasification of Coal under Pressure. *Industrial & Engineering Chemistry Process Design and Development* 17 (1), 92-98.

Bird, B.R., Stewart, W.E., Lightfoot, E.N., 2002. Transport Phenomena, 2nd ed. Wiley, New York.

Boroson, M.L, Howard, J.B, Longwell, J.P., Peters, W.A. 1989. Product yields and kinetics from the vapor phase cracking of wood pyrolysis tars. *AIChE Journal* 35(1), 120-128.

Bruni, G., Solimene, R., Marzochella, A., Salatino, P., Yates, J.G., Lettieri, P., Fiorentino, M. 2002. Self-segregation of high volatile fuel particles during devolatilization in a fluidized bed reactor. *Powder Technology* 128(1), 11-21.

Campoy, M., Gómez-Barea, A., Vidal, F.B., Ollero, P. 2009. Air-steam gasification of biomass in a fluidised bed: Process optimisation by enriched air. *Fuel Processing Technology* 90(5), 677-685.

Claderbank, P.H., Toor, F.D. 1971. Fluidized beds as catalytic reactors. In J.F. Davidson, D. Harrison eds. Fluidization, 1st ed. *Academic Press*, London..

Corella, J. Sanz, A. 2005. Modelling circulating fluidized bed biomass gasifiers. A pseudo-rigorous model for stationary state. *Fuel Processing Technology* 86(9), 1021-1053.

Davidson, J.F., Harrison, D. 1971. Fluidization. Academic Press, London, pp. 383-429.

Davidson, J.F., Harrison, D. 1963. Fluidised particles. 1st ed.. Cambridge University Press, Cambridge, UK.

De Souza-Santos, M.L. 1989. Comprehensive modelling and simulation of fluidized bed boilers and gasifiers. *Fuel* 68(12), 1507-1521.

De Souza-Santos, M.L. 2005. Solid fuels combustion and gasification (Modelling, simulation and equipment operation). I. Marcel Dekker. New York**,** pp. 237-240.

De Souza-Santos, M.L., 2007. A new version of CSFB, comprehensive simulator for fluidised bed equipment. *Fuel* 86(12-13), 1684-1709.

Dryer, F.L., Glassman, I. 1973. High-temperature oxidation of CO and CH_4. Proceedings of the 14th Symposium (International) on Combustion. The Combustion Institute, Pittsburgh. Pennsylvania, 987-1003.

Fane, A.G., Wen, C.Y. 1982. Fluidized-bed reactors. Chapter 8 in Handbook of Multiphase Systems. Ed. Hetsroni, G. Hemisphere Publishing Corporation, Washington.

Fiaschi, D., Michelini, M. 2001. A two-phase one-dimensional biomass gasification kinetic model. *Biomass & Bioenergy* 21(2), 121-132.

Field, M.A., Gill, D.W., Morgan, B.B., Hawksley, P.G.W. 1967. Reaction Rate of Carbon Particles. In: Chpater 6 of Combustion of pulverised coal. BCURA, Cheney & Sons, Ltd., Banbury. England.

Gerber, S., Behrendt F., Oevermann, M. 2010. An Eulerian modelling approach of wood gasification in a bubbling fluidized bed reactor using char as bed material. *Fuel* 89(10), 2903-2917.

Gil, J., Corella, J., Aznar, M.P., Caballero, M.A. 1999. Biomass gasification in atmospheric and bubbling fluidized bed: Effect of the type of gasifying agent on the product distribution. *Biomass & Bioenergy* 17(5), 389-403.

Gómez-Barea, A., Arjona, R., Ollero, P. 2005. Pilot-Plant Gasification of Olive Stone: a Technical Assesment. *Energy & Fuels* 19(2), 598-605.

Gómez-Barea, A. Leckner, B. 2010. Modelling of biomass gasification in fluidized bed. *Progress In Energy and Combustion Science* 36(4), 444-509.

Grace, J.R. 1971. An evaluation of models for fluidized bed reactors. *AIChE Symposium Series* 67, 159-167.

Grace, J.R. 1981. Fluidized bed reactor modelling: an overview. *ACS Symposium Series*, 168, 1-18.

Grace, J.R. 1984. Generalized models for isothermal fluidized bed reactors. Chpater 13 of Recent advances in engineering analysis of chemically reacting systems. Ed. L.K. Doraiswamy, Wiley, Eastern New Deli, pp. 237-255.

Grace, J.R. 1986a. Fluid beds as chemical reactors. Chapter 11 of Gas Fluidization Technology. Ed. D. Geldart, John Wiley & Sons, New York, pp. 287-341.

Grace, J.R. 1986b. Modelling and simulation of two-phase fluidized bed reactors. In: Chemical reactor design and technology. Ed. H.I. de Lasa, Martinus Nijhof Publishers, Den Haag, Netherlands, pp. 245-289.

Grace, J.R. 1986c. Contacting modes and behaviour classification of gas-solid and other two-phase suspensions. Canadian Journal Chemical Engineering 64(3), 353-363.

Grace, J.R., Abba, I.A. 2005. Recent progress in the modelling of fluidized-bed reactors. In: Proc. Industrial Fluidization South Africa, South African Institute. Mining & Metallurgy Symposium Series. Eds. Luckos, A. and Smit, Presentation S42. pp. 3-22.

Hajaligol, M.R., Howard, J.B., Longwell, J.P., Peters, W.A. 1982. Product compositions and kinetics for rapid pyrolysis of cellulose. *Industrial & Engineering Chemistry Process Design and Development* 21(3), 457-465.

Ho, T.C. Modelling. 2003. In: Chapter 9 in Handbook of fluidization and fluid particle systems. Ed. Yang, W.C., Marcel Dekker, New York, pp. 239-255.

Horio, M., Wen, C.Y. 1977. An assessment of fluidized-bed modelling. *AiChE Symposium Series* 73, 9-21.

JANAF database (therm.dat) from CHEMKIN file therm.dat v4.0, March, 2004. http://users.rowan.edu/~marchese/combustion04/kinetics/h2-chemkin/therm.dat

Jess, A. 1995. Reaktionskinetische Untersuchungen zur thermischen Zersetzung von Modellkohlenwasserstoffen. *Erdöl ErdgasKohle* 111, 479-484. German.

Ji, P., Feng, W., Chen, B. 2009. Production of ultrapure hydrogen from biomass gasification with air. *Chemical Engineering Science* 64(3), 582-592.

Jiang, H.-M., Morey, R.V. 1992. A numerical model of a fluidized bed biomass gasifier. *Biomass & Bioenergy* 3(6), 431-447.

Kaushal, P., Abedi, J., Mahinpey, N. 2010. A comprehensive model for biomass gasification in a bubbling fluidized bed reactor. *Fuel* 89(12), 3650-3661.

Kerinin, E.V., Shifrin, E.I. 1993. Mathematical model of coal combustion and gasification in a passage of an underground gas generator. *Combustion, Explosion and Shock Waves* 29(2), 148-154.

Kunii, D., Levenspiel, O. 1969. Fluidization Engineering. Wiley, New York, USA.

Kunii, D., Levenspiel, O. 1991. Fluidization Engineering. 2nd ed. Butterworth-Heinemann. Stoneham, Massachutssets, USA.

Leckner, B., Johnsson, F., Andersson, S. 1991. Expansion of a freely bubbling fluidized bed. *Powder Technology* 68(2), 117-123.

Li, X., Grace, J.R., Lim, C.J., Watkinson, A.P., Chen, H.P., Kim, J.R. 2004. Biomass gasification in a circulating fluidized bed. *Biomass & Bioenergy* 26(2), 171-193.

Li, C., Suzuki, K. 2009. Tar property, analysis, reforming mechanism and model for biomass gasification. An overview. *Renewable and Sustainable Energy Reviews* 13(3), 594-604.

Mahecha-Botero, A., Grace, J.R., Elnashaie, S.S.E.H., Lim, C.J. 2007. A comprehensive approach to reaction engineering. International Journal of Chemical Reactor Engineering 5(A17), 1-26.

Mahecha-Botero, A., Grace, J.R., Lim, C.J., Elnashaie, S.S.E.H., Boyd, T., Gulamhusein, A. 2009. Pure hydrogen generation in a fluidized bed membrane reactor: Application of the generalized comprehensive reactor model. *Chemical Engineering Science* 64(17), 3826-3846.

Mahecha-Botero. A. 2009. Comprehensive modelling and simulation of fluidized bed reactors for efficient production of hydrogen and other hydrocarbon processes. *PhD Thesis*. University of British Columbia, Vancouver, Canadá.

Mansaray, K.G., Al-Taweel, A.M., Ghaly, A.E., Hamdullahpur, F., Ugursal, V.I. 2000. Mathematical modelling of a fluidized bed rice husk gasifier. Part I – Model development. *Energy source* 22(1), 83-98.

Matsui, I. Kunii, D., Furusawa, T. 1985. Study of fluidized bed gasification of char by thermogravimetrically obtained kinetics. *Journal of Chemical Engineering of Japan* 18(2), 105-113.

Matsui, I., Koijma, T., Kunii, D., Furusawa, T. 1987a. Study of char gasification by carbon dioxide. 1. Kinetic study by thermogravimetric analysis. *Industrial & Engineering Chemistry Research* 26(1), 91-95.

Matsui, I., Koijma, T., Kunii, D., Furusawa, T 1987b. Study of char gasification by carbon dioxide. 2. Continuous gasification in fluidized bed. *Industrial & Engineering Chemistry Research* 26(1), 95-100.

May, W.G. 1959. Fluidized-bed reactor studies. *Chemical Engineering Progress* 55, 49-56.

McKendry, P. 2002. Energy production from biomass (part 3): gasification technologies. *Bioresource Technology* 83(1), 55-63.

Mori, S., Wen, C.Y. 1975. Estimation of Bubble Diameter in Gaseous Fluidized Beds. *AIChE Journal* 21(1), 109-115.

Narváez, I., Orío, A., Aznar. M.P., Corella, J. 1996. Biomass gasification with Air in an Atmospheric Bubbling Fluidized Bed. Effect of Six Operational Variables on the Quality of the Produced Raw Gas. *Industrial & Engineering Chemistry Research* 35(7), 2110-2120.

Natarajan, E., Öhman, M., Gabra, M., Nordin, A., Liliedahl, T. 1998. Experimental determination of bed agglomeration tendencies of some common agricultural residues in fluidized bed combustión and gasification. *Biomass & Bioenergy* 15(2), 163-169.

Nunn, T.R., Howard, J.B., Longwell, J.P., Peters, W.A. 1985. Product Compositions and Kinetics in the Rapid Pyrolysis of Sweet Gum Hardwood. *Industrial & Engineering Chemistry Process Design and Development* 24(3), 836-844.

Oevermann, M., Gerber, S., Behrendt, F. 2009. EulerGLagrange/DEM simulation of wood gasification in a bubbling fluidized bed reactor. Particuology 7(4), 307-316.

Öhman, M., Nordin, A., Bengt-Johan, S., Backman, R., Hupa, M. 2000. Bed agglomeration characteristics during fluidized bed combustión of biomass fuels. *Energy & Fuels* 14(1), 169-178.

Orcutt, J.C., Davidson, J.F. and Pigford, R.L. 1962. Reaction time distributions in fluidized catalytic reactors. *Chemical Engineering Progress Symosiu. Series* 58(38), 1-15.

Pallarés, D., Johnsson, F. 2006. Macroscopic modelling of fluid dynamics in large-scale circulating fluidized beds. *Progress in Energy Combustion Science* 32(5-6), 539-569.

Papadikis, K., Bridgewater, A.V., Gu, S. 2008. CFD modelling of the fast pyrolysis of biomass in fluidised bed reactors. Part A: Eulerian computation of the momentum transport in bubbling fluidised beds. *Chemical Engineering Science* 63(16), 4218-4227.

Papadikis, K., Bridgewater, A.V., Gu, S. 2009a. CFD modelling of the fast pyrolysis of biomass in fluidised bed reactors. Part B: Heat, momentum and mass transport in bubbling fluidised beds. *Chemical Engineering Science* 64(5), 1036-1045.

Papadikis, K., Gu, S., Bridgewater, A.V., Gerhauser, H. 2009b. Application of cfd to model fast pyrolysis of biomass. *Fuel Process Technology* 90(4), 504-512.

Papadikis, K., Gu, S., Bridgewater, A.V. 2009c. CFD modelling of the fast pyrolysis of biomass in fluidized bed reactors: modelling the impact of biomass shrinkage. *Chemical Engineering Journal* 149(1-3), 417-427.

Partridge, B.A., Rowe, P.N. 1966. Analysis of gas flow in a bubbling fluidized bed when cloud formation occurs. *Transaction of the Institution of Chemical Engineer*s 44, 335.

Petersen, I., Werther, J. 2005. Experimental investigation and modelling of gasification of sewage sludge in the circulating fluidized bed. *Chemical Engineering and Processing* 44(7), 717-736.

Puig-Arnavat, M., Bruno, C:, Coronas, A. 2010. Review and analysis of biomass gasification models. *Renewable & Sustainable Energy Review*s 14(9), 2841-2851.

Pyle, D.L. 1972. Fluidized bed reactors. Review. In: 1st chemical reaction engineering international sympomsium. *Advances in Chemical Society*, Washington, D.C.

Radmanesh, R., Chaouki, J., Guy, C. 2006. Biomass Gasification in a Bubbling Fluidized Bed Reactor: Experiments and Modelling. *AIChE Journal* 52(12), 4258-4272.

Robert, P.M.A., Felder. R.M., Ferrell. J.K. 1988. Modelling a Pilot-Scale Fluidized Bed Coal Gasification Reactor. *Fuel Processing Technology* 19(3), 265-290.

Ross, D.P., Yan, H.-M., Zhang, D.-K. 2004. Modelling of a laboratory-scale bubbling fluidised-bed gasifier with feeds of both char and propane. *Fuel* 83(14-15), 1979-1990.

Ross, D.P., Yan, H.-M., Zhong, Z., Zhang, D.-K. 2005. A non-isothermal model of bubbling fluidised-bed coal gasifier. *Fuel* 84(12-13), 1469-1481.

Shen, C.Y., Johnstone, H.F. 1955. Gas-solid contact in fluidized beds. *AIChE Journal* 1(3), 349-354.

Sit, S.P., Grace, J.R. 1981. Effect of bubble interaction on interphase mass transfer in gas fluidized beds. *Chemical Engineering Science* 36(2), 327-335.

Solimene, R., Marzocchella, A. Salatino, P. 2003. Hydrodynamic interaction between a coarse gas-emitting particle and a gas fluidized bed of finer solids. *Powder Technology* 133(1-3), 79-90.

Sofialidis, D., Faltsi, O. 2001. Simulation of biomass gasification in fluidized beds using computational fluid dynamics approach. Thermal Science 5(2), 95-105.

Toomey, R.D., Johnstone, H.F. 1952. Gaseous fluidization of solid particles. *Chemical Engineering Progress* 48(5), 220-226.

van Swaiij, W.P.M. 1985. Chemical reactors. In Fluidization, 2nd ed. Eds. Davidson, J.F., Clift, R. and Harrison, D., Academic Press, London.

Wang, Y., Yan, L. 2008. CFD studies on biomass thermochemical conversion. *International Journal of Molecular Science* 9(6), 1108-1130.

Wen, C.Y., Yu, Y.H. 1966. A Generalized Method for Predicting the Minimum Fluidization Velocity. *AIChE Journal* 12(3), 610-612.

Wen, C.Y., Chen, L.H. 1982. Fluidized Bed Freeboard Phenomena Entrainment and Elutriation. *AIChE Journal* 28(1), 117-128.

Werther, J., Hartge, E.-U. 2004. Modelling of Industrial Fluidized-Bed Reactors. *Industrial & Engineering Chemistry Research* 43(18), 5593-5604.

Wilke, C.R. 1950. Diffusional properties of multicompenent gases. *Chemical Engineering Progress* 46, 95-104.

Yan, H.M., Heidenreich, C., Zhang, D.K. 1998. Mathematical modelling of a bubbling fluidised-bed coal gasifier and the significance of 'net flow'. *Fuel* 77(9-10), 1067-1079.

Yan, H.M., Heidenreich, C., Zhang, D.K. 1999. Modelling of bubbling fluidised bed coal gasifiers. *Fuel* 78(9), 1027-1047.

Yates, J.G. 1975. Fluidised bed reactors. The Chemical Engineer, vol. 303, pp. 671-677.

Zimont, V. L., Trushin, Y.M. 1969. Total combustion kinetics of hydrocarbon fuels. *Combustion Explosion Shockwaves* 5(4), 391-394.

Chapter 4

MBHEF syngas conditioning: modelling approach and exergy optimisation

Contents

4.1. Introduction

From some time past, there is an increasing concern about global warming and its effects due to GHG emissions of anthropologic origin since fossil fuels are still the dominant source of global primary energy supply (Herzog, 2011). As stated in the introduction section, much effort has been addressed in research and development of less polluting fuel-to-energy processes such biomass conversion technologies, sustainable renewable energy systems, methods and tools to evaluate the availability of renewable energy sources and investigation of CO_2 capture and storage techniques.

Additionally, in the present days, there seems still to be a long way to improve the efficiency of every step in power production processes.

In the way to improve process efficiency and lower pollutant emissions many attention is being given on biomass gasification (BG). The interest in biomass as fuel mainly lays in the very low net GHG emissions compared to others fuels when it is processed by some of the thermal technology conversion (Ptasinski, 2008). Among all existing conversion routes, biomass gasification in fluidized beds (BGFB's) has been proven as a feasible and eco-friendly fuel-to-energy thermal conversion method (McKendry, 2002). However, this type of fuel conversion presents several drawbacks. One of the most important disadvantages of BGFB's is the unacceptable tar content in the raw syngas for power production in internal combustion engines, combined cycle gas turbine, fuel cells, chemical synthesis, compressors, etc. (Milne and Evans, 1998). The tar problem in BG underlie in its physical properties: a low dew point yielding the condensation of sticky and refractory slurries that can lead to operational problems as blockage and attrition in filters, heat exchangers, exit pipes, etc (Li and Suzuki, 2009). Thus, tar removal is key for a successful application of biomass-derived producer gas though is still a challenge that has to be solved (Gómez-Barea et al., 2012).

Gas cleaning systems for conditioning syngas produced by BG reactors have been extensively studied and reviewed along the time (Milne and Evans, 1998; Gómez-Barea et al., 2012) since gas quality requirements for different gas application changes with the technology development and improvement (Milne and Evans, 1998). The current work proposes the use of a Moving Bed Heat Exchanger Filters (MBHEF's) as hot gas clean-up system for removing tar and particulate material. The choice of a MBHEF as hot gas cleaning equipment is justified by: the possibility of operating at high temperatures (up to 700-800ºC, the exhaust gas temperature from the gasifier) in contrast to problems presented by others devices such as ceramic filters over 400ºC (Longanbach, 1998), no-clogging and non-pressure increase during operation (Smid et al., 2005a). All these advantages offered by the MBHEF system would avoid shut-down and its associated costs in comparison with traditional hot gas clean-up devices.

To date, MBHEF's have been studied because of offering particular advantages when cleaning hot gas exhaust from reactors such BFBG's in contrast to traditional equipment: ceramic filters, scrubbers, electrostatic precipitators or bag filters in order to remove particulate material. This part of the thesis is aimed at evaluating the use of a MBHEF for conditioning syngas from BG processes in order to give a usable gas for power production applications. The purpose of the model proposed is to provide a predictive tool for simulating such steady MBHEF operation and to give tars and particles reduction level maps. The MBHEF will be optimised (Soria-Verdugo et al., 2009) in order to improve the tars and particulate removal efficiency (η_{tars} and η_{dust} respectively) as well as the heat transfer and pressure drop.

Finally, concerning to the particulate removal, the optimisation of MBHEF study focuses on the tar removal point of view since very high particle collection efficiencies can be easily achieved in comparison to tar reduction levels (Hasler and Nussbaumer, 1999).

4.1.1. Gas quality requirements

The performance, investment and operational costs of a hot gas cleaning system depend on the syngas quality demanded and the reactor performance whereas the quality of the gas produced is determined by the end-use of the gas. The need of tar and particulate removal depends basically on the syngas application. For instance, the acceptable limit of tar concentration in a syngas for engine applications varies according to the author as the review of Milne and Evans (1998). In this study, the limits adopted were those proposed by Stassen (1993), Milne and Evans (1998) and Rabu et al. (2001) (table 4.1).

The tars nature and not the tars concentration is key for successful assessment of the suitability of syngas end-use as Gómez-Barea and Leckner (2009) report, since it has been demonstrated that gas containing 100mg/Nm^3 of tars with a dew point of 70ºC causes mechanical problems in engines but a gas with 5000mg/Nm^3 of tars and a dew point of 20ºC has been used without engines problems. Here, for the sake of simplicity, the tar removal analysis is conducted from a concentration point of view, not exclusively focused on the tar nature. Furthermore, gas derived from biomass and wastes contain others pollutant species such as nitrogen, sulfur compounds, alkaline metals and dust. All these contaminants can be removed by means of conventional devices downstream of the gasifier before condensing tars. Thus, tar conversion is of interest since it increases the heating value of syngas. For instance, the low heating value (LHV) of tars is estimated to be around 26-40MJ/kg (Thunman et al., 2001).

Contaminant	Allowable concentration	
	IC Engine	Gas Turbine
Tar (mg/Nm^3)	<50	<5
Particles (mg/Nm^3)	<50	<30
Particle size (μm)	<10	<5

Table 4.1: Fuel requirements for internal combustion engines and gas turbines (Stassen, 1993; Milne and Evans, 1998; Rabu et al., 2001).

4.2. Tar removal methods review

To accomplish the objectives of tar removal, tars behavior in reactors should be understood. This involves knowing tars nature (previously explained in **Chapter 3**) and its formation mechanisms (out of the scope of this PhD Thesis). As follows, tar removal technologies are briefly presented, pointing out their main strong and weak points. Finally, the MBHEF is chosen as technology solution for tar elimination in order to give syngas with tars content levels acceptable for end-use applications: gas turbines and internal combustion engines.

4.2.1. Tar removal methods

The tar removal technologies can be sort out in two categories: primary and secondary methods depending on the location in the BGFB process where tars are removed (figure 4.1).

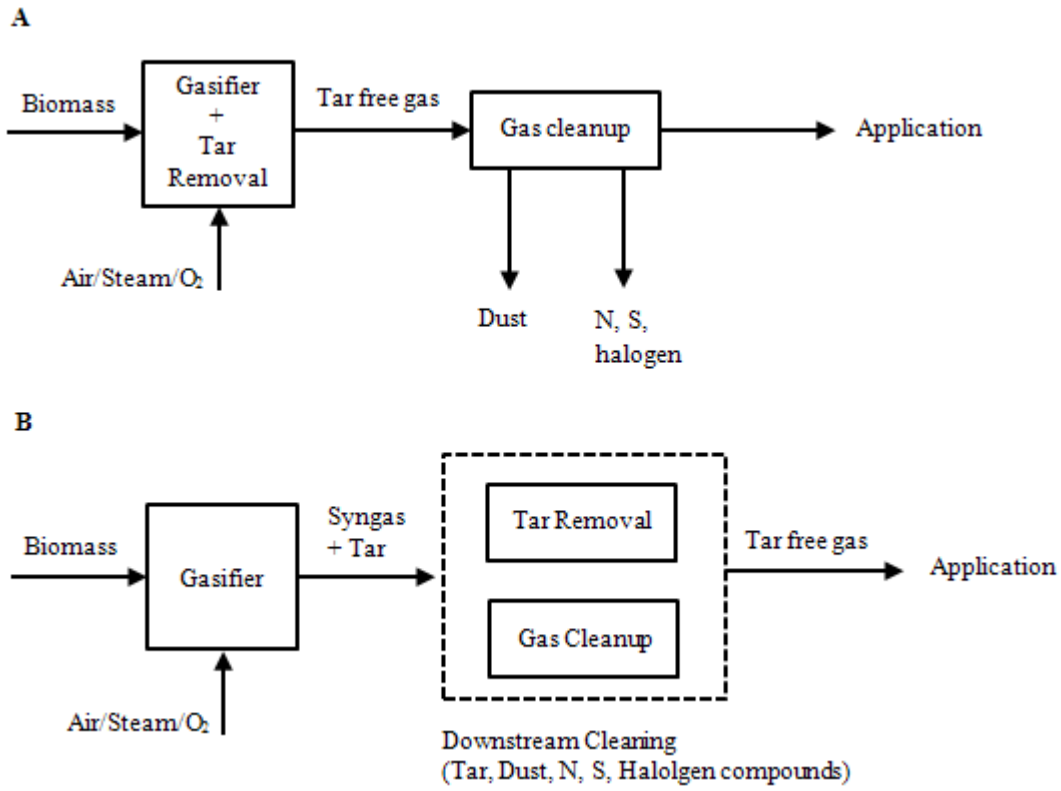

Figure 4.1: Tar removal by primary method (A) and secondary method (B), adopted from Devi et al. (2003).

Primary methods are addressed to prevent or convert tar formed inside the gasifier so that these types of technologies would save the use of secondary methods downstream. Three types of measures can be taken as primary methods: the proper design of reactor (Pan et al., 2006; Gómez-Barea et al., 2012), the right selection of operating conditions (Corella et al., 2006; Weerachanchai et al., 2009; Pipatmanomai and Kaewluan, 2011) and the use of proper bed additives/catalysts during gasification (Weerachanchai et al., 2009; Foscolo et al., 2009; Ruoppolo et al., 2009; Detournay et al., 2011).

On the other hand, secondary methods are aimed to treat the hot gas after the gasifier. They consist of chemical or physical treatment: thermal or catalytic cracking and mechanical methods such as use of electrostatic filters, ceramic filters, fabric filters, scrubbers and rotating particle separators.

In spite of the existence of a wide variety of tar removal technologies, not all of them are suitable from an economic point of view. Although secondary methods have been proven and shown as efficient, new trends address to the investigation of primary methods. In fact, recent works are focused on development and optimisation of primary tar technologies (Devi et al., 2003; Dou et al.; 2008; Arena et al., 2009; Ruoppolo et al., 2009; Schmidt et al., 2011). These works investigate the effect of metal-based and non-metallic catalysts in tar removal efficiency in BFBG.

According to the review of Devi et al. (2003), there are some remarks about the use of active bed material in BG processes:

- A change in product gas composition.
- An increase of H_2 content.
- A slight decrease of CO and an increase of CO_2 content.
- Almost no variation of CH_4.
- Dependence of catalytic activity on gasification conditions.
- Severe problems related to catalyst deactivation and carryover of fines.

However, the use of primary methods involves design modifications in reactors and/or changes in operating conditions in order to keep the quality and composition of the producer gas. Obviously, these syngas properties are desired to be constants when tar removal technologies are applied for satisfying quality syngas demand from markets. In the current paper, a cross-flow MBHEF device as secondary method is proposed to reduce tar levels in syngas saving costs derived from reactor design modifications or use of additives/catalysts.

MBHEF systems could be employed as a tar removal device. The cross-flow MBHEF concept for tar and particulate removal would provide a high contact area between gas and solids without either entrainment or elutriation of solids. Furthermore, to date, MBHEF systems have only been designed for heat transfer and hot gas particulate removal (Lozano et al., 1996; Henriquez and Macias-Machín, 1997; Smid et al., 2005b; Socorro et al., 2006; Soria-Verdugo et al., 2009). Dealing with BFBG reactors, MBHEF systems could also act as a preheater of the gasifying agent as the exhaust gas is cooled down and conditioned to be used for power production in internal combustion engines, gas turbines, etc (figure 4.2). Finally, all these properties would yield compact equipment with high gas cleaning efficiency and saving costs.

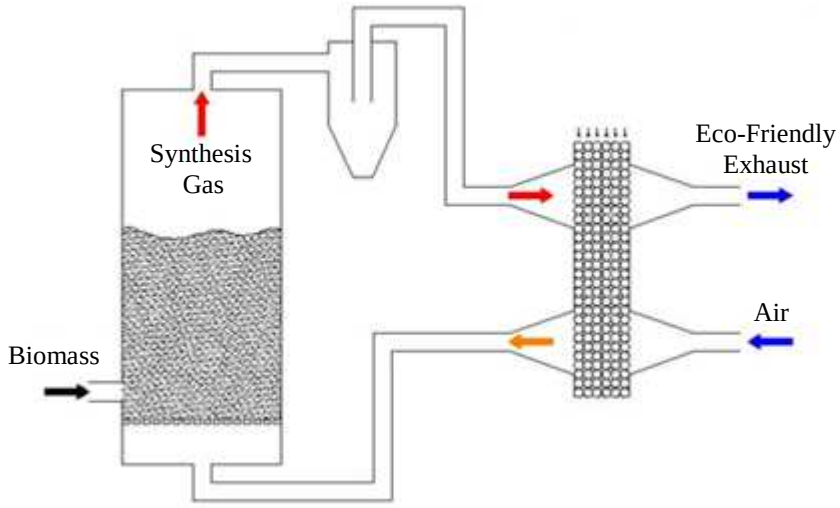

Figure 4.2: MBHEF syngas conditioning coupled to a BFBG reactor.

4.3. Model description

The analysis of the MBHEF operation is based on the coupled models of heat exchange, mass transfer and filtration of all species. Once the heat and mass transfer mechanisms

for tars removal is presented, the filtration mechanism for particulate collection is described.

4.3.1. MBHE model

The MBHEF device is featured by the cross-flow of a gas stream and a down-moving solid stream. When the gas is cool down by the particles, the condensable material (tars) would be removed from the gas flow into the solid mass flow, collected on the bottom part of the equipment. The gas inlet with condensable material enters the device and leaves it free of tars or with low tar content. Meanwhile, the liquid and solid phases act as interphase where condensation can take place yielding liquid film around particle surface.

Figure 4.3(B) represents a micro-scale zoom of the fixed bed and briefly describes heat and mass transfer between all phases: gas, liquid and solid and the direction of mass and energy flow. The heat and mass transfer processes are all coupled and take place between each pair of phases. The nomenclature used in defining governing equations denotes the couple of these processes in this way. Note that figure 4.3(A-B) addresses to the general case for removal of substance when its amount is appreciable, as for example.

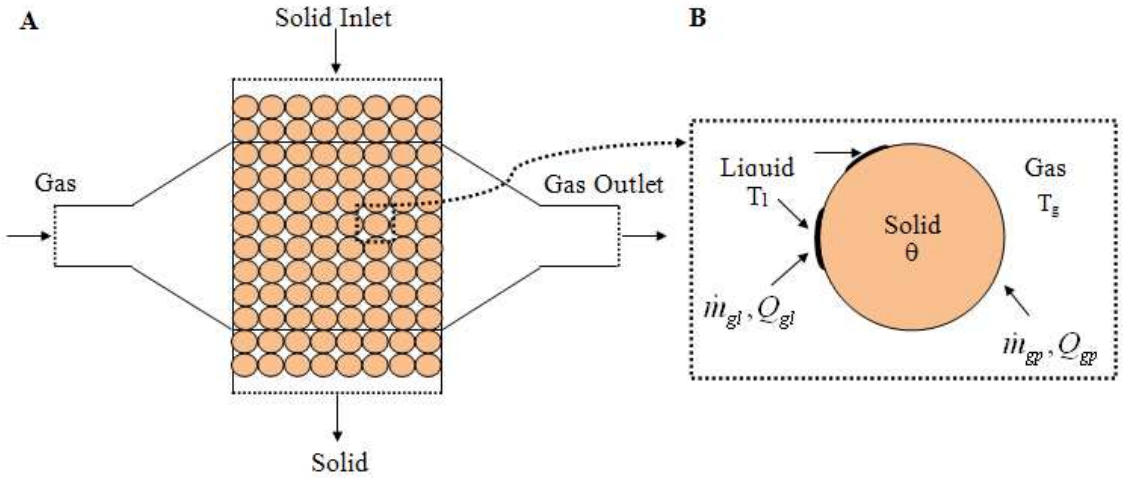

Figure 4.3: Schematic of a MBHE: for a general case with non-negligible phase condensable (A), and heat and mass transfer between all phases involved at particle-scale (B).

The energy and mass conservation equations can be applied to a typical MBHEF system, as shown in figure 4.4. This figure represents the mass balance in an arbitrary control element in the MBHEF device according to the general formulation. Neglecting chemical reaction the mass variation is only due to condensation. Then, gas phase loses mass in form of liquid phase which stays around the surface particle in the solid phase. The condensation rate would be related to the mass flux difference between two consecutive control volumes along one direction. Particularly, the condensate from gas phase would equal the mass flux gained by both solid and liquid phases.

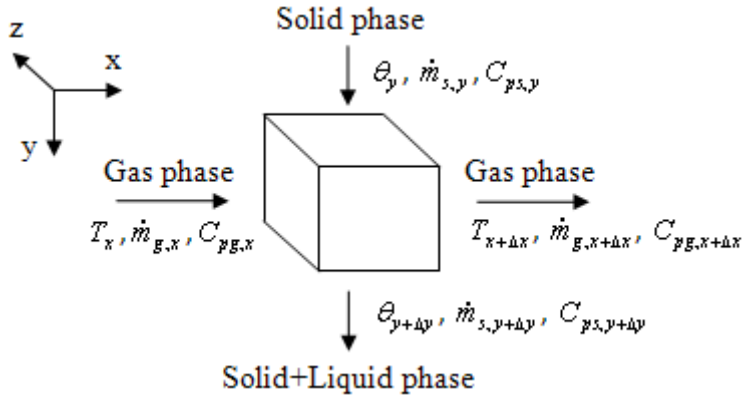

Figure 4.4: Mass balance in an arbitrary control volume inside the MBHEF.

Prior to study the performance of a MBHEF as tar removal equipment for conditioning syngas produced in BFBG reactors, heat and mass transfer inside the device is analysed. Generally, dealing with condensable species in fixed or fluidized beds means three phase systems. Assuming plug flow for gas, liquid and solid phases in cartesian coordinates, the energy and mass conservation equations in the general form can be written as Hu et al. (2011):

Gas phase energy equation

$$\begin{aligned}\varepsilon_g \rho_g c_{pg}\left(\frac{\partial T_g}{\partial t}+u_g\frac{\partial T_g}{\partial x}+v_g\frac{\partial T_g}{\partial y}+w_g\frac{\partial T_g}{\partial z}\right)= \quad & k_{gx}\frac{\partial^2 T_g}{\partial^2 x}+k_{gy}\frac{\partial^2 T_g}{\partial^2 y}+k_{gz}\frac{\partial^2 T_g}{\partial^2 z}\\ & +h_{gp}a_{gp}\left(\theta-T_g\right)+h_{gl}a_{gl}\left(T_l-T_g\right)\\ & -U_{gw}a_{gw}\left(T_g-T_\infty\right)+q_{rad}\\ & -\left(\sum_c^n \dot{m}_{gp,c}+\sum_c^n \dot{m}_{gl,c}\right)h_{fg,c}\\ & +\sum_r^{nr} G_{g,c}\Delta H_r\end{aligned} \tag{4.1}$$

Liquid phase energy equation

$$\begin{aligned}\varepsilon_l \rho_l c_{pl}\left(\frac{\partial T_l}{\partial t}+u_l\frac{\partial T_l}{\partial x}+v_l\frac{\partial T_l}{\partial y}+w_l\frac{\partial T_l}{\partial z}\right)= \quad & k_{lx}\frac{\partial^2 T_l}{\partial^2 x}+k_{ly}\frac{\partial^2 T_l}{\partial^2 y}+k_{lz}\frac{\partial^2 T_l}{\partial^2 z}\\ & +h_{lp}a_{lp}\left(\theta-T_l\right)+h_{gl}a_{gl}\left(T_g-T_l\right)\\ & -U_{lw}a_{lw}\left(T_l-T_\infty\right)+q_{rad}\\ & +\sum_c^n \dot{m}_{gl,c}h_{fg,c}+\sum_r^{nr} G_{l,c}\Delta H_r\end{aligned} \tag{4.2}$$

Solid phase energy equation

$$\begin{aligned}\varepsilon_p \rho_p c_{pp}\left(\frac{\partial \theta}{\partial t}+u_p\frac{\partial \theta}{\partial x}+v_p\frac{\partial \theta}{\partial y}+w_p\frac{\partial \theta}{\partial z}\right)= \quad & k_{px}\frac{\partial^2 \theta}{\partial^2 x}+k_{py}\frac{\partial^2 \theta}{\partial^2 y}+k_{pz}\frac{\partial^2 \theta}{\partial^2 z}\\ & +h_{gp}a_{gp}\left(T_g-\theta\right)+h_{lp}a_{lp}\left(T_l-\theta\right)\\ & -U_{pw}a_{pw}\left(\theta-T_\infty\right)+q_{rad}\\ & +\sum_c^n \dot{m}_{gp,c}h_{fg,c}+\sum_r^{nr} G_{p,c}\Delta H_r\end{aligned} \tag{4.3}$$

Gas phase mass equation for condensable species

$$\left(\frac{\partial}{\partial t}\left(\varepsilon_g C_c\right)+u_f\frac{\partial C_c}{\partial x}+v_f\frac{\partial C_c}{\partial y}+w_f\frac{\partial C_c}{\partial z}\right)= D_c\left(\frac{\partial^2 C_c}{\partial^2 x}+\frac{\partial^2 C_c}{\partial^2 y}+\frac{\partial^2 C_c}{\partial^2 z}\right) + G_{g,c}-\sum_c^n \dot{m}_{gp,c}-\sum_c^n \dot{m}_{gl,c} \tag{4.4}$$

Solid phase mass equation for condensable species

$$\left(\frac{\partial}{\partial t}\left(\varepsilon_p C_{c,p}\right)+u_p\frac{\partial C_{c,p}}{\partial x}+v_p\frac{\partial C_{c,p}}{\partial y}+w_p\frac{\partial C_{c,p}}{\partial z}\right)= D_{c,p}\left(\frac{\partial^2 C_{c,p}}{\partial^2 x}+\frac{\partial^2 C_{c,p}}{\partial^2 y}+\frac{\partial^2 C_{c,p}}{\partial^2 z}\right) + G_{p,c}+\sum_c^n \dot{m}_{gp,c}+\sum_c^n \dot{m}_{gl,c} \tag{4.5}$$

In this work, the liquid phase fraction (ε_l) is considered to be so small in terms of phase fraction, thus the liquid phase is assumed to be included in the solid phase. Because of the forming liquid film along the MBHEF dimensions is much less than the particle surface since the tar content is small, the contact area liquid-wall, a_{lw}, can be assumed as zero while the sum of specific area between gas and liquid, a_{gl}, and gas and solid, a_{gp}, is equals to the superficial particle area per unit volume, a_p. Furthermore, because of this assumption, the liquid phase properties as velocity components, temperature and condensation rate are assumed to be identical to the ones of the solid phase ($T_l=\theta$, $u_l=u_p$, $u_l=v_p$, $w_l=w_p$, for instance). Therefore, equations 4.2 and 4.3 can be added. All these hypothesis leads to:

Gas phase energy equation

$$\varepsilon_g\rho_g c_{pg}\left(\frac{\partial T_g}{\partial t}+u_g\frac{\partial T_g}{\partial x}+v_g\frac{\partial T_g}{\partial y}+w_g\frac{\partial T_g}{\partial z}\right)= k_{gx}\frac{\partial^2 T_g}{\partial^2 x}+k_{gy}\frac{\partial^2 T_g}{\partial^2 y}+k_{gz}\frac{\partial^2 T_g}{\partial^2 z} + h_p a_p\left(\theta-T_g\right) - U_{gw}a_{gw}\left(T_g-T_\infty\right)+q_{rad} - \sum_c^n \dot{m}_c h_{fg,c}+\sum_r^{nr} G_{g,c}\Delta H_r \tag{4.6}$$

Solid phase energy equation

$$\left(\varepsilon_p\rho_p c_{pp}+\varepsilon_l\rho_l c_{pl}\right)\left(\frac{\partial\theta}{\partial t}+u_p\frac{\partial\theta}{\partial x}+v_p\frac{\partial\theta}{\partial y}+w_p\frac{\partial\theta}{\partial z}\right)= \left(k_{px}+k_{lx}\right)\frac{\partial^2\theta}{\partial^2 x}+\left(k_{py}+k_{ly}\right)\frac{\partial^2\theta}{\partial^2 y} + \left(k_{pz}+k_{lz}\right)\frac{\partial^2\theta}{\partial^2 z}+h_p a_p\left(T_g-\theta\right) - U_{pw}a_{pw}\left(\theta-T_\infty\right)+q_{rad} + \sum_c^n \dot{m}_c h_{fg,c}+\sum_r^{nr} G_{p,c}\Delta H_r \tag{4.7}$$

Additionally, since the liquid phase fraction is much less than solid phase fraction, it can be assumed that ε_l is close to zero. Then, the heat diffusion terms related to ε_l (left side) and second derivatives liquid phase (right side) in equation 4.7 can be neglected in

comparison with the terms related to ε_p and second derivatives solid phase, respectively. Thus, Eq. 4.7 leads to the following energy conservation equation for the solid phase:

$$\varepsilon_p \rho_p c_{pp}\left(\frac{\partial\theta}{\partial t}+u_p\frac{\partial\theta}{\partial x}+v_p\frac{\partial\theta}{\partial y}+w_p\frac{\partial\theta}{\partial z}\right)= \begin{aligned} & k_{px}\frac{\partial^2\theta}{\partial^2 x}+k_{py}\frac{\partial^2\theta}{\partial^2 y}+k_{pz}\frac{\partial^2\theta}{\partial^2 z} \\ & -U_{pw}a_{pw}\left(\theta-T_\infty\right)+q_{rad} \\ & +h_p a_p\left(T_g-\theta\right)+\sum_c^n \dot{m}_c h_{fg,c}+\sum_r^{nr} G_{p,c}\Delta H_r \end{aligned} \quad (4.8)$$

This formulation, equations 4.6 and 4.8, can be simplified (table 4.2) for most cases with the following assumptions (points i-x based on Soria-Verdugo et al. (2009)):

i. Steady state.
ii. Two dimensional mass and energy evolution. 2D symmetry along z axis considered.
iii. Adiabatic operation: energy loss to the surroundings term is neglected.
iv. Heat transfer by conduction in both phases is negligible.
v. Solid phase is composed of inert, non-porous material particles. Thus, there is no pore-diffusion of heat and mass.
vi. No radial temperature distribution. Uniform temperature in the whole particle.
vii. One-dimensional gas and solid mass flow: $u_g >> v_g$, w_g and $v_p >> u_p, w_p$ can be assumed.
viii. Mass diffusion is much lower than mass convection (represented by u_g). In this way, second mass derivatives in equations 4.4 and 4.5 are not accounted for.
ix. No reaction between species.
x. Gas and solid phase fractions are assumed to be constant during operation.
xi. Ideal gas behavior is stated.
xii. Tar condensation takes place when gas temperature equals or is less than the tar dew point for the corresponding tar concentration (Li and Suzuki, 2009).
xiii. Physical and transport properties for gas species and gas-solid heat and mass transfer coefficients are evaluated with temperature at each point in the MBHEF (table 4.3).

Energy Balance	
Gas phase	**Solid phase**
$\varepsilon\rho_g c_{pg}\left(u_g\frac{\partial T}{\partial x}\right)= h_p a_e\left(\theta-T\right)-\sum_c^n \dot{m}_c h_{fg,c}$ (4.9)	$(1-\varepsilon)\rho_p c_{pp}\left(v_p\frac{\partial\theta}{\partial y}\right)= h_p a_e\left(T-\theta\right)+\sum_c^n \dot{m}_c h_{fg,c}$ (4.10)
Mass Balance (for tar compound)	
Gas phase	**Solid phase**
$u_g\frac{\partial C_c}{\partial x}=-\dot{m}_c=a_e k_m\left(C_c^*-C_c\right)$ (4.11)	$v_p\frac{\partial C_{c,p}}{\partial y}=\dot{m}_c=-u_g\frac{\partial C_c}{\partial x}$ (4.12)

Table 4.2: Energy and mass conservation equations.

Finally, to remark that the tar dew point is influenced by tar concentration so that in each mesh node a calculation strategy for solving conservation equations is required.

The dependence of tar dew point with its concentration and tar class was investigated by Kiel et al. (2004).

Property	Pure components	Mixtures	Reference
Viscosity	μ_c	μ_q	Bird et al. (2002)
Thermal conductivity	k_c	k_g	Bird et al. (2002)
Diffusivity	D_{ab} *1	D_q *2	*1Fuller et al. (1966) *2Wilke (1950)
Heat capacity	C_p		JANAF Database
Latent heat	h_{fg}		Thek and Stiel (1966)
Heat transfer coefficient	h_p		Achenbach (1995)
Mass transfer coefficient	k_m		Ranz (1952)
Effective interfacial area	a_e		Gandhidasan (2003)

Table 4.3: Correlations for estimating viscosity, thermal conductivity, diffusivity, heat capacity of gas species, latent heat and heat and mass transfer coefficients for packed beds.

4.3.2. Tars species

As explained previously, tar fraction in biomass comprises a wide variety of compounds with different properties affecting to devices. Hence, the choice of representative tars is critical for designing such equipment. Here, not all tar classes are considered since the work is focused in characterizing the performance of a MBHEF as tar removal method. Only tar classes with a tar dew point over 0ºC are taken into account: tar classes 2, 4 and 5 are lumps of interest. One specie is chosen as representative of each tar class: phenol, naphthalene and pyrene for tar class 2, 4 and 5, respectively, since they are usually predominant in concentration terms in BFBG processes (Kiel et al., 2004; Campoy-Naranjo, 2009).

The prediction of tar dew point variations due to tar concentration change because of condensation is made by a polynomic fitting of data based on the simple model developed by the ECN research institution (www.thersites.nl). The polynomic fitting, of 4-order, is based on the influence of tar concentration as logarithmic value as follows:

$$T_{dp,tar} = P(1)\left(\log_{10} C_{tar}\right)^4 + P(2)\left(\log_{10} C_{tar}\right)^3 + P(3)\left(\log_{10} C_{tar}\right)^2 P(4)\left(\log_{10} C_{tar}\right) + P(5) \qquad (4.13)$$

Table 4.4 shows the polynomic fitting coefficients for each tar class. The regression coefficient is also attached indicating the good agreement with results from www.thersites.nl.

Tar class	*P(1)*	*P(2)*	*P(3)*	*P(4)*	*P(5)*	R^2
2	0.0317	0.0862	11.361	133.110	2.364.992	0.9999
4	0.0392	0.0744	11.563	132.505	2.475.884	10.000
5	0.0452	0.1090	16.976	197.733	3.242.779	10.000

Table 4.4: Polynomic fitting coefficients for 4-grade polynomial for each tar class.

4.3.3. Filtration model

The filtration model proposed for the case of 2D-MBHEF is described by Lozano et al. (1996):

$$u_g \frac{\partial C_{p,g}}{\partial x} + v_p \frac{\partial C_{p,p}}{\partial y} = 0 \tag{4.14}$$

This equation relates the dust mass balances in both phases: the amount of dust deposited within a given bed volume, $C_{p,p,}$ and the dust concentration remaining in the gas, $C_{p,g}$ while the particle concentration profile in the gas follows an exponential law:

$$\frac{\partial C_{p,g}}{\partial x} = -\lambda C_{p,g} \tag{4.15}$$

Thus, the filtration process in a MBHEF device consists of the gas flow throughout the equipment while the moving bed collects dust. The rate at which the particle concentration in the gas falls is given by the filter coefficient, λ.

To sum up, the mass balance of dust in the gas and solid phase are shown in table 4.5, where equation 4.17 is computed after solving equation 4.14.

Dust mass balance in gas phase	Dust mass balance in solid phase
$\frac{\partial C_{p,g}}{\partial x} = -\lambda C_{p,g}$ (4.16)	$v_p \frac{\partial C_{p,p}}{\partial y} = -u_g \frac{\partial C_{p,g}}{\partial x}$ (4.17)

Table 4.5: Mass balance of dust in the gas and solid phases.

4.3.4. Calculation strategy

The conservation equations (4.6, 4.8, 4.9-12, 4.16-17), listed above, are expressed in terms of volumetric flow. For convenience, they are redefined in terms of mass flow multiplying by the control volume. These equations are approximated by first-order forward finite-difference expressions since they are first-order equations. Finally, the conservation equations are solved as non-dimensional equations (4.18-4.24), solving the energy balances by means of inverse matrix method. The definition of the dimensionless variables is indicated in the Appendix J.

Energy balance for gas and solid phases

$$\begin{pmatrix} 1+\frac{CNTU^*_{x+\Delta x}}{2} & -\frac{CNTU^*_{x+\Delta x}}{2} \\ -\frac{CNTU^*_{x+\Delta x} NTU^*_{x+\Delta x}}{2} & 1+\frac{CNTU^*_{x+\Delta x} NTU^*_{x+\Delta x}}{2} \end{pmatrix} \begin{pmatrix} T^*_{x+\Delta x} \\ \theta^*_{x+\Delta x} \end{pmatrix}$$
$$= \begin{pmatrix} \frac{CPG^*_x}{CPG^*_{x+\Delta x}}\left(T^*_x - T^*_{ref}\right) - \frac{CNTU^*_{x+\Delta x}}{2}\left(T^*_x - \theta^*_y\right) + \frac{\left(T^*_0 - \theta^*_0\right)}{STe^*_{x+\Delta x}} + T^*_{ref} \\ \frac{CPS^*_y}{CPS^*_{y+\Delta y}}\left(\theta^*_y - \theta^*_{ref}\right) + \frac{CNTU^*_{x+\Delta x}}{2}\left(T^*_x - \theta^*_y\right) + \frac{\left(T^*_0 - \theta^*_0\right)}{STe^*_{x+\Delta x}} + \theta^*_{ref} \end{pmatrix} \tag{4.18}$$

Where the coefficients NTU, CNTU, STe, CPG and CPS are defined in appendix J.

Mass balance for tar species in gas and solid phases

$$C^*_{g,x+\Delta x} = \frac{u_{g,x}}{u_{g,x+\Delta x}} C^*_{g,x} + \frac{\Delta x^* k_m a_e L}{u_{g,x+\Delta x}} \left(C^*_{s,y} - C^*_{g,x}\right) - \left(1 - \frac{u_{g,x}}{u_{g,x+\Delta x}}\right) \frac{C_{s,0}}{\left(C_{g,0} - C_{s,0}\right)} \quad (4.19)$$

$$C^*_{s,y+\Delta y} = C^*_{s,y} + \frac{\Delta y^* k_m a_e H}{u_p} \left(C^*_{g,x} - C^*_{s,y}\right) \quad (4.20)$$

Mass balance for water in gas and solid phases

$$C^*_{g,x+\Delta x} = \frac{u_{g,x}}{u_{g,x+\Delta x}} C^*_{g,x} + \frac{\Delta x^* L}{u_{g,x+\Delta x}} \left(k_m a_e \left(C^*_{s,y} - C^*_{g,x}\right) + \frac{\dot{m}_{evap}}{\left(C_{g,0} - C_{s,0}\right)} \right) - \left(1 - \frac{u_{g,x}}{u_{g,x+\Delta x}}\right) \frac{C_{s,0}}{\left(C_{g,0} - C_{s,0}\right)} \quad (4.21)$$

$$C^*_{s,y+\Delta y} = C^*_{s,y} + \frac{\Delta y^* H}{u_p} \left(k_m a_e \left(C^*_{g,x} - C^*_{s,y}\right) + \frac{\dot{m}_{cond}}{\left(C_{g,0} - C_{s,0}\right)} \right) \quad (4.22)$$

Mass balance for particulate material in gas and solid phases

$$C^*_{pg,x+\Delta x} = C^*_{pg,x} + -\lambda \Delta x^* L \left(C^*_{pg,x} + \frac{C_{pp,0}}{\left(C_{pg,0} - C_{pp,0}\right)} \right) - \frac{C_{pp,0}}{\left(C_{pg,0} - C_{pp,0}\right)} \quad (4.23)$$

$$C^*_{pp,y+\Delta y} = C^*_{pp,y} + \frac{\lambda \Delta y^* H}{u_p} \left(C^*_{pg,x} - \frac{C_{pp,0}}{\left(C_{pg,0} - C_{pp,0}\right)} \right) \quad (4.24)$$

The energy and mass balances in each node are solved according to the calculation method explained in figure 4.5. With the initial data, the MBHEF is simulated following this sequence: gas composition, physical, transport and thermodynamical properties, dust particle mass balance, tar/water condensation mass balance, energy balance and tars dew point for next node, along the y axis, first, and along the x axis then according to the figure 4.4 (The size step has been set as 1E-5 for convenience). The heat transfer and tars condensation are simulated with the characteristic node temperature for both phases, that is, the node "(x+x+Δx)/2,(y+y+Δy)/2". As the gas properties in the node "x+Δx,y" depend on the temperature in that node and the gas and solid temperatures are unknown, for the first calculation the characteristic node temperatures for both phases are assumed to be the ones in the node "x,y" in order to calculate the gas and solid temperatures for the nodes "x+Δx,y" and "x,y+Δy". In this way, there is a calculation error which is minimized by means of an iteration method to satisfy the energy balance for both phases. Therefore, this calculation sequence is repeated while the error in the outlet temperature of gas and solid phases does not satisfy the tolerance adopted (1E-3 in this PhD Thesis). Thus, the simulation of the performance of the MBHEF system is carried out along the y and x directions until the value of a variable X is less than the value stated as goal. This variable, called X_{goal}, can be either the gas temperature

exhaust (60ºC as the inlet gas temperature in engine applications) or the tar reduction efficiency in accordance to the two possible cases of interest: case 1 and 2.

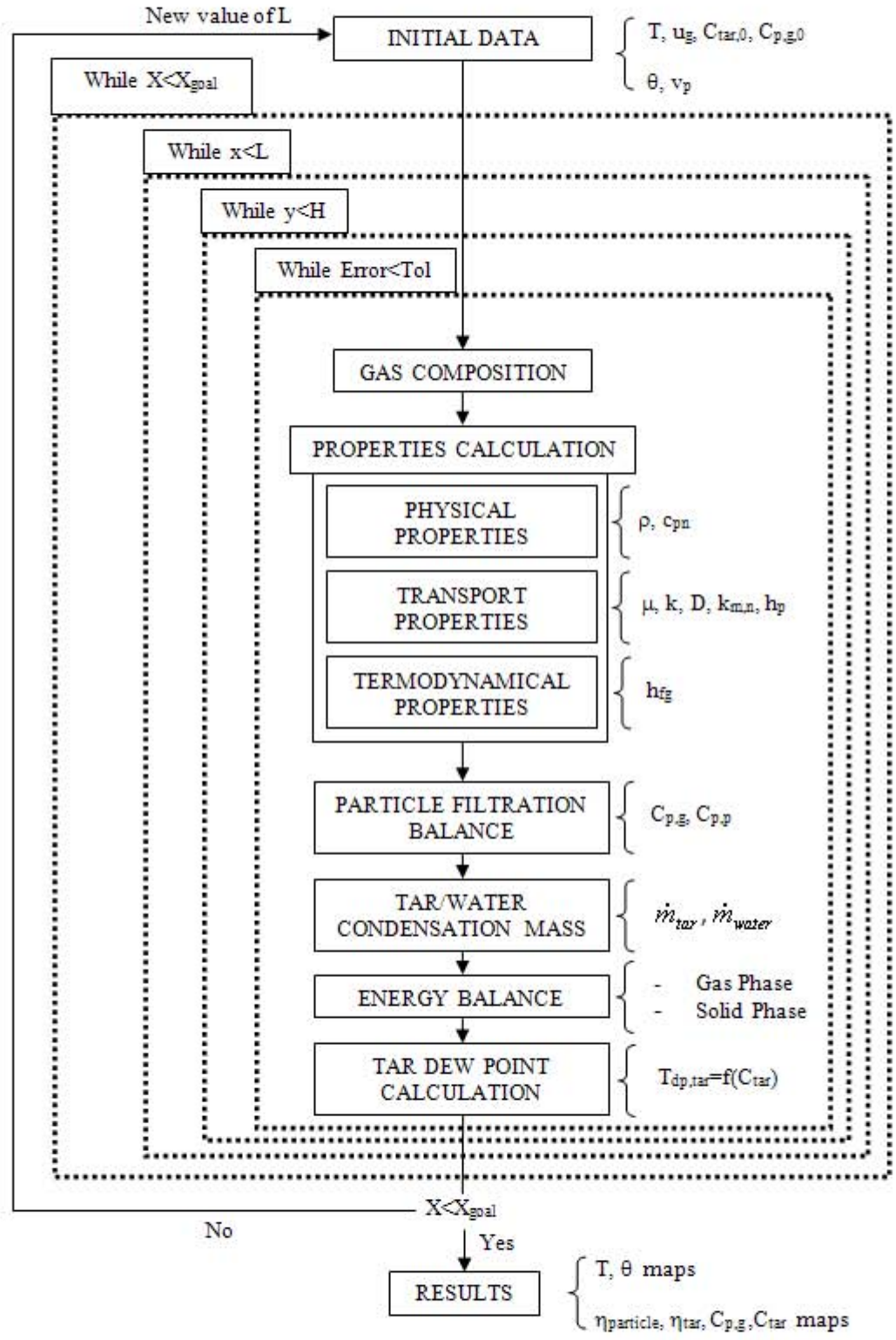

Figure 4.5: Scheme of the calculation strategy for simulating the tar removal in a MBHEF system.

4.4. Results and discussion

The performance of a MBHEF is studied using the composition (CO, CO_2, H_2, CH_4) from test 1 of experiments conducted by Gómez-Barea et al. (2009). The gas temperature and the water content are set as 700ºC and 10% of gas volume respectively, since they are typical results in gasification. Concerning the pollutant species, the typical tar content in syngas is around 20-50g/Nm^3 according to Gómez-Barea and Leckner (2010). Thus, we set the inlet tar concentration as 10g/Nm^3 for each representative species of condensable tar class so that all tars species account for 30g/Nm^3. Finally, inlet fines or dust particles content and others dust properties such particle size and density are set from the work of Lozano et al. (1996). The gas velocities employed, 0.5-3m/s, assure proper MBHEF operation with no ceasing of solid flow (Ginestra and Jackson, 1985) and the range 100μm-1mm of particle bed size is of interest. Table 4.6 shows the data of gas and solid properties used for simulations.

Gas composition (%, d.b.)		**Contaminant concentration (g/Nm^3)**		**Solid properties**	
O_2	0.0	tars class 2	10	Bed porosity, ε	0.4
CO	15.8	tars class 4	10	Bed particle size	100μm-1mm
CO_2	15.1	tars class 5	10	ρ_p (kg/m^3)	2150
H_2	8.7	Particle (fines or "dust")	8	c_p (J/kgK)	745
CH_4	5.1	Particle size (μm)	5	k_p (W/mK)	2.9
Q_{gas} (Nm^3/h)	4.6	Particle density (kg/m^3)	2100	v_p (cm/min)	5

Table 4.6: Data of gas and solid properties.

The MBHEF can be analysed from two different points of view. Firstly, the MBHEF can be built in order to get a proper temperature of the syngas to be fed to an internal combustion engine or gas turbine, normally, around 60ºC (we call this situation case 1). In this case, the removal efficiency of tars and fines particle is not of interest. Consequently, depending on the inlet tars and particle content, the MBHEF design could be enough or not to depurate the syngas flow. The equipment would act as a first cleaning measure and a second measure should be taken to adequate quality syngas for its power production use in mechanical engines. Secondly, the MBHEF can be designed to satisfy tars and particle levels (case 2). Thus, the gas temperature exhaust can be different (lower) from the 60ºC, the value set as inlet gas temperature in internal combustion engines and gas turbines. Then, the performance of the MBHEF should be analysed regarding two variables: the inlet gas temperature to internal combustion engines and gas turbines and the tars and particle removal efficiency, which are calculated by comparison with the corresponding inlet content values for both streams.

4.4.1. Syngas conditioning for engine applications requirements

Figure 4.6 shows the thermal performance of the MBHEF device: the temperature maps of gas (4.6A) and solid phase (4.6B) for the case of 700μm and 1.5m/s of gas velocity as example. The gas stream entering the MBHEF lowers its temperature while the downward moving bed increases its temperature until there is not temperature difference between both phases, what depends on the device dimensions. Consequently,

it can be seen that gas and solid streams leave the device with a different bulk temperature from the corresponding inlet values. Note that these equipment sizes may not mean energy and exergy optimised dimensions of MBHEF.

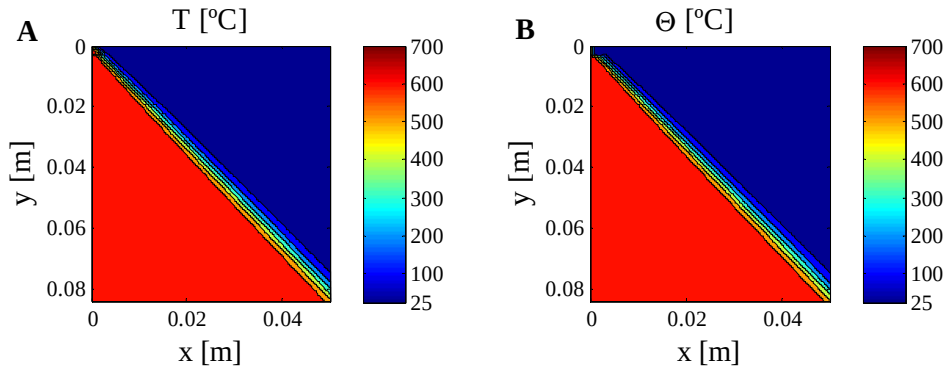

Figure 4.6: Contour maps of gas temperature (A) and solid temperature (B) for d_p=700µm and u_g=1.5m/s.

As expected, the tar condensation phenomenon is linked to heat transfer between phases since it depends on the tar dew point and then the tar concentration in the gas bulk according to Kiel et al. (2004). This will be explained as follows.

Figure 4.7A indicates the tar removal efficiency in the cross-sectional area along the *x* coordinate, that is, the gas flow direction. This map denotes the areas inside the device where tars condensation would take place. These condensation areas correspond to gas temperatures below the respective tar dew point of each tar class. The color indicates the order of magnitude of condensation. Instead of having a gradual condensation of tars, the condensation phenomenon takes places in a very narrow strip, almost unnoticeable. The use of small particle sizes promotes this condensation behavior. For example, the blue-colored region corresponds to a hot gas with a temperature higher than the tar dew point for each tar species while the red-like area, above the hot gas flow, would mean a colder syngas with lower tar content. Because of the small particle bed diameter, below 1mm, the specific area yields a narrow border between the coldest part of gas flow and the hottest region of gas flow as seen previously. This fact is consequence of the nature of particle beds which allows achieving huge specific areas enhancing heat and mass transfer. Therefore, the rapid heat transfer is accompanied by a fast tars condensation wherever the respective tar dew points are greater than local gas temperature.

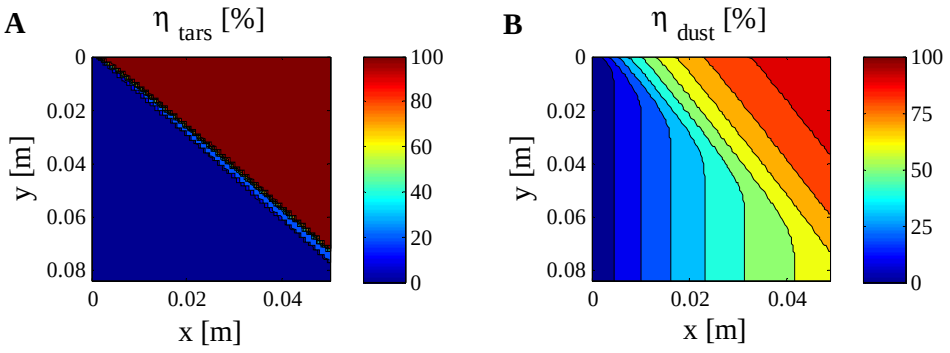

Figure 4.7: Contour map of tar removal efficiency (A) and dust collection efficiency (B) for d_p=700µm and u_g=1.5m/s.

The particulate matter reduction also takes place simultaneously with the heat and mass transfer involving tars condensation, denoted by figure 4.7B. According to the filtration model adopted for granular material, the dust collection efficiency follows the pattern shown in the map stated above (figure 4.7B). Due to the use of so small particle bed material, the collection of fine dust happens gradually along the device length.

On the contrary, Figure 4.8 shows the tar reduction efficiency profile along the equipment length, that is, the gas flow direction (tar class 2, red line; tar class 4, blue line and tar class 5, yellow line). The tar content in the gas bulk rapidly decreases because of the mentioned high specific area of the moving bed: for a gas flow of 4.6Nm^3/h and a 5cm length device, tar reduction efficiencies up to 90% or even more can be attained. Thus, the compact MBHEF could be employed as a first tar abatement measure followed by a second exhaustive method, for instance, a tar cracker.

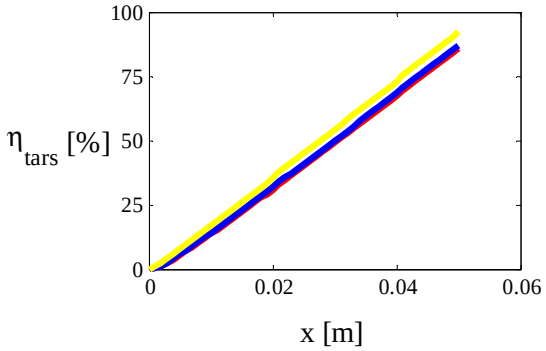

Figure 4.8: Tar removal efficiency profile along the gas flow direction in the MBHEF for tars classes 2 (red), 4 (blue) and 5 (yellow), respectively, for d_p=700μm and u_g=1.5m/s.

These trends in thermal and tar removal performance happen for the operating conditions range studied since the specific area is so high that promotes the heat exchange in much reduced dimensions of equipment.

As follows, dimensionless gas temperature and tar removal efficiencies maps are presented in figures 4.9(A-D) and 4.10(A-D). As it can be seen, the patterns are opposed: the lower gas temperature, the higher tar abatement efficiency with the position. These maps show the influence of particle bed size and superficial gas velocity as well as and the choice of operating conditions and equipment size for achieving the tar removal efficiency desired which would accomplish quality syngas requirements in internal engines.

In both figures, 4.9(A-D) and 4.10(A-D), it can be understood that the superficial gas velocity has a negative effect in the heat exchange and tar condensation. High gas velocities involve low residence times to reach the same gas outlet temperature and then, the same value of tar removal efficiency. This means that syngas with acceptable tar content levels for engine applications requires much compact devices with low gas velocities than with high values. The same is expected to occur with the particle bed size. Furthermore, the trends for gas temperature and tar content reduction are opposed since the tar abatement efficiency is linked to the tar dew point.

Figure 4.9(A-D) depicts the heat transfer process to cool down completely the syngas: from the inlet gas temperature to the inlet solid temperature. The maps

presented in figure 4.9 (A-D) shows the average gas temperature evolution with length as well as the influence of the superficial gas velocity. As it can be observed, the particle size of moving bed practically has the same influence on the gas temperature profile but the 1mm of particle bed diameter. For this particle diameter, a curve-like evolution is noticeable when the gas temperature is close to the inlet solid temperature. For particle sizes of 400 and 700µm the curves endings look very similar while for 100 µm is unnoticeable and for 1mm the slope is a little more pronounced. Besides, the effect of the superficial gas velocity when reaching the inlet solid temperature is also observed in a lower slope of the gas temperature profile and a higher device length to reach the same outlet gas temperature. This is more noticeable for greater gas velocities (1-3m/s). Finally, accordingly to the simulation results, it could be stated the existence of two linear profiles: a very long first one and a second one when the gas temperature is very close to the inlet solid temperature.

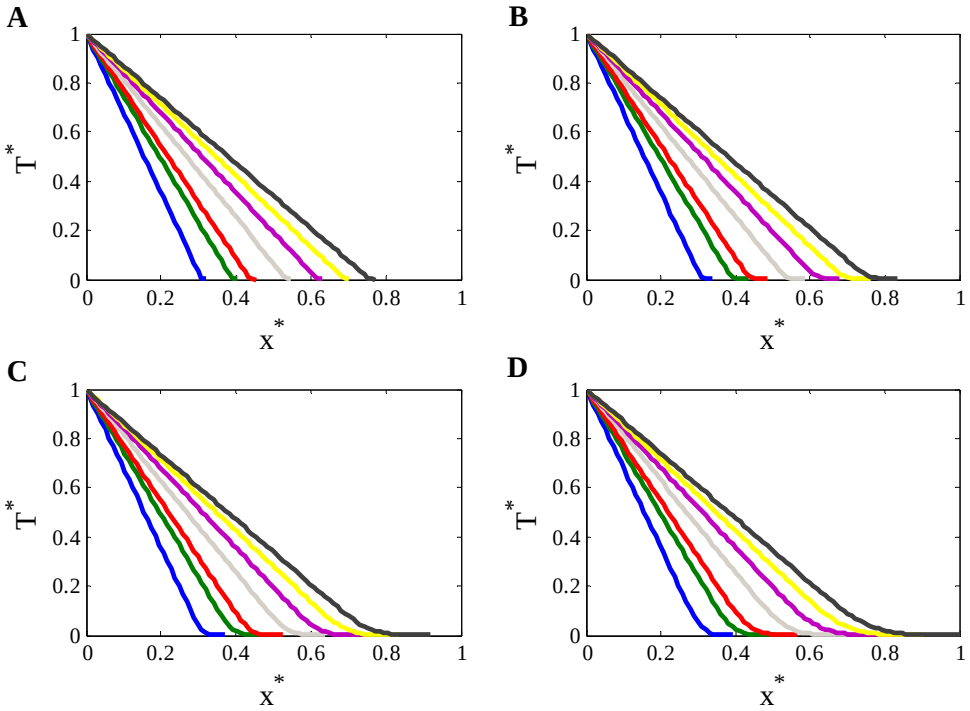

Figure 4.9: Dimensionless gas temperature map for particle bed size of 100µm (A), 400µm (B), 700µm (C) and 1mm (D) at 0.5(blue), 0.8(green), 1(red), 1.5(grey), 2(pink), 2.5(yellow) and 3m/s(black) of superficial gas velocity.

Concerning the tar removal efficiency maps, figure 4.10(A-D) shows the same trends described above, but now, the tar removal efficiency has the opposite evolution. The tar abatement efficiency, presented as the average tar removal efficiency of tar classes 2, 4 and 5, rises with the decrease of the superficial gas velocity and the particle size. As explained previously, the increase of the gas superficial velocity yields a decrease of the residence time of the gas inside the device so that greater tar content is removed from the gas bulk. In addition to this, the removal of tars is enhanced by the use of small bed particle sizes promoting high heat and mass transfer coefficients. Thus, this leads to compact equipment sizes saving costs in materials, building and operation.

These maps compare the equipment size required for achieving the tar removal efficiency desired or specified by the engine application. Thereafter, the same level of

tar reduction can be obtained at any gas velocity by making longer the MBHEF length. For example, for getting a tar removal efficiency of 50% for a gas flow at 0.5m/s, it would be needed a device twice times longer than blowing gas at 3m/s. However, if a tar content reduction of at least 95% is desired, the increase of the superficial gas velocity from 0.5 to 3m/s would require a MBHEF three times longer instead of just doubling the size. This point is very important since the size of the equipment is related to the pressure drop and therefore the operational costs as it will be analysed later on.

Finally, note that the dimensionless map for each particle size is constructed using the maximum length obtained in all designs, it is, for the range of particle size studied, the cases with 1mm of bed particle diameter (figure 4.10D). Furthermore, comparing the device performance for all particle bed diameters studied, the differences are slight at low gas velocities (0.-1.5m/s) while at high gas velocities (2-3m/s) they are noticeable. In the current study, tars with tar dew point above ambient temperature, 25ºC, have been investigated. Then, tar species with a tar dew point below the inlet solid temperature (ambient temperature in this work) would not be removed at 100%. Therefore, the resulting maps would show tar removal efficiency profile below 100% though the inlet solid temperature would be reached for the gas phase. As consequence, tar classes more refractory such as classes 1 and 3 would not be removed by the proposed method and further syngas conditioning aimed to eliminate tar classes 1 and 3 should be employed for satisfying tar content required in engines applications.

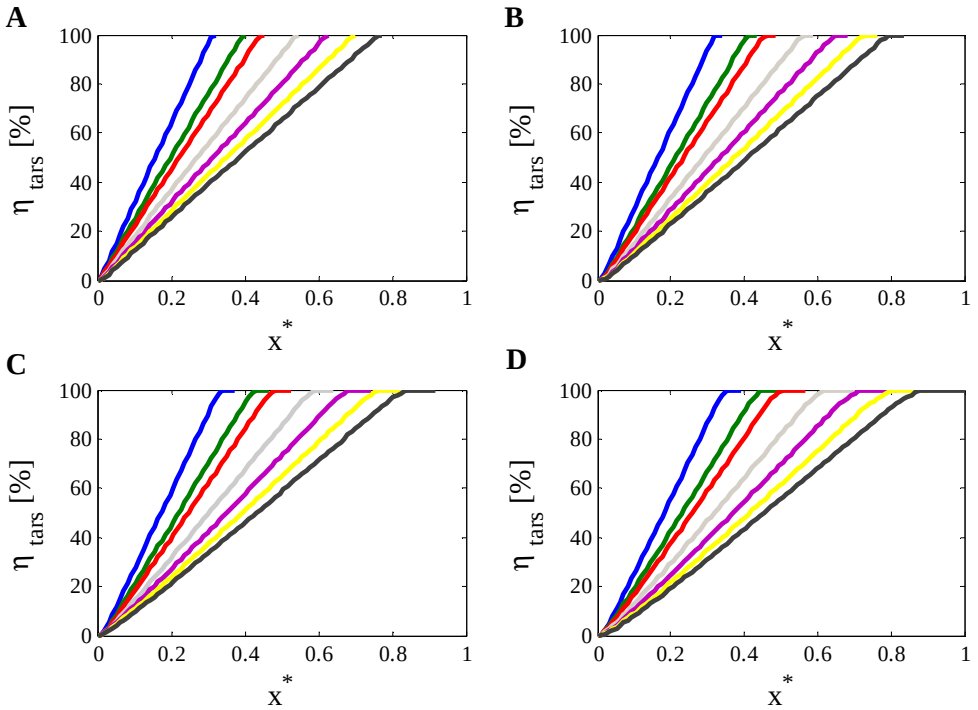

Figure 4.10: Dimensionless tar abatement efficiency map for particle bed size of 100µm (A), 400µm (B), 700µm (C) and 1mm (D) at 0.5(blue), 0.8(green), 1(red), 1.5(grey), 2(pink), 2.5(yellow) and 3m/s(black) of superficial gas velocity.

On the other hand, figure 4.11A shows the linear relationship of the length/width ratio with the gas velocity and the particle bed diameter to cool down the gas until the inlet temperature of solid flow. This figure stands out several important aspects in

designing a MBHEF. Firstly, the higher the gas velocity the longer the aspect ratio, that is, the longer the length since the residence time is decreasing with the gas velocity of gas for each particle size. Secondly, the relative importance of gas velocity and particle size remains practically unchanged but at low gas velocities (below 1m/s) the performance of MBHEF tends to be insensitive to the particle size. Thus, the gas velocity rules tars condensation. This will be relevant for choosing the map of operating conditions with saving operational costs. Thirdly, at high superficial gas velocities (1.5-3m/s) the particle bed diameter of moving bed gains relevance in the MBHEF design since the gap between lines grows with the gas velocity as denoted by the figure 4.11A. Although this figure allows us to check the relative importance of the two key operating parameters for design purposes of a MBHEF, figure 4.11B is a useful help in the choice of proper operating conditions of a MBHEF in terms of pressure drop and energy consumption for blowing the syngas flow.

The pressure drop (Ergun, 1952) along the moving bed increases with the particle bed and the gas velocity from 24 to 385kPa for 100µm of particle size, from 1.6 to 30.5kPa for 400µm, from 0.5 to 12.2kPa for 700µm and from 0.3 to 7.2kPa for 1mm. This means that the pressure drop can be a factor of 30 times greater at 3m/s than at 0.5m/s. Furthermore, the range analysed yields a power consumption of 98-1621W, 6.5-12.9W, 2.3-51.6W and 1.2-30.3W for 100µm, 400 µm, 700µm and 1mm respectively for conditioning a gas flow of 4.6Nm^3/h. Therefore, particle sizes above 400µm would yield acceptable tar content reduction with a relatively low pressure drop compared to the performance of a MBHEF employing 100µm particle size. Additionally, above 700µm, the pressure drop remains softly sensitive with the superficial velocity while below 400µm the pressure drop is more influenced.

To sum up, the analysis of the influence of the operating conditions in the pressure drop indicates that low values of superficial gas velocity (0.5m/s) and high particle size (700µm-1mm) should be recommended in order to save operational costs.

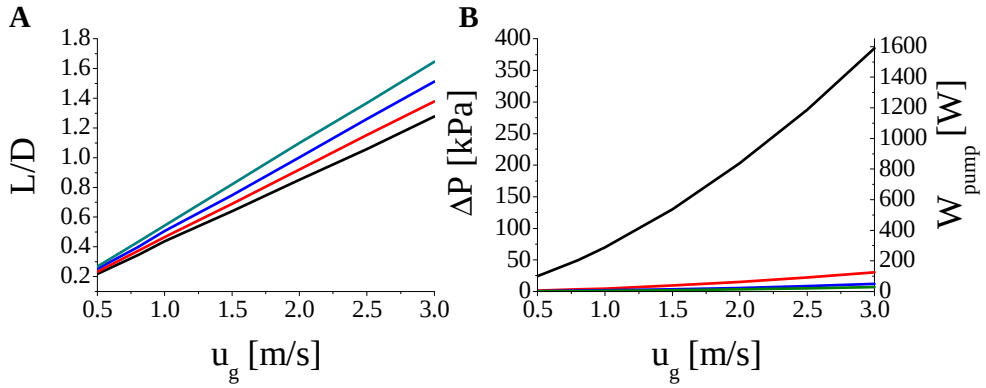

Figure 4.11: Influence of superficial gas velocity and particle size (100µm: black line, 400µm: red line, 700µm: blue line, and 1mm: green line) on the length-width ratio (A) and the pressure drop and power consumption (B).

Figure 4.12A denotes the influence of the outlet gas temperature in the average tar removal efficiency of all tar classes at 3m/s what would correspond to the case most unfavorable. As expected, the tar abatement level follows a decreasing linear

relationship with the outlet gas temperature. This is logical since its means that the length of the MBHEF is not enough to allow the heat exchange between both gas and solid phases completely. This has the same effect that increasing the gas velocity what would mean lower residence time. Then, there is less gas-solid contact yielding fewer tars condensation. In addition to this, all lines hardly change their slopes but the one corresponding to 1mm of particle bed diameter. Furthermore, considering the case of 1mm of particle bed diameter, it could be understood that this line would yield the minimum tar removal efficiency for tar classes 2, 4 and 5. For example, at 80ºC, 60ºC and 40ºC, above 80%, 85% and 91% of tar content reduction would be achieved respectively.

On the other hand, figure 4.12B depicts the dependence of dust collection efficiency for particulate matters of 5 and 10µm with the superficial gas velocity. These curves correspond to particle bed sizes of 400µm and 1mm. The two solid curves are related to filtration in a moving bed of 400µm which denote higher dust collection efficiencies than at 1mm of particle bed size, dash curves. In fact, the difference can be up to two times at low gas velocities (0.5-1.5m/s). Furthermore, the dust collection efficiency for dust of 10µm is higher than for 5µm since the relative particle size is lower as well as this gap is lower for low particle size (400µm). Then, low gas velocities and low bed particle sizes are desirable for getting dust collection efficiencies of at least to 80%. In order to get higher efficiencies in collecting dust material, a second gas flow treatment should be applied.

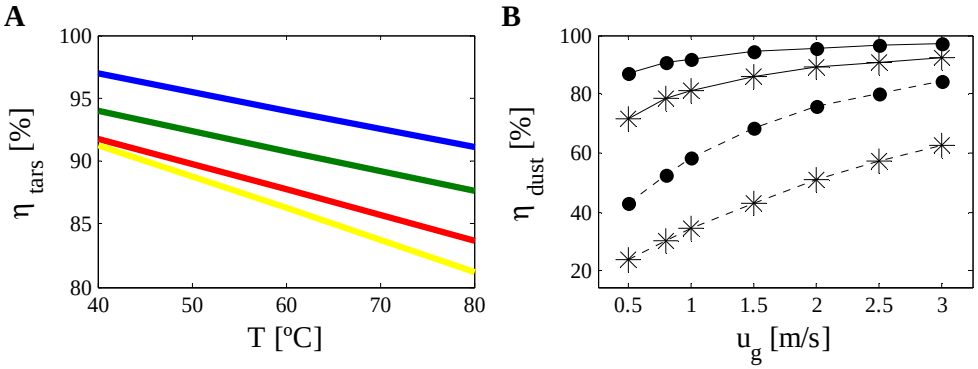

Figure 4.12: Tar removal efficiency with outlet gas temperature at several particle sizes: 100µm(blue), 400µm(green), 700µm(red) and 1mm(yellow) at 3m/s superficial gas velocity (A) and dust collection efficiency with superficial gas velocity at 400µm(-) and 1mm(- -) for 5(*) and 10µm(·) of dust (B).

As previously stated, the MBHEF equipment would yield high tar removal efficiencies, at least of the same order of those attained with the use of catalytic tar cracker, venture scrubber or sand bed filter at much lower temperatures and higher efficiencies than the ones achieved by means of wash tower, wet electrostatic precipitator, fabric filter, rotational particle separator and fixed bed adsorber (Hasler and Nussbaumer, 1997).

Finally, one point has to be considered. Because of using a moving bed, an additional stream with tarry material condensed would be produced as waste. Then, it would require a recovery or cleaning treatment in order to clean the moving bed of tars. The

current work proposes to recirculate the solid flow stream coming out from the moving bed to the BGFB reactor in order to clean-up it and avoid extra waste disposal problems: cleaning equipment and costs. Therefore, the moving bed should employ the same particle size than the one used in the bed of the BGFB reactor.

4.4.2. Effect of the temperature in the gas properties simulations

The figure 4.13(A-B) is aimed to analyse the influence of the temperature on the gas properties. To accomplish this, the effect of using constant and variables physical and transport properties with the temperature in the outlet gas temperature and the tar removal efficiency is shown in the figures 4.13A and 4.13B, respectively. These figures depict the profiles of differences between constant and variables properties for the gas temperature and the tar abatement efficiency in the gas flow direction at 700mm of particle size as for example. In general terms, the error committed is up to -43% for the gas temperature in the last 20% of length but the case of 0.5m/s of superficial gas velocity. The error also reaches around 26% of difference as consequence of decimals in the last positions of the MBHEF.

On the contrary, the discrepancies in the tar removal efficiency are visible in the very inlet of the device, being up to -70%. Then, the error tends to be around less ±5%.

Although performance errors are high as figure 4.13 denotes, the MBHEF size is so small in both design cases (1 and 2) that no to consider temperature influence in the gas properties would not imply noticeable divergence in equipment design. However, in the current study, the gas properties dependence with temperature has been employed.

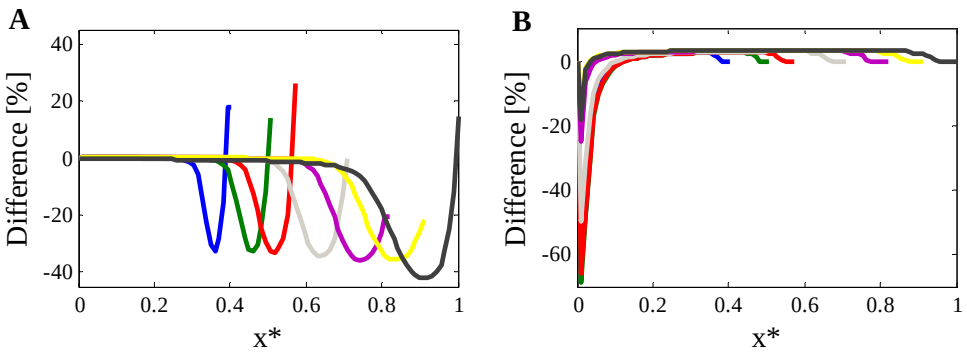

Figure 4.13: Dimensionless profiles of gas temperature error (A) and tar removal efficiency error (B) committed by using constant gas properties at 0.5(blue), 0.8(green), 1(red), 1.5(grey), 2(pink), 2.5(yellow) and 3m/s(black) of superficial gas velocity and 700μm of particle size.

4.4.3. Exergy analysis

An exergy analysis was performed in order to obtain more insight about the performance of a MBHEF system according to the choice of operating conditions. This analysis is based on the exergy balance:

$$A_d = \sum_j \left(1 - \frac{T_{ref}}{T_j}\right) Q_j + \dot{W}_{cv} + \sum_i \dot{m}_i a_{f,i} + \sum_o \dot{m}_o a_{f,o} \qquad (4.25)$$

The exergy balance yields the exergy destruction (A_d) accounting for the heat transfer, work developed (if it exists) and the mass flow contribution in the gas and solid phases.

In the figure 4.14, the exergy destruction profile along the length of the MBHEF is represented for two cases studied as examples. As it can be observed, the exergy destruction increase with the length since the heat and mass exchange between the gas and solid phases take place. As explained in figure 4.6, the temperature of the solid phase raises against the decrease of the gas temperature. Furthermore, the pressure drop also affects the exergy balance. Therefore, the exergy destruction increases rapidly at the inlet region. Then, the exergy tends to level out.

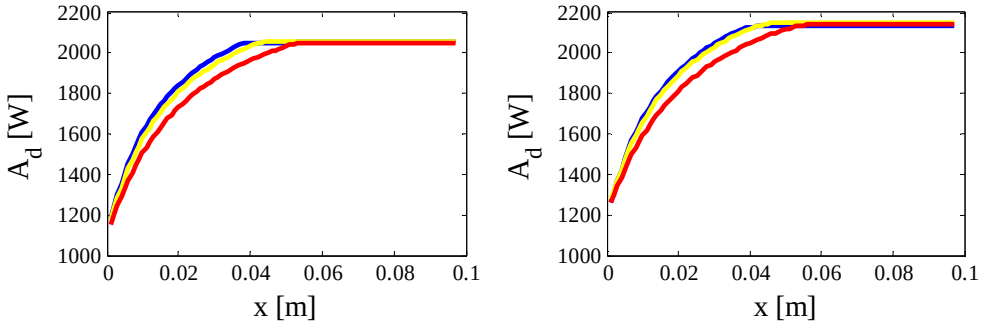

Figure 4.14: Exergy destruction profile along the length for particle bed size of 400µm (A) and 700µm (B) at 0.8m/s (blue line), 1m/s (yellow line) and 1.5m/s (red line) of superficial gas velocity.

On the other hand, figure 4.15 shows a map of exergy destruction with the MBHEF length. Here the dimensionless exergy destruction (A_d^*) is represented as the evolution of exergy destroyed compared to the maximum value attainable at the highest superficial velocity (here 3m/s).

The trends are identical since the only difference is the particle size. The exergy destruction follows the same relationship than the tar removal efficiency one, with two characteristic features. For a given axial position in the gas flow direction, the higher the gas velocity the lower the exergy destruction while for a given outlet gas temperature, the exergy destruction grows with the gas velocity because of the decrease of the residence time due to that it involves bigger device size. Furthermore, it is evident that the particle size influences the exergy destruction paying attention to the scale. Although there is hardly difference between 700µm and 1mm, the shape of the curves changes below 700µm. This can be observed in the increase of slope at the very inlet, followed by a more pronounced decrease at the tail of the curves for the smaller particle sizes. This effect is more obvious at high gas velocities (above 1.5m/s). In addition to this, at low particle sizes (100µm), the curves tend to separate each other being parallel even at low gas velocities in contrast to what happens to others particle bed diameters.

Finally, the particle bed size becomes relevant below 400µm in the exergy destruction map for choosing optimised operating conditions. From an exergy point of view, the highest gas velocity, the less exergy destruction because of less residence time to promote the heat exchange and tars condensation. However, this involves lower tar removal and dust collection efficiency. Then, the exergy destruction analysis stands out

low particle sizes (above 400µm) and gas velocities (below 1.5m/s) for minimizing the exergy destruction with high tar abatement and dust collection efficiencies.

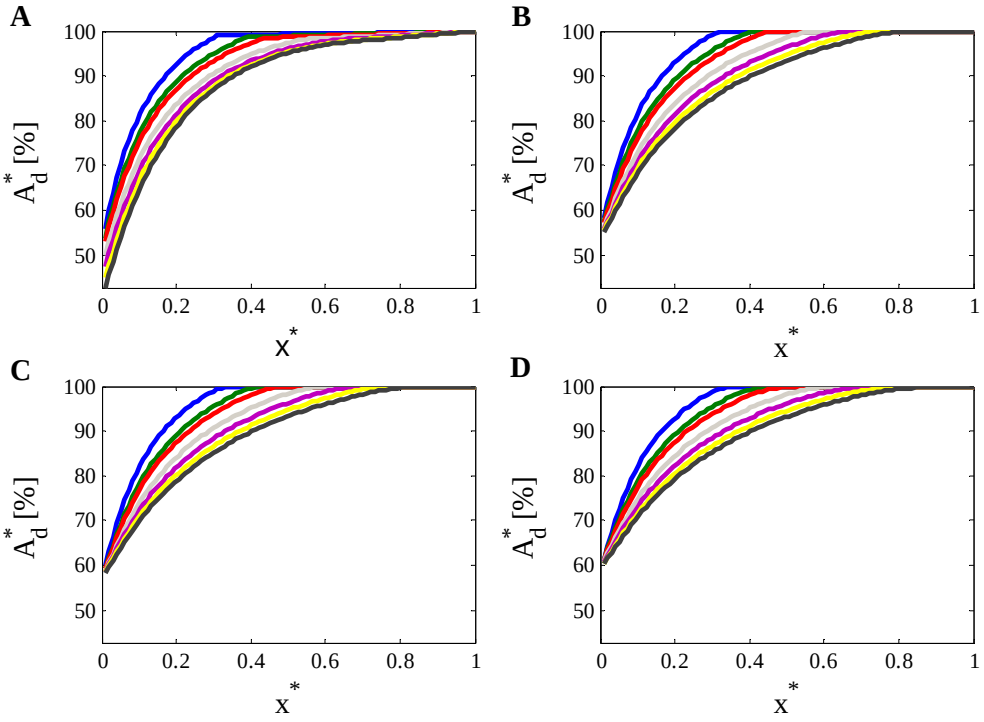

Figure 4.15: Exergy destruction map for particle bed size of 100µm (A), 400µm (B), 700µm (C) and 1mm (D) at 0.5(blue), 0.8(green), 1(red), 1.5(grey), 2(pink), 2.5(yellow) and 3m/s(black) of superficial gas velocity.

4.5. Conclusions

A tar and particle removal and exergy analysis of a MBHEF system has been performed varying the particle size of the bed material and the superficial gas velocity. Tar specie representatives of classes 2, 4 and 5 have been chosen. The general problem is addressed and simplified for a gas-solid cross-flow, neglecting conduction and energy losses terms.

According to the sensitivity analysis carried out, compact equipment yielding tar removal efficiencies up to 94% are attainable with the proper choice of operating conditions, superficial gas velocities of 0.5-3m/s and particle bed sizes of 100µm-1mm for example, for an outlet gas temperature of 60ºC. The superficial gas velocity and the particle size have been demonstrated as key parameters in designing compact equipment. Low superficial velocities promote high residence time and low pressure drop and then, slighter power consumption in contrast to higher gas velocities (above 1.5m/s). The opposed effect is found with the particle size of the bed. The smaller the particle size the higher gas-solid contact and therefore the higher the tar condensation rates and the tar removal efficiencies. However, small particle bed sizes would involve higher power consumption for blowing the gas flow through the moving bed. The pressure drop would depend on the gas flow to be conditioned and the particle size of the bed. Thus, particle bed sizes above 400µm should be recommended.

On the other hand, the dimensionless maps of temperature, tar abatement efficiency and exergy destruction obtained are addressed to help choosing the most suitable operating conditions in terms of tars removal efficiency, syngas cooling and exergy optimisation in order to save costs. However, as stated by these maps, the simultaneous economic and exergy optimisation of the MBHEF equipment is not possible.

Then, the MBHEF proposed here can be used as valuable and useful equipment for conditioning syngas to be fuelled in engine applications, saving operational costs in comparison with traditional cold syngas conditioning device. Further secondary treatment should be applied to improve the tar content removal if needed.

Finally, to remark that using the same particle bed size that the one employed in BGFB reactors, the solid flow stream leaving the MBHEF could be recirculated to the BGFB reactor. This would avoid extra waste disposal problems and costs.

4.6. Notation

A_d Exergy destruction, [W].

a Interfacial area, [m^2/m^3].

a_p Surface-volume particle ratio, [m^2/m^3].

C_c Concentration of specie “c” in gas phase in MBHEF, [kg/m^3].

$C_{p,g}$ Dust concentration in gas phase in MBHEF, [kg/m^3].

$C_{p,p}$ Dust concentration in solid phase in MBHEF, [kg/m^3].

$C_{c,p}$ Concentration of specie “c” in solid phase in MBHEF, [kg/m^3].

c_p Heat capacity, [J/kg K].

D Diffusivity of species in a multicomponent mixture of species, [m^2/s].

d_p Particle diameter, [m].

G Generation term, [kg/m^3 s].

h heat transfer coefficient by convection, [W/m^2 K].

$h_{fg,c}$ Latent heat of component “c”, [J/kg].

k Thermal conductivity, [W/m K].

k_m Fluid-particle mass transfer coefficient of component “m”, [m/s].

H Width of MBHEF, [m].

L Length of MBHEF, [m].

$\dot{m}$ Condensation rate of component “c”, [kg/m^3 s].

n Number of chemical species/components.

nc Number of condensable components.

nr Number of reactions.

Q Volume flow, [m^3/s]. Heat flux, [W/m^3].

q_{rad} Radiation heat loss [W/m^3].

T Fluid temperature, [K].

$T_{dp,tar}$ Tar dew point, [K].

u_g, v_g, w_g Gas velocity components, [m/s].

u_l, v_l, w_l Liquid velocity components, [m/s].

u_p, v_p, w_p Solid velocity components, [m/s].

U_w Overall phase to surroundings heat transfer coefficient, [W/m^2 K].

x, y, z Spatial coordinates, [m].

W_{pump} Power pumping of fluid, [J/s].

Abbreviations

BFB Bubbling Fluidized Bed.

CFB Circulating Fluidized Bed.

EF Entrained Flow.

FBD Fixed Bed Downdraft.

FBU Fixed bed Updraft.

MBHEF Moving Bed Heat Exchanger Filter.

PAH Polycyclic aromatic hydrocarbons.

syngas Synthesis gas.

Greek letters

ΔH_r Reaction enthalpy or reaction "r", [J/kg].

ΔP Pressure drop, [Pa].

ε Phase fraction, porosity of bed inert material, [-].

η Removal efficiency of tars/dust, [%].

θ Solid phase temperature, [K].

λ Filter coefficient [m^{-1}], mean free path of the gas molecules, [μm].

μ Viscosity, [kg/m s].

ρ Density, [kg/m^3].

Subscripts

0 Value of variable at the MBHEF inlet.

a First chemical specie in a binary system of components.

b Second chemical specie in a binary system of components.

c Arbitrary chemical specie.

cond Condensate.

cv Control volume.

dust Fine particles content/concentration. Fine particles. Fines.

e Effective.

evap Evaporate.

f Fluid.

g Gas phase.

l Liquid phase.

M Component or chemical specie.

p Particle, solid phase.

r Reaction arbitrary.

ref Reference state (25ºC and 1atm).

s Value of variable at the MBHEF outlet.

tars Tars content/concentration. Tars.

∞ Surroundings.

Superscripts

* Non-dimensional variable [-].

‾ Average value.

Bibliography

Achenbach, E. 1995. Heat and flow characteristics of packed beds. *Experimental Thermal and Fluid Science* 10(1), 17-27.

Arena, U., Zaccariello, L., Mastellone, M. L. 2009. Tar removal during the fluidized bed gasification of plastic waste. *Waste Management* 29(2), 783-791.

Bird, B.R., Stewart, W.E., Lightfoot, E.N., 2002. Transport Phenomena, 2nd ed. Wiley, New York.

Cao, Y., Wang, Y., Riley, J.T., Pan, W.P. 2006. A novel biomass air gasification process for producing tar-free higher heating value fuel gas. *Fuel Processing Technology* 87(4), 343-353.

Campoy-Naranjo, M. 2009. Gasificación de biomasa y residuos en lecho fluidizado: Estudios en planta piloto (Biomass and wastes gasification in fluidised bed: pilot plant studies). *PhD Thesis*. University of Sevilla, Spain. Spanish.

Campoy, M., Gómez-Barea, A., Vidal, F.B., Ollero, P. 2009. Air-steam gasification of biomass in a fluidised bed: Process optimisation by enriched air. *Fuel Processing Technology* 90(5), 677-685.

Corella, J., Toledo, J.M., Molina, G. 2006. Calculation of the conditions to get less than 2g tar/m_n^3 in a fluidized bed biomass gasifier. *Fuel Processing Technology* 87(9), 841-846.

Detournay, M., Hemati, M., Andreux, R. 2011. Biomass steam gasification in fluidized bed of inert or catalytic particles: Comparison between experimental results and thermodynamic equilibrium predictions. *Powder Technology* 208(2), 558-567.

Devi, L., Ptasinski, K. J., Janssen, F. J. J. G. 2003. A review of the primary mesures for tar elimination in biomass gasification processes. *Biomass & Bioenergy* 24, 125-140.

Dou, B., Pan, W., Ren, J., Chen, B., Hwang, J., Tae-U, Y. 2008. Removal of tar component over cracking catalysts from high temperature fuel gas. *Energy Conversion and Management*, 49(8), 2247-2253.

Ergun, S. 1952. Fluid flow through packed columns. *Chemical Engineering and Processing* 48 (2), 89-94.

Fuller, E.N., Schettler, P.D. Giddings,, J.C. 1966. A new Method for prediction of binary gas-phase diffusion coefficients. *Industrial & Engineering Chemistry* 58(5), 19-27.

Gandhidasan, P. 2003. Estimation of the effective interfacial area in packed-bed liquid desiccant contactors. *Industrial & Engineering Chemistry Research* 42(12), 3420-3425.

Ginestra, J.C., Jackson, R. 1985. Pinning of a bed of particles in a vertical channel by a crossflow of gas. Industrial Engineering Chemical Fundamentals, 24: 121-128.

Gómez-Barea, A., Leckner, B. 2009. Gasification of biomass and waste, in: M. Lackner, F. Winter, A.K. Agarwal eds., Handbook of Combustion, Vol. 4, Wiley-VCH, Weinheim, 365-397.

Gómez-Barea, A., Leckner, B. 2010. Modeling of biomass gasification in fluidized bed. *Progress In Energy and Combustion Science* 36(4), 444-509.

Gómez-Barea, A., Leckner, B., Villanueva-Perales, A., Nilsson, S., Fuentes-Cano, D. 2012. Improving the performance of fluidized bed biomass/waste gasifiers for distributed electricity: A new three-stage gasification system. *Applied Thermal Engineering*, In Press: 1-10.

Hasler, P., Nussbaumer, T., Buehler, R. 1997. Evaluation of gas cleaning technologies for small scale biomass gasifiers. Swiss Federal Office of Energy, Berne, Switzerland.

Hasler, P., Nussbaumer, T. 1999. Gas cleaning for IC engine applications from fixed bed biomass gasification. *Biomass and Bioenergy* 16(6), 385-395.

Henriquez, V., Macías-Machín, A. 1997. Hot gas filtration using a moving bed heat exchanger-filter (MHEF). *Chemical Engineering and Processing* 36(5), 353-361.

Herzog, H.J., 2011. Scaling up carbon dioxide capture and storage: from megatons to gigatons. *Energy Economics* 33(4), 597-604.

Hu, T., Hassabou, A.H., Spinnler, M., Polifke, W. 2011. Performance analysis and optimisation of direct contact condensation in a PCM fixed bed regenerator. *Desallination* 280(1-3), 232-243.

JANAF database (therm.dat) from CHEMKIN file therm.dat v4.0, March, 2004. http://users.rowan.edu/~marchese/combustion04/kinetics/h2-chemkin/therm.dat

Kaewluan, S., Pipatmanomai. 2011. Gasification of high moisture rubber woodchip with rubber waste in a bubbling fluidized bed. *Fuel Processing Technology* 92(3), 671-677.

Kiel, J. H. A., van Paasen, S. V. B., Neeft, J. P. A., Devi, L., Ptasinski, K. J., Janssen, F. J. J. G. 2004. Primary measures to reduce tar formation in fluidized-bed biomass gasifiers. *Final Report SDE project P1999-12. Energy Research Centre of the Netherlands, ECN. Report ECN-C-04-014, The Netherlands*.

Li, C., Suzuki, K. 2009. Tar property, analysis, reforming mechanism and model for biomass gasification. An overview. *Renewable and Sustainable Energy Reviews* 13(3), 594-604.

Longanbach, J.R. 1998. Preparing advanced coal-based power systems for the 21st century at the power systems development facility in Wilsonville, Alabama. *In: Proc. 23rd Int. Technical Conf. on Coal Utilization and Fuel Systems*, Clearwater, FL, USA, pp. 69-78.

Lozano, A., Henriquez, V., Macias-Machín, A. 1996. Modelling of a new crossflow moving-bed heat-exchanger/filter (MHEF). *Filtration & Separation* 33(1) 69-74.

McKendry, P. 2002. Energy production from biomass (part 3): gasification technologies. *Bioresource Technology* 83(1), 55-63.

Milne, T. A., Evans, R. J. 1998. Biomass gasifier "tars": their nature, formation and conversion. *National Renewable Energy Laboratory, NREL, Report no. NREL/TP-570-25357, Golden, CO, USA*.

Ptasinski, K.J. 2008. Thermodynamic efficiency of biomass gasification and biofuels conversion. *Biofuels Bioproducts Biorefining* 2(3), 239-253.

Rabu, L.P.L.M., Jansen, D. 2001. De-centralised power production using low-calorific value gas from renewable energy resource in gas turbines. ECN.

Ranz, W.E. 1952. Friction and transfer coefficients for single particles and packed beds. *Chemical Engineering Progress* 48(5), 247-253.

Rapagnà, S., Jand, N., Kiennemann, A., Foscolo, P.U. 2000. Steam-gasification of biomass in a fluidised-bed of olivine particles. *Biomass and Bioenergy* 19(3), 187-197.

Ruoppolo, G., Miccio, F., Piriou, B., Chirone, R. 2009. Biomass gasification in a catalytic fluidized reactor with beds of different materials. *Chemical Engineering Journal* 154(1-3), 369-374.

Schmidt, S., Giesa, S., Drochner, A., Vogel, H. 2011. Catalytic tar removal from bio syngas-Catalyst development and kinetic studies. *Catalysis Today* 175(1), 442-449.

Smid, J., Hsiau, S.S., Peng, C.Y., Lee, H.T. 2005a. Moving bed filters for hot gas cleanup. *Filtration and Separation* 42(6), 34-37.

Smid, J., Hsiau, S.S., Peng, C.Y., Lee, H.T. 2005b. Granular moving bed filters and adsorbers /GM-BF/A) – patent review: 1970-2000. *Advanced Powder Technology* 16(4), 301-345.

Socorro, M., Macías-Machín, A., Verona, J.M., Santana, D. 2006. Hot gas filtration and heat Exchange in a packed bed using lapilli as a granular medium. *Industrial & Engineering Chemistry Research* 45(23), 7957-7966.

Soria-Verdugo, A., Almendros-Ibáñez, J.A., Ruiz-Rivas, U., Santana, D. 2009. Exergy optimisation in a steady moving bed heat exchanger. *Annals of the New York Academy of Science*, 1161: 584-600.

Stassen, H.E.M. 1993. Strategies for upgrading producer gas from fixed bed gasifier systems to internal combustion engine quality. In: Graham, R.G., Bain, R., editors, Biomass gasification: hot-gas clean-up. IEA Biomass Gasification Working Group: 33-44.

Thek, R.E., Stiel, L.I. 1966. A new reduced vapor pressure equation. *AIChE Journal* 12(3), 599-602.

Thunman, H., Niklasson, F., Johnsson, F., Leckner, B. 2001. Composition of volatiles gases and thermochemical properties of wood for modelling of fixed or fluidized beds. *Energy & Fuels* 15(6), 1488-1497.

Weerachanchai, P., Horio, M., Tangsathitkulchai, C. 2009. Effects of gasifying conditions and bed materials on fluidized bed steam gasification of wood biomass. *Bioresource Technology* 100(3), 1419-1427.

Wilke, C.R. 1950. Diffusional properties of multicomponent gases. *Chemical Engineering Progress* 46(2), 95-104.

Chapter 5

Conclusions

A techno-economic feasibility analysis has been performed in order to assess the potential of *Cynara cardunculus* L. gasification for bioenergy production. The choice of this biomass underlies in its advantages against other energy crops: high biomass yield on poor quality soils and ease to be grown in non-irrigated land and to be well suited for seed propagation. All these features make cynara one of the most promising energy crops in the Mediterranean region and a suitable choice to the farmers.

The technical and economic analysis has been carried out on the basis of estimating the energy crop and power plant cost of cynara in the CAM context, with the comparison of two technological solutions: a combined cycle gas turbine and an internal combustion engine. In addition, this PhD thesis has also investigated the predictive capacity of the modelling approaches proposed for estimating the performance of the FBG reactor and the MBHEF in order to transform cynara into bioenergy (syngas) and clean the syngas from inadequate tars and dust levels.

The results show that cynara has the potential to provide around 42% of national biomass-based electricity supply, what would correspond to save roughly 66% of CO_2 emissions from combustion of fossil fuels in the CAM.

The cost of cynara-based electricity generation varies broadly and is affected by the biomass yield, technology solutions, operation and maintenance.

The results indicate that ICE power generators are the most suitable technologies when the power output required is below 8 MW. Such behavior is influenced by the electrical costs corresponding to the engines. On the contrary, for an installed electric capacity above 8 MW, CCGT plants are the best choice.

It has been determined that an 8 MW CCGT plant could produce electricity from *Cynara cardunculus* L. for 21.60 c€/kWh, as compared to 24.32 c€/kWh for electricity from an ICE plant. Furthermore, the results conclude that ICE plants are more expensive to run than CCGT plants at any scale. This trend is due to the ICE plant requires the maintenance of more rotating equipment than the CCGT solution.

Concerning the thermochemical conversion of cynara into syngas, the new proposed scheme focuses on biomass behavior and characterizes the phenomena occurring in the bubble phase: temperature peaks due to volatiles combustion and instantaneous devolatilization. This phase of the dense region in the FB has been demonstrated to act as “by-passing” hot spots influencing the ash-related problems. Thereby, the modelling

approach is able to help monitoring the location of bed agglomeration and ash sintering risk regions and then, to avoid operating conditions prone to cause FBR defluidization.

The sensitivity analysis of cynara gasification in a FB predicts a good gasification performance but the tar content, whose interval values estimated are above the typical range reported in the literature for air-blown FB gasifiers (~20-30g/Nm^3).

The comparison of simulations and experimental works stand out discrepancies that can be attributable to data heterogeneity found in the literature. Such variations are related to the uncertainty in tars lumping criteria, inaccuracy of tar cracking kinetics and different use of tars measurement methods, what makes very difficult to accurately model and predict such reactor behavior. This is in accordance to what Gómez-Barea and Leckner (2010) state: the devolatilization and kinetic expressions greatly affect simulation results and char and tar conversion are the processes whose modelling is least satisfactory. Thus, validation should be desired at lab-scale or larger scale in testing the models proposals. On the other hand, Basu and Kaushal (2009) also concluded that the major obstacle is to correctly fit kinetic parameters based on experimental research. This adjustment would be able to predict more accurately the reactor performance under a wider range of operating conditions.

In regards to the clean-up of the syngas produced in FBG reactors, the use of the modelling approach proposed in this PhD Thesis has shown that such secondary method is a feasible tool for reducing the levels of particulate and tars material with high efficiencies: 88% (as a minimum) with the proper choice of the operating conditions (particle size and superficial gas velocity) for an outlet gas temperature of 60ºC, the typical inlet temperature in internal combustion engines and gas turbines.

The sensitivity analysis carried out has demonstrated that the superficial gas velocity and particle velocity are key parameters in designing such compact equipment. It has been observed that low superficial velocities promote high residence time, low pressure drop and high tar removal efficiencies. The opposed effect is found with the particle size of the bed material. Thus, particle bed sizes above 400μm should be recommended.

The aim of the dimensionless maps of temperature, tar abatement efficiency and exergy destruction presented is to help elucidating the most suitable operating conditions in terms of tars removal efficiency, syngas cooling and exergy optimization. Nevertheless, these maps denote that the simultaneous economic and exergy optimization in the MBHEF is not attainable.

Therefore, the MBHEF proposed here can be used as valuable equipment for conditioning syngas to be fuelled in engine applications, saving operational costs in comparison with traditional cold syngas conditioning devices.

To conclude, this PhD Thesis has described the methodology to assess the bioenergy production via fluidized bed gasification from *Cynara cardunculus* L. This study can be applied to other biofuels and energy crops of interest such as Reed canary grass or Giant reed, as for example, of applicability in others regions whose bioenergy share does not match the national and international RES-related directives. Furthermore, the modelling approaches proposed for predicting the performance of FBG reactors and MBHEF as hot gas clean-up of syngas from such reactors have been shown as a feasible and useful tools in order to: 1) help other diagnosis methods for the prevention of bed

agglomeration and ash sintering in FBG reactors; 2) reduce particulate and tar levels in the syngas generated; 3) avoid downstream particulate and tars-related problems such as fouling, blockage and attrition and 4) save operational and maintenance costs by the optimization of studied operations with the use of the modelling approaches presented in this work. Thus, unscheduled shut-down of FBG reactors and downstream equipment should be avoided. The use and implementation of these proposed tools would help to optimise such operation processes and to save costs, meeting energy demands and being environmentally sustainable.

Finally, the technical and economic feasibility study of *Cynara cardunculus* L. gasification in a fluidized bed has been proven as a valuable and promising methodology to assess the bioenergy production from energy crops and biofuels.

Chapter 6

Appendix

Contents

The appendixes presented as follows are aimed to:

- Summarizes previous experimental works (Appendix A) for comparing simulations results with them in order to evaluate the FBG modelling approach.
- Shows physical, chemical and thermodynamical data as well as physical and thermodynamical properties estimation methods employed in the corresponding chapters of this PhD Thesis. These are applied for permanent gases and tars compounds (Appendixes B-F).
- Justify the choice of diffusivity estimation method for permanent gases and tars (Appendix G) by means of comparing the error magnitudes of each diffusivity estimation method.
- Show the low capability of evaporation of tars once they have condensed within their respective vapor pressure of sub-cooled liquids and solids (Appendix H).
- Justify the assumption made of neglecting the width film of water liquid condensed film and volume dust collected in the solid phase (Appendix I).

Simulation results indicate that the fraction of water condensed as liquid can be neglected as well as the volume of dust collected in the solid phase.

- To explain the coefficients of energy balance of gas and solid phases for MBHEF in equation (4.19).

Appendix A. Biomass FBG Facilities Data and Experimental Results

This appendix has a double utility. On the one hand, to show in a detailed manner the operating conditions such as pressure, bed temperature, equivalence ratio, fluidization state (U_0/U_{mf}), bed material, particle and density of bed material and reactor design (diameter and height of the bed and the freeboard regions), in table A1. On the other hand, this appendix also details the syngas quality of some important experimental works (tables A3-4) when gasified several biomasses (table A2) in previously presented fluidized bed reactors under typical operating conditions, also explained.

Facility/Reference	Gómez-Barea et al. (2005)	Narváez et al. (1996)	Gil et al. (1999)	Alimuddin and Lim (2008)	Campoy et al. (2009)
Bed diameter (m)	0.15	0.06	n.a.	0.04	0.15
Bed height	1.7	n.a.	n.a.	0.92	1.7
Freeboard diameter (m)	0.25	n.a.	n.a.	n.a.	0.25
Freeboard height (m)	2.5	n.a.	n.a.	0.92	2.5
Fluidizadization velocity (m/s)	0.8-1.4	$2U_{mf}$	$2\text{-}4U_{mf}$	n.a.	bubbling
Equivalence Ratio	0.17-0.31	0.20-0.45	0.18-0.45	0.17-0.23	0.24-0.38
Operation Temperature (ºC)	700-820	700-850	780-830	718-733	755-840
Operation Pressure	atmospheric	atmospheric	atmospheric	atmospheric	atmospheric
Bed material	Ofite	Sand	Sand	Sand	Ofite
d_p (μm)	380	320-500	n.a.	425-600	380
ρ_s (kg/m^3)	2620	n.a.	n.a.	1520	2620

Table A1: Data of biomass fluidized bed gasification reactors: design parameters, operational conditions ranges and bed material employed in different researches using air as gasifying agent. n.a.: not available.

Biomass/Reference	Gómez-Barea et al. (2005)	Narváez et al. (1996)	Gil et al. (1999)	Alimuddin and Lim (2008)	Campoy et al. (2009)
Proximate Analysis (%)					
LHV (MJ/kg)	16.2	18.0-18.4	n.a.	n.a.	17.1
Fixed carbon	19.7	16-17	n.a.	n.a.	n.a.
Volatile matter	66.9	81-83	n.a.	n.a.	n.a.
Moisture	7.6	10-20	10-20	n.a.	6.3
Ash	5.8	0.5-1.2	n.a.	n.a.	0.5
Ultimate Analysis (%)					
C	50.0	50.0	n.a.	n.a.	n.a.
H	6.5	5.7	n.a.	n.a.	n.a.
O	36.3	44.1	n.a.	n.a.	n.a.
N	0.8	0.1-0.3	n.a.	n.a.	n.a.
S	0.1	0.03	n.a.	n.a.	n.a.

Table A2: Data of biomass properties used in corresponding researches presented above. n.a.: not available.

Table A3 presents the syngas quality of FBG experiments conducted by Campoy et al. (2009) according to the reactor and operating conditions stated in table A1. This work indicates the operating conditions for each test and the yield in terms of dry basis gas composition (CO, CO_2, H_2 and CH_4), the gas flow rate, LHV, cold gasification and carbon conversion. Thus, simulations results obtained in **Chapter 3** may be compared within a wide range of operating conditions typical in biomass gasification.

Test	1	2	3	4	5	6	7	8	9
Operational conditions									
Biomass Flow Rate (kg/h)	11.5	12.2	12.2	15.0	15.0	12.4	10.0	16.2	12.0
Air Flow Rate (Nm^3/h)	17.0	17.0	17.0	17.0	17.0	11.9	9.1	10.6	7.7
O_2 Flow Rate (Nm^3/h)	0	0	0	0	0	1.5	1.2	1.4	1.0
Steam Flow Rate (kg/h)	0	2.5	5.1	3.2	6.0	3.7	5.6	4.7	6.5
Bed temperature (ºC)	812	804	789	786	755	808	790	781	765
Freeboard temperature (ºC)	716	721	709	708	709	715	715	716	695
Gas composition (%v/v,dry)									
CO	15.8	15.4	13.8	15.0	11.9	18.9	15.7	20.8	15.3
CO_2	15.1	15.9	17.0	16.2	18.6	17.6	18.8	15.8	20.3
H_2	8.7	11.9	13.3	14.0	16.2	16.4	18.3	20.0	22.3
CH_4	5.1	4.8	4.6	4.7	5.3	5.5	5.7	6.7	7.1
Process variables									
Gas Flow Rate (Nm^3/h,dry)	24.6	26.1	26.5	27.2	28.4	22.3	17.2	23.5	17.9
Gas yield (Nm^3 dry gas, N_2 free/kg dafb)	1.03	1.11	1.14	0.97	1.06	1.13	1.08	0.98	1.04
LHV (MJ/Nm^3 dry gas)	4.76	4.95	4.83	5.09	5.15	6.12	6.00	7.19	6.88
Cold Gasification Efficiency (%)	0.59	0.62	0.61	0.54	0.57	0.64	0.60	0.61	0.60
Carbon conversion (%)	0.93	0.90	0.92	0.90	0.91	0.94	0.95	0.96	0.96

Table A3: Experimental results of work developed by Campoy et al. (2009).

Table A4 shows the syngas quality of FBG experiments conducted by Narváez et al. (1996) according to the reactor and operating conditions stated in table A1 too. This work indicates the operating conditions for each test and the yield in terms of dry basis gas composition (CO, CO_2, H_2 and CH_4), the gas yield, LHV and tar content. Thus, simulations results obtained in **Chapter 3** may also be compared within a wide range of gasification operating conditions.

Test	1	2	3	4	5	6
Operational conditions						
Biomass Flow Rate (kg/h)	9.6	9.2	6.5	11.4	10.9	11.3
Air Flow Rate (Nl/min)	12.0	12.0	12.0	12.0	14.0	14.0
Bed temperature (ºC)	800	800	810	800	790	800
Freeboard temperature (ºC)	540	550	500	600	560	530
Gas composition (%v/v,dry)						
CO	14.0	13.0	10.0	13.0	13.0	18.0
CO_2	13.5	15.0	12.0	15.0	15.0	13.5
H_2	7.0	9.5	8.0	9.5	9.5	9.5
CH_4	3.0	2.7	2.4	2.7	2.7	4.5
Process variables						
Gas yield (Nm^3 dry gas/kg dafb)	2.3	2.5	2.5	2.1	2.4	2.1
LHV (MJ/Nm^3 dry gas)	4.3	4.6	3.7	4.6	4.6	6.3
Tar content (g/Nm^3)	3.733	7.163	2.987	2.011	2.011	9.981

Table A4: Experimental results of work developed by Narváez et al. (1996).

Appendix B. Physical and Structural Properties of Permanent Gases

Table B1 shows physical and structural properties of permanent gases: oxygen (O_2), carbon monoxide (CO), carbon dioxide (CO_2), methane (CH_4), hydrogen (H_2) and nitrogen (N_2) as well as water (H_2O) and ethane (C_2H_6). These parameters are keys for estimating transport properties such as viscosity, thermal conductivity and diffusivities in gas mixtures.

Chemical specie	***M* (g/mol)**	**T_c (K)**	**P_c (bar)**	**V_c (cm3/mol)**	**ε/k (K)**	**σ (A)**
O_2	32	155	50.43	73.4	106.7	5.967
CO	28	133	34.99	94.4	91.7	3.690
CO_2	44	304	73.84	94.0	195.2	3.941
CH_4	16	190	45.99	98.6	148.6	3.758
H_2	2	33	13.13	64.1	59.7	2.827
H_2O	18	647	220.64	55.9	809.1	2.641
N_2	28	126	34.00	89.2	71.4	3.798
C_2H_6	30	305	48,72	145.5	215.7	4.443

Table B1: Critical properties (temperature, pressure) and structural properties (molar volume, minimal potential energy, collision diameter) of chemical species of interest in the works dealt within this Thesis. Adapted from Poling et al. (2004) and Rowley et al. (2007).

Appendix C. Physical and Structural Properties of Tars

Table C1 shows physical and structural properties of tar compounds. These parameters are key for estimating transport properties: viscosity, thermal conductivity and diffusivities in gas mixtures. Here, a wide list of tar compounds is attached in order to show the influence of molecular weight in these properties.

Chemical specie	***M* (g/mol)**	**T_c (K)**	**P_c (bar)**	**V_c (cm3/mol)**	**ε/k (K)**	**σ (A)**
Benzene	78.11	562	48.95	89.1	412.3	5.349
Toluene	92.14	592	41.08	106.3	455.8	3.983
Phenol	94.11	694	61.30	87.9	534.4	3.739
Naphthalene	128.17	727	38.97	409.5	560	6.25
Acenaphthalene	154.21	800	35.18	487.5	616	6.62
Fluorene	166.22	824	33.76	521.5	635	6.77
Phenanthrene	178.23	872	32.43	555.5	671	6.91
Anthracene	178.23	874	32.43	555.5	673	6.91
Fluoranthene	202.26	919	30.73	619.5	707	7.17
Pyrene	202.25	928	30.73	619.5	715	7.17
Chrysene	228	983	27.41	701.5	757	7.47
Perylene	252.31	1030	26.08	765.5	793	7.69
Coronene	300.35	1101	23.70	893.5	848	8.10

Table C1: Critical properties (temperature, pressure) and structural properties (molar volume, minimal potential energy, collision diameter) of chemical species of interest in the works dealt within this Thesis, related to tars. Adapted from Poling et al. (2004) and Rowley et al. (2007).

If there is no data about ε/k and σ, they can be estimated according to Bird and Stewart (2002):

$$\varepsilon / \bar{k} = 0.77 T_c \qquad \text{(C.1)}$$

$$\sigma = 0.841 V_c^{1/3} \tag{C.2}$$

Table C2 reports molecular structures of tar compounds for accounting the number of aromatic rings when estimating diffusivities by the method of Fuller et al. (1966).

Benzene	Phenol	Naphthalene	Acenaphthalene	Fluorene	Phenanthrene
	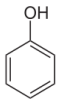	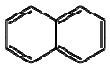	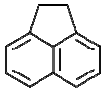	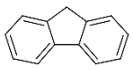	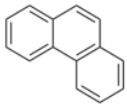
Anthracene	**Fluoranthene**	**Pyrene**	**Chrysene**	**Perylene**	**Coronene**
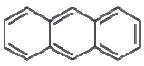	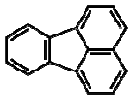	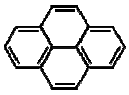	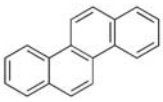	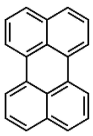	

Table C2: Molecular structure of tar species considered in the studies.

Appendix D. Thermodynamical Properties of Permanent Gases

The current appendix reports the estimation method to calculate the sensible heat capacity and enthalpy of permanent gases as well as for benzene as representative tar lump compound and char, as graphite, in **Chapter 3** and **Chapter 4**. These thermodynamic properties are calculated by means of polynomial correlations based on the JANAF coefficients, named a_1, a_2, a_3, a_4, a_5 and a_6.

$$c_p = R \cdot \left(a_1 + a_2 \cdot T + a_3 \cdot T^2 + a_4 \cdot T^3 + a_5 \cdot T^4\right) \tag{D.1}$$

$$H = RT\left(a_1 + \frac{1}{2}a_2 T + \frac{1}{3}a_3 T^2 + \frac{1}{4}a_4 T^3 + \frac{1}{5}a_5 T^4 + \frac{a_6}{T}\right) \tag{D.2}$$

As follows, tables D1 and D2 present the JANAF coefficients for the lower range (300-1000K) and upper range of temperatures (1000-4000/5000K) depending on the specie. All these coefficients, a_1, a_2, a_3, a_4, a_5 and a_6, allow us estimating specific calorific and enthalpy of chemical species of interest in this PhD Thesis: permanent gases (aforementioned), benzene (C_6H_6) and char (C as graphite).

Component	a_1	a_2	a_3	a_4	a_5	a_6	a_7
O_2	3.212936	1.127486E-3	-5.756150E-7	1.318770E-9	-8.768554E-13	-1.005249E3	6.0347380
CO	3.262452	1.511941E-3	-3.881755E-6	5.581944E-9	-2.474951E-12	-1.431054E4	4.8488970
CO_2	2.637077	7.803230E-3	-8.196187E-6	6.537897E-9	-2.520220E-12	-5.416773E4	1.188955E1
CH_4	7.787415	1.747668E-2	-2.783409E-5	3.049708E-8	-1.223931E-11	-9.825229E4	1.372219E1
H_2	3.298124	8.249442E-4	-8.143015E-7	-9.475434E-11	4.134872E-11	-1.012521E3	-3.2940940
H_2O	3.386842	3.474982E-3	-6.354696E-6	6.968581E-9	-2.506588E-12	-3.020811E4	2.5902330
N_2	3.298677	1.408240E-3	-3.963222E-6	5.641515E-9	-2.444855E-12	-1.020900E3	3.9503720
C_2H_6	1.462359	1.549567E-2	5.780507E-6	-1.257832E-8	4.586267E-12	-1.123918E4	1.443229E1
Benzene	-3.138012	4.723103E-2	-2.962208E-6	-3.262819E-8	1.718692E-11	8.890031E3	3.657573E1
C (graphite,s)	-6.705661E-1	7.181500E-3	-5.632921E-6	2.142299E-9	-4.168562E-13	-7.339498E1	2.6015960

Table D1: JANAF coefficients for range temperature of 300-1000K for the chemical species indicated in the table from JANAF database (2004).

Component	a_1	a_2	a_3	a_4	a_5	a_6	a_7
O_2	3.6975780	6.135197E-4	-1.258842E-7	1.775281E-11	-1.136435E-15	-1.233930E3	3.1891660
CO	3.0250780	1.442689E-3	-5.630828E-7	1.018581E-10	-6.910952E-15	-1.426835E4	6.1082188
CO_2	4.6105740	2.532962E-3	-1.070165E-6	2.026771E-10	-1.424958E-14	-5.479882E4	1.4496300
CH_4	1.6834790	1.023724E-2	-3.875129E-6	6.785585E-10	-4.503423E-14	-1.008079E4	9.6233950
H_2	2.9914230	8.249442E-4	-5.633829E-8	-9.231578E-12	1.582752E-15	-8.350340E2	-1.3551100
H_2O	2.6721460	7.000644E-4	-8.730260E-7	1.200996E-10	-6.391618E-15	-2.989921E4	6.8628170
N_2	2.9266400	1.487977E-3	-5.684761E-7	1.009704E-10	-6.753351E-15	-9.227977E2	5.9805280
C_2H_6	4.8259380	1.384043E-2	-4.557259E-6	6.724967E-10	-3.598161E-14	-1.271779E4	-5.2395070
Benzene	1.291074E1	1.723297E-2	-5.024211E-6	5.893497E-10	-1.947521E-14	3.664512E3	-5.002699E1
C (graphite,s)	1.4901660	1.662126E-3	-6.687204E-7	1.290880E-10	-9.205334E-15	-7.074019E2	-8.7177850

Table D2: JANAF coefficients for range temperature of 1000-4000/5000K for the chemical species indicated in the table from JANAF database (2004).

Table D3 shows the references values of enthalpy for main chemical species, used in chemical reactions enthalpy calculations.

Component	O_2	CO	CO_2	CH_4	H_2	H_2O	N_2	C_2H_6	Benzene	C (graphite,s)
H_{ref} **(J/mol)**	0	-101440	-393130	-74820	0	-241600	0	-83600	82760	0

Table D3: Values of reference enthalpy for main chemical species (Rowley et al., 2007).

Appendix E. Thermodynamical Properties of Tars

This appendix explains the estimation method of sensible heat capacity and vaporization latent heat of heterocyclic and PAH compounds acting as tar species.

There exist several methods for calculating the sensible heat capacity of organic compounds, but for convenience and due to the lack of data related to this property, two methods are adopted. In case of tar compounds such as naphthalene, phenanthrene or perylene, equation (E.1) is employed. In case of phenol, equation (E.2) is used for calculating its sensible heat capacity.

$$c_p = a + bT + cT^2 + dT^3 \tag{E.1}$$

$$c_p = C_1 + C_2\left(\frac{C_3/T}{\sinh(C_3/T)}\right)^2 + C_4\left(\frac{C_5/T}{\cosh(C_5/T)}\right)^2 \tag{E.2}$$

The correlation proposed by Poling et al. (2004) for rest of tars is a polynomial function with coefficients in table E1 while the correlation proposed by Rowley et al. (2007) for phenol is a hyperbolic function with coefficients C_1, C_2, C_3 and C_4 (table E2).

Chemical specie	***a***	***b***	***c***	***d***
Naphthalene	-71.55	0.8712	-6.88E-4	2.14E-7
Acenaphthalene	-95.83	1.1292	-9.85 E-4	3.46 E-7
Fluorene	-94.08	1.1586	-9.80 E-4	3.32 E-7
Phenanthrene	-92.33	1.1880	-9.75 E-4	3.18 E-7
Anthracene	-92.33	1.1880	-9.75 E-4	3.18 E-7
Fluoranthene	-108.83	1.3900	-1.26 E-4	4.54 E-7
Pyrene	-108.83	1.3900	-1.26 E-4	4.54 E-7
Chrysene	-113.11	1.5048	-1.26 E-4	4.22 E-7
Perylene	-129.61	1.7068	-1.55 E-4	5.58 E-7
Coronene	-162.61	2.1108	-2.11 E-3	8.29 E-7

Table E1: Coefficients for the c_p calculation of PAH compounds according to Poling et al. (2004).

Chemical specie	C_1	C_2	C_3	C_4	C_5
Phenol	$0.434*10^5$	$2.445*10^5$	$1.152*10^3$	$1.512*10^5$	507

Table E2: Coefficients for the c_p calculation of phenol according to Rowley et al. (2007).

The vaporization (condensation) latent heat for heterocyclics and PAH compounds are estimated at any temperature according to the equation proposed by Thek and Stiel (1996). This work also states out the value of exponent n_v as 0.375 or 0.38. Here, n_v is set as 0.38. This correlation estimates the latent heat of vaporization based on a known value. Here, the condensation latent heat at 25ºC, the reference temperature, is adopted as reference condensation latent heat. Table E3 indicates this value for corresponding tar compounds.

$$\Delta H_v = \Delta H_{v,ref} \left(\frac{1 - T_r}{1 - T_{r,ref}} \right)^{n_v} \tag{E.3}$$

T_r in equation (E.3) denotes the reduced temperature, calculated as the relationship between the temperature of interest and the temperature of critical point, for each specie. The temperature of critical point for each species is reported in table C1.

Chemical specie	ΔH_v at 25ºC (kJ/mol)
Phenol	75.41
Naphthalene	58.13
Acenaphthalene	67.20
Fluorene	71.26
Phenanthrene	79.91
Anthracene	68.92
Fluoranthene	69.26
Pyrene	76.82
Chrysene	106.01
Perylene	124.50
Coronene	104.68

Table E3: Values of vaporization heat of heterocyclic and PAH compounds at reference state (Poling et al., 2004; Rowley et al., 2007).

Appendix F. Diffusivity Coefficient Estimation Methods

The purpose of this appendix is to give basic guidelines to estimate diffusivity properties for gas mixtures at low pressure. Readers can obtain more detail information and insights in the corresponding references cited along this appendix and references therein. Furthermore, the current appendix deals with the main important diffusivity coefficient estimation methods, the procedure for estimating such properties, the errors associated and some advices in using them.

Table F1 presents ranges of order of magnitude for diffusivities of gas, liquid and solid states, in SI and CGS units. This table tries to show the relative importance of diffusivity coefficients of gases in mass transfer processes. It should be noted that diffusivity coefficient for gases ranges around from 10^{-4} to 10^{-6}. This values range, together to the particle diameter, control the mass transfer in condensation processes.

Continuous phase	D_i magnitude		D_i range		Comments
	m^2/s	cm^2/s	m^2/s	cm^2/s	
Gas at atmospheric pressure	10^{-5}	0.1	10^{-4} - 10^{-6}	1 - 10^{-2}	Accurate theories exist, generally within ±10% $D_iP \cong$ constant, $D_i \propto T^{1.66 \text{ to } 2.0}$
Liquid	10^{-9}	10^{-5}	10^{-8} - 10^{-10}	10^{-4} - 10^{-6}	Approximate correlations exist, generally within ±25%
Liquid occluded in solid matrix	10^{-10}	10^{-6}	10^{-8} - 10^{-12}	10^{-4} - 10^{-8}	Hard cell walls: D_{eff}/D_i=0.1 to 2.0. Soft cell walls: D_{eff}/D_i=0.3 to 0.9
Polymers and glasses	10^{-12}	10^{-8}	10^{-10} - 10^{-14}	10^{-6} - 10^{-10}	Aproximate theories exist for dilute and concentrated limits, strong composition dependance
Solid	10^{-14}	10^{-10}	10^{-10} - 10^{-34}	10^{-6} - 10^{-30}	Approximate theories exist, strong temperature dependance

Table F1: Rules of thumb for diffusivities from Cussler (1980), Schwartzberg and Chao (1982) and Poling et al. (2004). Table adapted from Green and Perry (2008).

Besides, the range of values for D_i and D_{ab} reported in table F1 can help to understand the relative error of estimation methods from table F2 for complex substance such as tar compounds in next appendix. A couple of methods presented here for complex molecules will be discussed in next appendix in order to show the inherent error of the methods in estimation results and the needless of an extreme accuracy for the purposes in the current work.

In table F2, some important methods for estimating the diffusivity coefficients of gas binary mixtures are presented. These methods are: Chapman and Enskog, Wilke and Lee, Fuller, Schettler and Giddings method for nonpolar compounds and Brokaw method for at least one polar compound in the binary mixture. The equations and the relative errors based on experimental values are also shown. As it can be observed, the error can be up to 9%. This points out that any estimation method of diffusivity coefficient can yield important deviation from experimental values for others species (tar compounds for example, shown in next appendix). Therefore, it does not matter which estimation method is used.

Equation		Error (%)	Authors	Reference
Binary mixtures - Low pressure - nonpolar				
$D_{ab} = \frac{0.001858 T^{3/2} M_{ab}^{1/2}}{P \sigma_{ab}^2 \Omega_D}$	(F.1)	7.3	Chapman and Enskog	Chapman and Cowling (1990)
$D_{ab} = \frac{\left(0.00217 - 0.0005 M_{ab}^{1/2}\right) T^{3/2} M_{ab}^{1/2}}{P \sigma_{ab}^2 \Omega_D}$	(F.2)	7.0	Wilke and Lee	Wilke and Lee (1955)
$D_{ab} = \frac{0.001 T^{1.75} M_{ab}^{1/2}}{P\left(\left(\sum_v\right)_a^{1/3} + \left(\sum_v\right)_b^{1/3}\right)^2}$	(F.3)	5.4	Fuller, Schettler and Giddings	Fuller et al. (1966)
Binary mixtures - Low pressure – polar				
$D_{ab} = \frac{0.001858 T^{3/2} M_{ab}^{1/2}}{P \sigma_{ab}^2 \Omega_D}$	(F.4)	9.0	Brokaw	Brokaw (1969)

Table F2: General accepted methods for estimating diffusivity coefficients of binary systems.

In all these equations, there are some structural, physical and chemical parameters to be calculated and estimated in order to obtain D_{ab}. Additionally, some of them follow different rules of estimation according to the method chosen. First of all, the influence of the molecular weight of compounds of binary mixtures is considered, but its definition differs with the method used. Then, M_{ab} is defined by Chapman and Cowling (1990), Wilke and Lee (1955) and Brokaw (1966) as:

$$M_{ab} = 2\frac{M_a M_b}{M_a + M_b} \tag{F.5}$$

On the contrary, Fuller et al. (1966) defines M_{ab} as:

$$M_{ab} = 1/M_a + 1/M_b \tag{F.6}$$

Concerning to the collisional diameter, σ, it can be estimated for nonpolar or polar compounds. Brokaw (1969) recommends adjusting this parameter by means of expression denoted in equation (F.8), which accounts for the value obtained from equation (F.7), according to the rest of methods (Wilke and Lee, 1955; Chapman and Cowling, 1990).

The rest of variables for a binary system are expressed in table F3 too. These parameters are based on boiling point properties (volume and temperature). Others estimation methods are based on critical properties as states the Joback method but here the previous one is used since diffusivity coefficients for permanent gases (O_2, CO, CO_2, H_2, H_2O, CH_4 and N_2) are defined following these rules. Besides, the diffusivity coefficients for tar compounds will be based on the same properties. Using the same method for both types of compounds, the systematic error in calculations will be the same. Finally, note that the corresponding values of each property are reported in tables of appendix C.

Nonpolar components mixtures			
$\Omega_D = \frac{1.06036}{T^{*0.1561}} + \frac{0.193}{e^{0.47635T^*}} + \frac{1.03587}{e^{1.52996T^*}} + \frac{1.76474}{e^{3.89411T^*}}$	(F.7)		
Mixtures with at least one polar component			
$\Omega_D^{'} = \Omega_D + \frac{0.19\delta_{ab}^2}{T^*}$	(F.8)	$T^* = \bar{k}T/\varepsilon_{ab}$	(F.9)
Binary system		**Individual component**	
$\sigma_{ab} = (\sigma_a \sigma_b)^{1/2}$	(F.10)	$\sigma = \left(\frac{1.585V_{bp}}{1+1.3\delta^2}\right)^{1/3}$	(F.11)
$\delta_{ab} = (\delta_a \delta_b)^{1/2}$	(F.12)	$\delta = \frac{1.94+10^3\mu_p^2}{V_{bp}T_{bp}}$	(F.13)
$\varepsilon_{as} = (\varepsilon_a \varepsilon_b)^{1/2}$	(F.14)	$\frac{\varepsilon}{\bar{k}} = 1.18(1+1.3\delta^2)T_{bp}$	(F.15)

Table F3: Parameters for estimating diffusivity coefficients by methods proposed by Chapman and Cowling (1990), Wilke and Lee (1955) and Brokaw (1969).

In case of using the Fuller-Schettler-Giddings method (1966), as it can be observed in equation (F.3), the diffusivity coefficient requires to calculate the contribution of each species in a binary mixture to the diffusivity value, it means. To accomplish this, this method accounts for the diffusion-volume. They can be atomic contribution of C, H, O, N, Cl, S and aromatic or heterocyclic rings or diffusion-volumes corresponding to simple molecule such as hydrogen, oxygen, water, etc, for example. The corresponding value of each component/specie is reported in below table, table F4. For estimating the structural diffusion-volume of tar compounds, it is mandatory to calculate the parameter ν_i, according to contribution of increments of C, H, O, N and aromatic rings of these molecules. Particularly, the number of aromatic rings has to be counted. To do this, the molecule structures of main tar compounds are presented in table C2 in the appendix C.

Atomic and structural diffusion-volume increments, ν_i (cm^3/mol)			
C	16.5	Cl	19.5
H	1.95	S	17.0
O	5.48	Aromatic ring	-20.2
N	5.69	Heterocyclic ring	-20.2
Diffusion-volumes for simple molecules, $\Sigma\nu_i$ (cm^3/mol)			
H_2	7.07	CO	18.9
D_2	6.70	CO_2	26.9
He	2.68	N_2O	35.9
N_2	17.9	NH_3	14.9
O_2	16.6	H_2O	12.7
Air	20.1	CCl_2F_2	114.8
Ar	16.1	SF6	69.7
Kr	22.8	Cl_2	37.7
Xe	37.9	Br_2	67.2
Ne	5.59	SO_2	41.1

Table F4: Atomic diffusion-volumes for use in estimating Dab by the method of Fuller et al. (1966).

In this thesis, Diffusivity coefficients of permanents gases for simulation campaign of biomass gasification in fluidized bed in **Chapter 3** are estimated by means of Wilke-Lee method (1955) while simulation campaign of MBHE filter in **Chapter 4**, the diffusivity coefficients of both permanent gases and tar compounds are estimated by the method of Fuller et al. (1966). The choice of different methods for these chapters underlies in the fact that for permanent gases there is enough valuable information for estimating these coefficients with the parameters σ and ε/k. The opposite occurs for tar compounds. The following appendix discusses the use of the last method.

Appendix G. Diffusivity Coefficient Methods Error Magnitude

This appendix tries to justify the choice of the estimation methods of diffusivity coefficients employed in **Chapter 3** and **Chapter 4** for tar compounds within the brief comparison of some experimental research.

Figure G1(A-B) shows the diffusivity coefficients of some tar compounds (benzene, phenol, naphthalene, acenaphthylene, phenanthrene, anthracene, pyrene and benz[a]anthracene) according to methods of Wilke and Lee (1955) and Fuller et al.

(1966), respectively. The purpose of these two figures is to show the trend of diffusivity coefficients for some important and representative tar compounds. It can be seen that the diffusivities ranges from around 10^{-5} up to near to10^{-6}. This indicates that the order of magnitude of diffusivities for all tar compounds comprised in the studies carried on within the current PhD Thesis are in concordance with the typical range reported in literature (see table F1). Besides, these estimated values are around one order of magnitude greater than the diffusivities of permanent gases at the same temperature. This result is consistent with the fundamentals of estimation methods reported in appendix F since the tar compounds have a molecular weight much greater than the one of permanent gases. In fact, the greater the molecular weight is the less temperature influence accounts for it. Additionally, the diffusivity at any temperature is lower.

This study concludes the less relative importance of diffusivity for tars in comparison with others parameters: superficial gas velocity, particle diameter and mass transfer controlling agents. Furthermore, this would be supported by the lack of available data about diffusivities of tars and the incertitude in the estimation, as discussed later on.

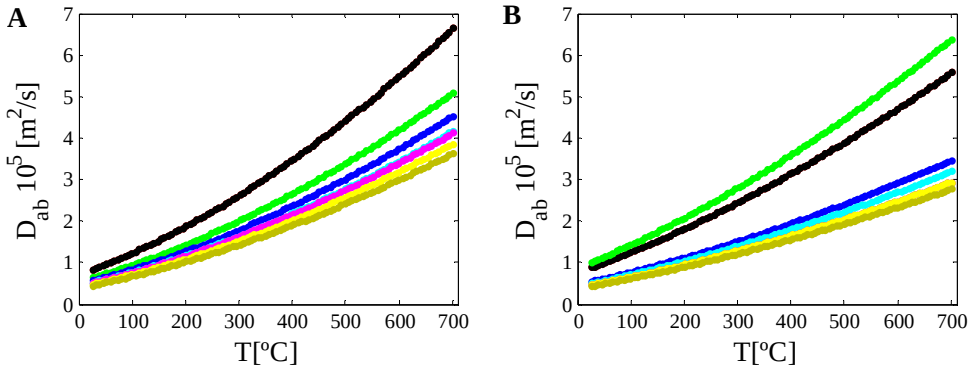

Figure G1: Diffusivity coefficients of benzene (black), phenol (red), naphthalene (green), acenaphthalene (dark blue), phenanthrene (light blue), anthracene (pink), pyrene (yellow) and benz[a]anthracene (olive) with temperature: Estimation methods of Wilke-Lee (1955) (A) and Fuller-Schettler-Giddings (1966) (B).

On the other hand, figure G2 denotes the relative difference between Wilke-Lee and Fuller-Schettler-Giddings methods for the tars compounds selected above. This figure remarks the increase of this difference between these two methods with temperature. Besides, this difference remains comprised around 0.9-1.2 interval for most tar species studies. However, naphthalene and anthracene yield greater differences.

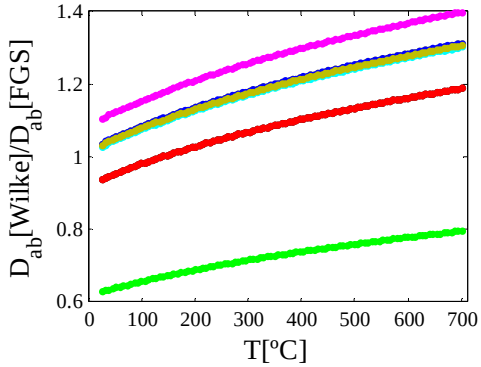

Figure G2: Comparison of Wilke-Lee and Fuller-Schettler-Giddings methods for estimating diffusivity coefficients of benzene (black), phenol (red), naphthalene (green), acenaphthalene (dark blue), phenanthrene (light blue), anthracene (pink), pyrene (yellow) and benz[a]anthracene (olive).

The following figure, G3(A-D) based on the work of Gustafson and Dickhut (1994), shows the error between experimental values and the corresponding estimations of diffusivities in air by means of methods proposed by Wilke and Lee (1955), Fuller et al. (1966) and Gustafson and Dickhut (1994), at several low temperatures for a reduced group of tar compounds (PAH and no PAH) as example: benzene, toluene, naphthalene, acenaphthylene, anthracene, phenanthrene, pyrene and benz[a]anthracene. As it can be seen from results depicted in these figures, the deviation from experiments can be up to 36% for some compounds (benzene, benz[a]anthracene) with the use of Wilke-Lee method. Others methods, as the one of Fuller et al. (1966) and Gustafson (1994), also yields considerable deviation when predicting the diffusivity coefficient of others compounds as toluene, naphthalene, phenanthrene or pyrene, for instance as figures G3(A-D) denote.

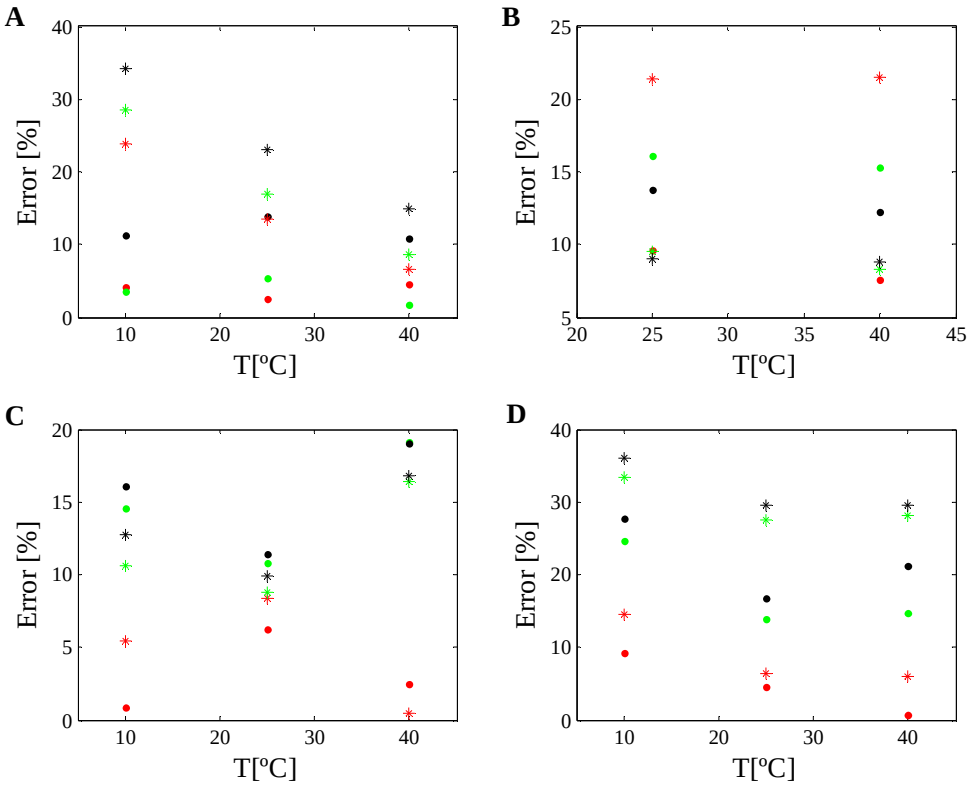

Figure G3: Error of diffusivity coefficients at 10, 25 and 40ºC of benzene (A·) and toluene (A*), naphthalene (B·) and acenaphtylene (B*), anthracene (C·) and phenanthrene (C*), pyrene (D·) and benz[a]anthracene (D*) using the estimation methods of Wilke and Lee (1955) (black), Fuller et al. (1966) (green) and Gustafson (1994) (red). Comparison performed with experimental values, adapted from Gustafson (1994).

The intrinsic error in estimating diffusivity coefficients is due to the basis adopted in each method. Here, as it was stated out in previous appendix, the methods employed are the ones proposed by Wilke and Lee (1955) and Fuller et al. (1966) in **Chapter 3** and **Chapter 4**, respectively. Thus, the error associated to each method has different origin. The main difference between the error associated to each methods, is basically due to the lack of experimental data for more complex compounds (tar, PAH, etc) and the assumption of Fuller et al. (1966): colliding molecules behave as spheres.

However, the possible difference of estimated value respect to the real one should not be of great concern because of results shown below. As Gustafson (1994) points out, the methods of Wilke and Lee (1955) and Fuller et al. (1966) overestimate diffusivities of smaller compounds and underestimate the diffusivities of the larger aromatic compounds when compared with experimental data.

Appendix H. Vapour Pressure above Liquid and Solid State for Tars

This appendix states out the low vapour pressure of both sub-cooled and solid state of some tars (naphthalene, acenaphthylene, anthracene, pyrene, benz[a]anthracene). This study reveals the low capacity of the tars compounds, especially PAHs, to evaporate once they have condensed. This phenomenon indicates that tars compounds will condensate if the gas stream is saturated, as it occurs in biomass gasification processes. This is due to theirs low vapour pressures.

To evaluate this behaviour, figure H1(A-B) show the influence of temperature in the vapour pressure above subcooled liquid and solid, respectively. Thus, the following correlations, equations (H.1-2), allow us to estimate the vapour pressure of the subcooled and solid states. The corresponding parameters are reported in table H1.

$$\ln(p_s) = -\frac{A}{T} + B \qquad \text{(H.1)}, \qquad \ln\frac{p_L}{p_S} = \frac{\Delta S_{fus}(T_m - T_a)}{RT_a} \qquad \text{(H.2)}$$

Tar compound	A (K)[*1]	B[*1]	T_m (K)[*2]	ΔS_{fus} (J/mol K)[*2]	Reference
Naphthalene	3960	14.30	353.45	53.73	[1] McCullogh et al. (1957), [*2] Sonnefeld et al. (1983)
Acenaphthylene	3822	12.77	335.12	50.00	[*1] Allen (1997), [*2] Sonnefeld et al. (1983)
Anthracene	4792	12.98	488.97	60.11	[*1] Goursot et al. (1970), [*2] Sonnefeld et al. (1983)]
Pyrene	4761	12.75	423.31	40.98	[*1] Goursot et al. (1970), [*2] Sonnefeld et al. (1983)
Benz[a]anthracene	4247	9.68	434.25	49.23	[*1] Lide (1992), [*2] Sonnefeld et al. (1983)

Table H1: Thermodynamic properties for estimating vapour pressure above subcooled liquid and solid for some tar compounds.

To remark that PAHs are all solid at ambient temperature so that it is necessary to use the subcooled liquid state as well as the solid state. Figures H1A and H1B denote the big difference of vapour pressure of both subcooled liquid and solid respect to atmospheric pressure for several tar species. It is noticeable how the vapour pressure is very low even at high temperatures (600-700ºC).

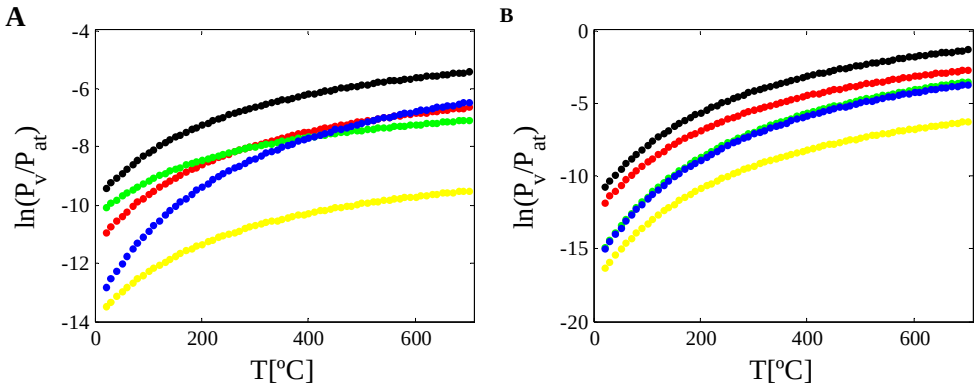

Figure H1: Vapour pressure of sub-cooled liquids (A) and solids (B) of naphthalene (black), acenaphthalene (red), anthracene (green), pyrene (dark blue) and benzene (light blue) with temperature.

Appendix I. Water liquid condensed film and volume dust collected in solid phase

This appendix is aimed to show the very low width of water condensed around the particles bed and the low volume ratio occupied by dust collected in the solid phase. These results justify the assumption of neglecting the width of material condensed or collected in the solid phase and therefore the uniform solid phase fraction.

For instance, for the gas humidity range stated in table I1, the water content condensed in the bed varies but with orders of magnitude of 1e-4-1e-3. In addition to this, the water film formed around the particle beds is the order of 1e-11-1e-9m in the range of 500µm to 5mm. As it can be seen, the range of gas humidity and the particle bed size covers a wide range of cases concluding as valid the assumption made concerning to uniformity of constant phase fractions of gas and solid streams.

Gas humidity (%)	**Gas humidity condensed (%)**	**m^3 water/m^3 bed**	**Water content bed (%)**	***d_p* of bed material**			
				500micras	**800micras**	**1mm**	**5mm**
				Water liquid film width (m)			
3	0	0	0	0	0	0	0
5	40.0	1.81E-6	1.81E-4	3.78E-11	6.05E-11	7.56E-11	3.78E-10
8	62.5	4.54E-6	4.54E-4	9.45E-11	1.51E-10	1.89E-10	9.45E-10
10	70.0	6.35E-6	6.35E-4	1.32E-10	2.12E-10	2.65E-10	1.32E-9
15	80.0	1.54E-5	1.54E-3	3.21E-10	5.14E-10	6.43E-10	3.21E-9
20	85.0	1.09E-5	1.09E-3	2.27E-10	3.63E-10	4.54E-10	2.27E-9
25	88.0	2.00E-5	2.00E-3	4.16E-10	6.65E-10	8.32E-10	4.16E-9
30	90.0	2.45E-5	2.45E-3	5.10E-10	8.17E-10	1.02E-9	5.10E-9
35	91.4	2.90E-5	2.90E-3	6.05E-10	9.68E-10	1.21E-9	6.05E-9

Table I1: Gas humidity condensed and water liquid film width formed around the particle bed for several particle bed diameters.

On the other hand, figure I1 depicts the contour maps of dust/bed volume ratio for the lowest and highest superficial gas velocities. Furthermore, these two cases are considered at low particle size (400µm) which yields a high dust collection as observed previously. For bigger particle diameters of moving bed, the dust collection efficiencies are expected to be smaller and then, the dust/bed volume ratio as well as in the same order of magnitude. Therefore, figure I1 denotes a possible maximum limit of dust deposited in the moving bed, particularly the figure I1B since a higher dust/bed ratio is

achieved. However, it can be seen that the region where the dust/bed volume ratio can be relatively noticeable is very small. It covers the very inlet, the first millimetres in figure I1B and up to half centimetre in figure I1A, matching the uniform phase fractions assumption too.

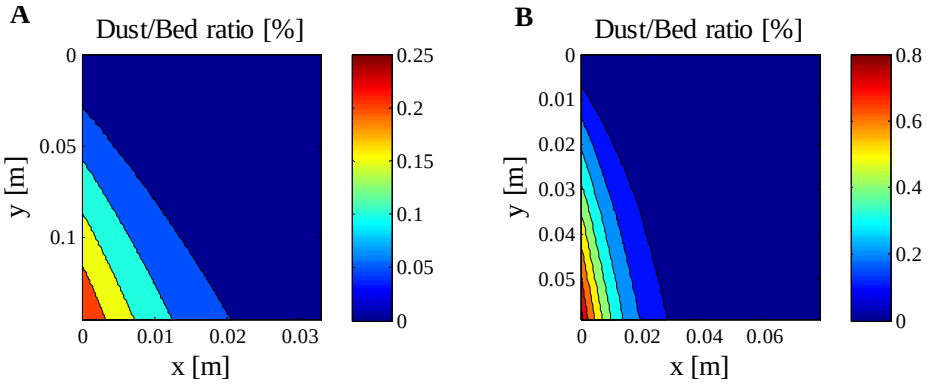

Figure I1: Dust/solids bed volume ratio maps for 400μm of particle bed at 0.5m/s (A) and 3m/s (B).

Appendix J. Coefficients of energy balance of gas and solid phases for MBHEF

This appendix explains in a detailed manner the corresponding coefficients of energy balance of gas and solid phases, equation (4.19). The coefficients NTU^*, $CNTU^*$ and STe^* are dimensionless while CPG^* and CPS^* have units of energy (J) per unit of volume (m^3) and time (s). Finally, these coefficients are defined as:

$$CNTU^*_{x+\Delta x} = \frac{ha_e \Delta x^* \Delta y^* H}{\left(m_g c_{pg,x+\Delta x} + \sum_{c=1}^{nc} m_{gc,x+\Delta x} c_{pgc,x+\Delta x}\right) // (LHH)} \tag{J.1}$$

$$NTU^*_{x+\Delta x} = \frac{m_g c_{pg,x+\Delta x} + \sum_{c=1}^{nc} m_{gc,x+\Delta x} c_{pgc,x+\Delta x}}{m_p c_{pp} + \sum_{c=1}^{nc} m_{pc,y+\Delta y} c_{plc,y+\Delta y}} \tag{J.2}$$

$$STe^*_{x+\Delta x} = \frac{m_g c_{pg,x+\Delta x} + \sum_{c=1}^{nc} m_{gc,x+\Delta x} c_{pgc,x+\Delta x}}{\sum_{c=1}^{nc} \dot{m}_c h_{f,gc}} \left(T_0^* - \theta_0^*\right) \tag{J.3}$$

$$CPG^*_x = \frac{m_g c_{pg,x} + \sum_{c=1}^{nc} m_{gc,x} c_{pgc,x}}{LHH} \tag{J.4}$$

$$CPS^*_y = \frac{m_p c_{pp} + \sum_{c=1}^{nc} m_{pc,y} c_{plc,y}}{LHH} \tag{J.5}$$

Concerning the definition of the dimensionless variables of interest in the MBHEF performance analysis, the non-dimension gas and solid temperatures and water, tars and dust concentration are expressed as follows:

$$T_x^* = \frac{T_x - \theta_0}{T_0 - \theta_0} \quad \text{(J.6)}, \qquad \theta_y^* = \frac{\theta_y - \theta_0}{T_0 - \theta_0} \quad \text{(J.7)}$$

$$C_{g,x}^* = \frac{C_{g,x} - C_{s,0}}{C_{g,0} - C_{s,0}} \quad \text{(J.8)}, \qquad C_{s,y}^* = \frac{C_{s,y} - C_{s,0}}{C_{g,0} - C_{s,0}} \quad \text{(J.9)}$$

$$C_{pg,x}^* = \frac{C_{pg,x} - C_{pp,0}}{C_{pg,0} - C_{pp,0}} \quad \text{(J.10)}, \qquad C_{pp,y}^* = \frac{C_{pp,y} - C_{pp,0}}{C_{pg,0} - C_{pp,0}} \quad \text{(J.11)}$$

Notation

a_e Effective interfacial area, [m^2/m^3].

c_p Heat capacity, [J/kg K].

D_i Diffusivity of the chemical specie “i”, [m^2/s].

D_{eff} Effective diffusivity of the chemical specie “i”, [m^2/s].

D_{ab} Diffusivity of the binary mixture of components “a” and “b”, [m^2/s].

d_p Particle diameter, [m].

H Enthalpy, [J/mol]. Height of device, [m].

H_{ref} Reference enthalpy of a substance, [J/mol].

h_p Gas-particle heat transfer coefficient, [W/m^2 K].

L Length of device, [m].

M Molecular weight, [g/mol].

M_{ab} Molecular weight of the binary mixture “ab”, [g/mol].

$\dot{m}$ Condensation rate of component “c”, [kg/m^3 s].

n_v Exponent for estimating the vaporization heat, [-].

P Pressure, [Pa].

P_{at} Atmospheric pressure, [Pa].

P_c Critical pressure of a substance, [bar].

p_L Vapour pressure of sub-cooled liquid, [Pa].

p_S Vapour pressure of solid, [Pa].

p_V Vapour pressure, [Pa].

R Ideal gas constant, [J/mol K].

T Temperature, [K].

T_a Atmospheric temperature, [K].

T_{bp} Boiling point, [K].

T_c Critical temperature of a substance, [K].

T_m Melting point of an arbitrary tar, [K].

T_r Reduced temperature, [K].

T^* Dimensionless temperature, [-].

U_0/ U_{mf} Fluidization state of a bed, [-].

V_{bp} Volume at the boiling point, [cm^3/mol].

V_c Critical volume, [cm^3/mol].

Abbreviations

CNTU Convection-sensible heat ratio for the gas phase in the moving bed, [-].

CPG Energy flow concentration of gas phase, [J/m^3 s].

CPS Energy flow concentration of solid phase, [J/m^3 s].

NTU Sensible heat ratio of gas and solid phases, [-].

Ste Stefan number, [-].

LHV Low Heating Value, [J/kg].

PAH Polycyclic aromatic hydrocarbons.

Greek letters

ΔH_v Vaporization heat, [kJ/mol].

ΔS_{fus} Fusion entropy, [J/mol K].

Δx^* Step size in the x axis, [-].

Δy^* Step size in the y axis, [-].

δ Dimensionless parameter for transport properties.

ε Minimum potential energy, [J].

ε/k Parameter for estimating transport properties, [K].

θ Solid temperature, [K].

μ_p Dipole moment, [D].

v_i Atomic and structural diffusion-volume increments, [cm^3/mol].

ρ_s Density of inert bed material, [kg/m^3].

Σv_i Diffusion-volume for simple molecules, [cm^3/mol].

σ Collision diameter, [Å].

Ω_D Collision integral for transport diffusivity of mixtures.

Subscripts

0 Value of variable at the system inlet.

a First chemical specie in a binary system of components.

ab Binary system of chemical species.

b Second chemical specie in a binary system of components.

bp Boiling point.

c Arbitrary chemical specie.

fus Fusion.

g Gas.

gc Gases [tars and H_2O] that can condensate.

nc Number of components.

p Particle phase.

pc Gases that have condensed in the particle phase.

pg Permanent gases.

ref Reference state (25ºC and 1atm).

v Vaporization.

x Coordinate in the x axis.

y Coordinate in the y axis.

Bibliography

Alimuddin, Z., Lim, M.T. 2008. Bubbling fluidized bed biomass gasification. Performance. process findings and energy analysis. *Renewable Energy* 33(10), 2339-2343.

Allen, J.O. 1997. Atmospheric partitioning of polycyclic aromatic hydrocarbons (PAH) and oxygenated PAH. *PhD Thesis*. University of Cambridge, Massachusetts, United States.

Bird, B.R., Stewart, W.E., Lightfoot, E.N., 2002. Transport Phenomena, 2nd ed. Wiley, New York.

Brokaw, R.S. 1969. Predicting transport properties of dilute gases. *Industrial & Engineering Chemistry Process Design and Development* 8, 240-253.

Campoy, M., Gómez-Barea, A., Vidal, F.B., Ollero, P. 2009. Air-steam gasification of biomass in a fluidised bed: Process optimisation by enriched air. *Fuel Processing Technology* 90(5), 677-685.

Chapman, S., Cowling, T.G. 1990. The mathematical theory of non-uniform gases: an account of the kinetic theory of viscosity, thermal conduction and diffusion in gases. Cambridge University Press, Cambridge, UK.

Cussler, E.L. 1980. Cluster diffusion in liquids. *AIChE Journal* 26 (1), 43-51.

Fuller, E.N., Schettler, P.D. Giddings,, J.C. 1966. A new Method for prediction of binary gas-phase diffusion coefficients. *Industrial & Engineering Chemistry* 58(5), 19-27.

Gil, J., Corella, J., Aznar, M.P., Caballero, M.A. 1999. Biomass gasification in atmospheric and bubbling fluidized bed: Effect of the type of gasifying agent on the product distribution. *Biomass & Bioenergy* 17(5), 389-403.

Gómez-Barea, A., Arjona, R., Ollero, P. 2005. Pilot-Plant Gasification of Olive Stone: a Technical Assesment. *Energy & Fuels* 19(2), 598-605.

Gómez-Barea, A., Leckner, B. 2010. Modeling of biomass gasification in fluidized bed. *Progress In Energy and Combustion Science* 36(4), 444-509.

Goursot, P., Girdhar, H.L. Westrum, E.F. Jr. 1970. Thermodynamics of polynuclear aromatic molecules: III. Heat capacities and enthalpies of fusion of anthracene. *Journal of Physical Chemistry* 74(12), 2538-2541.

Green, D.W., Perry, R.H. 2008. Perry's Chemical Engineers' Handbook, Chapter 5, 8th ed., McGraw-Hill, New York, pp 746.

Gustafson, K.R., Dickhut, R.M. 1994. Molecular diffusivity of polycyclic aromatic hydrocarbons in air. *Journal of Chemical and Engineering Data* 39 (2), 286-289.

JANAF database (therm.dat) from CHEMKIN file therm.dat v4.0, March, 2004. http://users.rowan.edu/~marchese/combustion04/kinetics/h2-chemkin/therm.dat

Lide, D.R. 1992. Handbook of Chemistry and Physics, 73th ed. CRC Press, Boca Raton, Florida, USA.

McCullough, J.P, Finke, H.L., Messerly, J.F., Todd, S.S., Kincheloe, T.C., Waddington, G. 1957. The low-temperature thermodynamic properties of naphthalene, 1-methylnaphthalene, 2-methylnaphthalene,1,2,3,4-tetrahydronaphthalene. *Journal of Physical Chemistry* 61(8), 1105-1116.

Poling, B.E., Prausnitz, J.M., O'Connell, J.P. 2004. The properties of gases and liquids. 5th ed., McGraw-Hill.

Rowley ,R.L., Wilding, W.V., Oscarson, J.L., Yang, Y., Zundel, N.A., Daubert, T.E., Danner, R.P. 2007. DIPPR® Data Compilation of Pure Chemical Properties, Design Institute for Physical Properties. AIChE, New York.

Schwartzberg, H.G., Chao, R.Y. 1982. Solute diffusivities in leaching processes. *Food Technology* 39(2), 73-86.

Sonnefeld, W.J., Zoller, W.H., May, W.E. 1983. Dynamic coupled-column liquid chromatographic determination of ambient temperature vapor pressures of polynuclear aromatic hydrocarbons. *Analytical Chemistry* 55(2), 275-280.

Thek, R.E., Stiel, L.I. 1966. A new reduced vapor pressure equation. *AIChE Journal* 12(3), 599-602.

Wilke, C.R. 1950. Diffusional properties of multicomponent gases. *Chemical Engineering Progress* 46(2), 95-104.

Wilke, C.R., Lee, C.Y. 1955. Estimation of Diffusion Coefficients for Gases and Vapors. *Industrial & Engineering Chemistry* 47(6), 1253-1257.

Notation

Ar Arquimeder number, [-].

A_{fb} Cross-sectional area of reactor in freeboard region, [m^2].

A_d Exergy destruction, [W].

A_T Cross-sectional area of the reactor at any height, [m^2].

a_B Interfacial area between bubbles and emulsion phases per unit bed volume unit, [m^2/m^3].

a Constant of the entrainment model, [m^{-1}]. Interfacial area, [m^2/m^3].

a_p Surface-volume particle ratio, [m^2/m^3].

C Molar concentration of species “i”, [mol/m^3].

C_{Bi} Molar concentration of species “i” in bubble phase, [mol/m^3].

C_c Concentration of specie “c” in gas phase in MBHEF, [kg/m^3].

$C_{c,p}$ Concentration of specie “c” in solid phase in MBHEF, [kg/m^3].

C_{Ei} Molar concentration of species “i” in emulsion phase, [mol/m^3].

$C_{p,g}$ Dust concentration in gas phase in MBHEF, [kg/m^3].

$C_{p,p}$ Dust concentration in solid phase in MBHEF, [kg/m^3].

C_{st} Specific transport cost [€km^{-1}].

c_D Drag coefficient, [-].

c_p Heat capacity, [J/kg K].

D Fluidized bed/reactor diameter, [m]. Diffusivity of species a in a multicomponent mixture of species, [m^2/s].

D_{eff} Effective diffusivity of the chemical specie “i”, [m^2/s].

D_{ab} Diffusivity of the binary mixture of components “a” and “b”, [m^2/s].

D_i Diffusivity of the chemical specie “i”, [m^2/s].

D_t Fluidized bed diameter, [m].

Da Damkohler number, [-].

d_B Bubble diameter, [m].

d_{B0} Initial bubble diameter at the distributor, [m].

d_{BM} Maximum bubble diameter due to total coalescences of bubbles, [m].

d_p Particle diameter, [m].

d_p^* Dimensionless particle diameter, [-].

d_r Discount rate [%].

ecc_i Cost of energy crop item i [€ha^{-1}].

F_{∞} Flux of particles above the transport disengaging height, [kg/m^{2}s].

F_B Biomass feeding the gasifier [t yr^{-1}].

F_{bex} Bed expansion factor [-].

F_s Flux of particles in the freeboard, [kg/m^{2}s].

f_{Bi} Molar flow of species “i” in bubble phase, [mol/s].

f_{Ei} Molar flow of species “i” in emulsion phase, [mol/s].

$f_e(y)$ Binary figure (0 or 1) to indicate wether power is produce in year y [h].

f_{fb} Molar flow of gaseous species “i” in the freeboard region, [mol/s].

$f_i(y)$ Number of times per hectare that cost item i occurs in year y in the plantation.

$f_j(y)$ Number of times that cost item j occurs in year y in the power plant.

f_{T0} Total molar flow at the reactor inlet, [mol/s].

$f_{yld}(y)$ Binary figure (0 or 1) to indicate whether the energy crop is harvested in year y.

fr Product CO/CO_2 ratio, [-].

f_{vol} Molar flow of volatiles release at any height in the FB region, [mol/s].

G Generation term, [kg/m^3 s].

g Gravity, [m^2/s].

K Adsorption kinetic constant [units depending on the reaction].

k Thermal conductivity, [W/m K]. Chemical reaction kinetic constant (units depending on the reaction).

k_{BE} Bubble-emulsion mass transfer coefficient, [m^3/m^2s].

k_m Fluid-particle mass transfer coefficient of component “m”, [m/s].

k_{SB} Stefan-Boltzmann constant, [W/m^2K^4].

H Enthalpy, [J/mol]. Height of device, [m]. Width of MBHEF, [m].

H_{BE} Bubble-emulsion heat transfer coefficient, [W/m^2 K].

H_{ref} Reference enthalpy of a substance, [J/mol].

h Fluidized bed/reactor height, [m]. Heat transfer coefficient by convection, [W/m^2 K].

$h_{fg,c}$ Latent heat of component “c”, [J/kg].

h_p Gas-particle heat transfer coefficient, [W/m^2 K].

i Number of energy crop cost items with different time pattern.

j Number of power plant cost items with different time pattern.

L Fluidized bed height, [m]. Length of device, [m].

L/D Fixed bed height/bed reactor diameter ratio, [-].

l_f Load factor [h].

M Molecular weight, [kg/kmol].

M_{ab} Molecular weight of the binary mixture “ab”, [g/mol].

$\dot{m}$ Condensation rate of component “c”, [kg/m^3 s].

m Visible bubble flow parameter, [-].

N Number of reactions.

N_g Number of homogeneous reactions and heterogeneous tar cracking reactions in freeboard region.

$N_{g\text{-}s}$ Number of heterogeneous gas-solid reactions in freeboard region.

N_i Chemical species in bubble and emulsion phase. total chemical species in the freeboard region that participate in homogeneous and heterogeneous tar cracking reactions.

n Number of chemical species/components. total number of years in the project lifetime.

nc Number of condensable components.

n_d Number of orifice openings in the distributor.

n_v Exponent for estimating the vaporization heat, [-].

nr Number of reactions.

OH Operation hours.

P Pressure, [Pa].

P_{at} Atmospheric pressure, [Pa].

P_c Critical pressure of a substance, [bar].

P_{net} Net installed electric capacity of the power plant [MWe].

Pr Prandlt number, [-].

p_L Vapour pressure of sub-cooled liquid, [Pa].

p_S Vapour pressure of solid, [Pa].

p_V Vapour pressure, [Pa].

ppc_j Cost of power plant cost item [€].

Q Volume flow, [m^3/s]. Heat flux, [J/s] or [W/m^3].

q_{rad} Radiation heat loss [W/m^3].

R Ideal gas constant, [J/mol K].

Re Reynolds number, [-].

r_{Bj} Reaction rate of homogenous reaction “j” in bubble phase, [mol/m^3s].

r_{Ej} Reaction rate of homogenous reaction “j” in emulsion phase, [mol/m^3s].

r_{sj} Reaction rate of heterogeneous reaction “j” in emulsion phase, [mol/m^3s].

$r_{g\,j}$ Reaction rate of homogeneous reaction “j” and heterogeneous tar cracking reactions in the gas fraction in the freeboard region, [mol/m^3s].

$r_{g\text{-}s\,j}$ Reaction rate of heterogeneous gas-solid reaction “j” in reactant solid fraction in the freeboard region, [mol/m^3s].

rot Harvest rotation cycle [yr].

Ste Stefan number, [-].

T Temperature, [K]. Fluid temperature, [K].

T_a Atmospheric temperature, [K].

T_{bp} Boiling point, [K].

T_c Critical temperature of a substance, [K].

$T_{dp,tar}$ Tar dew point, [K].

T_F Freeboard temperature, [K].

T_m Melting point of an arbitrary tar, [K].

T_R Standard temperature, [K].

T_r Reduced temperature, [K].

T^* Dimensionless temperature, [-].

t Time, [s].

U_0 Superficial gas velocity, [m/s].

U_0/ U_{mf} Fluidization state of a bed, [-].

U_B Bubble phase velocity, [m/s].

U_E Emulsion phase velocity, [m/s].

U_{mf} Minimum fluidization velocity, [m/s].

U_t Terminal velocity, [m/s].

U_w Overall bed to surroundings heat transfer coefficient, [W/m^{2}K].

u^* dimensionless gas velocity, [-].

u_{br} Velocity of a single bubble in an infinite freely-bubbling bed, [m/s].

u_g, v_g, w_g Gas velocity components, [m/s].

u_l, v_l, w_l Liquid velocity components, [m/s].

u_p, v_p, w_p Solid velocity components, [m/s].

V_{bp} Volume at the boiling point, [cm^3/mol].

V_c Critical volume, [cm^3/mol]. Vehicles capacity (t).

W_{pump} Power pumping of fluid, [J/s].

X_{char} Conversion of char.

x_{fines} Elutriable/entrainable solid material fraction [-].

x Spatial coordinate, [m].

y Spatial coordinates, [m].

yld average annual yield of energy crop [t ha^{-1} yr^{-1}].

Z Acentric factor.

z Spatial coordinate, [m]. Height, [m]. Axial position, [m].

z_{fb} Position of freeboard surface, [m].

$z_{reactor}$ Position of exit of reactor, [m].

Abbreviations

BBFBG	Biomass Bubbling Fluidization Gasifier.
BFB	Bubbling Fluidized Bed.
BFBG	Bubbling Fluidized Bed Gasifier.
BGFB	Biomass Gasification in Fluidized Bed.
BTC	Biomass transport costs.
CAM	Autonomous Community of Madrid.
CCGT	Combined Cycle Gas Turbine.
CEC	Commission of the European Communities.
CFB	Circulating Fluidized Bed.
CFD	Computational fluid-dynamics.
CHNS	Carbon, hydrogen, nitrogen, sulphur content.
CNTU	Convection-sensible heat ratio for the gas phase in the moving bed, [-].
COE	Cost of electricity [€/kWh].
CPG	Energy flow concentration of gas phase, [J/m^3 s].
CPS	Energy flow concentration of solid phase, [J/m^3 s].
CSTR	Continuous Stirred Tank Reactor.
CV	Calorific value.

DM	Dry matter.
ICE	Internal Combustion Engine.
EB	Energy balance.
EF	Entrained Flow.
ER	Equivalence Ratio. Air-Biomass ratio.
FB	Fluidized Bed.
FBD	Fixed Bed Downdraft.
FBG	Fluidized Bed Gasifier. Fluidized Bed Gasification.
FBR	Fluidized Bed Reactor.
FBGR	Fluidized Bed Gasification Reactor.
FBU	Fixed bed Updraft.
FS	Fluidization State, [-].
GHG	Greenhouse gases.
GIS	Geographic Information System.
GT	Gas Turbine.
HHV	High heating value.
HRSG	Heat Recovery and Steam Generator.
ICE	Internal Combustion Engine.

KM Kinetic model.

LHV Low heating value [MJ/Nm^3]. In **Chapter 2** [GJ t^{-1}].

MB Mole balance.

MBHEF Moving Bed Heat Exchange Filter.

MT Mass Transport.

NTU Sensible heat ratio of gas and solid phases, [-].

O&M Operation & Management.

OEB Overall energy balance in the limits of the fluidized bed region.

PAH Polycyclic aromatic hydrocarbons.

PFR Plug Flow Reactor.

RES Renewable energy source.

ST Steam Turbine.

Ste Stefan number, [-].

syngas Synthesis gas.

TC Total plant cost.

TCI Total capital investment.

TDC Total direct costs.

TOC Total operating costs.

UCM Uniform Conversion Model.

Greek letters

α Stoichiometric coefficient for char combustion reaction.

β Stoichiometric coefficient for char gasification reaction.

ΔH Reaction enthalpy, [J/mol].

ΔH_r Reaction enthalpy of reaction “r”, [J/kg].

ΔH_v Vaporization heat, [kJ/mol].

ΔP Pressure drop, [Pa].

ΔS_{fus} Fusion entropy, [J/mol K].

Δx^* Step size in the x axis, [-].

Δy^* Step size in the y axis, [-].

δ Dimensionless parameter for transport properties, [-].

ε Phase fraction, porosity of bed inert material, [-]. Minimum potential energy, [J].

ε_B Volume fraction of bubbles. void fraction of bubble phase at any reactor height.

ε_{fb} Volume fraction of gas in the freeboard region at any reactor height.

ε_{fb}^* Volume fraction of solids in the freeboard region at any reactor height.

ε_{kb} Boltzmann constant [m^2 kg s^{-2} K^{-1}].

ε_{mf} Porosity of bed inert material.

ε_p Emissivity of bed inert material.

ε/k Parameter for estimating transport properties, [K].

η Removal efficiency of tars/dust, [%].

η_{net} Net power plant efficiency.

θ Solid phase temperature, [K].

λ Filter coefficient [m^{-1}], mean free path of the gas molecules, [μm].

μ Viscosity, [kg/m s].

μ_p Dipole moment, [D].

v_i Atomic and structural diffusion-volume increments, [cm^3/mol].

v_{ij} Stoichiometric coefficient for gaseous species “i” in reaction “j”.

v_{nj} Stoichiometric coefficient for solid species “n” in reaction “j”.

ρ Density of gas, [kg/m^3].

ρ_s Density of inert bed material, [kg/m^3].

Σv_i Diffusion-volume for simple molecules, [cm^3/mol].

σ Collision diameter, [Å].

ϕ Contribution factor for pairs of species in a mixture in the properties calculation.

φ Phase in the fluidized bed.

Ω_D Collision integral for transport diffusivity of mixtures.

Ω_k Stockmayer potential.

Ω_μ Lennard-Jones potential.

Subscripts

0 Value of variable at any system inlet.

a First chemical specie in a binary system of components.

ab Binary system of chemical species.

B Bubble phase in bed region.

b Second chemical specie in a binary system of components.

bed Bed region. Inert particles bed.

bp Boiling point.

c Arbitrary chemical specie.

cond Condensate.

cv Control volume.

dev Devolatilization.

drying Heat of evaporation.

dust Fine particles content/concentration. Fine particles. Fines.

E Emulsion phase in bed region.

e Effective.

evap Evaporate.

ext External.

f Fluid. Fluidized bed.

fb Freeboard region.

fus Fusion.

g Gas phase. Gas.

gc Gases [tars and H_2O] that can condensate.

i Chemical species “i” involved or not in a reaction in bubble and emulsion phase. Chemical species “i” involved or in a reaction in the freeboard region.

im Property of chemical specie “i” in a mixture of components.

j Chemical reaction.

l Liquid phase.

loss Energy loss to surroundings.

M Component or chemical specie.

m Stoichiometric coefficient in chemical reactions, number of atoms of an

element.

mf Minimum fluidization.

mix Gas mixture.

n n stoichiometric coefficient in chemical reactions, number of atoms of an element.

nc Number of components.

ncg Non-combustible gases.

p Particle. Particle phase. Solid phase.

pc Gases that have condensed in the particle phase.

pg Permanent gases.

preh Preheater.

r Reaction. Reaction arbitrary.

ref Reference state (25ºC and 1atm).

s Value of variable at the MBHEF outlet. Solid.

syngas Synthesis gas.

T Total.

t Terminal.

tars Tars content/concentration. Tars.

vis Visible.

vol Volatiles.

x Coordinate in the x axis.

y Coordinate in the y axis.

∞ Surroundings.

Superscripts

* Non-dimensional variable [-].

‾ Average value.

Bibliography

Abba, I.A., Grace, J.R., Bi, H.T., Thompson, M.L. 2003b. Spanning the flow regimes: a generic fluidized bed reactor model. *AIChE Journal* 49(7), 1838–1848.

Achenbach, E. 1995. Heat and flow characteristics of packed beds. *Experimental Thermal and Fluid Science* 10(1), 17-27.

Adler, P.R., Del Grosso, S.J., Parton, William J. 2007. Life-cycle assessment of net greenhouse-gas flux for bioenergy cropping systems. *Ecological Applications* 17(3), 675-691.

Agarwal, P.K., Linjewile, T.M. 1995. The influence of product CO/CO_2 ratio on the ignition and temperature history of petroleum coke particles in incipiently gas-fluidized beds. *Fuel* 71, 12-16.

Agblevor, F.A., Besler, S., Wiselogel, A.E. 1995. Fast pyrolysis of stored biomass feed-stocks. *Energy & Fuels* 9(4), 635-640.

Aho, M., Gil, A., Taipale, R., Vainikka, P., Vesala, H. 2008. A pilot-scale fireside deposit study of co-firing Cynara with two coals in a fluidized bed. *Fuel* 87(1), 58-69.

Alimuddin, Z., Lim, M.T. 2008. Bubbling fluidized bed biomass gasification. Performance. process findings and energy analysis. *Renewable Energy* 33(10), 2339-2343.

Allen, J.O. 1997. Atmospheric partitioning of polycyclic aromatic hydrocarbons (PAH) and oxygenated PAH. *PhD Thesis*. University of Cambridge, Massachusetts, United States.

Altafini, C.R., Wamder, P.R., Barreto, R.M. 2003. Prediction of working parameters of a wood waste gasifier through an equilibrium model. *Energy Conversion and Management* 44(17), 2763-2777.

Angelis-Dimakis, A., Biberacher, M., Domínguez, J., Fiorese, G., Gadocha, S., Gnansounou, E., Guariso, G., Kartalidis, A., Panichelli, L., Pinedo, I., Robba, M. 2011. Methods and tools to evaluate the availability of renewable energy sources. *Renewable and Sustainable Energy Reviews* 15(2), 1182-1200.

Arena, U., Zaccariello, L., Mastellone, M. L. 2009. Tar removal during the fluidized bed gasification of plastic waste. *Waste Management* 29(2), 783-791.

Arvelakis, S., Gehrmann, H., Beckmann, M., Koukios, E.G. 2003. Agglomeration problems during fluidized bed gasification of olive-oil residue: evaluation of fractionation and leaching as pre-treatments. *Fuel* 82(10), 1261-1270.

Babu, S.P., Shah, B., Talwalker, A. 1978. Fluidization correlations for coal gasification materials-minimum fluidization velocity and fluidized bed expansion ratio. *AIChE Journal Symp. Ser.* 74, 176-186.

Baratieri, M., Baggio, P., Bosio, B., Grigiante, M., Longo, G.A. 2009. The use of biomas syngas in IC engines and CCGT plants: A comparative analysis. *Applied thermal Engineering* 29(16), 3309-3318.

Bartels, M., Lin, W., Nijenhuis, J., Kapteijn, F., van Ommen, J.R. 2008. Agglomeration in fluidized beds at high temperatures: mechanisms, detection and prevention. *Progress In Energy and Combustion Science* 34(5), 633-666.

Basu, P, Kaushal, P. 2009. Modeling of pyrolysis and gasification of biomass in fluidized beds: a review. *Chemical Product and Process Modeling* 4(1), 21 (47 pp.). ISSN (Online) 1934-2659, DOI: 10.2202/2659.1338.

Basu, P. 2010. Biomass gasification and pyrolysis. Practical design. Eds. Elsevier, Oxford, UK.

Bauen, A., Berndes, G., Juginger, M., Londo, M., Vuille, F., Ball, R., Bole, T., Chudziak, C., Faaij, A., Mozaffarian, H. 2009. Bioenergy – A sustainable and Reliable Energy Source. A review of Status and Prospects. Main Report. International Energy Agency Bioenergy.

Beenackers, A.A.C.M. 1999. Biomass gasification in moving beds, a review of European technologies. *Renewable Energy* 16(1-4), 1180-1186.

Belgiorno, V., De Feo, G., Della Rocca, C., Napoli, R.M.A. 2003. Energy from gasification of solid wastes. *Waste Management* 23(1), 1-15.

Bhaskar, T., Bhavya, B., Singh, R., Naik, D.V., Kumar, A., Goyal, H.B.. 2011. Chapter 3 - Thermochemical conversion of biomass to biofuels. In Ashok Pandey, Christian Larroche, Steven C. Ricke, Claude-Gilles Dussap, and Edgard Gnansounou, editors, Biofuels, pages 51-77. Academic Press, Amsterdam. ISBN 978-0-12-385099-7.

Biba, V., Macak, J., Klose, E.J., Malecha, J. 1978. Mathematical Model for the Gasification of Coal under Pressure. *Industrial & Engineering Chemistry Process Design and Development* 17 (1), 92-98.

Bird, B.R., Stewart, W.E., Lightfoot, E.N., 2002. Transport Phenomena, 2nd ed. Wiley, New York.

Boroson, M.L, Howard, J.B, Longwell, J.P., Peters, W.A. 1989. Product yields and kinetics from the vapor phase cracking of wood pyrolysis tars. *AIChE Journal* 35(1), 120-128.

Bridgwater, A.V. 1994a. Catalysis in thermal biomass conversion. *Applied Catalysis A-General* 116(1-2), 5-47.

Bridgwater, A.V., Meier, D., Radlein, D. 1999. An overview of fast pyrolysis of biomass. *Organic Geochemistry* 30(12), 1479-1493.

Bridgwater, A.V. 2003. Renewable fuels and chemicals by thermal processing of biomass. *Chemical Engineering Journal* 91(23), 87-102.

Brokaw, R.S. 1969. Predicting transport properties of dilute gases. *Industrial & Engineering Chemistry Process Design and Development* 8, 240-253.

Bruni, G., Solimene, R., Marzochella, A., Salatino, P., Yates, J.G., Lettieri, P., Fiorentino, M. 2002. Self-segregation of high volatile fuel particles during devolatilization in a fluidized bed reactor. *Powder Technology* 128(1), 11-21.

Burvall, J. 1997. Influence of harvest time and soil type on fuel quality in reed canary grass (phalaris arundinacea l.). *Biomass & Bioenergy* 12(3), 149-154.

Campoy-Naranjo, M. 2009. Gasificación de biomasa y residuos en lecho fluidizado: Estudios en planta piloto (Biomass and wastes gasification in fluidised bed: pilot plant studies). *PhD Thesis*. University of Sevilla, Spain. Spanish.

Campoy, M., Gómez-Barea, A., Vidal, F.B., Ollero, P. 2009. Air-steam gasification of biomass in a fluidised bed: Process optimisation by enriched air. *Fuel Processing Technology* 90(5), 677-685.

Cao, Y., Wang, Y., Riley, J.T., Pan, W.P. 2006. A novel biomass air gasification process for producing tar-free higher heating value fuel gas. *Fuel Processing Technology* 87(4), 343-353.

Caputo, A.C., Palumbo, M., Pelagagge, P.M., Scacchia, F. 2005. Economics of biomass energy utilization in combustion and gasification plants: effects of logistic variables. *Biomass & Bioenergy* 28(1), 35-51.

Chapman, S., Cowling, T.G. 1990. The mathematical theory of non-uniform gases: an account of the kinetic theory of viscosity, thermal conduction and diffusion in gases. Cambridge University Press, Cambridge, UK.

Christou, M., Fernandez, J., Gosse, G., Venturi, G., Bridgwater, A., Scheurlen, K., Obernberger, I., Van be Beld, B., Soldatos, P., Reinhardt, G. 2005. Bio-energy chains from perennial crops in south europe. BIO-ENERGY CHAINS.

Claderbank, P.H., Toor, F.D. 1971. Fluidized beds as catalytic reactors. In J.F. Davidson, D. Harrison eds. Fluidization, 1st ed. *Academic Press*, London.

Commission of the European Communities (CEC). 2005. Biomass action plan. Technical Report, COM(2005) 628 final.

Corella, J. Sanz, A. 2005. Modeling circulating fluidized bed biomass gasifiers. A pseudo-rigorous model for stationary state. *Fuel Processing Technology* 86(9), 1021-1053.

Corella, J., Toledo, J.M., Molina, G. 2006. Calculation of the conditions to get less than 2g tar/m_n^3 in a fluidized bed biomass gasifier. *Fuel Processing Technology* 87(9), 841-846.

Cornelissen, S., Koper, M., Deng, Y.Y. 2012. The role of bioenergy in a fully sustainable global energy system. *Biomass and Bioenergy* 41, 21-33.

Cussler, E.L. 1980. Cluster diffusion in liquids. *AIChE Journal* 26 (1), 43-51.

Davidson, J.F., Harrison, D. 1963. Fluidised particles. 1st ed.. Cambridge University Press, Cambridge, UK.

Davidson, J.F., Harrison, D. 1971. Fluidization. Academic Press, London, pp. 383-429.

Davidsson, K.O., A mand, L.E., Leckner, B, Kovacevik, B., Svane, M., Hagstrom, M., Pettersson, J.B.C., Pettersson, J., Asteman, H., Svensson, J.E.; Johansson, L.G. 2007. Energy & Fuels 21 (1), 71–81.

De Souza-Santos, M.L. 1989. Comprehensive modelling and simulation of fluidized bed boilers and gasifiers. *Fuel* 68(12), 1507-1521.

De Souza-Santos, M.L. 2005. Solid fuels combustion and gasification (Modelling, simulation and equipment operation). I. Marcel Dekker. New York**,** pp. 237-240.

De Souza-Santos, M.L., 2007. A new version of CSFB, comprehensive simulator for fluidised bed equipment. *Fuel* 86(12-13), 1684-1709.

Demirbas, A. 2006. Global renewable energy sources. Energy Sources, Part A: Recovery, Utilization and Environmental Effects 28(8), 779-792.

Detournay, M., Hemati, M., Andreux, R. 2011. Biomass steam gasification in fluidized bed of inert or catalytic particles: Comparison between experimental results and thermodynamic equilibrium predictions. *Powder Technology* 208(2), 558-567.

Devi, L., Ptasinski, K. J., Janssen, F. J. J. G. 2003. A review of the primary mesures for tar elimination in biomass gasification processes. *Biomass & Bioenergy* 24, 125-140.

Dornburg, V., Faaij, A.P.C., Verweij, P., Langeveld, H., van de Ven, G., van Keulen, H., van Diepen, K., Meeusen, M., Banse, M. Ros, J. 2008. Biomass Assessment. Assessment of Global Biomass Potentials and Their Links to Food, Water, Biodiversity, Energy Demand and Economy. Netherlands Environmental Assessment Agency.

Dornburg, V., van Vuuren, D., van de Ven, G., Langeveld, H., Meeusen, M., Banse, M., van Oorschot, M., Ros, J., Jan van den Born, G., Aiking, H. 2010. Bioenergy revisited: key factors in global potentials of bioenergy. *Energy Environmental Science* 3(3), 258-267.

Dou, B., Pan, W., Ren, J., Chen, B., Hwang, J., Tae-U, Y. 2008. Removal of tar component over cracking catalysts from high temperature fuel gas. *Energy Conversion and Management*, 49(8), 2247-2253.

Dryer, F.L., Glassman, I. 1973. High-temperature oxidation of CO and CH_4. Proceedings of the 14^{th} Symposium (International) on Combustion. The Combustion Institute, Pittsburgh. Pennsylvania, 987-1003.

ECOFYS. 2011. Financing renewable energy in the European energy market. Technical Report, ECOFYS Netherlands BV.

Encinar, J.M., Gónzalez, J.F., González, J. 2000. Fixed-bed pyrolysis of Cynara cardunculus L. Product yields and compositions. *Fuel Processing Technology* 68(3), 209-222.

Erb, K.H., Haberl, H., Krausman, F., Lauk, C., Plutzar, C., Steinberger, J.K., Müller, C., Bondeau, C., Waha, K., Pollack, G. 2009. Eating the planet: Feeding and Fuelling the World Sustainably, Fairly and Humanely – A scoping Study. Institute of Social Ecology, Potsdam, Institute of Climate Impact Research. Social Ecology Working Paper 116. Vienna. ISSN 1726-3816.

Ergun, S. 1952. Fluid flow through packed columns. *Chemical Engineering and Processing* 48 (2), 89-94.

Evans, A., Strezov, V., Evans, T.J. 2010. Sustainability considerations for electricity generation from biomass. *Renewable and Sustainable Energy Reviews* 14(5), 1419-1427.

Fane, A.G., Wen, C.Y. 1982. Fluidized-bed reactors. Chapter 8 in Handbook of Multiphase Systems. Ed. Hetsroni, G. Hemisphere Publishing Corporation, Washington.

Fernández, J., Curt, M.D. 2004. Low-cost biodiesel from cynara oil. Proceedings of the 2nd World Conference and Exhibition on Biomass for Energy, Industry and Climate Protection, pag. 109-113, 10-14 May, Rome, Italy.

Fernández, J., Curt, M.D. 2005. State of the art of *Cynara cardunculus L*. as an energy crop. Proceedings of the 14th European Biomass Conference, pag. 22-25, 17-21 October, Paris, France.

Fernández, J., Curt, M.D., Aguado, P.L. 2006. Industrial applications of *Cynara cardunculus* L. for energy and other uses. *Industrial Crops and Products*, 24(3), 222-229. ISSN 0926-6690. 2005 Annual Meeting of the Association for the Advancement of Industrial Crops: The International Conference on Industrial Crops and Rural Development.

Fernández, J., Sánchez, J., Esteban, B., Checa, M., Aguado, P.L., Curt, M.D., Mosquera, F., Romero, L. 2009. Potential lignocellulosic biomass production from dedicated energy crops in marginalized agricultural land of Spain. Proceedings of the 17th European Biomass Conference, pag. 131-137, June-July, Hamburg, Germany.

Fiaschi, D., Michelini, M. 2001. A two-phase one-dimensional biomass gasification kinetic model. *Biomass & Bioenergy* 21(2), 121-132.

Field, M.A., Gill, D.W., Morgan, B.B., Hawksley, P.G.W. 1967. Reaction Rate of Carbon Particles. In: Chpater 6 of Combustion of pulverised coal. BCURA, Cheney & Sons, Ltd., Banbury. England.

Fischer, G., Schrattenholzer, L. 2001. Global bioenergy potentials through 2050. *Biomass and Bioenergy*, 20(3), 151-159.

Foley, G., Barnard, G. 1985. Biomass Gasification in Developing Countries. Earthscan, London, UK.

Fuller, E.N., Schettler, P.D. Giddings,, J.C. 1966. A new Method for prediction of binary gas-phase diffusion coefficients. *Industrial & Engineering Chemistry* 58(5), 19-27.

Gandhidasan, P. 2003. Estimation of the effective interfacial area in packed-bed liquid desiccant contactors. *Industrial & Engineering Chemistry Research* 42(12), 3420-3425.

GEA 2012: Global Energy Assessment 2012 – Towards a Sustainable Future. Cambridge University Press, Cambridge, UK and New York, USA and the International Institute for Applied Systems Analysis (IIASA), Laxenburg, Austria.

Geldart, D. 1973. Types of Gas Fluidization. *Powder Technology* 7(5), 285-292.

Gerber, S., Behrendt F., Oevermann, M. 2010. An Eulerian modeling approach of wood gasification in a bubbling fluidized bed reactor using char as bed material. *Fuel* 89(10), 2903-2917.

Gil, J., Corella, J., Aznar, M.P., Caballero, M.A. 1999. Biomass gasification in atmospheric and bubbling fluidized bed: Effect of the type of gasifying agent on the product distribution. *Biomass & Bioenergy* 17(5), 389-403.

Ginestra, J.C., Jackson, R. 1985. Pinning of a bed of particles in a vertical channel by a crossflow of gas. Industrial Engineering Chemical Fundamentals, 24: 121-128.

Gómez-Barea, A., Arjona, R., Ollero, P. 2005. Pilot-Plant Gasification of Olive Stone: a Technical Assesment. *Energy & Fuels* 19(2), 598-605.

Gómez-Barea, A., Leckner, B. 2009. Gasification of biomass and waste, in: M. Lackner, F. Winter, A.K. Agarwal eds., Handbook of Combustion, Vol. 4, Wiley-VCH, Weinheim, 365-397.

Gómez-Barea, A., Leckner, B. 2010. Modeling of biomass gasification in fluidized bed. *Progress In Energy and Combustion Science* 36(4), 444-509.

Gómez-Barea, A., Leckner, B., Villanueva-Perales, A., Nilsson, S., Fuentes-Cano, D. 2012. Improving the performance of fluidized bed biomass/waste gasifiers for distributed electricity: A new three-stage gasification system. *Applied Thermal Engineering*, In Press: 1-10.

Gómez-Hernández, J., Soria-Verdugo, A., Villa-Briongos, J., Santana, D. 2012. Fluidized bed with a rotating distributor operated under defluidization conditions. *Chemical Engineering Journal* 195, 198-207.

Goursot, P., Girdhar, H.L. Westrum, E.F. Jr. 1970. Thermodynamics of polynuclear aromatic molecules: III. Heat capacities and enthalpies of fusion of anthracene. *Journal of Physical Chemistry* 74(12), 2538-2541.

Grace, J.R. 1971. An evaluation of models for fluidized bed reactors. *AIChE Symposium Series* 67, 159-167.

Grace, J.R. 1981. Fluidized bed reactor modeling: an overview. *ACS Symposium Series*, 168, 1-18.

Grace, J.R. 1984. Generalized models for isothermal fluidized bed reactors. Chpater 13 of Recent advances in engineering analysis of chemically reacting systems. Ed. L.K. Doraiswamy, Wiley, Eastern New Deli, pp. 237-255.

Grace, J.R. 1986a. Fluid beds as chemical reactors. Chapter 11 of Gas Fluidization Technology. Ed. D. Geldart, John Wiley & Sons, New York, pp. 287-341.

Grace, J.R. 1986b. Modeling and simulation of two-phase fluidized bed reactors. In: Chemical reactor design and technology. Ed. H.I. de Lasa, Martinus Nijhof Publishers, Den Haag, Netherlands, pp. 245-289.

Grace, J.R. 1986c. Contacting modes and behaviour classification of gas-solid and other two-phase suspensions. Canadian Journal Chemical Engineering 64(3), 353-363.

Grace, J.R., Abba, I.A. 2005. Recent progress in the modeling of fluidized-bed reactors. In: Proc. Industrial Fluidization South Africa, South African Institute. Mining & Metallurgy Symposium Series. Eds. Luckos, A. and Smit, Presentation S42. pp. 3-22.

Green, D.W., Perry, R.H. 2008. Perry's Chemical Engineers' Handbook, Chapter 5, 8th ed., McGraw-Hill, New York, pp 746.

Greenhalf, C.E., Nowakowski, D.J., Bridgwater, A.V., Titiloye, J., Yates, N., Riche, A., Shield, I. 2012. Thermochemical characterisation of straws and high yielding perennial grasses. *Industrial Crops and Products* 36(1), 449-459.

Gustafson, K.R., Dickhut, R.M. 1994. Molecular diffusivity of polycyclic aromatic hydrocarbons in air. *Journal of Chemical and Engineering Data* 39 (2), 286-289.

Haines, A., Kovats, R.S., Campbell-Lendrum, D., Corvalan, C. 2006. Climate change and human health: Impacts, vulnerability and public health. *Journal of the Royal Institute of Public Health* 120(7), 585-596.

Hajaligol, M.R., Howard, J.B., Longwell, J.P., Peters, W.A. 1982. Product compositions and kinetics for rapid pyrolysis of cellulose. *Industrial & Engineering Chemistry Process Design and Development* 21(3), 457-465.

Hasler, P., Nussbaumer, T., Buehler, R. 1997. Evaluation of gas cleaning technologies for small scale biomass gasifiers. Swiss Federal Office of Energy, Berne, Switzerland.

Hasler, P., Nussbaumer, T. 1999. Gas cleaning for IC engine applications from fixed bed biomass gasification. *Biomass and Bioenergy* 16(6), 385-395.

Henriquez, V., Macías-Machín, A. 1997. Hot gas filtration using a moving bed heat exchanger-filter (MHEF). *Chemical Engineering and Processing* 36(5), 353-361.

Herzog, H.J., 2011. Scaling up carbon dioxide capture and storage: from megatons to gigatons. *Energy Economics* 33(4), 597-604.

Herzog, H., Drake, E., Adams, E. 1997. CO2 Capture, reuse and storage technologies for mitigating global climate change: a white paper, final report. DOE No DE-AF22-96PC01257. Energy Laboratory, Massachusetts Institute of Technology, Massachusetts, USA.

Herzog, H., Golomb, D. 2004. Carbon Capture and Storage from Fossil Fuel Use. In Encyclopedia of Energy (C.J. Cleveland, ed.) et al. pp. 277-287. Elsevier Science Inc., New York, USA.

Ho, T.C. Modeling. 2003. In: Chapter 9 in Handbook of fluidization and fluid particle systems. Ed. Yang, W.C., Marcel Dekker, New York, pp. 239-255.

Hoogwijk, M., Faaij, AA., Eickhout, B. de Vries, B., Turkenburg, W. 2005. Potential of biomass energy out to 2100, for four IPCC SRES land-use scenarios. *Biomass & Bioenergy* 29(4), 225-257.

Horio, M., Wen, C.Y. 1977. An assessment of fluidized-bed modeling. *AiChE Symposium Series* 73, 9-21.

Hu, T., Hassabou, A.H., Spinnler, M., Polifke, W. 2011. Performance analysis and optimization of direct contact condensation in a PCM fixed bed regenerator. *Desallination* 280(1-3), 232-243.

JANAF database (therm.dat) from CHEMKIN file therm.dat v4.0, March, 2004. http://users.rowan.edu/~marchese/combustion04/kinetics/h2-chemkin/therm.dat

Jess, A. 1995. Reaktionskinetische Untersuchungen zur thermischen Zersetzung von Modellkohlenwasserstoffen. *Erdöl ErdgasKohle* 111, 479-484. German.

Ji, P., Feng, W., Chen, B. 2009. Production of ultrapure hydrogen from biomass gasification with air. *Chemical Engineering Science* 64(3), 582-592.

Jiang, H.-M., Morey, R.V. 1992. A numerical model of a fluidized bed biomass gasifier. *Biomass & Bioenergy* 3(6), 431-447.

Johansson, T.B., McCormickm K., Neij, L., Turkenburg, W. 2004. The potentials of renewable energy thematic background paper, January 2004.

Juniper Consultancy Services Ltd. 2000. Pyrolysis & gasification of waste: a worldwide technology & business review. Volume 2: Technologies & Processes.

Kaushal, P., Abedi, J., Mahinpey, N. 2010. A comprehensive model for biomass gasification in a bubbling fluidized bed reactor. *Fuel* 89(12), 3650-3661.

Kaewluan, S., Pipatmanomai. 2011. Gasification of high moisture rubber woodchip with rubber waste in a bubbling fluidized bed. *Fuel Processing Technology* 92(3), 671-677.

Kerinin, E.V., Shifrin, E.I. 1993. Mathematical model of coal combustion and gasification in a passage of an underground gas generator. *Combustion, Explosion and Shock Waves* 29(2), 148-154.

Kiel, J. H. A., van Paasen, S. V. B., Neeft, J. P. A., Devi, L., Ptasinski, K. J., Janssen, F. J. J. G. 2004. Primary measures to reduce tar formation in fluidized-bed biomass gasifiers. *Final Report SDE project P1999-12. Energy Research Centre of the Netherlands, ECN. Report ECN-C-04-014, The Netherlands.*

Kunii, D., Levenspiel, O. 1969. Fluidization Engineering. Wiley, New York, USA.

Kunii, D., Levenspiel, O. 1991. Fluidization Engineering, 2nd ed. Butterworth-Heinemann. Stoneham, Massachutssets, USA.

Leckner, B., Johnsson, F., Andersson, S. 1991. Expansion of a freely bubbling fluidized bed. *Powder Technology* 68(2), 117-123.

Lee, T.-Y., Chen, C.L. 2009. Wind-photovoltaic capacity coordination for a time-of-use rate industrial user. *IE transactions on Renewable Power Generation* 3(2), 152-167.

Lewandowski, I., Scurlock, J.M.O., Lindvall, E., Christou, M. 2003. The development and current status of perennial rhizomatous grasses as energy crops in the us and europe. *Biomass & Bioenergy* 25(4), 335-361.

Li, X., Grace, J.R., Lim, C.J., Watkinson, A.P., Chen, H.P., Kim, J.R. 2004. Biomass gasification in a circulating fluidized bed. *Biomass & Bioenergy* 26(2), 171-193.

Li, C., Suzuki, K. 2009. Tar property, analysis, reforming mechanism and model for biomass gasification. An overview. *Renewable and Sustainable Energy Reviews* 13(3), 594-604.

Lide, D.R. 1992. Handbook of Chemistry and Physics, 73th ed. CRC Press, Boca Raton, Florida, USA.

Longanbach, J.R. 1998. Preparing advanced coal-based power systems for the 21st century at the power systems development facility in Wilsonville, Alabama. *In: Proc. 23rd Int. Technical Conf. on Coal Utilization and Fuel Systems*, Clearwater, FL, USA, pp. 69-78.

Lozano, A., Henriquez, V., Macias-Machín, A. 1996. Modelling of a new crossflow moving-bed heat-exchanger/filter (MHEF). *Filtration & Separation* 33(1) 69-74.

Mahecha-Botero, A., Grace, J.R., Elnashaie, S.S.E.H., Lim, C.J. 2007. A comprehensive approach to reaction engineering. International Journal of Chemical Reactor Engineering 5(A17), 1-26.

Mahecha-Botero, A., Grace, J.R., Lim, C.J., Elnashaie, S.S.E.H., Boyd, T., Gulamhusein, A. 2009. Pure hydrogen generation in a fluidized bed membrane reactor: Application of the generalized comprehensive reactor model. *Chemical Engineering Science* 64(17), 3826-3846.

Mahecha-Botero. A. 2009. Comprehensive modelling and simulation of fluidized bed reactors for efficient production of hydrogen and other hydrocarbon processes. *PhD Thesis*. University of British Columbia, Vancouver, Canadá.

Mansaray, K.G., Al-Taweel, A.M., Ghaly, A.E., Hamdullahpur, F., Ugursal, V.I. 2000. Mathematical modelling of a fluidized bed rice husk gasifier. Part I – Model development. *Energy source* 22(1), 83-98.

Martiskainen, M., Coburn, J. 2011. The role of information and communication technologies (ICTs) in household energy consumption/prospects for the UK. *Energy Efficiency* 4(2), 209-221.

May, W.G. 1959. Fluidized-bed reactor studies. *Chemical Engineering Progress* 55, 49-56.

Matsui, I. Kunii, D., Furusawa, T. 1985. Study of fluidized bed gasification of char by thermogravimetrically obtained kinetics. *Journal of Chemical Engineering of Japan* 18(2), 105-113.

Matsui, I., Koijma, T., Kunii, D., Furusawa, T. 1987a. Study of char gasification by carbon dioxide. 1. Kinetic study by thermogravimetric analysis. *Industrial & Engineering Chemistry Research* 26(1), 91-95.

Matsui, I., Koijma, T., Kunii, D., Furusawa, T 1987b. Study of char gasification by carbon dioxide. 2. Continuous gasification in fluidized bed. *Industrial & Engineering Chemistry Research* 26(1), 95-100.

McCullough, J.P, Finke, H.L., Messerly, J.F., Todd, S.S., Kincheloe, T.C., Waddington, G. 1957. The low-temperature thermodynamic properties of naphthalene, 1-methylnaphthalene, 2-methylnaphthalene,1,2,3,4-tetrahydronaphthalene. *Journal of Physical Chemistry* 61(8), 1105-1116.

McKendry, P. 2002. Energy production from biomass (part 3): gasification technologies. *Bioresource Technology* 83(1), 55-63.

Milne, T. A., Evans, R. J. 1998. Biomass gasifier “tars”: their nature, formation and conversion. *National Renewable Energy Laboratory, NREL, Report no. NREL/TP-570-25357, Golden, CO, USA.*

Monti, A., Di Virgilio, N., Venturi, G. 2008. Mineral composition and ash content of six major energy crops. *Biomass & Bioenergy* 32(3), 216-223.

Mori, S., Wen, C.Y. 1975. Estimation of Bubble Diameter in Gaseous Fluidized Beds. *AIChE Journal* 21(1), 109-115.

Mosquera, F., Sánchez, J., Esteban, B., Checa, M., Aguado, P.L., Curt, M.D., and Fernández, J. 2011. Assessment of the potential biomass production from cardoon

(*Cynara cardunculus* L.) in the autonomous community of Madrid. Proceedings of the 19th European Biomass Conference, pages 404-408.

Nakicenovic, N. Grubler, A., McDonald, A. 1998. Global Energy Perspectives. International Institute for Applied Systems Analysis (IIASA) and World Energy Council (WEC) (eds). Cambridge University Press, Cambridge, UK.

Narváez, I., Orío, A., Aznar. M.P., Corella, J. 1996. Biomass gasification with Air in an Atmospheric Bubbling Fluidized Bed. Effect of Six Operational Variables on the Quality of the Produced Raw Gas. *Industrial & Engineering Chemistry Research* 35(7), 2110-2120.

Natarajan, E., Öhman, M., Gabra, M., Nordin, A., Liliedahl, T. 1998. Experimental determination of bed agglomeration tendencies of some common agricultural residues in fluidized bed combustión and gasification. *Biomass & Bioenergy* 15(2), 163-169.

Neves, D., Thunman, H., Matos, A., Tarelho, L., Gómez-Barea, A.2011. Characterization and prediction of biomass pyrolysis products. *Progress In Energy and Combustion Science* 37(5), 611-630.

Nunn, T.R., Howard, J.B., Longwell, J.P., Peters, W.A. 1985. Product Compositions and Kinetics in the Rapid Pyrolysis of Sweet Gum Hardwood. *Industrial & Engineering Chemistry Process Design and Development* 24(3), 836-844.

Oasmaa, A., Kuoppala, E., 2003. Fast pyrolysis of forestry residue. 3. Storage stability of liquid fuel. *Energy & Fuels* 17(4), 1075-1084.

Odero, D., Gilbert, R., Ferrell, J., Helsel, Z. 2008. Production of giant reed for biofuel. SS-AGR-318, pages 1-4.

Oevermann, M., Gerber, S., Behrendt, F. 2009. EulerGLagrange/DEM simulation of wood gasification in a bubbling fluidized bed reactor. Particuology 7(4), 307-316.

Öhman, M., Nordin, A., Bengt-Johan, S., Backman, R., Hupa, M. 2000. Bed agglomeration characteristics during fluidized bed combustión of biomass fuels. *Energy & Fuels* 14(1), 169-178.

Olofsson, I., Nordin, A., Sönderlimd, U. 2005. Initial review and evaluation of process technologies and systems suitable for cost-efficient medium-scale gasification for biomass to liquid fuels. ISSN 1653-0551. ETPC Report 05-02, Energy Technology & Thermal Process Chemistry, University of Umeå, Sweden.

Orcutt, J.C., Davidson, J.F. and Pigford, R.L. 1962. Reaction time distributions in fluidized catalytic reactors. *Chemical Engineering Progress Symosiu. Series* 58(38), 1-15.

Özbay, N., Apaydin-Varol, E., Uzun, B.B., Pütün, A.E. 2008. Characterization of bio-oil obtained from fruit pulp pyrolysis. *Energy* 3(8), 1233-1240.

Pallarés, D., Johnsson, F. 2006. Macroscopic modelling of fluid dynamics in large-scale circulating fluidized beds. *Progress in Energy Combustion Science* 32(5-6), 539-569.

Panoutsou, C. 2007. Socio-economic impacts of energy crops for heat generation in northern greece. *Energy Policy* 35(12), 6046-6059.

Panwar, N.L., Kaushik, S.C., Kothari, S. 2011. Role of renewable energy sources in environmental protection: A review. *Renewable and Sustainable Energy Reviews* 15(3), 1513-1524.

Papadikis, K., Bridgewater, A.V., Gu, S. 2008. CFD modelling of the fast pyrolysis of biomass in fluidised bed reactors. Part A: Eulerian computation of the momentum transport in bubbling fluidised beds. *Chemical Engineering Science* 63(16), 4218-4227.

Papadikis, K., Bridgewater, A.V., Gu, S. 2009a. CFD modelling of the fast pyrolysis of biomass in fluidised bed reactors. Part B: Heat, momentum and mass transport in bubbling fluidised beds. *Chemical Engineering Science* 64(5), 1036-1045.

Papadikis, K., Gu, S., Bridgewater, A.V., Gerhauser, H. 2009b. Application of cfd to model fast pyrolysis of biomass. *Fuel Process Technology* 90(4), 504-512.

Papadikis, K., Gu, S., Bridgewater, A.V. 2009c. CFD modeling of the fast pyrolysis of biomass in fluidized bed reactors: modeling the impact of biomass shrinkage. *Chemical Engineering Journal* 149(1-3), 417-427.

Papazoglou, E.G., Rozakis, S. 2011. Cardoon cultivation for combined bioenergy production and cadmium phytoextraction: an economic evaluation. Proceedings of the 3rd International CEMEPE & SECOTOX Conference, pag. 637-642, June, Skiathos island, Greece.

Partridge, B.A., Rowe, P.N. 1966. Analysis of gas flow in a bubbling fluidized bed when cloud formation occurs. *Transaction of the Institution of Chemical Engineer*s 44, 335.

Petersen, I., Werther, J. 2005. Experimental investigation and modelling of gasification of sewage sludge in the circulating fluidized bed. *Chemical Engineering and Processing* 44(7), 717-736.

Poling, B.E., Prausnitz, J.M., O'Connell, J.P. 2004. The properties of gases and liquids. 5th ed., McGraw-Hill.

Ptasinski, K.J. 2008. Thermodynamic efficiency of biomass gasification and biofuels conversion. *Biofuels Bioproducts Biorefining* 2(3), 239-253.

Puig-Arnavat, M., Bruno, C:, Coronas, A. 2010. Review and analysis of biomass gasification models. *Renewable & Sustainable Energy Review*s 14(9), 2841-2851.

Pyle, D.L. 1972. Fluidized bed reactors. Review. In: 1st chemical reaction engineering international sympomsium. *Advances in Chemical Society*, Washington, D.C.

Rabu, L.P.L.M., Jansen, D. 2001. De-centralised power production using low-calorific value gas from renewable energy resource in gas turbines. ECN.

Radmanesh, R., Chaouki, J., Guy, C. 2006. Biomass Gasification in a Bubbling Fluidized Bed Reactor: Experiments and Modeling. *AIChE Journal* 52(12), 4258-4272.

Ranz, W.E. 1952. Friction and transfer coefficients for single particles and packed beds. *Chemical Engineering Progress* 48(5), 247-253.

Rapagnà, S., Jand, N., Kiennemann, A., Foscolo, P.U. 2000. Steam-gasification of biomass in a fluidised-bed of olivine particles. *Biomass and Bioenergy* 19(3), 187-197.

Reed, T.B., Levie, B. 1984. A simplified model of the stratified downdraft gasifier. In: The International Bio-Energy Directory and Handbook. Washington, D.C., USA, pp. 379-389.

Resch, G., Held, A., Faber, T., Panzer, C., Toro, F., Haas, R. 2008. Potentials and prospects for renewable energies at global scale. *Energy Policy* 36(11), 4048-4056.

Robert, P.M.A., Felder. R.M., Ferrell. J.K. 1988. Modelling a Pilot-Scale Fluidized Bed Coal Gasification Reactor. *Fuel Processing Technology* 19(3), 265-290.

Rogner, H.H. et al. 2004. Energy resources. In World Energy Assessment – 2004 update. United Nations Development United Nations Department of Economic Affairs, World Energy Council, 2004 (Chapter 5).

Ross, D.P., Yan, H.-M., Zhang, D.-K. 2004. Modelling of a laboratory-scale bubbling fluidised-bed gasifier with feeds of both char and propane. *Fuel* 83(14-15), 1979-1990.

Ross, D.P., Yan, H.-M., Zhong, Z., Zhang, D.-K. 2005. A non-isothermal model of bubbling fluidised-bed coal gasifier. *Fuel* 84(12-13), 1469-1481.

Rowley ,R.L., Wilding, W.V., Oscarson, J.L., Yang, Y., Zundel, N.A., Daubert, T.E., Danner, R.P. 2007. DIPPR® Data Compilation of Pure Chemical Properties, Design Institute for Physical Properties. AIChE, New York.

Ruoppolo, G., Miccio, F., Piriou, B., Chirone, R. 2009. Biomass gasification in a catalytic fluidized reactor with beds of different materials. *Chemical Engineering Journal* 154(1-3), 369-374.

Sankari, H.S., Mela, T.J.N 1998. Characteristics of reed canary grass (phalaris arundinacea l.) breeding lines compared at three experimental sites in Finland. Biomass for Energy and Industry: 10th European Conference and Technology Exhibition: Proceedings of the International Conference, pages 894–896.

Schmidt, S., Giesa, S., Drochner, A., Vogel, H. 2011. Catalytic tar removal from bio syngas-Catalyst development and kinetic studies. *Catalysis Today* 175(1), 442-449.

Schröder, E. 2004. Experiments on the pyrolysis of large beechwood particles in fixed beds. *Journal of Analytical Applied Pyrolysis* 71(2), 669-694.

Schwartzberg, H.G., Chao, R.Y. 1982. Solute diffusivities in leaching processes. *Food Technology* 39(2), 73-86.

Secretaria de Estado de Energía. 2010. La energía en España. Technical Report, Ministerio de Industria, Turismo y Comercio.

Shell. 2008. Shell energy scenarios to 2050. Shell International BV.

Shi, L., Chew, M.Y.L. 2012. A review on sustainable design of renewable energy systems. *Renewable and Sustainable Energy Reviews* 16(1), 192-207.

Siegel, G.J. 2005. Overview of gasification technologies. Global Energy and Energy Project (GCEP) Advanced Coal Workshop, Provo, UT.

Sims, R.E.H. 2004. Renewable energy: a response to climate change. *Solar Energy*, 76(1-3), 9-17.

Smeets, E.M.W., Faaij, A.P.C., Lewandowski, I.M., Turkenburg, W.C. 2007. A bottom-up assessment and review of global bio-energy potentials to 2050. *Progress In Energy and Combustion Science* 33(1), 56-106.

Smid, J., Hsiau, S.S., Peng, C.Y., Lee, H.T. 2005a. Moving bed filters for hot gas cleanup. *Filtration and Separation* 42(6), 34-37.

Smid, J., Hsiau, S.S., Peng, C.Y., Lee, H.T. 2005b. Granular moving bed filters and adsorbers /GM-BF/A) – patent review: 1970-2000. *Advanced Powder Technology* 16(4), 301-345.

Socorro, M., Macías-Machín, A., Verona, J.M., Santana, D. 2006. Hot gas filtration and heat Exchange in a packed bed using lapilli as a granular medium. *Industrial & Engineering Chemistry Research* 45(23), 7957-7966.

Sonnefeld, W.J., Zoller, W.H., May, W.E. 1983. Dynamic coupled-column liquid chromatographic determination of ambient temperature vapor pressures of polynuclear aromatic hydrocarbons. *Analytical Chemistry* 55(2), 275-280.

Soria-Verdugo, A., Almendros-Ibáñez, J.A., Ruiz-Rivas, U., Santana, D. 2009. Exergy optimization in a steady moving bed heat exchanger. *Annals of the New York Academy of Science*, 1161: 584-600.

Stassen, H.E.M. 1993. Strategies for upgrading producer gas from fixed bed gasifier systems to internal combustion engine quality. In: Graham, R.G., Bain, R., editors, Biomass gasification: hot-gas clean-up. IEA Biomass Gasification Working Group: 33-44.

Thek, R.E., Stiel, L.I. 1966. A new reduced vapor pressure equation. *AIChE Journal* 12(3), 599-602.

Thunman, H., Niklasson, F., Johnsson, F., Leckner, B. 2001. Composition of volatiles gases and thermochemical properties of wood for modeling of fixed or fluidized beds. *Energy & Fuels* 15(6), 1488-1497.

Toomey, R.D., Johnstone, H.F. 1952. Gaseous fluidization of solid particles. *Chemical Engineering Progress* 48(5), 220-226.

Tsai, W.T., Lee, M.K., Chang, Y.M. 2007. Fast pyrolysis of rice husks: product yields and compositions. *Bioresource Technology* 98(1), 22-28.

van den Broek, R., van den Burg, T., van Wijk, A., Turkenburg, W.. 2000. Electricity generation from eucalyptus and bagasse by sugar mills in Nicaragua: A comparison with fuel oil electricity generation on the basis of costs, macro-economic impacts and environmental emissions. *Biomass & Bioenergy* 19(5), 311-335.

Van Loon, S., Koppejan, J. 2008. The Handbook of Biomass Combustion and Co-firing. Task 32. Earthscan, London.

van Swaiij, W.P.M. 1985. Chemical reactors. In Fluidization, 2nd ed. Eds. Davidson, J.F., Clift, R. and Harrison, D., Academic Press, London.

Van Vuuren, Detlef, .P., Van Vliet, J., Stehfest, E. 2009. Future bio-energy potential under various natural constraints. *Energy Policy* 37(11), 4420-4230.

Wang, Y., Yan, L. 2008. CFD studies on biomass thermochemical conversion. *International Journal of Molecular Science* 9(6), 1108-1130.

Weerachanchai, P., Horio, M., Tangsathitkulchai, C. 2009. Effects of gasifying conditions and bed materials on fluidized bed steam gasification of wood biomass. *Bioresource Technology* 100(3), 1419-1427.

Wen, C.Y., Yu, Y.H. 1966. A Generalized Method for Predicting the Minimum Fluidization Velocity. *AIChE Journal* 12(3), 610-612.

Wen, C.Y., Chen, L.H. 1982. Fluidized Bed Freeboard Phenomena Entrainment and Elutriation. *AIChE Journal* 28(1), 117-128.

Werther, J., Hartge, E.-U. 2004. Modeling of Industrial Fluidized-Bed Reactors. *Industrial & Engineering Chemistry Research* 43(18), 5593-5604.

Wilke, C.R. 1950. Diffusional properties of multicomponent gases. *Chemical Engineering Progress* 46(2), 95-104.

Wilke, C.R., Lee, C.Y. 1955. Estimation of Diffusion Coefficients for Gases and Vapors. *Industrial & Engineering Chemistry* 47(6), 1253-1257.

WBGU: Future Bioenergy and Sustainable Land Use. 2009. Earthscan.

Yan, H.M., Heidenreich, C., Zhang, D.K. 1998. Mathematical modelling of a bubbling fluidised-bed coal gasifier and the significance of 'net flow'. *Fuel* 77(9-10), 1067-1079.

Yan, H.M., Heidenreich, C., Zhang, D.K. 1999. Modelling of bubbling fluidised bed coal gasifiers. *Fuel* 78(9), 1027-1047.

Yates, J.G. 1975. Fluidised bed reactors. The Chemical Engineer, vol. 303, pp. 671-677.

Zakhidov, R.A., 2008. Central Asian countries energy system and role of renewable energy sources. Applied Solar Energy 44(3), 218-223.

Zimont, V. L., Trushin, Y.M. 1969. Total combustion kinetics of hydrocarbon fuels. *Combustion Explosion Shockwaves* 5(4), 391-394.

Zwart, R.W.R. 2009. Gas cleaning downstream biomass gasification. *Status Report. Energy Research Centre of the Netherlands, ECN. Report ECN-E-08-078 Petten, The Netherlands.*